Dissertation zur Erlangung des Doktorgrades
der Fakultät für Chemie und Pharmazie
der Ludwig-Maximilians-Universität München

Improved synthetic gene delivery vehicles for advanced bioimaging-guided tumor-targeted application of the sodium iodide symporter (NIS) as theranostic gene

Sarah Christine Urnauer
geb. Hacker

aus

Pfarrkirchen, Deutschland

2017

Erklärung

Diese Dissertation wurde im Sinne von § 7 der Promotionsordnung vom 28. November 2011 von Frau Professor Dr. C. Spitzweg betreut und von Herrn Professor Dr. E. Wagner vor der Fakultät für Chemie und Pharmazie vertreten.

Eidesstattliche Versicherung

Diese Dissertation wurde eigenständig und ohne unerlaubte Hilfe erarbeitet.

München, 07.12.2017

Sarah Urnauer

Dissertation eingereicht am	12.10.2017
1. Gutachter:	Prof. Dr. Ernst Wagner
2. Gutachterin:	Prof. Dr. Christine Spitzweg
Mündliche Prüfung am	30.11.2017

Table of contents

1. Introduction

1.1 Cancer and metastasis

Genetic and epigenetic alterations drive normal cells to turn into tumor cells [1-3]. Based on the level of aggressiveness, tumors are divided into two subclasses: (1) benign tumors that develop locally and (2) malignant tumors, also termed as cancer, which are characterized by a high potential to migrate and invade in other tissues. In recent years, intensive research allowed a better understanding of the complex processes of carcinogenesis of primary tumors as well as migration, invasion and formation of secondary tumors in the process of metastasis. This multistep process consists of a collaborative network between tumor cells and the tumor microenvironment including tumor stroma and tumor-associated cells [3].
As a result of an increasing number of elderly people, increasing risk factors, high incidence of therapy resistance and relapse, in both developed and developing countries, cancer presents one of the most common cause of death worldwide [4]. Differences in morphological and phenotypical tumor characteristics between patients, primary tumor and metastases and within the tumor itself, termed as tumor heterogeneity, evolved as major bottleneck for effective treatment, as tumor heterogeneity is attributed to therapy resistance as well as limited and diverging efficacy of cancer therapeutics [5]. Although a strong variety in individual tumor properties were identified, certain capabilities are common for all cancer types: sustaining proliferative signaling, evading growth suppressors, activating invasion and metastasis, enabling replicative immortality, inducing angiogenesis, resisting cell death, deregulating cellular energetics, avoiding immune destruction, as well as genome instability and mutation, tumor-promoting inflammation and the importance of the microenvironment in the tumorigenesis process [3]. These hallmarks of cancer as well as new insights in the tumor biology, gained over the last decades, promote the development of individualized concepts for prevention, detection and therapy of cancer that consider special patients' needs.

1.2 Diagnostic and therapeutic approaches for cancer

Due to the fact that cancer screening evolved as an important healthcare issue, nowadays a clinical cancer diagnosis is often made before symptoms become apparent. Diagnostic procedures have improved considerably over the last decades. In addition to endoscopy and biopsy as invasive methods, noninvasive methods such as computed tomography (CT),

magnetic resonance imaging (MRI), x-rays, scintigraphy and positron-emission tomography (PET) allow exact localization of the tumorous tissue and provide important information for the selection of the best and most suitable treatment strategy in the clinical routine.

For localized tumors, surgery and radiation are the most effective treatment opportunities [6], however, especially for advanced cancer stages, therapeutics for systemic application are urgently required. As starting point, agents that destroy rapidly dividing cells were identified to act as cancer therapeutics. However, chemotherapeutics, basically acting via DNA-damaging mechanisms, exhibit strong toxicities due to unselective effects in normal cells and patients show a high degree of recurrence or chemo-resistance [6]. A big step forward was made in 1946, where for the first time, a cancer-specific strategy was applied and thyroid cancer was treated with ^{131}I after thyroidectomy based on the findings that thyroid cancer cells are capable of concentrating iodide due to the expression of the sodium iodide symporter (NIS) [7].

Due to new insights in the complex tumor biology gained over the last years, cancer treatment strategies turned from relatively unspecific options to more elaborate therapy concepts, which focus on selective and mechanisms based processes in a targeted fashion. Targeted therapy strategies use the fact that in addition to the unique character of each cancer type, some alterations are shared between several tumor types. Growth factor receptors, signaling molecules, cell-cycle proteins and components of the microenvironment or the angiogenesis process serve as targets [6]. Currently approved targeted agents for cancer therapy for a broad range of malignancies are monoclonal antibodies and small molecules (tyrosine kinase inhibitors).

In the last years, cancer gene therapy emerged as highly promising tool to intervene in cancer homeostasis. Gene therapy in general describes the introduction of genetic material in cells with the intention to interact and interfere with aberrant physiological processes for a therapeutic intervention [8]. This adaptable treatment approach offers new perspectives to respond to special patients' needs in an individualized manner. Replacement or silencing of malfunctioning genes can be conducted by RNA interference via siRNA or microRNA, peptide nucleic acids or via the CRISPR-Cas methodology [9] and insertion of new genes can be directed via application of peptides, proteins or plasmid DNA (pDNA) [10-12].

The tremendous progress over the last years and the effectiveness of cancer gene therapy is mirrored by the recent approval in the US of the first cancer gene therapy for leukemia [13]. In this therapy concept, human T-cells are engineered *ex vivo* to produce special receptors that bind to epitopes on malignant cells. These anti-CD19-CAR retroviral vector-transduced autologous T-cells are then reinjected to destroy the cancerous B-cells [14, 15].

Aiming at high therapeutic efficacy and safe application, a great number of genes with various modes of action have been investigated. In the last 20 years, the sodium iodide

symporter (NIS) emerged as highly promising target gene for cancer therapy, as it combines a cytotoxic function, which can induce cell destruction, with a diagnostic function that allows exact localization and level of transgene expression based on its ability to mediate uptake of diagnostic and therapeutic radionuclides, such as radioiodide [16].

1.3 The sodium iodide symporter (NIS)

The human sodium iodide symporter (NIS; SLC5A5) is a 643-amino acid transmembrane plasma protein that is localized mainly in the thyroid and consists out of 13 transmembrane domains (Fig.1).

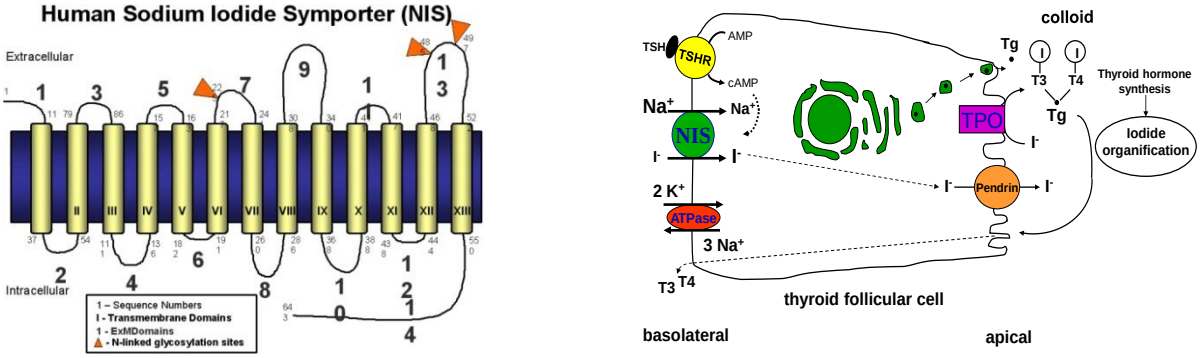

Fig. 1: *Structure of the human sodium iodide symporter (NIS) transmembrane protein (left) and illustration of a thyroid follicular cell and the function of NIS in the process of thyroid hormone synthesis (right). With permission reproduced from Spitzweg et al., J Clin Endocrinol Metab, 2001.*

The active transport of iodide (I^-) with cotransportation of two sodium ions (Na^+) into the thyroid is the first and crucial step in the biosynthesis of thyroid hormones [17]. This uptake is driven by a sodium gradient, established by the Na^+/K^+-ATPase, which is also located at the basolateral membrane. In a next step, I^- is transported across the apical membrane by a chloride/iodide transporter (pendrin) and the process of iodide organification takes place. Herein, I^- is oxidized to iodine (I_2) catalyzed by the thyroperoxidase (TPO) and then I_2 is incorporated into tyroglobulin (Tg) in the process of thyroid hormone synthesis. After TSH stimulation, iodinated Tg is internalized from the follicular lumen and proteolytically cleaved in lysosomes to tri-iodothyronine (T_3) and tetra-iodothyronine (T_4) that are then released into the bloodstream [18]. Thyroid hormones are essential for pre- and postnatal development as well as for multiple metabolic cell processes. This indispensable function highlights the enormous importance of NIS for human health [19].

Besides the ability to transport I^-, NIS further mediates the uptake of other anions, such as selenium cyanate ($SeCN^-$), thiocynate (SCN^-), chlorate (ClO_3^-), nitrate (NO_3^-), perchlorate (ClO_4^-), bromide (Br^-), tetrafluoroborate (BF_4^-), perrhenate (ReO_4^-) and astatide (At^-) [20, 21].

In addition to the thyroidal expression, NIS can also be detected in several other nonthyroidal tissues, such as stomach, lactating breast, salivary glands and kidneys. Various functions of I^- in these tissues are discussed. In the salivary glands, I^- is supposed to act as antimicrobial substance, whereas in lactating breast I^- is secreted into the milk and serves as nutrient to the newborn. Unlike in the thyroid, in these tissues probably no or only low levels of organification of iodide is performed and iodide uptake is not TSH dependent [22-24].

1.3.1 NIS as theranostic tool for thyroid cancer

The fist therapeutic use of the iodide uptake ability of NIS was in 1939 to treat hyperthyroidism by application of radioiodide (^{131}I) and in 1946 to treat thyroid cancer after thyroidectomy [7]. This indicated the starting point of the most effective systemic anticancer radiotherapy strategy to date.

Due to the continuing capacity of a majority of differentiated thyroid cancers (DTC) to express NIS, the NIS-mediated accumulation of radioiodide can further be used to image the extent of tumor spread and possible metastases with subsequent dosimetric calculations of the tumor absorbed dose as basis for consecutive ^{131}I treatment. Whole body ^{123}I- or ^{131}I -scintigraphy has been used for diagnostic purposes for many years [17]. Large efforts were made in establishing new imaging modalities as well as application of new tracers. Besides scintigraphy using y-camera, single photon emission computed tomography (SPECT) and PET imaging allow a more precise diagnosis and exact localization of the tumorous tissues with improved sensitivity and resolution of images using various diagnostic radionuclides (i.e. ^{123}I, ^{124}I, ^{125}I, $^{99m}TcO_4^-$, ^{188}Re, ^{18}F-TFB) [17, 18].

After diagnostic evaluation and exact calculation of the suitable dose for therapy, effective treatment of thyroid cancer can be performed by application of therapeutic radionuclides (^{131}I, ^{188}Re, ^{211}At). This therapeutic concept for DTC using the ionizing radiation of ^{131}I to induce toxic effects in cancer cells represents an efficient strategy with high response rates, which is mirrored by the low mortality of DTC patients even in metastatic stage [25]. The toxic effects are provoked by a destruction of cellular proteins and DNA double strand breaks with subsequent apoptosis [26].

Further, the high efficacy of radioiodide therapy is supported by a bystander effect based on the crossfire effect of the beta-emitter ^{131}I, which implies that the cytotoxic effect is not only limited to transduced cells, but also affects surrounding cells [27] (Fig. 2).

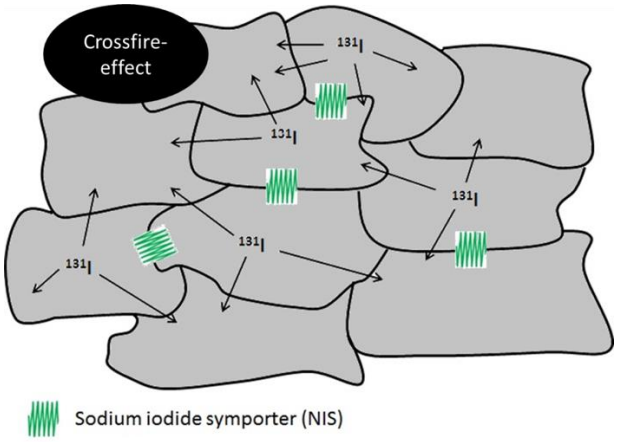

Fig. 2: *NIS expression in tumor cells is associated with a bystander effect based on the crossfire effect of the beta-emitter ^{131}I. This increases the therapeutic effectiveness by affecting non-NIS expressing cells.*

This translational approach for diagnosis and therapy, which resulted in the termination of NIS as “theranostic” gene [28], may represent a promising therapy approach even in nonthyroidal cells after successful NIS gene transfer.

1.3.2 NIS for cancer gene therapy

The identification and cloning of the NIS gene sequence in 1996 [29, 30] opened the exciting prospect to administer NIS as theranostic gene even in nonthyroidal cancer types.

The beneficial concept of image-based targeted radioiodide therapy, with NIS as non-immunogenic human gene and protein, enables safe and efficient application of various radionuclides with a well-known therapeutic window and the ability to adjust dosage in a personalized way with regard to individual tumor radio-responsiveness, co-morbidities and side effects in patients [16, 31, 32]. Based on the ability of NIS to transport various radionuclides, a broad range of imaging modalities can be applied to investigate pharmacokinetic and pharmacodynamic capabilities of different NIS gene delivery vectors and subsequent NIS gene expression in the target tissue. The reporter function further allows calculation of the extent of radionuclide uptake that correlates with cell viability, as only viable cells are able to concentrate iodide [33].

Limited native NIS expression in other tissues restricts negative and undesired effects in healthy cells. Moreover, pretreatment with L-T_4 reduces NIS expression in the thyroid and, therefore, minimizes thyroidal radionuclide uptake, which protects the thyroid from tissue damage and enables prolonged circulation of radionuclides in the body for tumoral uptake [34].

The efficacy of the dual imaging and therapy concept of NIS has been investigated in several preclinical as well as clinical studies using various tumor models and delivery systems with

an enormous potential for a future clinical use [35-51]. Although, in NIS transduced cells, the organification process is not performed, the accumulated dose in the tumor tissue was high enough for a significant therapeutic effect and prolonged accumulation of iodide in transfected cells was demonstrated [47, 52]. As a result of the promising preclinical achievements, NIS as theranostic gene entered clinical trial (NCT00788307, NCT01846091, NCT02068794, NCT02364713, NCT02192775, NCT00450814, NCT03017820, NCT01503177).

Nevertheless, for systemic application, where naked NIS DNA would undergo a rapid enzymatically degradation in blood and tissue, further progress is required, as the efficiency of the NIS gene therapy concept is dependent on the employed delivery system. One promising method is the application of mesenchymal stem cells that are genetically engineered to stably express NIS (eMSCs). Due to their excellent tumor-homing property, NIS-armed MSCs migrate to tumor cells and NIS can be used for vector imaging and therapy. In combination with tumor specific promotors, specific expression can be accomplished only in tumor tissue and undesired effects on nontarget tissue can be reduced [45]. In a collaboration project between Prof. Dr. Christine Spitzweg and Prof. Dr. Peter Nelson, successful NIS gene expression was obtained after administration of adoptively transferred MSCs under the control of the constitutively active cytomegalovirus (CMV) promoter [42], as well as tumor-selective promotors, such as RANTES (regulated on activation, normal T-cell expressed and presumably secreted)/CCL5 promoter [43, 44] and a hypoxia responsive HIF1α-promotor [45]. With these concepts, successful vector imaging could be performed in hepatocellular cancer xenograft models and in a colon cancer metastases model with subsequent therapeutic application of radioiodide that resulted in significantly decelerated tumor growth and prolonged animal survival [42-45].

A further method is the application of viral vectors, which constitutes the most common delivery system in preclinical and clinical studies. The frequent use of viral vectors is owed to the enormous transfection efficiency as a result of their inherent genome editing capacity. In the group of Christine Spitzweg, genetically engineered replication-selective oncolytic adenoviruses were applied, in which the E1a gene is driven by the mouse alpha-fetoprotein promoter and the NIS gene is inserted in the E3 region (Ad5-E1/AFP-E3/NIS). NIS enabled detailed imaging of vector biodistribution and a combinatorial treatment concept of oncolytic virotherapy with radioiodide treatment (radiovirotherapy) [35]. To reduce the negative impact of neutralizing antibodies, widespread expression of the coxsackie-adenovirus receptor (CAR) and adenovirus sequestration by the liver, coating with poly(amidoamine) dendrimers (PAMAM-G5) was performed. Liver detargeting and effective tumor retargeting was obtained [37]. This strategy was further improved by coating the viral particles with PAMAM coupled to

the epidermal growth factor receptor (EGFR)-specific ligand GE11 to obtain a higher level of tumor selectivity [37].

1.4 Cationic oligomers as nonviral gene delivery vehicles

Since viral delivery systems face significant disadvantages regarding immunogenicity, uncontrolled replication, oncogenesis after integration of viral genetic information in human chromosomal DNA, limited loading capacity and sophisticated production processes [9], synthetic carriers emerged as powerful systems that imitate viral behavior. The synthetic systems can be designed in a fashionable manner with multifunctional domains that address the challenges of improved safety, exact targeting and easy upscaling [53].

Nonviral carriers for nucleic acid delivery can be divided into three subclasses: cationic polymers (polyplexes after DNA complexation), cationic lipids (lipoplexes after DNA complexation) and a combination of these two systems: lipid-polymer-based nanoparticles (lipopolyplexes) [54].

The first use of nonviral delivery systems for NIS gene transfer was performed by Kathrin Klutz in Prof. Dr. Christine Spitzweg's group in close collaboration with Prof. Dr. Ernst Wagner, using pseudodendritic oligoamines with high intrinsic tumor affinity (G2-HD-OEI) [38, 40]. High tumor accumulation and NIS expression in the target tissue was obtained. However, accumulation was dependent on the enhanced permeability and retention (EPR) effect, which bears limitations for small fenestrated and low vascularized tumors. A big step forward was made by the successful application of LPEI-PEG-GE11/NIS in a subcutaneous HCC tumor model [39]. Incorporation of the peptide GE11 as EGFR-specific ligand allowed specific tumor targeting and enhanced internalization rates could be achieved.

1.4.1 Oligomer-based nonviral NIS gene delivery process and major challenges

Nevertheless, efficient and tumor-selective delivery with nonviral synthetic systems remains a major issue [55, 56]. Various extra- and intracellular barriers have to be considered for targeting the tumor tissue [56-58]. Formation of stable structures is essential to protect the nucleic acid in the blood stream and avoid rapid enzymatic degradation. Anionic DNA can be condensed with cationic polymers and lipooligomers, as a result of an electrostatic force driven by the entropy process. After reaching the target tissue, the (lipo)-polyplex can bind via its ligand to the corresponding cell surface structure, whereupon the (lipo)-polyplex is internalized mainly through endocytosis. Escape of the endosome and release into the

cytosol enables trafficking to the nucleus, where the gene information is processed [55, 56] (Fig.3).

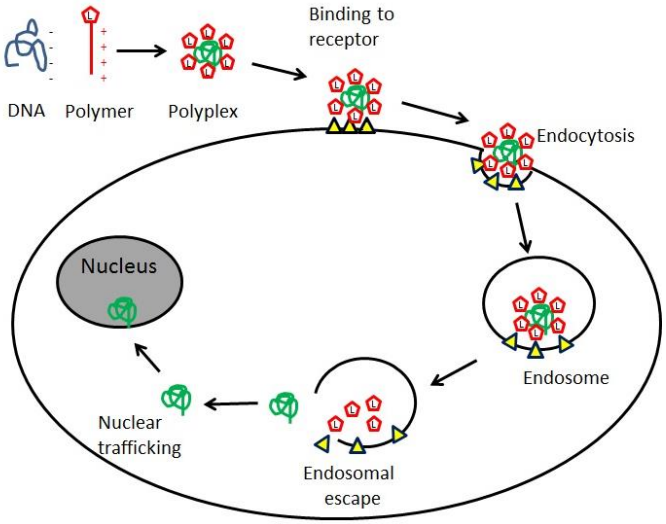

Fig. 3: *Uptake process after complexing of NIS DNA with cationic polymers and systemic application via active ligand targeting and endocytosis into tumor cells.*

However, for this optimized process, several requirements have to be fulfilled:

1. Capability of the polymer to stably compact the nucleic acid, while being able to release the DNA after cellular uptake in a controlled fashion
2. Prolonged circulation time in the blood stream
3. Ideal size for systemic application
4. Protection from enzymatic degradation before delivery and reduced interaction with extracellular components
5. Tumor specific targeting and efficient uptake in tumor cells along with minimal off-target effects
6. Ability to escape out of the endosome
7. Biocompatibility and biodegradability

On the basis of the substantial benefits of nonviral carriers acting as “artificial viruses” these systems may represent a promising strategy for safe and specific NIS gene delivery. The requirements for successful gene delivery stated above, may be addressed by functionalizing the nonviral delivery system in specialized synthesis strategies.

1.4.2 Functionalization of nonviral oligomers

1.4.2.1 DNA complexation

Formation of stable complexes with ideal size and stability is a prerequisite for systemic application of the genetic information. The critical issue of nanoparticle size is reflected by rapid clearing of particles < 5 nm [59]. Furthermore, only particles up to 400 nm can benefit from the EPR effect and only particles up to 200 nm are supposed to enter the cell via a clathrin-dependent active pathway [60-62]. Reduced interactions with extracellular components in the blood stream to ensure long-term stability of the genetic information, low self-aggregation, low immunogenicity, as well as the optimal balance to degrade after cellular uptake to release the genetic information are further important capacities. This can be addressed by influencing charge density of the used cationic oligomer for compaction and by further implementation of hydrophobic sections.

Polyethyleneimine (PEI) has been the most prominent cationic carrier for pDNA delivery as it bears high transfection efficiency *in vitro* and *in vivo* [63]. The linear form of PEI (LPEI) with different molecular weight ranges (Fig. 4) allows controlling of stability, transfection efficiency and safety to some degree [64].

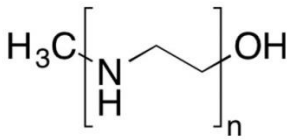

Fig. 4: *Chemical sturcture of linear polyethyleneimine (LPEI).*

High amount of protonable secondary amine groups in the LPEI structure result in a high density of cationic charges and hence enormous efficiency in DNA compaction. The transfection capacity is dependent on the molecular weight of the formulation. High molecular weight PEIs show intense transduction efficiency compared to reduced effects with low molecular weight PEI. Likewise, with increasing molecular weight, cytotoxicity is increasing and a balance between efficacy and cytotoxicity is essential for *in vivo* application. Therefore, the ideal balance between transfection efficiency and biocompatibility is the limiting factor of the application of LPEI. Along with a high degree of polydispersity of LPEI structures and the uncontrollability of polyplex formation, currently, better and more biocompatible structures are being developed [65].

Using solid-phase supported synthesis [66], precise, biodegradable sequence-defined polymers with structure-activity relationships have been designed. Exemplary structures for a sequence defined polymer can be seen in Figure 5 and a schematic structure of a sequence defined lipooligomers is displayed in Figure 6.

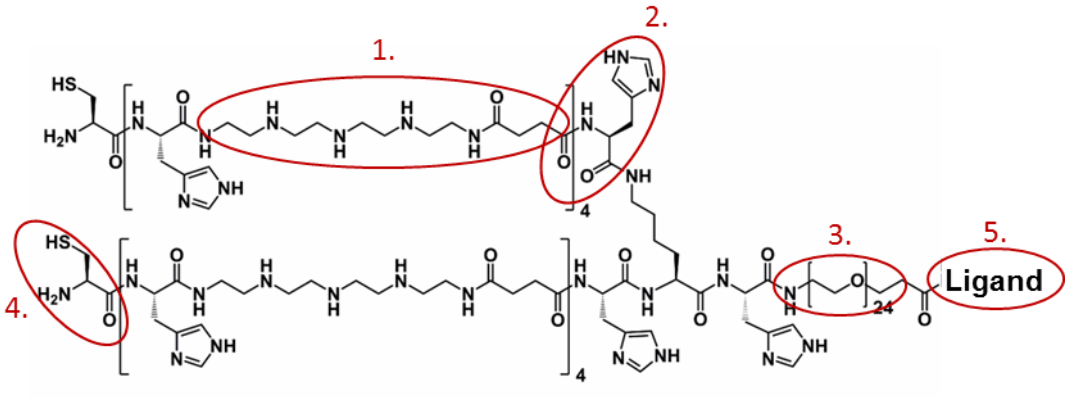

Fig. 5: *Schematic structure of an exemplary two-arm sequence defined oligomer. 1. Diamino ethane domain with artificial aminoacids for DNA binding and buffering capacity (here: Stp); 2. Amino acids with additional buffering capacity (here: histidine); 3. Shielding domain (here: polytheylene glycol; PEG); 4. Reactive sites for crosslinking; 5. Ligand for active tumor cell targeting. Modified figure adapted from [67].*

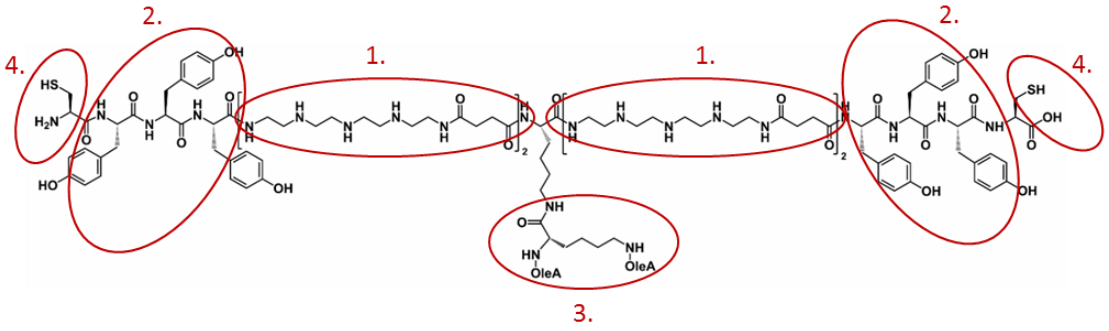

Fig. 6: *Schematic structure of an exemplary sequence defined lipooligomer (here the topology of **454**). 1. Diamino ethane domain with artificial aminoacids for DNA binding and buffering capacitiy (here: Stp); 2. Amino acids with additional buffering capacity (here: histidines); 3. Lipid domain (Oleic acid; OleA) for hydrophobic interaction with endosomal membrane; 4. Reactive sites for crosslinking and postmodification with shielding domain and specific targeting ligands. Modified figure adapted from [67].*

These structures contain a diaminoethane motif, which mimics the PEI structure. Repeating units of various artificial amino acids such as succinoyl-tetraethylenepentamine (Stp), succinoyl-pentaethylene hexamine (Sph) or glutaryl-triethylene tetraamine (Gtt) equip the polymer with a functional site that exhibits optimal DNA condensation ability along with enhanced biodegradability and low toxicity [68, 69].

1.4.2.2 Shielding

The positive surface charge of polyplexes is responsible for efficient cellular uptake as it allows interaction with negatively charged plasma membranes, but also increases the risk of

self-aggregation, binding of extracellular components and unspecific cell attachment [70]. Incorporation of non-cationic hydrophilic copolymers enables sufficient surface shielding and consequently results in a higher safety profile and lower immunogenicity of polyplexes. Hydrophilic domains, such as polyethylene glycol (PEG), saccarides or poly(N-(2-hydroxypropyl)methacrylamide) (pHPMA) were applied to obtain better tolerated nanoparticles with reduced cytotoxicity [71-74].

Integration of a shielding domain can be performed by covalent attachment or by postintegration onto predefined nanoparticles (Fig.7) [75]. The postintegration approach may represent an advantageous strategy, as diminished particle compaction and uncontrolled complex formation were detected in various systems, when using polyplexes with covalentely bound PEG [76, 77].

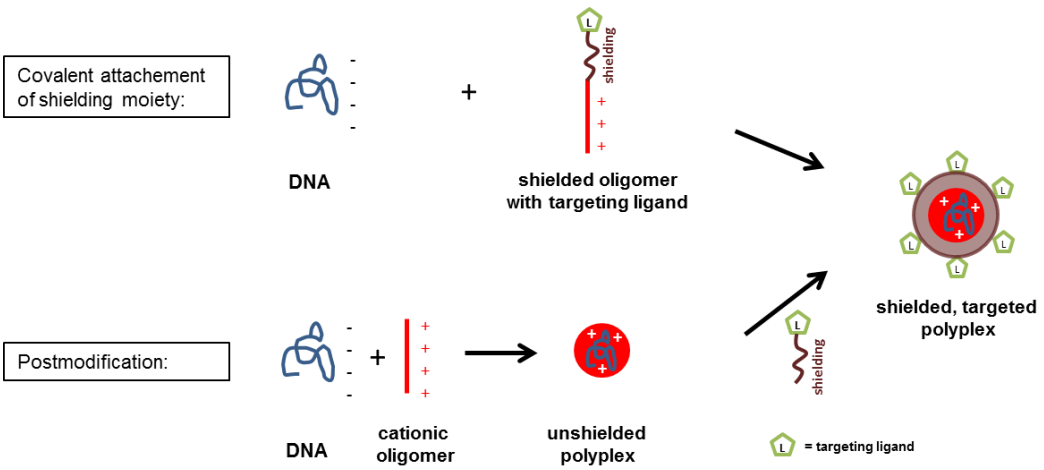

Fig. 7: *Schematic illustration of different approaches to obtain shielding: covalent attachment of shielding and postmodification of preformed complexes.*

For *in vivo* application enhanced shielding is a mandatory requirement; however reduced level of membrane interaction reveal decreased transfection efficiency. This phenomenon is described as the “PEG-dilemma” [78]. To reduce the impact of shielding on transfection efficiency, active targeting is applied to minimize this effect.

1.4.2.3 Specific tumor cell targeting

Exploiting the individual tumor characteristics of increased vascularization and enhanced permeability due to leaky vascular structure [79, 80], unspecific accumulation of nonviral delivery vehicles in the tumor tissue can be obtained. This effect is referred to as “enhanced permeability and retention” (EPR) effect [81]. However, the lack of specific tumor targeting also results in effects in non-target cells as well as reduced efficacy in poor vascularized tumors and metastases [53, 56, 57]. Therefore, active ligand-mediated targeting represents

an elegant method to improve tumor specificity with enhanced transgene expression to compensate reduced transfection efficiency due to active surface shielding in tumoral tissues and reduced side effects in non-target organs [57].

Various receptors are overexpressed in a high range of tumor types and play a crucial role in tumor progression and metabolic maintenance and can function as suitable targets. Antibodies and their fragments that recognize different epitopes on the receptor have been applied; however their use *in vivo* is limited. Large size, rapid clearing from the bloodstream and sensitivity against temperature, pH, salt concentration and organic solvents make it difficult to transfer their applicability into clinical application. Therefore, the focus switched to the identification of short, specific peptide ligands with the advantages of easy synthesis, smaller particles, reduced immune reactivity and improved stability [82].

Several peptide ligands have been developed and tested in the laboratory of Prof. Dr. Ernst Wagner to target various receptors, such as the folate receptor [61], cMET/hepatocyte growth factor receptor [69], epidermal growth factor receptor (EGFR) [39, 68], transferrin receptor (TfR) [83] and integrin receptors [68].

In addition to single receptor targeting, dual targeting approaches have been performed. The simultaneous targeting of various receptors may enhance particle uptake by receptor crosslinking that mimics biphasic uptake of viral vectors [84-86], as well as improve efficacy and reduce therapy resistance by addressing the phenomenon of tumor heterogeneity with expression of several surface receptors at variable levels [68, 87, 88].

1.4.2.4 Endosomal escape

After cellular uptake, release into the cytosol is the next crucial step. A high amount of protonable functions in the polymer backbone is associated with a high buffering capacitiy. LPEI with the repeating structure of two aliphatic carbon groups and amino nitrogen contains a high content of protonable amine groups with high cationic charge density and buffering capacity in the endosome [63, 65]. Two possible effects that support the endosomal escape are discussed. The so called “proton sponge effect”, where the absorption of protons lead to an increased influx of chloride and water that results in swelling and vesicle rupture and the “needle effect”, which states that a pH dependent increase in cationic charge density destabilize directly the phospholipid membrane of the endosome [65].

For new generation sequence-defined oligomers, building blocks of artificial amino acids, which contain a diaminoethane motif, were assembled. These domains contain a high amount of protonable groups, which equip the polyplex with buffering capacity. Additional histidines for buffering can further be integrated to improve endosomal escape for adequate release of polymers in target cells. Another option is the incorporation of lipid domains, such

as oleic acid, stearic acid and cholesterol to enhance hydrophobic interaction of polyplexes and the endosomal membrane, where the lytic activity entails enhanced release in the cytosol [55, 56, 58, 69].

2. Aims of the thesis

Gene therapy has great potential to become an efficient and novel tool for cancer therapy in the clinical setting. In particular, the sodium iodide symporter (NIS) evolved as highly promising target gene taking advantage of its theranostic function to serve as both, reporter and therapy gene. Based on the advanced approaches in NIS gene therapy performed in the laboratory of Prof. Dr. Christine Spitzweg, the next logical step, which should be attempted in this thesis, was to broaden the application of nonviral methods of NIS gene delivery to more advanced tumor stages with regard to tumor heterogeneity as well as to develop and apply more efficient and more biocompatible vectors with the prospect of clinical translation.

The first aim of this thesis was to investigate novel peptide ligands for their suitability to function as highly effective and specific targeting moieties for nonviral NIS gene delivery. Three ligands (B6, GE11, cMBP) were coupled to established vectors and should be applied in different tumor models in order to obtain a broad platform of ligands that can be used in regard to various receptor expression levels of different tumors.

To adequately reflect the clinical situation for successful translation to human clinical trials, the second aim was to investigate the feasibility of established vectors in advanced tumor models. A hepatic colon cancer metastases model should be used to investigate the potential of the nonviral EGFR-targeted NIS gene therapy approach. In this setup, ^{18}F-tetrafluoroborate (TFB) should be applied as novel NIS PET tracer that promises higher resolution and more differentiated images. The suitability for imaging of small metastases after NIS gene delivery should be examined followed by evaluation of therapeutic efficacy after application of ^{131}I.

The third aim was to enhance efficacy as well as to minimize response failure in regard to tumor heterogeneity. As one of the most powerful strategies to circumvent resistance in the clinical situation is the combination of different therapy strategies, a dual combination of two different targeting ligands for cMET and EGFR should be performed. By using this double bifunctional strategy, simultaneous targeting of two receptors should be performed, together with utilizing the theranostic function of the NIS gene to allow monitoring of gene delivery efficiency by noninvasive imaging of tumoral NIS expression and therapeutic intervention by application of cytotoxic ^{131}I.

As next aim, to further improve systemic application with regard to safety, biocompatibility and transduction efficacy, novel sequence defined vectors based on solid phase supported synthesis should be applied. These sequence-defined vectors with various functional domains were coupled to a cMET-specific ligand and utilized, for the first time, *in vivo* for tumor specific NIS gene delivery to obtain bioimaging of functional NIS gene expression in tumorous tissue and therapy of hepatocellular cancer.

Shielding and covalent attachment of hydrophobic ligands, which are prerequisites for *in vivo* application, can result in diminished particle compaction and hence increased sizes of nanoformulations. As final aim, a post-integration concept of a shielding and binding domain in preformed nanoparticles should be established to avoid the limitations of prePEGylation. Analytical characteristics and transfection efficiency using luciferase and NIS as reporter genes should be determined. This critical step should pioneer future *in vivo* application of the novel strategy for successful NIS gene delivery exhibiting improved chemical features regarding size and stability, a higher biocompatibility as well as a possible combination with more hydrophobic ligands.

3. Systemic tumor-targeted sodium iodide symporter (NIS) gene therapy of hepatocellular carcinoma mediated by B6 peptide polyplexes

This chapter has been adapted from:

Urnauer S[1*], Klutz K[1*], Grünwald GK[1], Morys S[2], Schwenk N[1], Zach C[3], Gildehaus FJ[3], Rödl W[2], Ogris M[2,4], Wagner E[2], Spitzweg C[1]. Systemic tumor-targeted sodium iodide symporter (NIS) gene therapy of hepatocellular carcinoma mediated by B6 peptide polyplexes. J Gene Med. 2017 May; 19(5).

*[1]Department of Internal Medicine IV, University Hospital of Munich, LMU Munich, Germany, [2]Department of Pharmacy, Center of Drug Research, Pharmaceutical Biotechnology and Center for Nanoscience (CeNS), LMU Munich, Germany, [3]Department of Nuclear Medicine, University Hospital of Munich, LMU Munich, Germany [4]Present address: Division of Clinical Pharmacy and Diagnostics, University of Vienna, Vienna, Austria, * S.U. and K.K. contributed equally*

3.1 Abstract

Non-viral polymer-based gene transfer represents an adaptable system for tumor-targeted gene therapy, as various design strategies of shuttle systems together with the mechanistic concept of active tumor targeting lead to improved gene delivery vectors resulting in higher tumor specificity, efficacy and safety.

Using the sodium iodide symporter (NIS) as theranostic gene, non-viral gene delivery vehicles based on linear polyethylenimine (LPEI), polyethylene glycol (PEG) and coupled with the synthetic peptide B6 (LPEI-PEG-B6), which specifically binds to tumor cells, were investigated in a hepatocellular carcinoma (HCC) xenograft model for tumor-selectivity and transduction efficiency.

In vitro incubation of three different tumor cell lines with LPEI-PEG-B6/NIS resulted in significant increase in iodide uptake activity as compared to untargeted and empty vectors. After establishment of subcutaneous HuH7 tumors, NIS-conjugated nanoparticles were injected intravenously followed by analysis of radioiodide biodistribution using ^{123}I-scintigraphy showing significant perchlorate-sensitive iodide accumulation in tumors of LPEI-PEG-B6/NIS-treated mice (8.0±1.5% ID/g ^{123}I; biol. half-life 4 h). After four cycles of repetitive polyplex/^{131}I applications, significant delay of tumor growth was observed, which was associated with markedly improved survival in the therapy group.

These results clearly demonstrate that systemic *in vivo* NIS gene transfer using nanoparticle vectors coupled with B6 tumor-targeting ligand is capable of inducing tumor-specific radioiodide uptake. This promising gene therapy approach opens the exciting prospect of NIS-mediated radionuclide therapy in metastatic cancer together with the possibility of combining several targeting ligands to enhance selective therapeutic efficacy in a broad field of cancer types with various receptor expression profiles.

3.2 Introduction

The sodium iodide symporter (NIS) acts as key mediator of thyroidal iodide uptake and accumulation, which is required for thyroid hormone synthesis [89]. Due to its iodide-concentrating ability, NIS forms the basis of multimodal molecular imaging of tumorous tissue by NIS-mediated cellular uptake of various radionuclides, such as ^{123}I, ^{125}I, ^{124}I, ^{131}I, ^{188}Re, ^{211}At, as well as effective treatment of differentiated thyroid cancer by application of ^{131}I [48, 90]. Radioiodide therapy has been used clinically for many decades and represents an approved anticancer therapy in thyroid cancer with a well-understood therapeutic window and safety profile [91]. Cloning of NIS in 1996 [29, 30], as one of the major milestones in thyroidology in the last 20 years, opened the way for the use of this potent dual reporter and therapy gene concept in the treatment of a broad range of cancer types by targeting NIS to non-thyroidal cancer cells. Extensive characterization of the applicability of NIS as diagnostic and therapeutic gene by several research groups including our own [35-47, 49, 92-95], revealed NIS as remarkable and powerful tool to detect and treat different extrathyroidal cancer types, even in metastatic disease [16, 50, 96, 97]. The high incidence of hepatocellular carcinoma (HCC) due to late diagnosis and poor prognosis along with limited treatment strategies urgently requires the development of new treatment strategies. For this purpose the NIS gene therapy concept may represent a promising strategy [98].

However, the major obstacle of current NIS gene therapy is lack of efficient and tumor specific systemic gene delivery approaches. For future medical application, in particular in metastatic cancer, the design of improved vector systems with high transduction efficacy, low systemic toxicity and outstanding specific tumor targeting ability is of high importance. In this regard, several non-viral gene delivery systems including lipoplexes, polyplexes and other nanoparticles have been evaluated [56, 99-107]. The polycationic molecule polyethylenimine (PEI) has been shown to be an efficient non-viral gene delivery vector both *in vitro* and *in vivo* [108-113]. The transfection strategy was further improved by using the linear form of PEI (LPEI), the designated “gold standard” [114] which has also been used in clinical studies [111, 115]. However, biocompatibility and low biodegradability remain critical issues especially when systemic administration is considered [116-118]. A step towards improved biocompatibility was made by conjugating LPEI with polyethylene glycol (PEG) of optimal molecular weight to shield interactions with blood components, while sustaining delivery performance and transfection efficiency [76, 119-121]. To improve gene delivery to tumor sites and enhance availability of the relevant substance within the tumor, while reducing systemic toxicity at the same time, active receptor targeting displays an advantageous strategy.

Using the ligand-receptor-interaction platform for tumor-specific cellular uptake, we already investigated the epidermal growth factor receptor (EGFR)-specific ligand GE11 and a cMET-binding peptide (cMBP2), which were coupled to a polymer backbone, together with our NIS gene therapy concept. Both ligands demonstrated high tumor specificity *in vivo* after systemic application of polyplexes resulting in high iodide accumulation in tumor areas mediated by NIS expression [39, 46]. With the aim of providing a broad platform of ligands for variable surface receptor expression levels, in this study, we selected the peptide sequence CGHKAKGPRK (B6) as tumor-binding peptide, which was originally obtained from a phage display screen on TfR-binding [122]. Recently, we confirmed B6 as a ligand that promotes cell binding of nanoparticles [68, 88], although the real cellular receptor remains unidentified and is most probably different from TfR [123]. But irrespective of the nature of the cellular target receptor, the new fully synthetic LPEI-PEG-B6 conjugates demonstrate encouraging tumor targeting properties, which were investigated by using the dual function of NIS as reporter and therapy gene.

Consequently, in the current study, we evaluated the efficacy of the non-viral ligand-mediated gene delivery vehicle based on the potent LPEI-PEG platform coupled with the tumor-targeting peptide B6 for systemic NIS gene delivery in a human hepatocellular carcinoma (HCC) xenograft mouse model.

3.3 Materials and methods

Cell culture

The human HCC cell line HuH7 (JCRB0403; Japanese Collection of Research Bioresources Cell Bank, Osaka, Japan) was cultured in Dulbecco's modified eagle medium (DMEM; 1 g/l glucose; Sigma-Aldrich, St.Louis, Missouri, USA), the second HCC cell line Hep3B (HB-8064; American Type Culture Collection (ATCC, Manassas, VA) was cultured in Eagle's Minimum Essential Medium (EMEM; Sigma-Aldrich) and the breast cancer cell line MDA-MB-231 (ATCC) was cultured in Dulbecco's modified eagle medium (DMEM; 4 g/l glucose; Sigma-Aldrich, St.Louis, Missouri, USA). All three media were supplemented with 10% (v/v) fetal bovine serum (FBS Superior, Biochrom/Merck Milipore, Berlin, Germany) and 1% (v/v) penicillin/streptomycin (Sigma-Aldrich). Cells were maintained at 37°C and 5% CO_2 in an incubator with 95% humidity. Cell culture medium was replaced every second day and cells were passaged at 85% confluency.

Plasmid and polymer synthesis

The NIS cDNA was synthesized by GENEART (Regensburg, Germany) codon-optimized (pCpG-hCMV-NIS driven by the human elongation factor 1α promotor and human cytomegalovirus enhancer element) for gene expression in human tissue and cloned as described previously [39].

The synthesis of LPEI-PEG-B6 and LPEI-PEG-Cys was performed by Wolfgang Rödl (Department of Pharmacy, Pharmaceutical Biotechnology, LMU) by coupling heterobifunctional (poly)ethylene glycol (NHS-PEG-OPSS, 2 kDa, Rapp Polymere GmbH, Tübingen, Germany) via N-hydroxy succiniminyl ester to amine groups of linear polyethylene imine (LPEI) followed by a purification step via cation exchange chromatography. The B6 peptide (CGHKAKGPRK) was synthesized by solid phase peptide synthesis and coupled to the terminal OPSS group (orthopyridyl disulfide). A final purification step by size exclusion chromatography was performed on a Superdex 75 column (GE Healthcare Europe GmbH, Freiburg, Germany). LPEI-PEG-Cys was synthesized analogously using cysteine instead of the B6 peptide. The resulting conjugates were dialyzed against HBS (20 mM HEPES pH 7.4, 150 mM NaCl) and stored at -80°C as 1 - 5 mg/ml stock solutions until further use.

Polyplex formation

Polymer and plasmid DNA (pDNA) were diluted in same volumes of HEPES (2-[4-(2-hydroxyethyl)piperazin-1-yl]ethanesulfonic acid)-buffered glucose (HBG: 20 mmol/l HEPES, 5% glucose (w/v) at pH 7.4) at PEI conjugate/plasmid (c/p) - ratio (w/w) of 0.8. Polymers

were added to the DNA by rapid mixing and incubated at room temperature for 20 min prior to use [124].

Particle size measurements

Experiments were performed together with Stephan Morys (Department of Pharmacy, Pharmaceutical Biotechnology, LMU). Particle sizes of polyplexes were measured by dynamic laser-light scattering (DLS; Zetasizer Nano ZS, Malvern Instruments, Worcestershire, U.K.) and transmission emission microscopy (TEM; JEM 1011, Jeol, Freising, Germany). For DLS measurement, 2 µg pDNA was complexed with polymers in a total volume of 60 µl. After 20 min of incubation at room temperature, 740 µl of 10 mM sodium chloride solution (pH 7.4) was added and samples were measured. For TEM experiments, samples were prepared with 1 µg DNA in a total volume of 100 µl. The formvar/carbon coated 300 mesh copper grids (Ted Pella Inc., Redding, USA) were activated by mild plasma cleaning. The grids were then incubated with 20 µl of the polyplex solution for 1 min. Excess liquid was blotted off using filter paper until the grid was almost dry. Prior to staining, the grids were washed with 5 µl of staining solution for 5 s. Then the copper grids were incubated for 20 s with 5 µl of a 2% aqueous uranyl formate solution, excess liquid was blotted of using filter paper, followed by air-drying for 30 min. TEM was performed at 80 kV.

Serum stability measurements

Experiments were performed together with Stephan Morys (Department of Pharmacy, Pharmaceutical Biotechnology, LMU). Stability of polyplexes was determined in 90% FBS by DLS. Polyplexes were prepared with 8 µg pDNA in a total volume of 50 µl HBG. After incubation for 20 min 30 µl of HBG and 720 µl FBS were added to reach a final concentration of 90% FBS. 60 µl were placed in a DTS1070 cuvette and values for t=0 min were measured. Then polyplexes were incubated under continuous shaking at 37°C in serum and aliquots were taken for further measurements after 0, 1, 2, 4, 24, 48 h. For each time point measurement from 15 runs were averaged.

Transient transfection and iodide uptake assay

For *in vitro* transfection experiments, cells were grown to 60 - 80% confluency. Cells were incubated for 4 h with polyplexes (final DNA concentration of polyplexes was 2 µg/ml), in the absence of serum and antibiotics followed by incubation with growth medium for 24 h. Transfection efficiency was determined by measurement of iodide uptake activity at steady-state conditions as described previously [47]. Results were normalized to cell survival measured by cell viability assay (see below) and expressed as cpm/A620 nm.

Cell viability assay

After transfection, cell viability was analyzed. Cells were incubated with a commercially available MTT (3-(4,5-dimethylthiazol-2-yl)-2,5-diphenyltetrazolium bromide) reagent (Sigma-Aldrich) for 2 h at 37°C followed by a washing step with PBS (phosphate-buffered saline). The formazan product was measured after incubation with 10% DMSO (v/v) (dimethyl sulfoxide) in isopropanol at 620 nm in a Sunrise microplate absorbance reader (Tecan, Männedorf, Switzerland).

Cellular internalization

HuH7 cells were seeded in 24-well plates at a density of 50 000 cells per well. 24 h later culture medium was replaced with 400 µl fresh growth medium and cells were incubated for 45 min with polyplexes LPEI-PEG-B6/NIS or LPEI-PEG-Cys/NIS or empty polyplexes LPEI-PEG-B6/HBG which served as control. For pDNA polyplexes (c/p 0.8) in 100 µl HBG 1 µg pDNA was used, where 20% of the nucleic acid was Cy5-labeled. Cells were then washed with 500 µl PBS/1000 I.U. heparin for 15 min on ice to remove polyplexes on the cell surface. After washing with PBS, cells were detached with trypsin/EDTA and taken up in PBS with 10% FBS. Cellular uptake was determined by measurement of the excitation of Cy5 at 635 nm and detection of emission at 665 nm on a BD Accuri C6 flow cytometer (BD Bioscience). Cells were gated by forward/sideward scatter and pulse width for exclusion of doublets. Propidium iodide (PI, Sigma Aldrich) was used to discriminate between viable and dead cells. Experiments were performed in triplicates.

Analysis of NIS mRNA expression using quantitative real-time polymerase chain reaction (qPCR)

Total RNA was isolated from HuH7 cells and HuH7 tumors or other tissues using the RNeasy Mini Kit (Qiagen, Hilden, Germany) according to the manufacturer's recommendations. Single stranded oligo (dT)-primer cDNA was generated using Superscript III Reverse Transcriptase (Invitrogen). Following primers were used: hNIS: (5`-ACACCTTCTGGACCTTCGTG-3´) and (5`-GTCGCAGTCGGTGTAGAACA-3´), GAPDH: (5`-GAGAAGGCTGGGGCTCATTT-3´) and (5`-CAGTGGGGACACGGAAGG-3´). qPCR was performed with the cDNA from 1µg RNA using the SYBR green PCR master mix (Quiagen) in a Rotor Gene 6000 (Corbett Research, Morthlake, New South Wales, Australia). Relative expression levels were calculated using the comparative $\Delta\Delta C_t$ method and internal GAPDH for normalization.

Establishment of xenograft tumors in nude mice

HuH7 xenografts were established in female CD-1 nu/nu mice (Charles River, Sulzfeld, Germany) by subcutaneous injection of $5x10^6$ HuH7 cells suspended in 100 µl PBS into the flank region. Animals were maintained under specific pathogen-free conditions with free access to mouse chow and water *ad libitum*. The experimental protocol was approved by the regional governmental commission for animals (Regierung von Oberbayern).

Tumor-specific NIS gene transfer and radioiodide uptake studies in vivo

Experiments started when tumors had reached a size of 8 - 10 mm after a 10-day pretreatment with L-thyroxin (L-T4; 5 mg/ml; Sigma-Aldrich) in drinking water to suppress thyroidal iodide uptake. For systemic *in vivo* NIS gene transfer polyplexes (c/p 0.8) were applied intravenously (i.v.) via the tail vein at a DNA dose of 2.5 mg/kg (50 µg DNA in 250 µl HBG, final DNA concentration of polyplexes for *in vivo* studies: 200 µg/ml). Four groups of mice were established and treated as follows: (1) LPEI-PEG-B6/NIS (n=9); (2) LPEI-PEG-B6/NIS+NaClO4 (sodium perchlorate; 2 mg/mouse; Sigma Aldrich) (n=9); (3) LPEI-PEG-B6/Antisense-NIS (n=9), (4) LPEI-PEG-Cys/NIS (n=9). 24 h after polyplex application, mice received an intraperitoneal (i.p.) injection of 18.5 MBq (0.5 mCurie (mCi)) ^{123}I and iodide biodistribution was assessed using a gamma camera equipped with UXHR collimator (Ecam, Siemens, Germany) as described previously [93]. Regions of interest were quantified and expressed as a fraction of the total initial dose of applied radioiodide per gram tumor tissue (% ID/g). The retention time within the tumor was determined by serial scanning after radionuclide injection and dosimetric calculations were performed according to the concept of *Medical Internal Radiation Dose* (MIRD) with a dosis factor from the RADAR-group (www.doseinfo-radar.com).

Immunofluorescence analysis of NIS protein expression

Immunofluorescence staining on frozen tissue sections derived from HuH7 tumors after systemic gene delivery was performed using a mouse monoclonal antibody directed against hNIS (kindly provided by John C. Morris, Mayo Clinic, Rochester, MN, USA) as described previously [125]. Sections were imaged on an Olympus BX41 microscope (Olympus, Shimjukum Tokio, Japan) equipped with an Olympus XC30 CCD camera (Olympus).

Radioiodine therapy study in vivo

Following a 10-day L-T4 pre-treatment, mice bearing subcutaneous HuH7-tumors received 55.5 MBq (1.5 mCi) ^{131}I as a single i.p. injection 24 h after systemic application of LPEI-PEG-B6/NIS (n=11) or LPEI-PEG-B6/Antisense-NIS (n=9). As an additional control, mice were treated with saline instead of ^{131}I after injection of LPEI-PEG-B6/NIS (n=9) or received saline instead of polyplexes and iodide (n=9). Polyplex/^{131}I or saline cycle was conducted four times

on days 0/1, 3/4, 7/8 and 14/15. Tumor sizes were measured before treatment and daily thereafter for up to five weeks and tumor volume estimated using the equation: tumor volume = length x width x height x 0.52.

Indirect immunofluorescence assay

Immunofluorescence staining was performed on dissected frozen tumor tissues, which were fixed in 80% methanol at 4°C for 5 min and acetone at -20°C for 2 min. After rehydration in PBS and blocking with 12% bovine serum albumin/PBS for 30 min at room temperature, incubation with a rabbit polyclonal antibody against human Ki67 (Abcam, Cambridge, UK; dilution 1:1000) and a rat monoclonal antibody against mouse CD31 (BD Pharmingen, Heidelberg, Germany; dilution 1:200) was performed. A secondary anti-rabbit Alexa488-conjugated antibody (Jackson ImmunoResearch, West Grove, Pennsylvania, USA) for Ki67 staining and secondary anti-rat Cy3-conjugated antibody (Jackson ImmunoResearch) for CD31 staining were used. Nuclei were counterstained with Hoechst bisbenzimide (5 mg/ml) and sections were embedded in Fluorescent Mounting Medium (Dako, Hamburg, Germany). An Axiovert 135 TV fluorescence microscope equipped with an AxioCam MRm CCD camera and AxioVision Re. 4.8. Software (Carl Zeiss, Munich, Germany) was used for examination of stained sections.

Statistical methods

All *in vitro* experiments were carried out in triplicate. Results are expressed as mean +/- SD of triplicates. Statistical significance was tested using Student´s t test. *P* values ≤0.05 were considered significant (**p*≤0.05, ***p*≤0.01, ****p*≤0.001).

3.4 Results

Particle Sizes

DLS measurements revealed an average particle size of 107.1 nm for LPEI-PEG-B6/NIS, 135.3 nm for LPEI-PEG-Cys/NIS and 120.5 nm for LPEI/NIS, each with a PDI (polydisersity index) between 0.135 and 0.231, where 1.0 represents highest polydispersity (Fig. 1A).

TEM measurements showed two different particle subtypes, linear and round particles in all three polymer solutions (LPEI-PEG-B6/NIS, LPEI-PEG-Cys/NIS and LPEI/NIS) with sizes between 40 and 150 nm (Fig.1 B).

A

Polyplex	Average Size (nm)	PDI
LPEI-PEG-B6/NIS	107.1	0.231
LPEI-PEG-CYS/NIS	135.3	0.144
LPEI/NIS	120.5	0.135

B

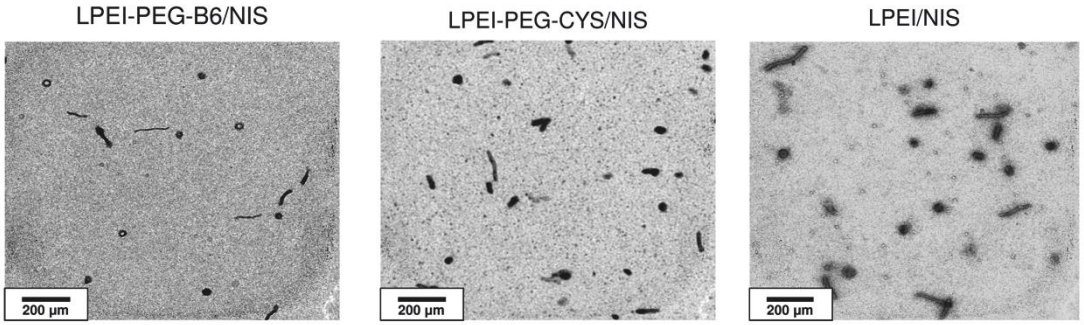

Fig. 1: (A,B) *DLS measurements showed particle sizes between 107-135 nm for all three polymer solutions LPEI-PEG-B6/NIS, LPEI-PEG-Cys/NIS and unPEGylated LPEI/NIS, demonstrating no clear difference in size (A). Detailed structure of polyplexes was obtained by TEM, which revealed two particle subtypes in all there solutions: linear (100-200 nm) and round particles (30-60 nm) (B). Experiments were performed together with Stephan Morys (Department of Pharmacy, Pharmaceutical Biotechnology, LMU). Adapted from [126].*

Serum stability

Polyplex stability and changes in size distribution were analyzed in 90% FBS and determined by DLS. Time points for size measurements were set at t=0, 1, 2, 4, 24 and 48 h. Only time points 0 h (red in Fig. 1 C-F), 4 h (green in Fig. 1 D-F) and 24 h (blue in Fig. 1 D-F) are shown, as time points 1 h and 2 h did not show any differences to time points 0 h and/or 4 h and no further changes were observed after 48 h compared to 24 h.

The peak pattern of FBS can be seen in Fig. 1 C and did not change over 48 h. For all three polymer solutions (LPEI-PEG-B6/NIS (Fig. 1D), LPEI-PEG-Cys/NIS (Fig. 1E) and LPEI/NIS (Fig. 1F)) the same peaks were detected as for the polyplex-free 90% FBS solution at 0 h, though an additional peak >1000 nm was detected for LPEI/NIS. This peak was not seen in both PEGylated polyplex mixtures. After 4 h, this additional peak ranging from 1-10 µm was

obtained in all three polyplex solutions. No further changes in particle sizes were detected after 48 h.

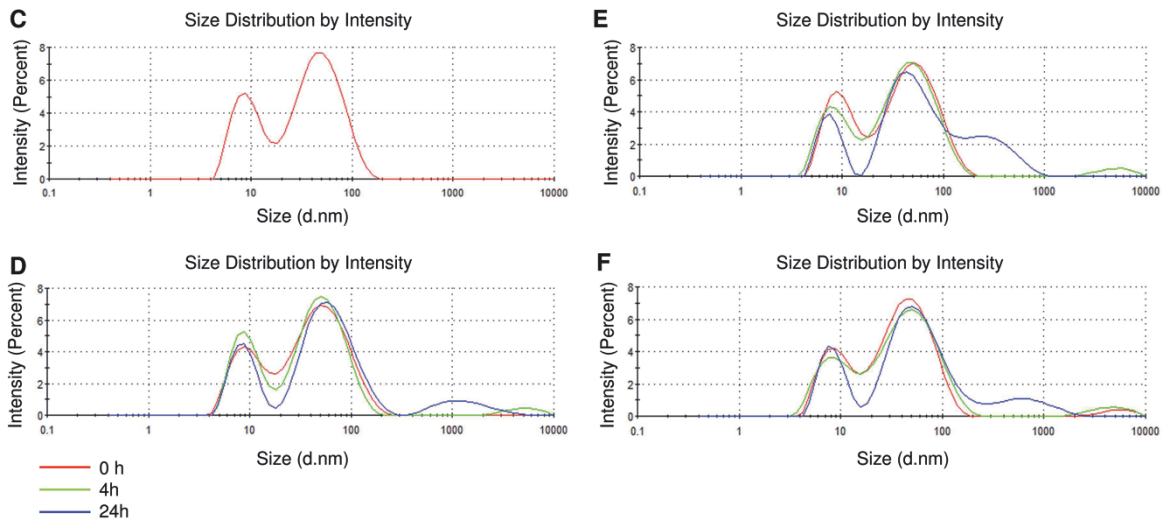

Fig. 1: (C,D) *Polyplex stability and change in size distribution was analyzed in 90% FBS with DLS. The peak pattern of FBS did not change over 48 h (C). All three polymer solutions (LPEI-PEG-B6/NIS (D), LPEI-PEG-Cys/NIS (E) and LPEI/NIS (F) in 90% FBS demonstrated same peaks as the pure FBS solution at 0 h (red line), only in the LPEI/NIS solution, a peak >1000 nm was detected, where in both PEGylated polyplex mixtures, this peak was not obtained. After 4 h an additional peak ranging from 1-10 µm was obtained in all three polyplex solutions. Experiments were performed together with Stephan Morys (Department of Pharmacy, Pharmaceutical Biotechnology, LMU). Adapted from [126].*

Tumor cell-targeted NIS gene transfer in vitro

Transfection conditions using LPEI-PEG-B6/NIS were optimized in HuH7 cells by measurement of perchlorate-sensitive iodide uptake activity 24 h after application of polyplexes (data not shown). An optimal PEI conjugate: pDNA (c/p) ratio of 0.8 (w/w) was found to result in highest transfection efficiency at lowest cell cytotoxicity. This ratio was used in all subsequent experiments. 24 h after transfection with LPEI-PEG-B6/NIS, all three cell lines showed a significant increase in ^{125}I accumulation as compared to cells incubated with LPEI-PEG-B6/Antisense-NIS. Transfection with untargeted LPEI-PEG-Cys/NIS polyplexes resulted in significantly lower iodide uptake activity in all three cell lines, exhibiting similar ratios of LPEI-PEG-B6/NIS to LPEI-PEG-Cys/NIS transfected cells (Fig. 2A). Furthermore, no perchlorate-sensitive iodide uptake above background level was observed in cells transfected with the empty vector LPEI-PEG-B6/HBG.

Transfections of all three cell lines did not result in cell cytotoxicity shown by MTT assay (Fig. 2B).

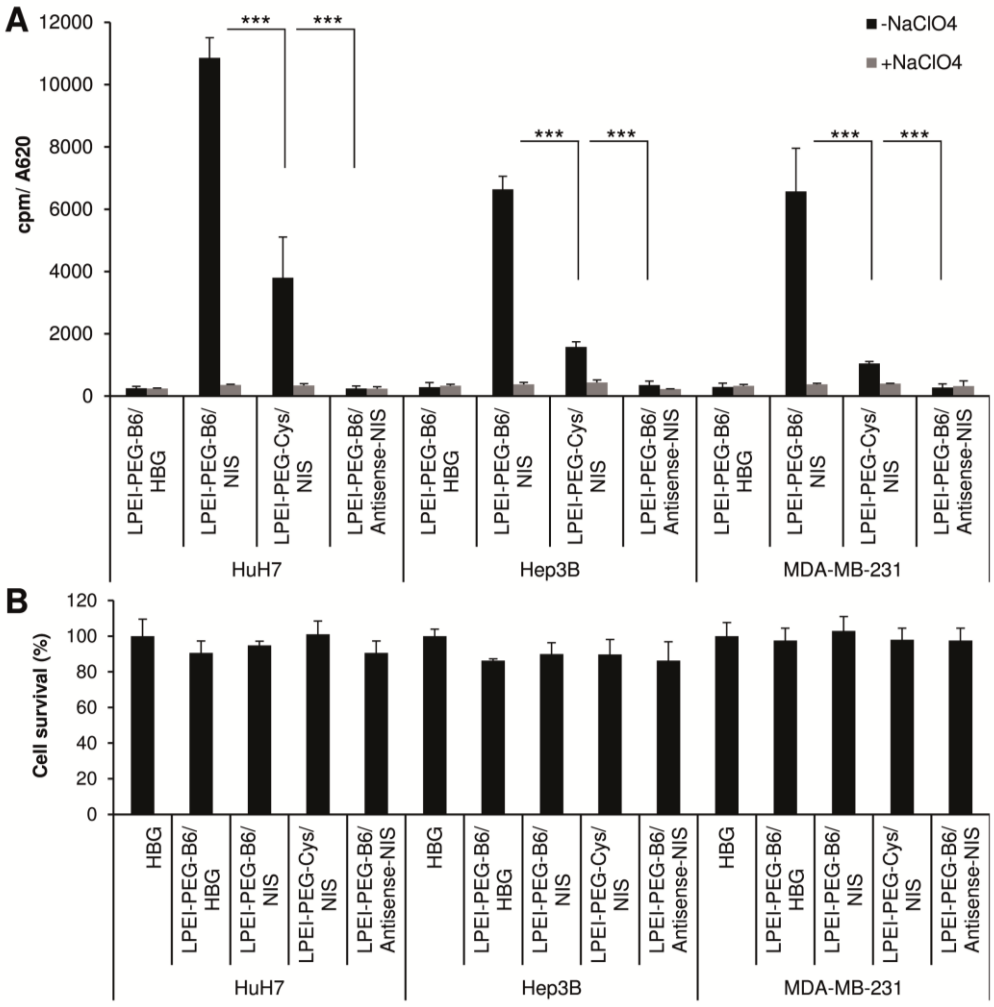

Fig. 2: (A,B) *Iodide uptake was measured in HuH7, Hep3B and MDA-MB-231 cells following in vitro transfection with LPEI-PEG-B6/NIS, control polyplexes LPEI-PEG-Cys/NIS, LPEI-PEG-B6/Antisense-NIS or empty vectors LPEI-PEG-B6/HBG. Cells transfected with LPEI-PEG-B6/NIS showed an increase in perchlorate-sensitive ^{125}I accumulation. After transfection with LPEI-PEG-Cys/NIS, iodide uptake was decreased to approx. 70%. No perchlorate-sensitive iodide uptake above background level was observed in cells transfected with LPEI-PEG-B6/Antisense-NIS or without DNA (A). No effects on cell viability after transfections were obtained shown by MTT assay (B) (***p <0.001). Adapted from [126].*

Cellular uptake and NIS gene expression in vitro

To verify the advantageous targeting effect of LPEI-PEG-B6, uptake of Cy5-labeled NIS-DNA was measured by flow cytometry. After 45 min of polyplex incubation, HuH7 cells demonstrated a higher cellular uptake of LPEI-PEG-B6/NIS polyplexes compared to LPEI-PEG-Cys/NIS (Fig. 2C), which was further demonstrated on the molecular level by analyzing NIS gene expression by qPCR. Cells transfected with the targeted B6-polyplex showed high NIS mRNA expression levels compared to cells treated with LPEI-PEG-Cys/NIS (Fig 2D).

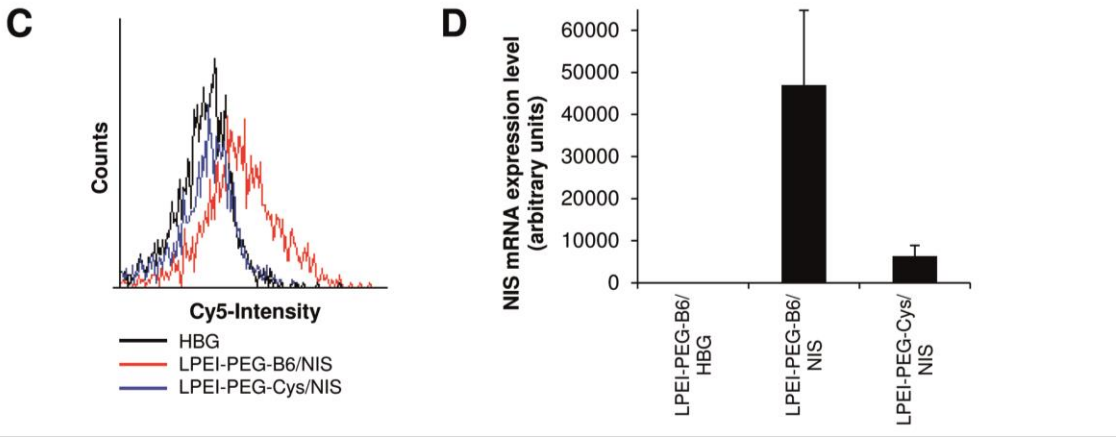

Fig. 2: (C,D) *Flow cytometry uptake studies with Cy5-labeled DNA revealed the beneficial targeting by B6, showing a marked shift towards a higher Cy5-intensity of LPEI-PEG-B6/NIS transfected cells (C).These results were further confirmed on molecular level, where higher NIS mRNA expression levels after transfection with LPEI-PEG-B6/NIS could be detected by qRT-PCR in comparison to incubation with LPEI-PEG-Cys/NIS polyplexes (D). Adapted from [126].*

Induction of iodide accumulation after systemic tumor-targeted NIS gene transfer in vivo

To investigate iodide uptake activity in HuH7 tumors after systemic *in vivo* NIS gene transfer, ^{123}I biodistribution was monitored in tumor bearing mice 24 h after administration of NIS polyplexes (Fig. 2). High levels of iodide uptake were observed in 80% of HuH7 tumors following systemic injection of LPEI-PEG-B6/NIS (Fig. 2A), whereas no significant iodide uptake was observed in non-target organs, including lungs and liver, confirming tumor-specificity of LPEI-PEG-B6-mediated NIS gene delivery. No iodide accumulation was detected in tumors after application of LPEI-PEG-B6/Antisense-NIS (Fig. 2C), and weak tumoral iodide accumulation was observed after application of LPEI-PEG-Cys/NIS (Fig. 2D). To confirm that tumoral iodide uptake was indeed NIS-mediated, LPEI-PEG-B6/NIS-injected mice received sodium-perchlorate (2 mg, i.p.) 30 min prior to ^{123}I administration, which almost completely blocked tumoral iodide accumulation in addition to the physiological iodide uptake in stomach and thyroid gland (Fig. 2B). As determined by serial scanning, approximately 8.0±1.5% ID/g ^{123}I was accumulated in NIS-transduced tumors with a biological half-life of 4 h after application of LPEI-PEG-B6/NIS (Fig. 2E). Considering a tumor mass of 1 g and an effective half-life of 6 h for ^{131}I, a tumor-absorbed dose of 50 mGy/MBq ^{131}I was calculated.

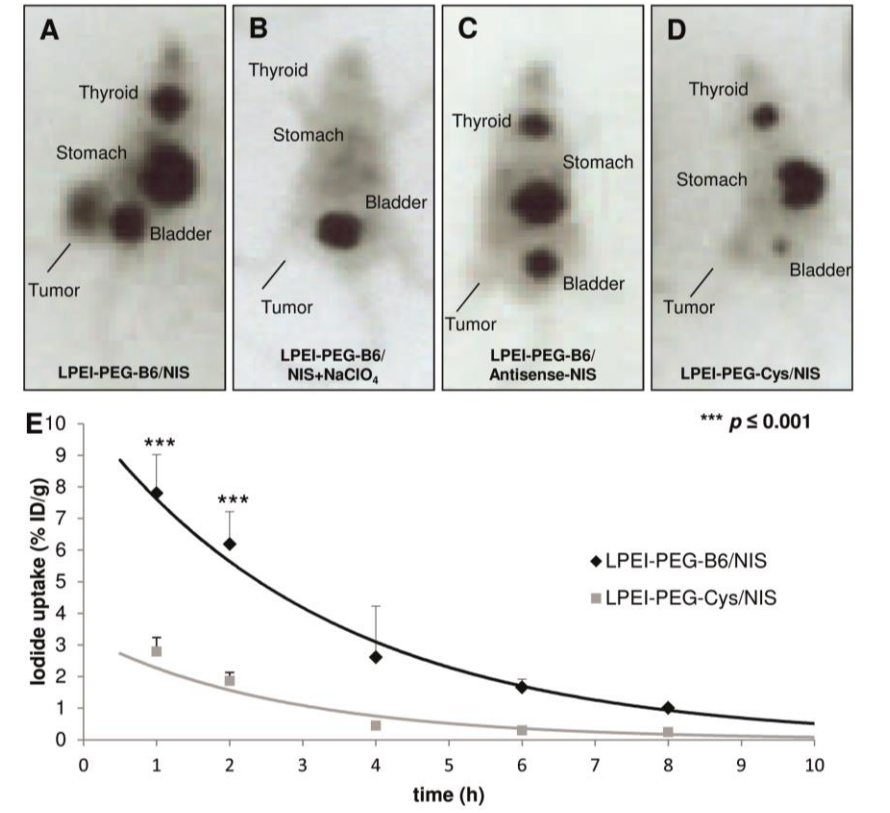

Fig. 3: *Gamma-camera imaging of mice harboring HuH7 tumors 3 h after an i.p. injection of 18.5 MBq ^{123}I 24 h after LPEI-PEG-B6-mediated NIS gene delivery revealed significant tumor-specific iodide accumulation (A), which was completely abolished upon pretreatment with perchlorate (B). In contrast, mice treated with control polyplexes LPEI-PEG-B6/Antisense-NIS (C) or LPEI-PEG-Cys/NIS (D) showed no significant tumoral iodide uptake. Iodide was also accumulated physiologically in thyroid, stomach and bladder (A, C, D).*
Serial ^{123}I-scanning of HuH7 tumors after systemic LPEI-PEG-B6-mediated NIS gene delivery was detected over time with a maximum tumoral iodide uptake of 8.0±1.5% ID/g tumor with a biological half-life of 4 h (E). Adapted from [126].

Analysis of NIS protein expression in HuH7 tumors

Immunofluorescence analysis of HuH7 tumors after systemic application of LPEI-PEG-B6/NIS revealed an intense heterogeneous staining pattern of membrane-associated NIS-specific immunoreactivity (Fig. 4A, arrows), whereas LPEI-PEG-Cys/NIS (Fig. 3B) treated mice showed much less tumoral NIS expression. In contrast, HuH7 tumors of mice treated with LPEI-PEG-B6/Antisense-NIS showed no evident NIS-specific immunoreactivity (Fig. 4C).

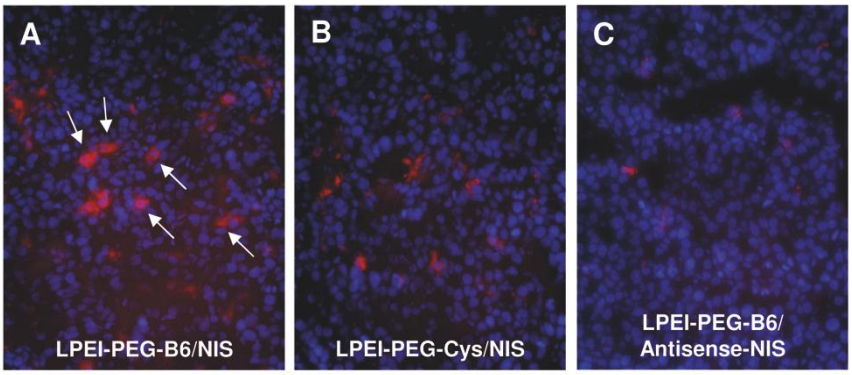

Fig. 4: (A-C) *Immunofluorescence staining of HuH7 tumors 24 h after LPEI-PEG-B6/NIS application using a hNIS specific antibody showed clusters of primarily membrane-associated NIS-specific immunoreactivity (A). In contrast, HuH7 tumors treated with the control polyplexes (LPEI-PEG-Cys/NIS (B), LPEI-PEG-B6/Antisense-NIS (C)), did not reveal NIS-specific immunoreactivity. Magnification: 100x. Adapted from [126].*

Analysis of NIS mRNA expression by quantitative real-time PCR analysis

NIS mRNA level 24 h after systemic NIS gene transfer were analyzed on various tissues by quantitative real-time PCR (qPCR) with a pair of NIS-specific oligonucleotide primers. High levels of NIS gene expression were induced in HuH7 tumors after systemic injection of LPEI-PEG-B6/NIS (Fig. 4D), whereas only low background levels were detected after application of LPEI-PEG-B6/Antisense-NIS and LPEI-PEG-Cys/NIS. As expected, administration of the competitive NIS inhibitor sodium-perchlorate had no influence on NIS mRNA expression in NIS-transduced tumors. Furthermore, analysis of non-target organs such as lungs and liver, showed no significant NIS mRNA expression above background level (Fig. 4D).

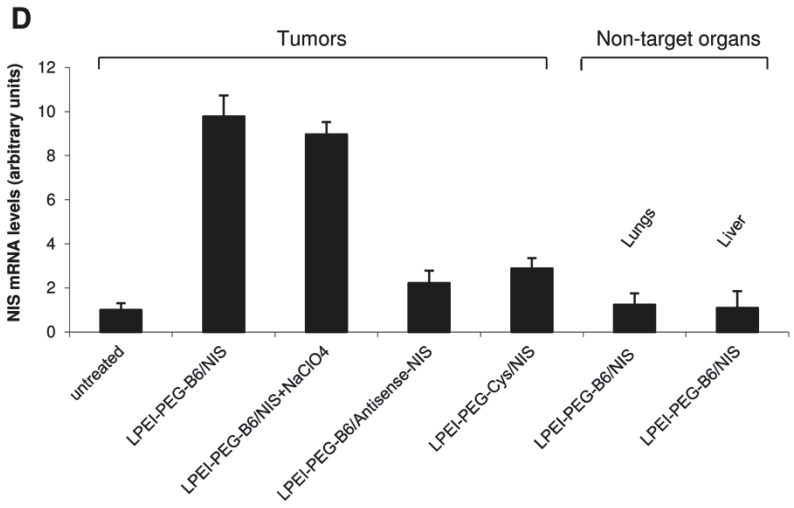

Fig. 4: (D) *Analysis of human NIS mRNA expression by qPCR demonstrated high levels of NIS mRNA in HuH7 tumors after systemic LPEI-PEG-B6-mediated NIS gene transfer with or without sodium-perchlorate pretreatment. Only a low background level of NIS mRNA expression was detected in untreated tumors, which was set as one arbitrary unit. Moreover, no significant NIS expression above background level was found in tumors after application of LPEI-PEG-B6/Antisense-NIS and LPEI-PEG-Cys/NIS, whereas non-target organs showed no significant NIS mRNA expression after treatment of LPEI-PEG-B6/NIS. Adapted from [126].*

Radioiodine therapy studies after in vivo NIS gene transfer

24 h after systemic administration of polyplexes, a therapeutic dose of 55.5 MBq ^{131}I or saline was administered (days 0/1). The cycle consisting of systemic NIS gene transfer followed by radioiodine was repeated three times on days 3/4, 7/8 and 14/15. Mice treated with LPEI-PEG-B6/NIS and ^{131}I showed a significant delay in tumor growth as compared to all control groups (Fig. 5A). While all the mice in the control groups had to be killed within 3 weeks after the onset of the experiments due to excessive tumor growth, 70% of mice in the therapy group survived up to 5 weeks after therapy start (Fig. 5B).

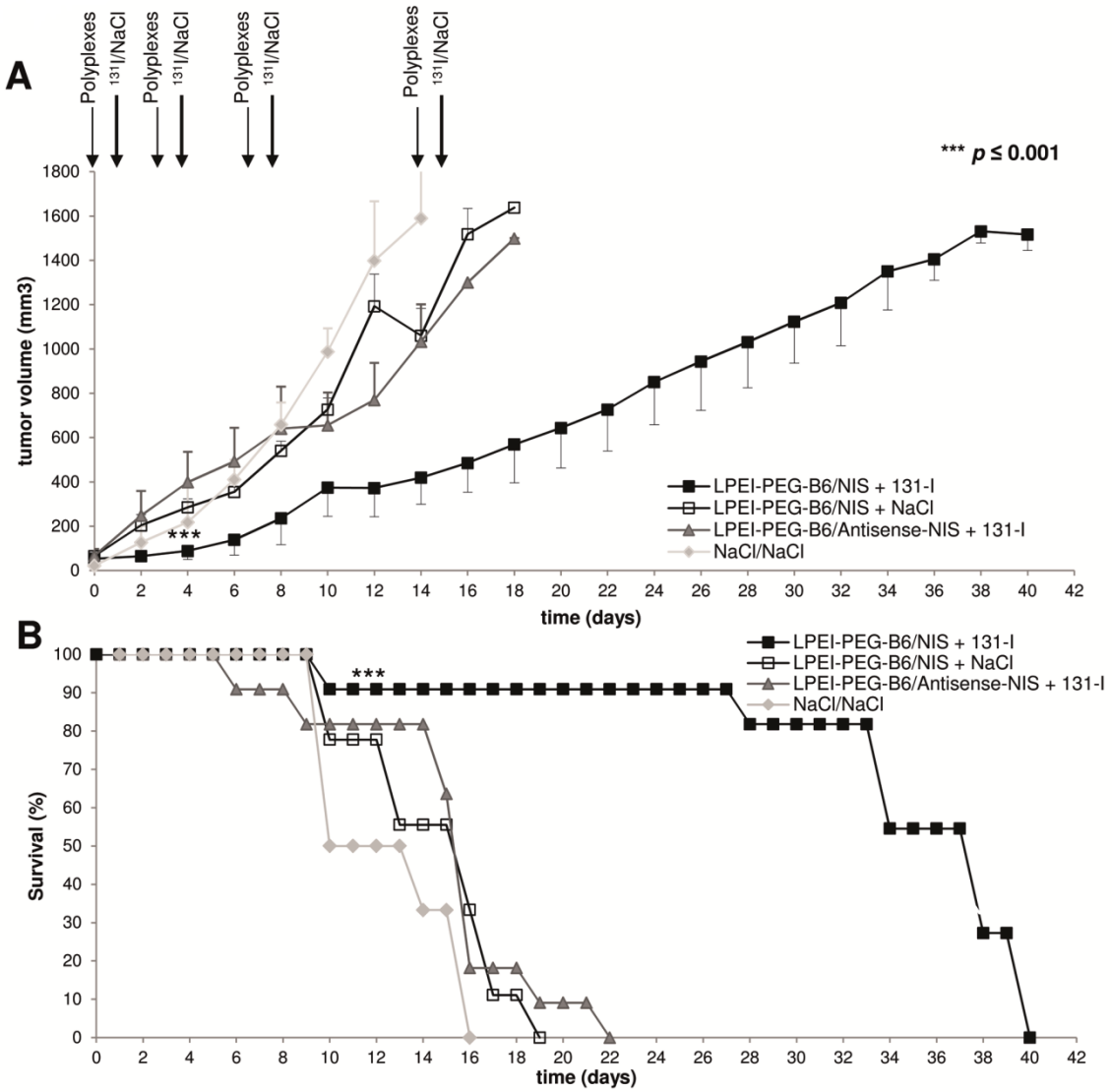

Fig. 5: (A,B) *Radioiodide treatment of HuH7 tumors after systemic polyplex-mediated NIS gene transfer in vivo. 24 h after i.v. polyplex injection (small arrow), 55.5 MBq ^{131}I were injected i.p. (big arrow). This treatment cycle was repeated on days 3/4, 7/8 and 14/15. ^{131}I therapy after systemic LPEI-PEG-B6/NIS application resulted in a significant delay in tumor growth (A) which was associated with markedly improved survival (B, Kaplan-Meier-plot) as compared to control groups that were injected with saline only, with LPEI-PEG-B6/NIS followed by saline application, or with LPEI-PEG-B6/Antisense-NIS followed by ^{131}I application. Adapted from [126].*

Immunofluorescence analysis

Three to four weeks after treatment, mice were sacrificed, tumors were dissected and processed for immunofluorescence analysis using a Ki67-specific antibody (green) to identify tumor cell proliferation and an antibody against CD31 (red) to label blood vessels (Fig. 5). NIS-transduced tumors (LPEI-PEG-B6/NIS) (Fig. 5C) exhibited a considerably lower intratumoral blood vessel density and proliferation index after ^{131}I therapy compared to tumors of mice that received saline instead of ^{131}I (Fig. 5D).

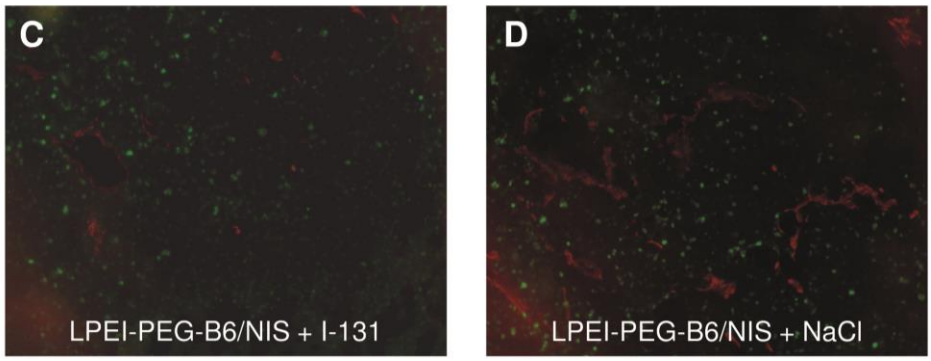

Fig. 5: (C,D) *Immunofluorescence analysis using a Ki67-specific antibody (green) and an antibody against CD31 (red, labeling blood vessels) showed significantly decreased proliferation and blood vessel density in NIS-transduced tumors following ^{131}I treatment (A) as compared to tumors of mice that received saline instead of ^{131}I (B). Tumor sections were counterstained with Hoechst. Magnification 100x. Adapted from [126].*

3.5 Discussion

The growing global incidence of cancer [127] together with increasing resistance to conventional chemo- and/or radiotherapy result in limited success of cancer therapy concepts [128], thus highlighting the importance to develop novel therapeutic alternatives, especially for HCC, where a high percentage of patients is diagnosed at a late stage when no curative therapies are available [98].

The existing therapeutic concept for differentiated thyroid cancer using the ionizing radiation of ^{131}I to induce toxic effects in cancer cells represents an efficient strategy with high response rates, which are mirrored by the low mortality of patients even in metastatic stage [25]. The thyroidal expression of NIS that is maintained in the majority of differentiated thyroid cancer cells enables uptake of various radionuclides (^{123}I, ^{125}I, ^{124}I, ^{131}I, ^{188}Re, ^{211}At) into the cell. This capability of concentrating iodide forms the molecular basis for multimodal non-invasive imaging of functional NIS expression by ^{123}I-scintigraphy and ^{124}I-/^{18}F-tetrafluoroborate positron emission tomography (PET), as well as exact dosimetric calculations before proceeding to therapeutic application of ^{131}I [27, 50, 51, 129, 130]. After identification and cloning of NIS in 1996 [29, 30], it was possible, to transfer this beneficial and powerful concept of image-based targeted therapy to other tumor types and opened the prospect of radioiodide therapy in non-thyroidal tumor tissues. Preclinical and first clinical applications of NIS (NCT00788307, NCT01846091, NCT02068794) [49, 131] as theranostic gene have been intensively investigated and several research groups, including our own, have shown the feasibility and the enormous potential of NIS for the treatment of different extra-thyroidal cancer types after systemic gene delivery, including cellular (mesenchymal stem cells), virus- and polymer-based gene delivery vehicles [35-40, 42-46]. Based on the extensive experience gained over the last decades in the clinical application of radioiodide in thyroid cancer patients, the NIS gene therapy approach offers a promising new alternative in the treatment of cancer together with an already well-known therapeutic window, which, in addition, allows adjustment of dosage in a personalized manner with respect to individual tumor radio-responsiveness, co-morbidities and side effects in patients.

However, using radioiodide to detect and treat distant cancer metastases requires improved efficiency of systemic gene delivery systems to ensure sufficient functional tumor-selective NIS expression. For *in vivo* gene delivery, a series of additional extracellular barriers have to be considered. Interactions of particles with plasma proteins, erythrocytes or non-target tissues, aggregation and clearance of transfection particles by the reticuloendothelial system (RES) and the restricted extravasation of transfection particles from the bloodstream limit the availability of relevant substances in target tissues [132]. The key feature of non-viral gene delivery vehicles for systemic administration is the formation of stable and non-toxic vectors

that can compact and sufficiently deliver genetic materials specifically into tumor cells with high efficiency [70, 133]. LPEI (with average molecular weight of 22 kDa), the “gold standard” of PEI-based gene carriers, shows remarkable transfection efficiency along with high stability of DNA complexes. Since LPEI exhibits dose dependent cytotoxicity, a more biocompatible system was developed by inserting a short PEG chain to reduce interactions with blood components. Recent advances in the identification of the ideal shielding agents with optimal molecular weight led to improved carries with high delivery performance and reduced cytotoxicity (LPEI-PEG2kDa) [119]. The advantage of short PEG chains was also highlighted in most recent work [76, 134]. LPEI-PEG2kDa as biocompatible and technically feasible starting point for complete synthetic targeting conjugates was further modified by biological targeting strategies to direct these synthetic gene delivery particles towards the tumor site by taking advantage of the special architecture of tumors and unique tumor properties [39, 88, 119]. Tumor cells are often characterized by a high proliferation rate and subsequent up-regulation of growth factor receptors such as EGFR, cMET or TfR characteristic for rapidly dividing cells. Therefore, tumor targeting ligands were applied that recognize their cognate receptors on the cell membrane of target cells, resulting in receptor-mediated endocytosis of polyplexes. Cell-targeting ligands included vitamins, carbohydrates, peptides, proteins and antibodies [56, 83, 135-139].

In consideration of pharmaceutical production, the use of whole protein ligands such as transferrin or EGF may be challenging in advanced synthesis and storage stability of LPEI conjugates. For a future medical application, synthetic systems such as small specific targeting peptides would be favorable [88]. The short peptide B6, which was originally isolated as TfR-specific ligand in a phage display array [122], was selected as targeting ligand for this study and coupled to the LPEI-PEG-platform. Former studies have already demonstrated the strong tumor cell binding promoting capacity of B6 [68, 88, 140], which resulted in a high tumor-specific gene delivery, and makes B6 a promising and interesting ligand for improving the concept of NIS gene delivery. However, as recent studies discovered that the corresponding receptor is most probably different from TfR, exact binding and interaction mechanisms of B6 remain unclear [123].

But even without knowing the exact cellular receptor, on the basis of the outstanding tumor cell binding capacity of the B6 ligand and with the focus of a possible future combination of two subsidiary targeting ligands to mimic the potent dual-receptor binding concept of viruses [68], B6 serves as promising ligand for further optimization of the NIS gene therapy concept.

For characterization of LPEI-PEG-B6/NIS and evaluation of a possible impact of the PEG shielding domain and the B6 ligand on particle size, shape and stability, DLS and TEM measurements were performed. DLS revealed particles of 107 nm in size for LPEI-PEG-B6/NIS polyplexes in comparison to 135 nm for LPEI-PEG-Cys/NIS polyplexes. These minor

differences in size were further examined by TEM, which revealed two different particle types: round and linear formed particles with no clear difference between LPEI-PEG-B6/NIS, LPEI-PEG-Cys/NIS and LPEI/NIS polyplexes. The combination with PEG as shielding agent to obtain longer circulation and reduced interactions with blood components [138] did not result in any alterations in size or shape in comparison to the PEG-free LPEI/NIS polyplexes. Building on these results, the size of polyplexes does not seem to be a crucial parameter for transfection efficiency both *in vitro* and *in vivo*, as particles <200 nm are postulated to be taken up into cells by clathrin dependent pathways, our particle sizes lay in the scope of being internalized by an active pathway [62].

In addition to polyplex size, behavior and stability of polyplexes after systemic application is a major point that influences efficiency of targeted LPEI-PEG-B6-mediated gene transfer. Interactions with serum components after systemic application may lead to aggregation and/or DNA degradation and hence to diminished targeted gene transfer and gene expression. Polyplex stability was analyzed in 90% FBS by DLS over 48 h. As internal control 90% FBS without polyplexes was measured. No change in peak formation was observed over 48 h. Solutions containing polyplexes showed the same pattern of peaks as the 90% FBS control. As the main polyplex peak is expected to be at 50-150 nm, likely the second FBS peak mashed the polyplex peak, which lies in the same region. In the LPEI/NIS polyplex solution a peak >1000 nm was detected at 0 h, whereas in both PEGylated polyplex mixtures (LPEI-PEG-B6/NIS and LPEI-PEG-Cys/NIS), this peak was not seen, confirming findings that non-PEGylated polyplexes are less stable than PEGylated ones [56]. After 4 h, this additional peak ranging from 1-10 µm was found in all three polyplex solutions. No further changes in particle sizes were detected after 48 h. These results demonstrate that a high amount of our compact polyplexes exhibit a long stability (4-24 h), with no fast and major aggregation or dissociation in serum, suggesting lasting stability, which is a prerequisite for tumor targeting and retention in tumor tissues.

To evaluate the capability of B6 as targeting ligand for non-viral NIS gene delivery, the reporter function of NIS was used to demonstrate tumor-specific NIS-mediated iodide uptake. LPEI-PEG-B6 polymers were complexed with human NIS (hNIS) cDNA under the control of the strong human elongation factor 1 alpha promoter and *in vitro* transfection of three different tumor cell lines resulted in significantly increased iodide uptake activity. A significantly lower uptake was obtained in cells that were treated with polyplexes where the targeting ligand was replaced by cysteine (LPEI-PEG-Cys/NIS).

To further investigate the beneficial targeting using B6 polyplexes that was observed in the iodide uptake assay, cell uptake studies with labeled DNA were performed to compare specific polyplex-mediated transfection of targeted LPEI-PEG-B6/NIS and untargeted LPEI-PEG-Cys/NIS in HuH7 cells. The advantageous conjugation to the ligand could be verified by

a higher Cy5 activity in LPEI-PEG-B6/NIS transfected cells. qPCR complemented these results by showing higher NIS mRNA expression levels in LPEI-PEG-B6/NIS treated cells.

After this proof of concept by *in vitro* studies, the diagnostic function of NIS was further used for demonstration of vector biodistribution and functional NIS expression *in vivo*. Mice carrying HuH7 xenografts showed a tumor-specific ^{123}I accumulation of 8.0±1.5 % ID/g with a biological half-life of 4 h and a tumor absorbed dose of 50 mGy/MBq ^{131}I 24 h after an i.v. injection of LPEI-PEG-B6/NIS. In line with these results, tumors of animals that received untargeted LPEI-PEG-Cys/NIS polyplexes showed significantly lower tumoral iodide uptake, further confirming the ligand-mediated enhanced tumor specificity of LPEI-PEG-B6. The low, but measurable iodide uptake activity in HCC tumors after LPEI-PEG-Cys/NIS treatment suggests that passive tumor targeting due to the "enhanced permeability and retention-effect" is sufficient for a low level of tumoral NIS transduction [81], which can be significantly increased after coupling to the tumor specific ligand B6. Besides tumoral uptake, significant radioiodine accumulation was observed in tissues physiologically expressing NIS, including stomach and thyroid, as well as in the urinary bladder (average of approximately 10% ID, depending on diuretic activity) due to elimination of radioiodine through the kidneys. NIS specificity could be confirmed by pretreatment with the NIS-specific inhibitor perchlorate, resulting in an almost complete inhibition of radioiodide uptake in the tumor and tissues that physiologically express NIS. Results of both *in vitro* and *in vivo* experiments using the B6 ligand strongly underline the high tumor specificity and ligand-dependent uptake of polyplexes, especially when comparing to unspecific LPEI-PEG-Cys/NIS polyplexes by using the reporter function of NIS.

In addition, NIS-mediated uptake could further be confirmed by immunohistochemical staining of human NIS protein in tumor sections. LPEI-PEG-B6-treated mice exhibited NIS-specific immunoreactivity in tumor tissue, which was primarily membrane-associated and occurred in clusters. The patchy staining pattern nicely correlates with earlier experiments using G2-HD-OEI polyplexes for systemic NIS gene transfer in a syngeneic neuroblastoma mouse model [38] and with a study using EGFR-targeted polymers (LPEI-PEG-GE11) for targeting the NIS gene to HCC xenografts.

As next step, the therapeutic impact of radioiodide after B6-mediated gene transfer was tested. The systemic NIS gene transfer, which resulted in tumor-specific iodide uptake activity in HCC tumor-bearing mice, was sufficiently high for a significant therapeutic effect of ^{131}I. The used beta-emitting radioisotope ^{131}I exhibits a high bystander effect, based on the crossfire effect of ^{131}I, which had a cytotoxic effect not only in transfected cells, but even proximate cells (2.4 mm). After four cycles of systemic polyplex application followed by ^{131}I injection, tumor-bearing mice showed a significant delay of tumor growth associated with a significantly prolonged survival for up to 40 days after therapy onset and convincingly prove

the promising tumor specific targeting effect of nonviral delivery systems coupled to the targeting ligand B6.

The applied therapy scheme consisting of 4 treatment cycles was applied in reference to commonly used multi-cycle treatment schemes used in current anti-cancer treatments. As immunohistochemical staining revealed heterogeneous NIS staining, we aimed at optimizing NIS transduction levels by repetitive NIS gene transfer into the heterogeneous tumor tissue in order to optimize therapeutic efficacy [141-143].

Due to the persistent and growing problem of drug resistance in cancer treatment, it is becoming more difficult to apply and develop efficient therapy concepts [144, 145]. Various processes that result in decreased response to drug-induced tumor cell growth inhibition are hypothesized, including altered membrane transport, modified genetic responses, as well as induced changes in expression levels of growth factor receptor [145]. Therefore, even for the new method of a cytoreductive gene therapy approach based on NIS gene delivery, the evaluation of novel targeting ligands is of high relevance to have a broad ligand-portfolio for the treatment of different cancer types with variable receptor expression and back-up alternatives for ligands, when resistance or decreased receptor expression occurs.

Regardless of the exact resistance mechanism, one of the most powerful strategies to circumvent resistance is the combination of different therapy strategies. In this context, a future dual combination of ligands may not only increase the efficacy of the therapy approach, but as well minimize the possibility of non-response by targeting two different receptor pathways. We have already investigated the EGFR-specific non-viral NIS gene delivery using GE11 as ligand coupled to the LEI-PEG-backbone. High transduction efficiency of LPEI-PEG-GE11/NIS was confirmed by significant EGFR-specific iodide accumulation both *in vitro* and *in vivo* resulting in significant delay of tumor growth associated with prolonged survival of animals after therapeutic application of ^{131}I [40]. Levels of specific tumor accumulation and therapeutic efficacy of NIS gene transfer mediated by non-viral delivery vehicles with the targeting ligand B6, are comparable to the study using the EGFR-specific ligand GE11 [39], thus opening the exciting prospect of a future combination of these two highly effective ligands for multiple target sites.

Tumor localization may have an impact on results due to differences in blood vessel density and permeability and infiltration of macrophages, which abolish DNA [79]. Consequently, as a next step toward clinical application, we are currently planning to investigate the efficacy of our LPEI-PEG-B6/NIS polyplexes in an advanced orthotopic HCC tumor model or metastases model that better reflect the natural tumor environment, including microenvironment and stroma, of HCC patients and therefore allows a better prediction of therapy outcome.

In conclusion, the current study demonstrated that using B6 as targeting ligand for systemic NIS gene delivery shows considerable promise for effective tumor targeting with high levels of NIS gene and protein expression that lead to a strong therapeutic effect of radioiodide. This paves the way for the use of B6-targeted non-viral delivery vehicles to specifically introduce NIS to cancer tissue even in a combinatorial ligand set-up depending on the individual receptor expression and represents an innovative concept to improve efficacy and safety of systemic NIS gene delivery in a broad range of cancer types.

3.6 Acknowledgements

The authors are grateful to SM Jhiang, Ohio State University, Columbus, OH, USA, for supplying the full-length human NIS cDNA and to JC Morris, Mayo Clinic, Rochester, MN, USA, for providing the NIS mouse monoclonal antibody. We also thank M Strigl (Department of Nuclear Medicine, LMU Munich, Germany) for assistance with therapy studies. A Vetter and M Willhauck are gratefully acknowledged for experimental support. This work was supported by grants from the Deutsche Forschungsgemeinschaft within the Collaborative Research Center SFB824 (project C 08) to C Spitzweg as well as within the Priority Programme SPP1629 to C Spitzweg and PJ Nelson (SP 581/6-1, SP581/6-2, NE 648/5-2), the Cluster of Excellence Nanosystems Initiative Munich (NIM) to E Wagner and by a grant from the Wilhelm-Sander-Stiftung to C Spitzweg (2014.129.1).

4. EGFR-targeted nonviral NIS gene transfer for bioimaging and therapy of disseminated colon cancer metastases

This chapter has been adapted from:

Urnauer S[1], Müller AM[1], Schug C[1], Schmohl KA[1], Tutter M[1], Schwenk N[1], Rödl W[2], Morys S[2], Ingrisch M[3], Bertram J[4], Bartenstein P[5], Clevert DA[3], Wagner E[2], Spitzweg C[1]. EGFR-targeted nonviral NIS gene transfer for bioimaging and therapy of disseminated colon cancer metastases. Oncotarget. 2017 Sep; 8(54):92195-92208

[1]Department of Internal Medicine IV, University Hospital of Munich, LMU Munich, Germany, [2]Department of Pharmacy, Center of Drug Research, Pharmaceutical Biotechnology, LMU Munich, Germany [3]Department of Clinical Radiology, University Hospital of Munich, LMU Munich, Germany [4]Department of Nuclear Medicine, Radiopharmacy, Klinikum rechts der Isar der Technischen Universität München, Munich, Germany, [5]Department of Nuclear Medicine, University Hospital of Munich, LMU Munich, Germany

4.1 Abstract

Liver metastases present a serious problem in the therapy of advanced colorectal cancer (CRC), as more than 20% of patients have distant metastases at the time of diagnosis with less than 5% being cured. Consequently, new therapeutic approaches are of major need together with high-resolution imaging methods that allow highly specific detection of small metastases.

The unique combination of reporter and therapy gene function of the sodium iodide symporter (NIS) may represent a promising theranostic strategy for CRC liver metastases allowing non-invasive imaging of functional NIS expression and therapeutic application of ^{131}I. For targeted NIS gene transfer polymers containing linear polyethylenimine (LPEI), polyethylene glycol (PEG) and the epidermal growth factor receptor (EGFR)-specific ligand GE11 were complexed with human NIS DNA (LPEI-PEG-GE11/NIS). Tumor specificity and transduction efficiency were examined in high EGFR-expressing LS174T metastases by non-invasive imaging using ^{18}F-tetrafluoroborate (^{18}F-TFB) as novel NIS PET tracer. Mice that were injected with LPEI-PEG-GE11/NIS 48 h before ^{18}F-TFB application showed high tumoral levels (4.8±0.6% of injected dose) of NIS-mediated radionuclide uptake in comparison to low levels detected in mice that received untargeted control polyplexes. Three cycles of intravenous injection of EGFR-targeted NIS polyplexes followed by therapeutic application of 55.5 MBq ^{131}I resulted in marked delay in metastases spread, which was associated with improved animal survival.

In conclusion, these preclinical data confirm the enormous potential of EGFR-targeted synthetic polymers for systemic NIS gene delivery in an advanced multifocal CRC liver metastases model and open the exciting prospect of NIS-mediated radionuclide therapy in metastatic disease.

4.2 Introduction

Metastatic dissemination of tumor cells is mostly responsible for the high mortality of patients with colorectal cancer (CRC), especially due to late diagnosis. Although the incidence of CRC is decreasing, CRC is the third leading cause of cancer-related death worldwide [45, 127, 146]. For early stages, surgical resection represents the first-line therapy concept, while in advanced stages a combination of surgical resection and chemotherapy are applied. As the 5-year survival of patients at the metastatic stage is about 6%, new potent therapeutic options are highly important [147].

For evaluation of novel CRC therapy approaches, especially in metastatic disease, it is a prerequisite to have models that give a detailed reflection of the morphological and molecular situation of cancer. Therefore, the establishment of advanced preclinical models that mimic human metastases, tumor microenvironment and tumor stroma are indispensable to obtain a valuable prediction of the therapeutic efficacy of new treatment strategies for a future application in humans [148, 149]. To this end, a human colon carcinoma metastases model was established by injecting CRC cells directly into the spleen. This resulted in induction of multifocal liver metastases highly similar to the metastatic process in humans, where the liver represents the most common metastatic site in patients with CRC [150].

A new evolving sector in cancer treatment is based on gene therapy [11], as utilizing and manipulating the particular biological characteristics of tumor cells provide a wide range of possible interactions to target different steps of the carcinogenesis process. In recent years there have been many attempts to knock out genes that are involved in tumor formation, growth and dissemination, to introduce suicide genes as well as inserting new genes containing specific anti-tumoral functions [10]. In this regard, the sodium iodide symporter (NIS) represents an advantageous and highly efficient target gene, as functional NIS gene expression allows exact localization of the tumorous tissue by administration of NIS specific tracers such as ^{123}I, ^{124}I and the novel NIS positron-emissions-tomography (PET) tracer ^{18}F-tetrafluoroborate (^{18}F-TFB) and at the same time gives the possibility of cytotoxic radioiodide treatment.

This dual concept, which is based on the iodide uptake activity of NIS [30], was proven by several groups including our own using a broad spectrum of gene delivery vehicles, such as viral vectors, mesenchymal stem cells and non-viral polymer-based vectors [27, 35-45, 47, 92, 93, 129]. Especially non-viral polymeric vehicles proved to be advantageous both technically and biologically due to the ease of adjusting chemical properties of synthetic particles for increased efficacy and biocompatibility [9, 12]. A modular synthesis concept allows incorporation of functional groups, such as polyethylene glycol (PEG) to achieve shielding against blood components *in vivo* and polymers can specifically be designed to

interact with individual tumor tissue properties to achieve tumor specific targeting [119]. To this end, polymers were coupled to ligands that bind to receptors overexpressed on the tumor cell, which results in tumor-directed uptake of delivery vehicles and minimizes off-target effects. In former studies, we tested polyplexes with an EGFR-specific targeting peptide (GE11) as NIS gene delivery vehicles in a subcutaneous HuH7 xenograft tumor model [39] as well as in orthotopic pancreatic ductal adenocarcinoma [151], which resulted in high tumor-specific NIS-mediated iodide accumulation.

To take the next step in the translation of this novel theranostic NIS gene strategy from laboratory scale to the clinical situation, in the current paper, we applied the NIS pDNA polyplexes in a high EGFR-expressing tumor model of metastatic colorectal cancer. This setting mimics the complex and functional environment of metastases including tumor stroma and tumor microenvironment and serves as ideal model for evaluation of the feasibility of the NIS gene therapy concept after EGFR-targeted nonviral gene transfer. In addition, the combination with the novel NIS PET tracer ^{18}F-TFB as improved diagnostic tool is utilized for optimized localization of single metastases and the therapeutic potency after application of ^{131}I is evaluated.

4.3 Materials and methods

Cell culture

The human colon carcinoma cell line LS174T (ATCC-CCL188; American Type Culture Collection, Manassas, VA) was cultured in Eagle's Minimum Essential Medium (EMEM; Sigma-Aldrich, St.Louis, MO) supplemented with 10% (v/v) fetal bovine serum (FBS Superior, Biochrom/Merck Milipore, Berlin, Germany), 5% (v/v) L-glutamine (Sigma-Aldrich) and 1% (v/v) penicillin/streptomycin (Sigma-Aldrich). Cells were maintained at 37°C and 5% CO_2 in an incubator with 95% humidity. Cell culture medium was replaced every second day and cells were passaged at 80% confluency.

Plasmid and polymer synthesis and polyplex formation

Polymer syntheses were carried out by Stephan Morys and Wolfgang Rödl (Department of Pharmacy, Pharmaceutical Biotechnology, LMU). Polymers with LPEI-PEG backbone (EGFR-targeted: LPEI-PEG-GE11; control polymer without ligand: LPEI-PEG-Cys) and codon-optimized human NIS cDNA (NIS pDNA) were synthesized as described previously [39, 46]. Polymers and cDNA were diluted in same volumes of HEPES (2-[4-(2-hydroxyethyl)piperazin-1-yl]ethanesulfonic acid)-buffered glucose (HBG: 20 mmol/l HEPES, 5% (w/v) glucose at pH 7.4) at a N/P ratio of 6 (w/w). Polymers were added to the DNA by rapid mixing and incubated at room temperature for 20 min prior use [124]. For *in vitro* studies the concentration of DNA for polyplex formation was 2 µg/ml, for *in vivo* studies 200 µg/ml.

EGFR expression levels in vitro

1×10^6 LS174T cells were detached with trypsin, centrifuged and incubated with an EGFR-specific antibody (1:100; monoclonal mouse IgG1 - Dako, Glostrup, Denmark) or with an IgG-anti-mouse antibody (BD Bioscience, Franklin Lakes, USA) as negative control in FACS buffer (PBS with 10% FBS) for 1 h on ice. Cells were washed with FACS buffer and incubated with an AlexaFluor 488 labeled goat anti-mouse secondary antibody (1:400 - Invitrogen, Langenselbold, Germany) for 1 h on ice. After washing, cells were resuspended in FACS buffer and flow cytometry analysis was performed on a BD Accuri C6 flow cytometer (BD Bioscience, Franklin Lakes, USA). Cells were gated by forward/sideward scatter and pulse width for exclusion of doublets. PI (propidium iodide, Sigma-Aldrich) was used for discrimination between viable and dead cells.

Transfection studies

CRC cells LS174T were plated at a density of 1×10^6 cells per well, grown to 60 - 80% confluency in 6-well plates and incubated for 24 h with either LPEI-PEG-GE11/NIS, LPEI-PEG-Cys/NIS or empty polymer LPEI-PEG-GE11/HBG. Transfection efficiency was determined by measurement of iodide uptake activity at steady-state conditions as described previously [47]. Results were normalized to cell survival measured by cell viability assay (see below) and expressed as cpm/A620.

Cell viability assay

Cell viability after transfection was analyzed after incubation of cells with a commercially available MTT reagent (Sigma-Aldrich) for 2 h at 37°C followed by a washing step with PBS (phosphate-buffered saline). The formazan product was measured after incubation with 10% DMSO (v/v) (dimethyl sulfoxide) in isopropanol at 620 nm in a Sunrise microplate absorbance reader (Tecan, Männedorf, Switzerland).

Establishment of hepatic colorectal metastases in nude mice

For the establishment of CRC metastases in female CD-1 nu/nu mice (Charles River, Sulzfeld, Germany), animals were fully anesthetized and after laparotomy, 50 µl of tumor cell suspension (1×10^6 cells in 1×PBS) was injected into the upper splenic pole. After 3 days, the abdominal wall was re-opened at the same site and a splenectomy was performed. Mice were pre- and post-treated with Metacam (0.5 mg/kg) to minimize wound pain and reduce risk of inflammation. 2-3 weeks after intrasplenic injection mice bore multifocal liver metastases. Mice were sacrificed when healthy liver tissue reached less than 30%, in case of weight loss of more than 10% of initial weight, or when impairment of breathing, drinking or eating behavior was observed. Animals were maintained under specific pathogen-free conditions with access to mouse chow and water *ad libitum*. The experimental protocol was approved by the regional governmental commission for animals (Regierung von Oberbayern) and all animal experiments were carried out according to the guidelines of the German law of protection of animal life.

EGFR-immunohistochemistry staining

Immunohistochemistry staining of EGFR on paraffin-embedded tumor tissue was performed as described previously [152].

PET imaging studies after systemic NIS gene transfer in vivo

Experiments started 2-3 weeks after intrasplenic injection of tumor cells. To demonstrate tumor-specific NIS expression *in vivo*, mice received polyplexes systemically via the tail vein (i.v.) at a DNA dose of 2.5 mg/kg (50 µg DNA in 250 µL HBG). Mice were treated as follows:

(1) LPEI-PEG-GE11/NIS (n=5); (2) LPEI-PEG-Cys/NIS (n=3); (3) LPEI-PEG-GE11/NIS + $NaClO_4$ (n=2): pretreatment with an i.p. injection of 2 mg of the competitive NIS inhibitor sodium perchlorate ($NaClO_4$) 30 min before PET tracer administration. 48 h after polyplex injection the novel NIS PET tracer ^{18}F-TFB (10 MBq; synthesized by the Radiopharmacy, Klinikum rechts der Isar, TU Munich, as described previously [96]) was applied i.v. and tracer accumulation in metastatic liver areas was determined by small-animal PET (Inveon, SIEMENS Preclinical Solutions, Erlangen, Germany). Regions of interest were analyzed with the software Inveon Acquisition Workplace (Siemens) and quantified using Inveon Research Workplace (Siemens) and expressed as a fraction of the total amount of initial dose (% of ID). The retention time of the tracer ^{18}F-TFB within metastases was determined by serial scanning after 0.5 h, 1 h and 2 h. To suppress thyroidal iodide uptake, a 10-day pretreatment with L-thyroxin (L-T4; 5 mg/ml; Sigma-Aldrich) in drinking water was conducted before PET-imaging.

Analysis of NIS mRNA expression by quantitative real-time PCR

For quantification of NIS expression in metastatic tissue, total RNA was isolated using the RNeasy Mini Kit (Qiagen, Hilden, Germany) according to the manufacturer's recommendations. Reverse transcription was performed using SuperScript III First-Strand Synthesis System (Thermo Fisher Scientific, Waltham, Massachusetts, USA). Quantitative real-time PCR was run with the QuantiTect SYBR Green PCR Kit (Qiagen) in a Mastercycler ep gradient S PCR cycler (Eppendorf, Hamburg, Germany). Relative expression levels were calculated from $_{\Delta\Delta}C_t$ values normalized to internal β-actin. As primers, the following sequences were used:

hNIS: (5'ACACCTTCTGGACCTTCGTG-3') and (5'-GTCGCAGTCGGTGTAGAACA-3'),

β-Actin: (5'AGAAAATCTGGCACCACACC-3') and (5'-TAGCACAGCCTGGATAGCAA-3').

Immunohistochemistry analysis of NIS protein expression

Immunohistochemical staining of paraffin embedded tumor tissue derived from hepatic metastases sections after NIS gene delivery were performed using a mouse monoclonal antibody directed against human NIS (kindly provided by John C Morris, Mayo Clinic, Rochester, MN, USA) as described previously [42, 153]. Immunohistochemically stained sections were imaged on an Olympus BX41 microscope equipped with an Olympus XC30 CCD camera (Olympus, Shimjukum Tokio, Japan).

Radioiodide therapy studies

Therapy trials were started two weeks after intrasplenic injection, when mice showed low hepatic metastases load (<20%), which was determined by CEUS. To this end, animals were

injected i.v. with either LPEI-PEG-GE11/NIS followed by an i.p. application of 55.5 MBq ^{131}I or saline 48 h later or received saline only (LPEI-PEG-GE11/NIS + ^{131}I (n=9); LPEI-PEG-GE11/NIS + NaCl (n=9); NaCl + NaCl (n=9)). The cycle consisting of systemic NIS gene transfer followed by radioiodide was repeated for a total of three times on days 0/2, 3/5 and 7/9.

Hepatic colorectal metastases load was monitored by CEUS as described by Eichhorn *et al*. [154]. CEUS was performed on an Acuson Sequoia 512 (Siemens) in combination with a 15L8W ultrasound probe using the Cadence contrast pulse sequencing technology. Metastases were imaged in brightness-mode with a frequency of 14 MHz and a mechanical index of 0.2 or less. The contrast agent SonoVue (Bracco, Milano, Italy) was applied via a tail vein catheter. Hepatic contrast agent distribution and accumulation in normal liver tissue and metastases was recorded on digital cine clips before and up to 30 s after the application of the contrast agent at a frame rate of 8-10 Hz. Digital cine clips were exported in a Digital Imaging and Communications in Medicine (DICOM) format for off-line analysis with VueBox (Bracco Suisse, Geneve, Switzerland) using a bolus kinetic model as described previously [45]. In a blinded experimental set-up, hepatic metastases load was estimated by an experienced radiologist with more than 16 years' experience in CEUS measurement using high-end ultrasound devices. For estimation of perfusion and contrast agent uptake, region of interests were drawn around the entire liver of each animal. The contrast agent concentration was estimated using pre-defined calibration curves [154].

Two independent therapy trials were conducted. For the first trial, the follow-up CEUS measurements were performed on days 8 and 12 after therapy start, in the second therapy trial a single follow-up CEUS measurement was performed on day 5. For evaluation of sonographic parameters, only animals from the second therapy trial with CEUS measurement on day 5, where clips were analyzable due to hepatic in-flow of the contrast agent, were included in calculations to enable a parallel comparison of all three treatment groups (LPEI-PEG-GE11/NIS + ^{131}I (n=2); LPEI-PEG-GE11/NIS + NaCl (n=2); NaCl + NaCl (n=3)).

Indirect immunofluorescence assay

Immunofluorescence staining was performed on dissected frozen tumor tissues as described previously [46]. A rabbit polyclonal antibody against human Ki67 (Abcam, Cambridge, UK; dilution 1:1000) and a rat monoclonal antibody against mouse CD31 (BD Pharmingen, Heidelberg, Germany; dilution 1:200) were used. For detection, an anti-rabbit Alexa488-conjugated secondary antibody (Jackson ImmunoResearch, West Grove, Pennsylvania, USA) for Ki67 staining and an anti-rat Cy3-conjugated secondary antibody (Jackson ImmunoResearch) for CD31 staining were applied. Nuclei were counterstained with Hoechst

bisbenzimide (5 mg/ml) and sections were embedded in Fluorescent Mounting Medium (Dako, Hamburg, Germany). ImageJ software (NIH) was used for quantification of proliferation (Ki67-staining) and blood vessel density (CD31-staining) by analyzing 6 visual fields per metastatic liver section of every mouse.

Statistics

All *in vitro* experiments were carried out at least in triplicates. Results are expressed as mean ± SEM, mean fold change ± SEM and, for survival plots, in percent. Statistical significance was calculated by two-tailed Student's *t*-test. *P* values ≤0.05 were considered significant (Student's *t*-test: $*p \leq 0.05$; $**p \leq 0.01$; $***p \leq 0.001$). For therapy studies, in addition, Mann-Whitney *U* test was performed. *P* values ≤0.05 were considered significant (Mann-Whitney *U* test: $^{\#}p \leq 0.05$; $^{\#\#}p \leq 0.01$; $^{\#\#\#}p \leq 0.001$).

4.4 Results

NIS-mediated iodide uptake studies in vitro

To evaluate optimal transfection conditions for complexes of LPEI-PEG-GE11 and NIS pDNA (LPEI-PEG-GE11/NIS polyplexes) in human CRC cells LS174T, which showed EGFR expression as determined by FACS analysis (Fig 1A), radioiodide uptake activity was evaluated 24 h after polyplex application. To obtain highest transfection rate with lowest impact on cell viability, a nitrogen/phosphate (N/P) ratio of 6 was chosen for all subsequent experiments. At 24 h after transfection with EGFR-targeted LPEI-PEG-GE11/NIS polyplexes, cells demonstrated a significantly higher uptake of ^{125}I in comparison to cells that were incubated with LPEI-PEG-Cys/NIS, where the targeting ligand was replaced by cysteine. Additional pretreatment of cells transfected with LPEI-PEG-GE11/NIS with the NIS-specific inhibitor perchlorate resulted in decreased uptake levels, comparable to the background levels measured after transfection with empty polymer in HBG buffer (LPEI-PEG-GE11/HBG) (Fig. 1B). No effects on cell viability after transfections were detected (Fig. 1C).

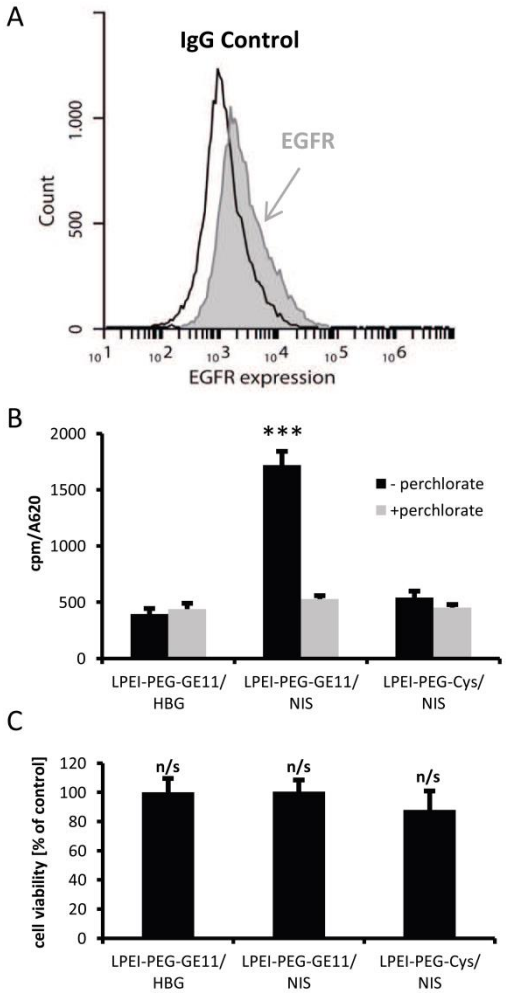

Fig. 1: *Incubation of EGFR expressing (**A**) LS174T cells with polyplexes at an N/P ratio of 6 resulted in high transduction efficiency and EGFR-specificity of NIS-encoding LPEI-PEG-GE11/NIS (n=4) polyplexes compared to polyplexes without ligand (LPEI-PEG-Cys/NIS; n=4) and empty polymers (LPEI-PEG-GE11/HBG; n=4) (**B**). Pre-treatment with the NIS-specific inhibitor perchlorate resulted in reduced iodide uptake confirming NIS-specificity. Cell viability was not affected by polyplex-mediated NIS gene transfer (**C**) (*p≤0.05; **p≤0.01; *** p≤0.001; n/s = not significant). Results are reported as mean ± SEM. Adapted from [155].*

^{18}F-TFB PET imaging after EGFR-targeted NIS gene delivery

Once animals had developed hepatic colon cancer metastases (Fig. 2A,B), tumor sections were dissected and investigated for EGFR-expression. High EGFR expression levels were detected in metastatic areas by immunohistochemical staining, whereas in normal liver tissue only low EGFR expression was observed (Fig. 2C). Based on these results, animals with hepatic metastases received EGFR-targeted polyplexes LPEI-PEG-GE11/NIS or control polyplexes LPEI-PEG-Cys/NIS and functional NIS expression was imaged by 3-dimensional high resolution small animal PET 48 h after polyplex injection. High accumulation of the NIS PET tracer ^{18}F-TFB was detected in metastases of animals that received LPEI-PEG-GE11/NIS polyplexes (Fig. 2D). Serial scanning revealed an accumulated dose of 4.8±0.6 % of initial dose (ID) (Fig. 2G). Non-targeted gene delivery via LPEI-PEG-Cys polymers resulted in a significantly reduced tumoral tracer uptake of 2.2±0.6 % of ID (Fig. 2E,G). ^{18}F-TFB uptake was also observed in physiologically NIS-expressing tissue (thyroid, mammary glands, salivary glands and stomach), as well as in the urinary bladder that is responsible for radionuclide elimination (Fig. 2D,E). To verify that the tracer uptake in metastases was indeed NIS-mediated, LPEI-PEG-GE11/NIS-injected mice were additionally treated with the competitive NIS inhibitor perchlorate 30 min before tracer administration (Fig. 2F). In these animals, NIS-mediated tracer accumulation was blocked in metastases and in tissues that exhibit endogenous NIS expression.

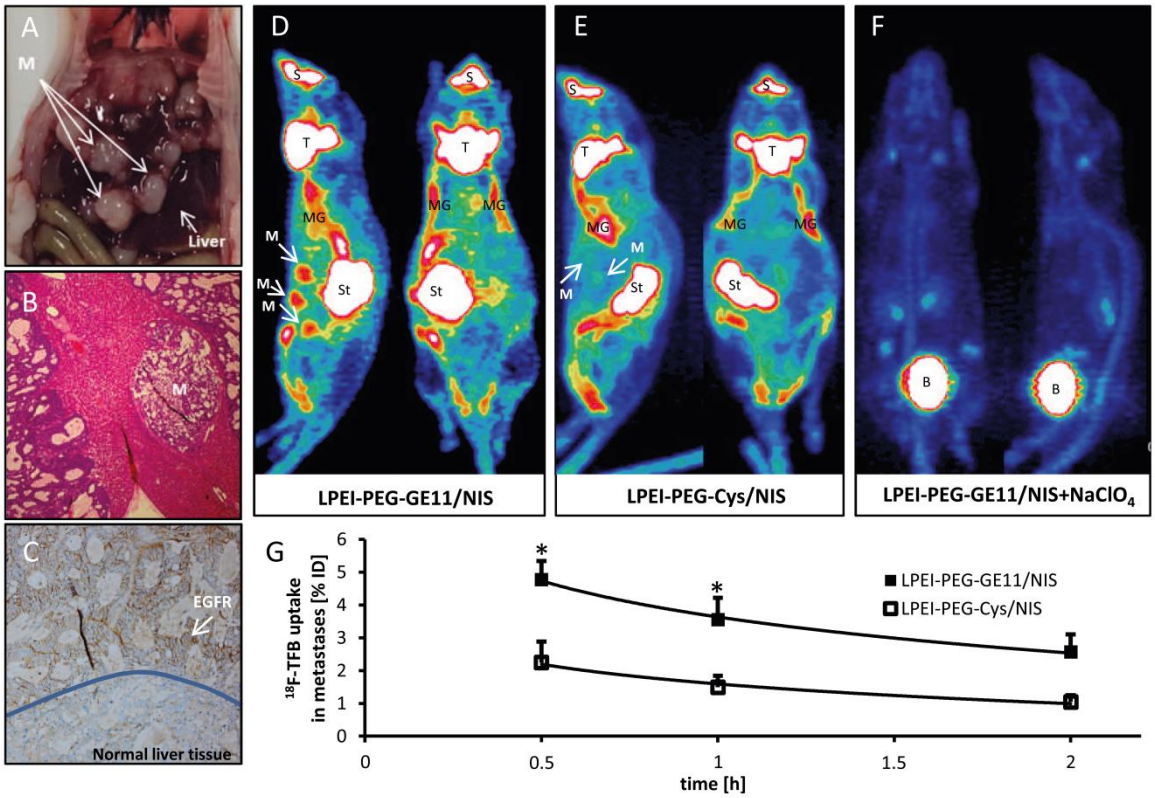

Fig. 2: *Hepatic colon cancer metastases (**A, B**) showed high EGFR expression (**C**) in contrast to normal liver tissue. Significant tumor-specific accumulation of the NIS PET tracer ^{18}F-TFB was detected in metastases of animals that received LPEI-PEG-GE11/NIS (**D**; n=5) in contrast to mice injected with control vectors (**E**; n=3). To verify NIS-mediated tracer uptake, LPEI-PEG-GE11/NIS-injected mice received the competitive NIS inhibitor perchlorate 30 min before tracer administration (**F**; n=2), which blocked NIS-mediated tracer accumulation in metastases and tissues that exhibit endogenous NIS expression. Serial scanning revealed an accumulated dose of 4.8±0.6% of injected dose (**G**) (*p≤0.05). Results are reported as mean ± SEM. (M=metastases; S=nasal secretion; T=thyroid; MG=mammary gland; St=stomach; B=bladder). Adapted from [155].*

Ex vivo analysis of NIS expression in CRC metastases

To determine NIS mRNA expression in liver metastases by qPCR, mice were sacrificed 48 h after polyplex administration and tumors dissected. High NIS mRNA expression was detected in metastatic areas in mice injected with LPEI-PEG-GE11/NIS as compared to untreated tumors. In addition, low NIS mRNA expression levels were observed in tumors of mice treated with the control vector LPEI-PEG-Cys/NIS (Fig. 3A).

For further evaluation of NIS protein expression, tumor sections were stained with a human NIS-specific antibody. Immunohistochemical staining revealed areas of NIS-specific immunoreactivity in metastatic tissue of LPEI-PEG-GE11/NIS-treated mice, whereas surrounding normal liver and tumors from mice treated with the control vector LPEI-PEG-Cys/NIS showed no NIS-specific immunoreactivity (Fig. 3B).

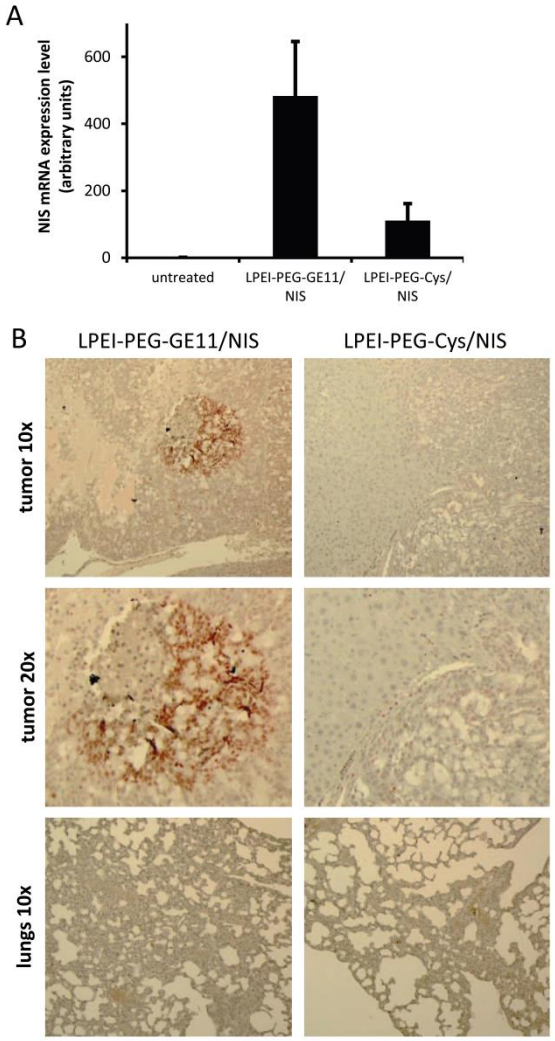

Fig. 3: *qPCR revealed high NIS mRNA expression in metastatic areas of mice injected with LPEI-PEG-GE11/NIS (n=5) compared to untreated tumors (n=2) and low NIS mRNA expression levels were observed in tumors of mice that were treated with the control vector LPEI-PEG-Cys/NIS (n=3) (**A**). Results are reported as mean ± SEM. Immunohistochemical staining confirmed NIS expression specifically in metastatic tissue of LPEI-PEG-GE11/NIS treated mice. NIS-specific immunostaining was visible only in metastatic tissue and occurred in clusters. No NIS expressing cells were found in normal liver tissue (**B**). Adapted from [155].*

NIS-mediated ^{131}I therapy

Metastases-bearing mice were treated with three cycles of either LPEI-PEG-GE11/NIS followed by ^{131}I (therapy group) or saline 48 h later or received saline only. Mice in the therapy group showed a significant reduction of tumor growth reflected in hepatic metastases load as determined by contrast-enhanced ultrasound (CEUS), while aggressive tumor growth was observed in both control groups (Fig. 4A). The reduced tumor growth in the therapy group resulted in an enhanced survival of these animals of up to 15 days post therapy start in contrast to control animals, that died within 8 days (NaCl/NaCl group) or 13 days (LPEI-PEG-GE11/NaCl group) (Fig. 4B).

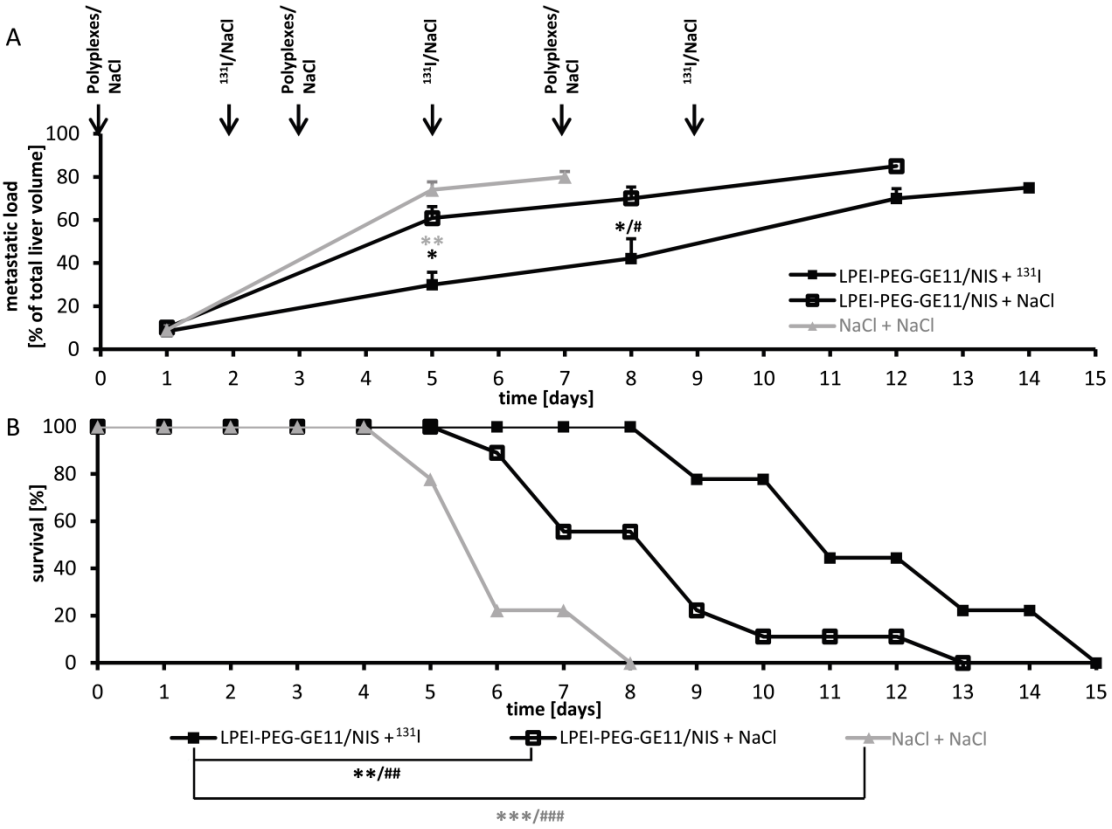

Fig. 4: *Metastases-bearing mice were treated with three cycles of either LPEI-PEG-GE11/NIS followed by ^{131}I (n=9) or saline (n=9) 48 h later or received saline only (n=9). Hepatic tumor load (**A**) and animal survival (Kaplan-Meier-Plot) (**B**) of the three different treatment groups were compared (Student's t-test: *p≤0.05; **p≤0.01; ***p≤0.001; Mann-Whitney U test: $^{\#}$p≤0.05; $^{\#\#}$p≤0.01; $^{\#\#\#}$p≤0.001). Results are either reported as mean ± SEM for tumor volumes or in percent for survival plots. Adapted from [155].*

For sonographic measurements 100 µl of the contrast agent SonoVue, which consists of gas-filled microbubbles (diameter 2.5 µm), was intravenously applied. CEUS images showing the entire liver on day 5 after therapy start revealed a more homogenous uptake of contrast agent with only small areas with lower contrast agent uptake that represent metastases in animals that received LPEI-PEG-GE11/NIS + ^{131}I (Fig. 5A). In comparison both control groups, which exhibit higher hepatic metastases load with highly hypovascularized central areas, showed severely inhomogeneous contrast agent uptake (Fig. 5B,C). To determine perfusion of disseminated liver metastases, echo signals were calculated by including the perfusion of the entire liver. A typical distribution of contrast agent in the LPEI-PEG-GE11/NIS + ^{131}I group was detected, which showed a maximum peak of liver uptake 10 s after injection, followed by a quick tail off due to elimination. In the control groups no peak was observed. Regions of interest (ROI) were drawn around the entire liver to calculate and compare perfusion in the different treatment groups. While therapy animals that received LPEI-PEG-GE11/NIS + ^{131}I revealed an increased overall signal, decreased amount of contrast agent uptake in the liver of control animals was detected (Fig. 5D).

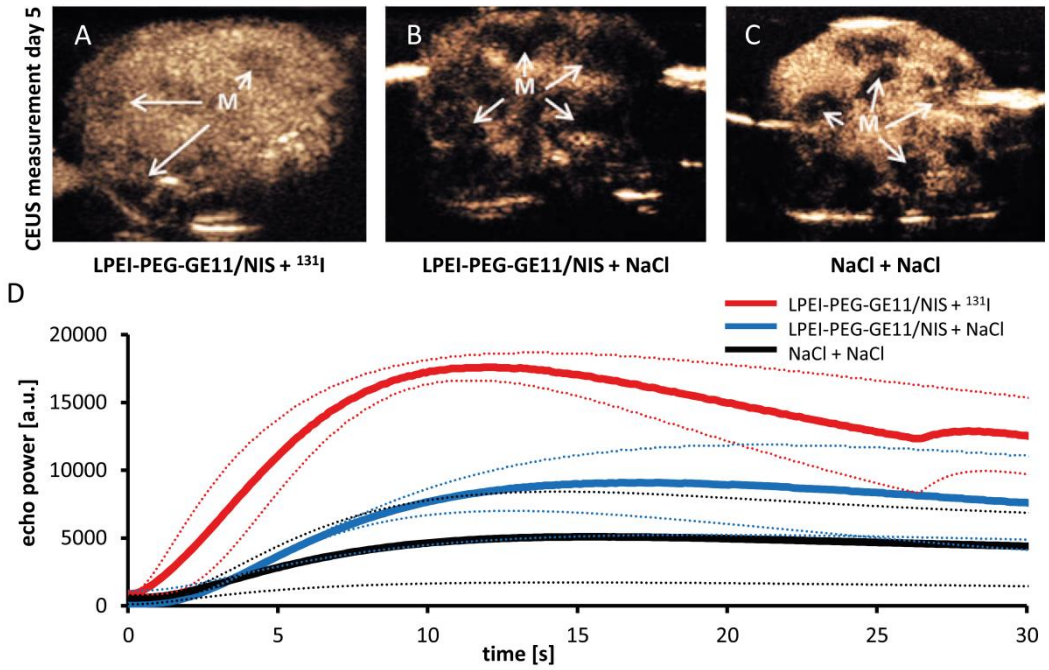

Fig. 5: *CEUS imaging of the entire liver on day 5 after therapy start revealed strong differences in contrast agent uptake and perfusion between therapy (**A;** LPEI-PEG-GE11/NIS + ^{131}I) and control groups (**B;** LPEI-PEG-GE11/NIS + NaCl and **C;** NaCl + NaCl). Due to hypovascularization of metastases and necrotic areas metastases (M) appear dark. Animals treated with ^{131}I showed an overall enhanced contrast agent signal and a higher maximum uptake (**D**), in comparison to both control groups, which exhibited higher hepatic metastases load, reduced amount of healthy hepatic tissue and thus overall decreased perfusion levels. Adapted from [155].*

Immunofluorescence staining for tumor cell proliferation and blood vessel density

Metastatic liver tissue of mice after therapy was examined for cell proliferation with a Ki67-specific antibody (green) and for blood vessel density with a CD31-specific antibody (red) (Fig. 6A-C). Ki67 and CD31 staining in metastatic tissue differs from staining of normal liver tissue (Fig. 6D). Metastatic tissue of LPEI-PEG-GE11/NIS-treated mice that received ^{131}I showed significantly decreased proliferation and lower blood vessel density as compared to control groups (Fig.6 E,F).

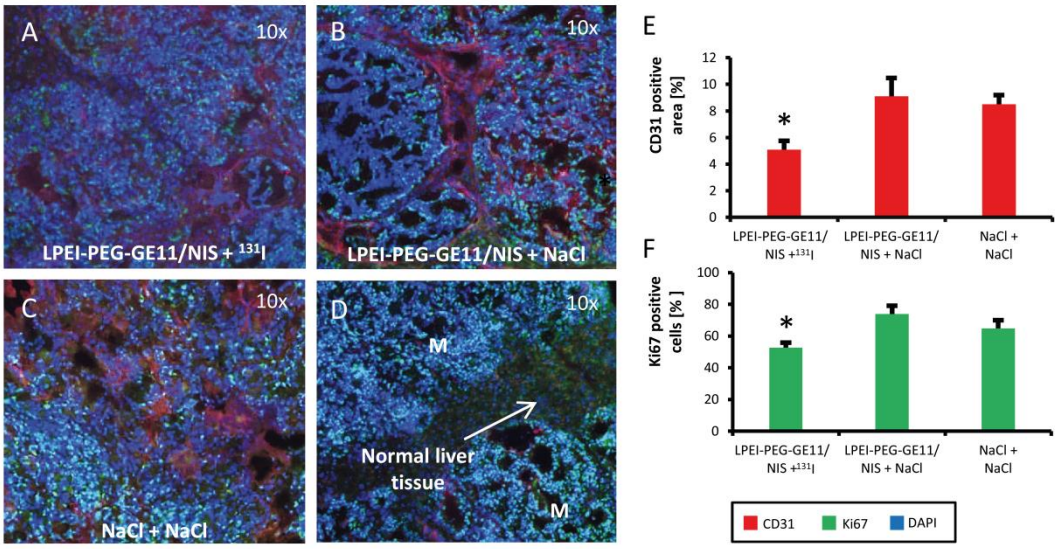

Fig. 6: *Frozen metastatic tissue sections of the three different treatment groups exhibited reduced cell proliferation (green; Ki67) and blood vessel density (red; CD31) in animals treated with LPEI-PEG-GE11/NIS + ^{131}I (**A**) (n=9) compared to control groups that received LPEI-PEG-GE11/NIS + NaCl (**B**) (n=9) or NaCl + NaCl (**C**) (n=9). Differences in Ki67 and CD31 staining between metastatic tissue and normal liver tissue can be seen in (**D**). Higher cell proliferation and increased pattern of vascularization of tissue surrounding metastases along with low vascularization inside metastases was found in both control groups (**E, F**). Results are reported as mean ± SEM. Adapted from [155].*

4.5 Discussion

In the emerging field of theranostics, which combine the capacities to function as imaging tool as well as a therapeutic agent, NIS has been evaluated as promising and beneficial target for cancer gene therapy. Due to its iodide concentration ability, NIS expression in nonthyroidal tumor cells induced by targeted gene transfer enables noninvasive tumor monitoring and exact localization of the tumorous tissue by various imaging modalities (y-camera, PET, SPECT) and tracers (^{123}I, ^{188}Re, ^{124}I, ^{18}F-TFB, ^{18}F-SO_4) before therapeutic radionuclide application (^{131}I, ^{188}Re, ^{211}At). The dual mechanism of NIS has been investigated in several nonthyroidal tumor models [35-51] and the concept of NIS gene therapy is currently under clinical evaluation for local treatment of prostate cancer after intratumoral application of adenoviral NIS gene carriers (NCT00788307, NCT01846091, NCT02068794) [49, 131]. Based on these results, the powerful image-based cytoreductive NIS gene therapy approach may also represent a promising cancer treatment strategy even for metastatic disease.

However, a worthwhile evaluation of novel therapeutics for clinical use against metastases remains challenging. Thus, tumor models that give a detailed reflection of the natural processes in tumorigenesis, invasion and angiogenesis are highly important, especially for metastases formation, which is defined by a multi-step process. This process involves cell migration of tumor cells via blood vessels and lymphatic vessels to distant sites followed by generation of one or more micro-metastases that transform to macroscopic metastases with a unique microenvironment that is formed of the tumor cells themselves, tumor stroma and tumor-associated cells [3].

With respect to the high incidence of CRC as third most common cancer worldwide [146], which lacks new therapeutic options with clinical benefits, improved response and survival, especially for metastatic CRC where only a low percentage of patients are eligible for surgery, we established an *in vivo* metastases colon cancer model to investigate the NIS gene therapy concept as a new treatment option for CRC metastases. The CRC cell line LS174T, which was well characterized *in vitro* and showed promising results after NIS gene transfections, was injected directly into the mouse spleen, which results in tumor cell migration via the splenic vein and portal vein to the liver with cell invasion into the liver followed by formation of small metastases. After three days a splenectomy was performed to eradicate interference from a primary tumor in the spleen. With about 90% of mice developing liver metastases, this model is highly reproducible and metastases in other tissues, e.g. in the lungs were not observed.

To obtain effective NIS gene expression specifically in metastases, potent carrier systems are required. Various vector systems for systemic NIS gene transport have been

investigated, including mesenchymal stem cells, viral and nonviral vehicles [35-46]. Nonviral vectors as part of the nanotechnology field showed promising features for a targeted delivery to tumor tissue due to the variable design strategies, which allow adjustment on efficacy, biocompatibility and safety conditions [119]. Since the epidermal growth factor receptor (EGFR) is overexpressed in a high range of CRC tumors [156, 157], it represents an auspicious target for tumor-specific NIS gene delivery via actively targeted nanoparticle transfer. Based on promising earlier *in vivo* results [39, 151], for NIS gene transfer to metastatic CRC tissue, LPEI-PEG-based polymers coupled to the EGFR-specific ligand GE11 were applied. LPEI as nonviral gene shuttle vector demonstrates high DNA binding capacity along with high transduction efficiency *in vitro* and *in vivo* and has already been evaluated in human clinical studies (NCT00712530) [158]. The additional PEG-shielding domain enables higher colloidal stability after systemic application and allows a safer *in vivo* application by reducing interactions with serum proteins and aggregation.

In vitro transfection studies in CRC LS174T cells using EGFR-targeted LPEI-PEG-GE11/NIS polyplexes resulted in significant perchlorate-sensitive ^{125}I accumulation, whereas transfections with untargeted polyplexes showed only low iodide uptake over background levels. These results confirm the advantage of EGFR-targeting compared to the Cys control that lacks a specific cell-binding structure. This has already been demonstrated in former studies using various high EGFR expressing cell lines such as HuH7 liver cancer cells and SKOV-3 ovarian carcinoma cells [39]. Perchlorate sensitivity of LPEI-PEG-GE11/NIS transfected cells confirmed NIS-mediated uptake.

Liver sections with metastases derived from intrasplenic injection of LS174T cells where stained for EGFR. High expression levels could be detected in the metastatic tissue providing the basis for EGFR-targeted NIS gene transfer *in vivo*. To be able to see NIS expression in single metastases and thereby confirming the suitability of our EGFR-targeted vectors for NIS gene delivery, we applied the novel NIS PET tracer ^{18}F-TFB. Due to the small size of metastases with a diameter of around 1-5 mm, a precise evaluation for exact quantitative calculations of radionuclide uptake was required. Compared to the drawbacks of ^{124}I as tracer with its long half-life, low positron yield, high positron energy, high energy gamma emission, limited availability and complex and expensive production, the new NIS PET tracer ^{18}F-TFB promises a higher resolution and more differentiated images [96]. TFB was identified to be a substrate for NIS and by coupling ^{18}F to TFB an ideal PET tracer with a short half-life and higher resolution images was developed [96]. Once mice had developed metastases, 2-3 weeks after tumor cell injection, animals were injected with LPEI-PEG-GE11/NIS or LPEI-PEG-Cys/NIS at a N/P ratio of 6. At 48 h after polyplex administration, mice received an intraperitoneal dose of 10 MBq ^{18}F-TFB. To demonstrate that tracer uptake was indeed NIS dependent, a subgroup of the LPEI-PEG-GE11/NIS mice was injected with

the NIS specific inhibitor perchlorate 30 min prior to ^{18}F-TFB application. Whereas metastases could nicely be detected in the LPEI-PEG-GE11/NIS group due to strong NIS-mediated ^{18}F-TFB accumulation, only weak radionuclide uptake was detected in metastases of the control group.

After this first series of encouraging animal imaging experiments, which confirmed high NIS expression in single metastases, the therapeutic efficacy of this approach was investigated. Animals received three cycles of polyplexes followed by ^{131}I or saline application 48 h later or received saline only. Hepatic metastases load was monitored by conventional sonography and CEUS performed by an experienced radiologist in a blinded, randomized trial. Significantly reduced hepatic metastases load was detected in the LPEI-PEG-GE11/NIS group that received ^{131}I, which was associated with prolonged survival, compared to both control groups.

For a detailed evaluation of the therapeutic effect, contrast agent distribution and liver perfusion were determined. As a consequence of the strong dissemination of small metastases pervading the entire liver, the evaluation of single metastasis was not feasible. Consequently, regions of interest (ROI) were drawn around the entire liver to calculate and compare perfusion in the different treatment groups.

For sonographic measurements 100 µl of the contrast agent SonoVue, which consists of gas-filled microbubbles (diameter 2.5 µm), was intravenously applied. The process of contrast agent distribution in the liver consists of two dynamic phases. First, the arterial phase, which starts a few seconds after injection of the contrast agent, followed by the portal phase, where an overall enhancement of perfusion of normal liver tissue takes place [159]. The typical distribution of contrast agent results in a maximum peak of liver uptake and is followed by a quick elimination by respiration and elimination by the liver [160]. The majority of liver metastases derived from colorectal cancer is hypovascularized and shows contrast agent accumulation only at the periphery of the lesion [159, 161]. This pattern of increased vascularization of the tissue surrounding metastases along with low vascularization inside metastases could be confirmed by immunofluorescence analysis of vascularization (CD31-staining). Moreover, the extensive spread of the LS174T derived metastases in control mice lead to highly necrotic areas in the center of metastases, further diminishing vascularization inside metastases [162, 163].

Due to this hypovascularization of metastases together with a lower fractional vascular volume of metastases compared to normal liver tissue, absence of portal supply and a greater extent of necrotic areas, metastases generally appear dark [161, 164]. Hence, the livers of therapy animals that were injected with LPEI-PEG-GE11/NIS + ^{131}I, where a reduced hepatic metastases load was detected, exhibit a more homogenous contrast agent uptake with only small areas that appear dark and represent metastases. In contrast, both control

groups showed strongly inhomogeneous agent distribution and a high extent of metastases pervading the livers. Owing to the higher hepatic metastases load and thus reduced amount of healthy hepatic tissue where contrast agent uptake and perfusion can be detected, this resulted in overall decreased perfusion levels of control animals.

As hypovascularization often constitutes a major drawback for efficient delivery, in this study an active EGFR targeting approach was used. Hereby, gene delivery is not only dependent on the enhanced permeability and retention effect (EPR), where hypervascularization is an essential prerequisite for effective accumulation of vectors at the target site [165]. Efficacy of the active EGFR targeting strategy was proven by imaging and therapy studies. Further, different sizes of polyplexes and contrast agent particles may affect liver distribution. Sizes of polyplexes were detected to have an average size of around 100 nm, whereas particles of the contrast agent are specified to be at 2.5 µm. Thus, polyplexes are able to reach even small blood vessels.

In addition, the bystander effect that is associated with radioiodide therapy supports an effective treatment of non-transfected tumor cells in the surrounding tumor tissue due to the crossfire effect of the beta-emitter ^{131}I of up to 2.4 mm. Hence, areas with diminished blood vessel density benefit from this bystander effect and can be efficiently destroyed even though they do not exhibit sufficient vascularization.

In conclusion, our data clearly demonstrate the potential of LPEI-PEG-GE11 carrier systems to target the NIS gene to hepatic CRC liver metastases. NIS as reporter gene allows for quantification of the extent of gene expression and quantitative analysis of tracer uptake. In its function as therapeutic gene, after applying the therapeutic tracer ^{131}I, NIS-mediated ^{131}I accumulation induces decelerated metastatic tumor growth with prolonged animal survival. The established metastases model is a valuable tool to reflect the clinical situation on a morphological and molecular level and serves as an ideal advanced tumor model to investigate our EGFR-targeted NIS-mediated gene therapy approach.

4.6 Acknowledgments

We are grateful to Sissy M Jhiang (Ohio State University, Columbus, OH, USA) for supplying the full length human NIS cDNA. We thank Barbara Ungern-Sternberg, Rosel Oos, Karin Bormann-Giglmaier (Department of Nuclear Medicine, Ludwig-Maximilians-University, Munich, Germany) and Jessica Schuster (Department of Radiotherapy and Radiation Oncology, Laboratory for Experimental Radiology, Ludwig-Maximilians-University, Munich, Germany) for their assistance with animal care and imaging studies. We thank Doris Mayr (Department of Pathology, University Hospital of Munich, LMU Munich, Germany) for performing EGFR-staining.

This work was supported by grants from the Deutsche Forschungsgemeinschaft within the Collaborative Research Center SFB824 (project C 08) to C Spitzweg as well as within the Priority Programme SPP1629 to C Spitzweg and PJ Nelson (SP 581/6-1, SP581/6-2, NE 648/5-2), the Cluster of Excellence Nanosystems Initiative Munich (NIM) to E Wagner and by a grant from the Wilhelm-Sander-Stiftung to C Spitzweg (2014.129.1).

5. Dual-targeting strategy for improved nonviral gene transfer of the theranostic sodium iodide symporter

This chapter has been adapted from the submitted manuscript:

Urnauer S[1], Schmohl KA[1], Tutter M[1], Schug C[1], Schwenk N[1], Morys S[2], Ziegler S[3], Bartenstein P[3], Clevert DA[4], Wagner E[2], Spitzweg C[1]. Dual-targeting strategy for improved nonviral gene transfer of the theranostic sodium iodide symporter. [submitted mansucript]

[1]Department of Internal Medicine IV, University Hospital of Munich, LMU Munich, Germany, [2]Department of Pharmacy, Center of Drug Research, Pharmaceutical Biotechnology, LMU Munich, Germany, [3]Department of Nuclear Medicine, University Hospital of Munich, LMU Munich, Germany, [4]Department of Clinical Radiology, University Hospital of Munich, LMU Munich, Germany

5.1 Abstract

Purpose: Tumor heterogeneity poses a major problem in cancer therapy, not only between patients, but even between primary tumor and metastases and within the tumor itself. To address the variability of tumor characteristics and improve gene delivery for therapy of hepatocellular cancer (HCC), a dual-targeting approach was performed.

Experimental Design: For tumor-targeted gene delivery, synthetic LPEI-PEG_{2kDa}-based polymer backbones were coupled to tumor-specific peptide ligands GE11 for EGFR-targeting or cMBP for cMET-targeting and mixed at equal amounts (1:1) before complexing with pDNA. The dual-targeting approach was used to deliver the sodium iodide symporter (NIS) gene to orthotopic HCC xenografts. NIS as well characterized theranostic gene allows diagnostic analysis of functional NIS gene expression by noninvasive imaging and effective anticancer radioiodide therapy.

Results: Enhanced tumor specificity and transduction efficiency of dual-targeted polyplexes in comparison to single-targeted polyplexes were demonstrated *in vitro* using tumor cell lines with different EGFR and cMET expression levels. Taking advantage of the reporter function of NIS *in vivo*, ^{124}I-PET-imaging of mice bearing orthotopic HCC xenografts revealed higher levels of tumor-specific NIS-mediated radionuclide uptake after dual-targeting. Evaluating the therapeutic efficacy of this bispecific concept, mice received 3 cycles of dual-targeted polyplexes followed by ^{131}I or saline 48h later. Significantly reduced tumor growth and perfusion in ^{131}I-treated animals was detected along with prolonged survival.

Conclusions: The dual-targeting approach resulted in higher tumor-specific radioiodide accumulation and significant therapeutic efficacy in an advanced orthotopic HCC model. This bifunctional strategy enhances the applicability of the NIS gene therapy concept in heterogeneic tumors.

5.2 Translational relevance

Tumor heterogeneity, within and between tumors, may have severe implications for tumor therapy, especially for targeted gene therapy, where single-targeted approaches often result in limited efficacy and therapy resistance. Polymer-formulated nonviral vectors provide a potent delivery platform for cancer therapy. To improve applicability of polymers for future clinical use in a broad range of patients and cancer types, tumor heterogeneity is a crucial aspect that has to be taken into account. The current study evaluates the beneficial effect of simultaneously targeting EGFR and cMET for nonviral gene delivery of the theranostic sodium iodide symporter (NIS). Imaging studies based on the reporter function of NIS and therapeutic application of radioiodide provided evidence for enhanced tumor-specific gene delivery after dual-targeting. This highlights the benefits of a bifunctional strategy with improved efficacy for a future clinical translation allowing efficient targeting of heterogeneic tumors with variable receptor expression levels.

5.3 Introduction

Hepatocellular cancer (HCC), one of the most common cancers worldwide, is characterized by high mortality and resistance to conventional chemo- and radiotherapies [98]. The limited success of available treatment options is attributed to the complex prooncogenic microenvironment of chronic liver diseases that often proceed the development of HCC, as well as the high level of tumor heterogeneity [166, 167]. Tumor heterogeneity not only occurs between patients, but even between primary tumor and metastases and within the tumor itself and represents a major hurdle for the development of effective therapy strategies for HCC patients [166]. Against this background, even individualized and molecularly targeted therapy strategies as promising novel approaches for HCC treatment have to be designed in a way that takes heterogenous tumor characteristics into account.

Nonviral delivery vectors have been confirmed as potent agents for the delivery of genes specifically to tumor cells for cancer gene therapy. High precision synthesis allows the design of multifunctional systems for effective tumor cell targeting [168]. Functional groups for nucleic acid binding, as well as endosomal buffering can be complemented by a shielding domain that improves *in vivo* biocompatibility and lateral stabilization by crosslinking of polyplexes [119, 169]. Most importantly for specific tumor targeting, incorporation of active targeting ligands provides the mechanistic rationale to enhance tumor-specific binding, cellular uptake and transfection efficiency. Various ligands that bind receptors that are highly expressed in a wide range of tumors, including epidermal growth factor receptor (EGFR), cMET/hepatocyte growth factor receptor (HGFR), transferrin receptor, integrin receptors and folate receptor, have served as promising candidates for molecularly targeted cancer gene therapy [39, 68, 69, 88, 123, 126, 151, 169]. Nevertheless, efficacy of nanoparticle-based carriers often varies after translation from *in vitro* conditions to *in vivo* models and between different tumor models [170], which is most likely attributable to tumor heterogeneity.

One promising strategy to minimize the effect of tumor heterogeneity and resistance to cancer therapies in the clinical setting is the combination of different therapeutics that either show different pharmacological modes of action or have different targets [171]. In the present study, a dual receptor targeting strategy for a single nanotherapeutic using LPEI-PEG_{2kDa}-based nonviral vectors for delivery of the potent theranostic sodium iodide symporter (NIS) gene was developed. To reduce the impact of variable receptor expression levels due to inter- and intratumoral heterogeneity, GE11 and cMBP were chosen as ligands for EGFR- and cMET-targeting, respectively. Both ligands proved to be highly specific and effective in single-targeting experiments [39, 46, 68, 69, 123, 151]. By simultaneously targeting both receptors, the postulated crosstalk between cMET/HGFR and EGFR [172] and enhanced

particle uptake by receptor crosslinking that mimics biphasic uptake of viral vectors by binding to two different receptor types, can be exploited to increase efficacy [84-86].

Since its cloning in 1996 [30], NIS has proven its function as potent theranostic gene and is already being investigated clinically in cancer patients [30, 47, 49, 94, 129, 131, 173, 174]. The transduction efficiency *in vitro* and *in vivo* can be monitored by taking advantage of the reporter function of NIS that allows determination of radionuclide uptake in transfected cells. This enables exact localization of tumorous tissue by noninvasive bioimaging as well as quantification of trapped radionuclides (^{125}I, ^{123}I, ^{124}I, ^{18}F-TFB). At the same time, NIS provides the possibility for an effective treatment strategy by application of ^{131}I, ^{188}Re and ^{211}At [41, 175].

In the current study, nonviral NIS gene transfer was investigated *in vitro* in different tumor cell lines by comparison of the dual-targeting strategy to single-targeting of EGFR or cMET. Based on these results, the efficacy of polyplexes for dual-targeting and single-targeting was further examined in an orthotopic *in vivo* model of HCC using the reporter function of NIS for noninvasive positron emission tomography (PET) imaging followed by evaluation of the therapeutic efficacy of the dual-targeting approach.

This novel approach utilizes two bifunctional strategies: (1) simultaneous targeting of two receptors to improve efficacy and reduce effects of variable receptor expression levels in heterogeneic tumors and (2) using the dual function of NIS for monitoring of the efficiency of gene delivery by noninvasive imaging of tumoral NIS expression as well as effectiveness of therapeutic intervention after application of ^{131}I for cancer treatment.

5.4 Materials and methods

Plasmid and polymer synthesis and polyplex formation

Polymers with LPEI-PEG_{2kDa}-backbone were synthesized by coupling heterobifunctional (poly)ethylene glycol (NHS-PEG-OPSS, 2 kDa, Rapp Polymere GmbH, Tübingen, Germany) to amine groups of linear polyethylene imine (LPEI) via N-hydroxy succiniminyl ester followed by a cation exchange chromatography purification step as described previously [39, 126]. Specific targeting was achieved by coupling peptide ligands to the polymer backbone. GE11 was used for EGFR-targeting (LPEI-PEG-GE11; peptide sequence: YHWYGYTPQNVI) and cMBP was applied for cMET-targeting (LPEI-PEG-cMBP; peptide sequence: KSLSRHDHIHHH). The conjugates were stored at -80°C as 1-5 mg/ml stock solutions until further use. Polyplexes were formed by complexing polymer with codon-optimized human NIS plasmid DNA [46, 126]. Polymers and cDNA, diluted in the same volumes of HEPES (2-[4-(2-hydroxyethyl)piperazin-1-yl]ethanesulfonic acid)-buffered glucose (HBG: 20 mmol/l HEPES, 5% (w/v) glucose at pH 7.4) at a nitrogen/phosphate (N/P) ratio of 6 (w/w), were mixed and incubated at room temperature for 20 min prior to use [124].

For single-targeted polyplex solutions, 100% of polymer was added, for dual-targeted polyplexes a 1:1 mixture of cMET-targeted and EGFR-targeted polymers was prepared (total N/P=6) before adding to DNA and then complexed with pDNA. For *in vitro* studies the DNA concentration for polyplex formation was 2 µg/ml, for *in vivo* studies 200 µg/ml.

Particle size measurements

Particle sizes of single-targeted and dual-targeted polyplexes were determined by transmission emission microscopy (TEM; JEM 1011, Jeol, Freising, Germany). Samples were prepared with 1 µg DNA in a total volume of 100 µl. The formvar/carbon coated 300 mesh copper grids (Ted Pella Inc., Redding, USA) were activated by mild plasma cleaning. Subsequently, the grids were incubated for 1 min with 20 µl of the polyplex solution. Excess liquid was blotted off using filter paper until the grid was almost dry. Then, the grids were washed with 5 µl of staining solution for 5 s and incubated for 20 s with 5 µl of a 2% aqueous uranyl formate solution. Excess liquid was blotted off using filter paper, followed by air-drying for 30 min. TEM was performed at 80 kV.

Cell culture

The HCC cell line HuH7 (JCRB0403; Japanese Collection of Research Bioresources Cell Bank, Osaka, Japan) was cultured in Dulbecco's modified eagle medium (DMEM; 1 g/l glucose; Sigma-Aldrich, St.Louis, Missouri, USA). The breast cancer cell line MCF-7 (American Type Culture Collection, Manassas, Virginia, USA) was cultured in Dulbecco's

modified eagle medium (DMEM; 4 g/l glucose; Sigma-Aldrich). The human follicular thyroid carcinoma cell line FTC-133 (Sigma-Aldrich) was cultured in DMEM/F12 (Sigma-Aldrich). All media were supplemented with 10% (v/v) fetal bovine serum (FBS Superior, Biochrom/Merck Millipore, Berlin, Germany) and 1% (v/v) penicillin/streptomycin (Sigma-Aldrich).
Cells were maintained at 37°C and 5% CO_2 in an incubator with a relative humidity of 95%. Cell culture medium was replaced every second day and cells were passaged at 80% confluency.

EGFR and cMET receptor expression levels in vitro

0.8-1 × 10^6 cells were detached with trypsin/EDTA (Sigma-Aldrich), washed with phosphate buffered saline (PBS; Sigma-Aldrich) supplemented with 10% fetal bovine serum (FBS; Sigma-Aldrich) and incubated with an EGFR-specific antibody (1:200; monoclonal mouse IgG1, Dako, Glostrup, Denmark) or with an antibody that detects human cMET/HGFR (1:200; monoclonal mouse IgG1, R&D Systems, Minneapolis, Minnesota, USA) or with an IgG-anti-mouse antibody (1:200; BD Biosciences, Franklin Lakes, New Jersey, USA) as negative control for 1 h on ice. Then, cells were washed with PBS with 10% FBS and incubated with an AlexaFluor 488 labeled goat anti-mouse secondary antibody (1:400; Invitrogen, Langenselbold, Germany) for 1 h on ice. Cells were washed and resuspended in PBS with 10% FBS for analysis, which was performed on a BD Accuri C6 flow cytometer (BD Biosciences). Cells were gated by forward/sideward scatter and pulse width for exclusion of doublets. PI (propidium iodide; Sigma-Aldrich) was used for discrimination between viable and dead cells.

Cellular binding and internalization

Cells were seeded in 24-well plates at a density of 50 000 cells per well. After 24 h, cell culture medium was replaced with 400 µl fresh growth medium. Cells were transfected with polyplexes for single-targeting, i.e. LPEI-PEG-GE11/NIS or LPEI-PEG-cMBP/NIS (subsequently specified as EGFR-targeting or cMET-targeting respectively) or polyplexes formed with a 1:1 mixture of polymers for simultaneous cMET- and EGFR-targeting (subsequently labeled as dual-targeting). HBG served as control. For pDNA polyplexes (N/P=6) in 100 µl HBG 1 µg pDNA was used, where 20% of the nucleic acid was Cy5-labeled. To determine cellular association, polyplexes were added to cells and incubated for 30 min on ice. Afterwards, cells were washed twice with 500 µL PBS, detached with trypsin/EDTA and resuspended in PBS with 10% FBS.
For cell uptake experiments, cells were incubated for 30 min with polyplexes. Cells were then washed with 500 µl PBS/1000 I.U. heparin for 15 min on ice to remove polyplexes on the cell surface. Cells were then detached with trypsin/EDTA and taken up in PBS with 10% FBS.

Samples were examined on a BD Accuri C6 flow cytometer by determination of the excitation of Cy5 at 635 nm and detection of emission at 665 nm. Cells were gated by forward/sideward scatter and pulse width for exclusion of doublets. PI was used to discriminate between viable and dead cells.

Transfection studies

Cells were plated at a density of 2×10^5 cells per well in 6-well plates and incubated for 45 min with polyplexes for dual-targeting or single EGFR- or cMET-targeting. Transfection efficiency was determined by measurement of iodide uptake activity at steady-state conditions 24 h after transfection as described previously [47].

Cell viability assay

Cell viability 24 h after transfection was analyzed after incubation of cells with a commercially available MTT reagent (Sigma-Aldrich) for 2 h at 37°C followed by a washing step with PBS. The formazan product was measured after incubation with 10% DMSO (v/v) (dimethyl sulfoxide) in isopropanol at 620 nm in a Sunrise microplate absorbance reader (Tecan, Männedorf, Switzerland).

Establishment of orthotopic HuH7 xenografts

For orthotopic HCC xenografts in female CD-1 nu/nu mice (Charles River, Sulzfeld, Germany), 1×10^6 HuH7 cells resuspended in 50 µl were injected into the liver after laparotomy of 7-week old mice under full anesthesia. Animals were pre- and post-treated with Metacam (0.5 mg/kg). Mice were sacrificed when healthy liver tissue dropped below 30% as determined by sonography or animals showed any other symptoms of illness. Animals were maintained under specific pathogen-free conditions with access to mouse chow and water *ad libitum*. The experimental protocol was approved by the regional governmental commission for animals (Regierung von Oberbayern) and all animal experiments were carried out according to the guidelines of the German law of protection of animal life.

EGFR and cMET receptor expression levels in vivo

Receptor immunofluorescence staining was performed on dissected frozen tumor tissues. Tissues were fixed in 80% methanol for 5 min at 4 °C and acetone for 2 min at −20 °C. PBS was used for rehydration and sections were blocked with 12% bovine serum albumin/PBS for 30 min at room temperature. An EGFR-specific antibody (1:100; monoclonal mouse IgG, Dako) or a cMET-specific antibody (1:100; monoclonal mouse IgG1, R&D Systems) were used and sections were incubated for 1 h. Afterwards, sections were incubated with an anti-

mouse Alexa 488-conjugated secondary antibody (1:200; BD Pharmingen, Heidelberg, Germany). For nuclei counterstaining Hoechst bisbenzimide (1:1000; 5 mg/ml) was applied and sections were embedded in Fluorescent Mounting Medium (Dako). Stained sections were examined using an Axiovert 135 TV fluorescence microscope equipped with an AxioCam MRm CCD camera and AxioVision Rel. 4.8. software (Carl Zeiss, Munich, Germany).

PET imaging studies after systemic NIS gene transfer in vivo

Experiments started 5-6 weeks after intrahepatic injection of tumor cells. For determination of tumor specific NIS expression and subsequent NIS mediated iodide uptake, animals received LPEI-PEG-GE11/NIS polyplexes for EGFR-targeting (n=6), LPEI-PEG-cMBP/NIS for cMET-targeting (n=4) or both for dual-targeting (n=7). Polyplexes were administered systemically via the tail vein (intravenously, i.v.) at a DNA dose of 2.5 mg/kg (50 µg DNA in 250 µL HBG). At 48 h after polyplex injection mice received the NIS-specific PET tracer ^{124}I and accumulation in tumor tissue was determined by small-animal PET (Inveon, SIEMENS Preclinical Solutions, Erlangen, Germany). Serial scanning was performed after 1 h, 3 h and 5 h. Regions of interest were analyzed with the software Inveon Acquisition Workplace (Siemens), quantified using Inveon Research Workplace (Siemens) and expressed as a fraction of the total amount of initial dose (% of ID). To suppress thyroidal iodide uptake, a 10-day pretreatment with L-thyroxine (L-T4; 5 mg/ml; Sigma-Aldrich) in drinking water was conducted before PET-imaging. To verify NIS specific uptake, pretreatment with an intraperitoneal (i.p.) injection of 2 mg of the competitive NIS inhibitor sodium perchlorate ($NaClO_4$) 30 min before PET tracer administration (n=2) was performed.

Immunohistochemical analysis of NIS protein expression

Immunohistochemical NIS staining of paraffin embedded tumor tissue derived from hepatic tumor sections after NIS gene delivery was performed using a mouse monoclonal antibody directed against human NIS (1:1000; Merck Millipore) as described previously [42, 153]. Immunohistochemically stained sections were imaged on an Olympus BX41 microscope equipped with an Olympus XC30 CCD camera (Olympus, Shimjukum Tokio, Japan).

Radioiodide therapy studies

Three weeks after intrahepatic tumor cell injection, when mice have received a 10-day pretreatment with L-T4 in drinking water, therapy trials were started. Animals were randomly distributed to two groups. Animals received an i.v. injection of a solution of polplexes for dual-targeting followed by an i.p. application of 55.5 MBq ^{131}I (n=8) or saline (n=8) 48 h later. The

cycle consisting of systemic NIS gene transfer followed by radioiodide was repeated for a total of three times on days 0/2, 3/5 and 7/9.

Tumor growth was monitored by conventional sonography and tumor perfusion was determined by contrast-enhanced ultrasound (CEUS) after application of 100 µl of the contrast agent SonoVue® (Bracco, Switzerland) on an Acuson Sequoia 512 (Siemens) combined with a 15L8W ultrasound probe using the Cadence contrast pulse sequencing technology.

The experiment was performed in a blinded experimental setup and evaluated by an experienced radiologist. CEUS was performed as described previously [45] and the contrast agent concentration was estimated using pre-defined calibration curves [154].

Indirect immunofluorescence assay

Immunofluorescence staining of Ki67 and CD31 was performed on dissected frozen tumor tissues via as described previously [46]. For Ki67, a rabbit polyclonal antibody against human Ki67 (1:200; Abcam, Cambridge, UK;) and an anti-rabbit Alexa488-conjugated secondary antibody (1:400; Jackson ImmunoResearch, West Grove, Pennsylvania, USA) were used. For CD31, a rat monoclonal antibody against mouse CD31 (1:200; BD Pharmingen, Heidelberg, Germany) was used. For detection, an anti-rat Cy3-conjugated secondary antibody (1:400; Jackson ImmunoResearch) was applied. Hoechst bisbenzimide (1:1000; 5 mg/ml) was used for nuclei counterstaining and sections were embedded in Fluorescent Mounting Medium (Dako). ImageJ software (NIH, Bethesda, MD, USA) was used for quantification of proliferation (Ki67-staining) and blood vessel density (CD31-staining) by analyzing 6 visual fields per tumor section of every mouse.

Statistics

All in vitro experiments were carried out at least in triplicates. Results are expressed as mean ± SEM, mean fold change ± SEM and, for survival plots, in percent. Statistical significance was calculated by two-tailed Student's t-test. P values ≤0.05 were considered significant (*p≤0.05; **p≤0.01; ***p≤0.001).

5.5 Results

Particle sizes

To investigate whether different solutions of polyplexes result in unequal particle sizes, TEM measurements were performed. All three polyplex solutions for EGFR-targeting, cMET-targeting and dual-targeting were analyzed. No significant differences between the three solutions were observed and TEM measurements revealed two different particle subtypes: linear and round particles. Sizes of globular particles were determined to be approximately 50 nm and sizes of linear particles were analyzed to be 15-20 nm thin and up to 200 nm long (Fig. 1).

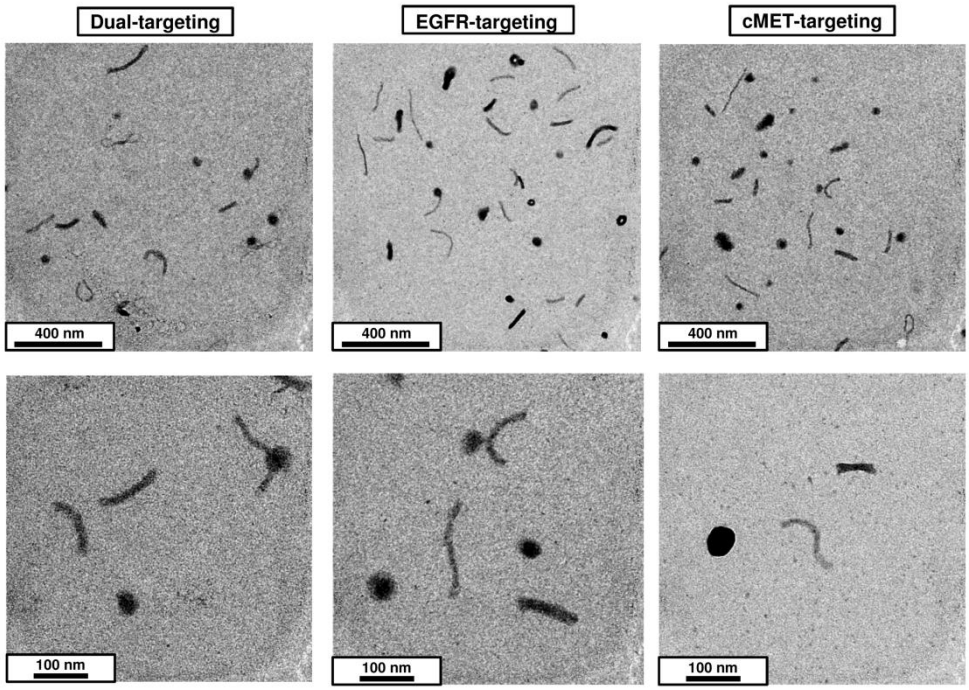

Fig. 1: *TEM size measurements of formed polyplexes revealed two different particle subtypes with no significant differences between the polyplex solutions for dual- or single-targeting. Globular particles were approximately 50 nm in size and linear particles were up to 200 nm in size. Adapted from submitted manuscript.*

EGFR and cMET expression levels

Three different cell lines were used for subsequent *in vitro* studies and were investigated for their EGFR and cMET expression levels. The human HCC cell line HuH7 and the human breast cancer cell line MCF-7 were identified to have both high EGFR and cMET cell surface expression. In contrast, the human follicular thyroid carcinoma cell line FTC-133 showed low expression levels for both receptors (Fig. 2).

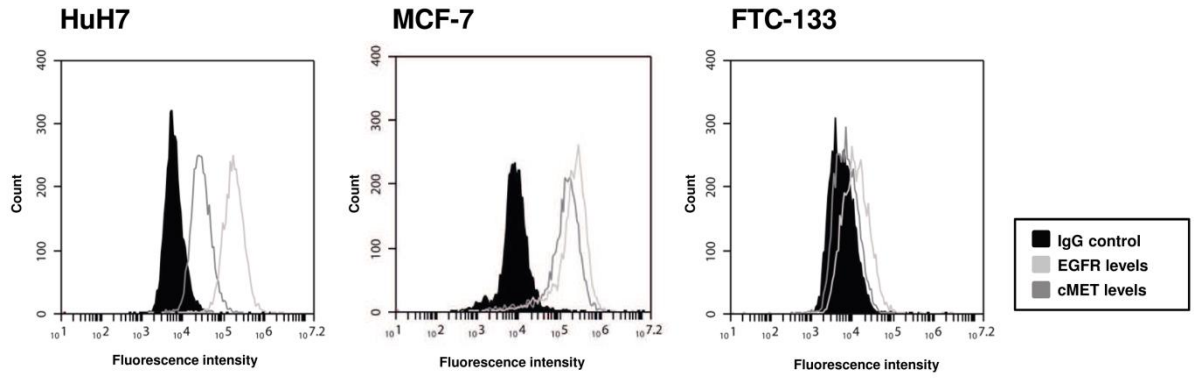

Fig. 2: *The human HCC cell line HuH7, the human breast cancer cell line MCF-7 and the human follicular thyroid carcinoma cell line FTC-133 were investigated for EGFR and cMET expression levels by flow cytometry. HuH7 and MCF-7 cells were found to have both high EGFR and cMET cell surface expression. FTC-133 cells showed low receptor expression levels for cMET and EGFR. An IgG-anti-mouse antibody served as control. Adapted from submitted manuscript.*

Comparison of dual-targeting and single-targeting for NIS gene transfer in vitro

The three different human tumor cell lines were transfected with polyplex solutions to investigate single-targeting vs. dual-targeting in relation to cell surface receptor expression. Cellular binding and cellular uptake were measured by detection of fluorescence intensity of polyplexes containing Cy5-labelled NIS DNA (Fig. 3A-C). Binding was measured after a short incubation time of 30 min and revealed higher mean fluorescence intensity (MFI) values for dual-targeting (black bars), whereas MFI values for the single-targeted polyplexes, especially EGFR, were lower (Fig. 3D; red bars for EGFR-targeting, blue bars for cMET-targeting). In the low EGFR and cMET-expressing cell line FTC-133, the dual-targeting strategy resulted in lower MFI values than obtained after single cMET-targeting transfection (Fig. 3D).

Uptake levels confirmed the trend seen in the binding studies, as a significantly higher MFI was detected for HuH7 and MCF-7 cells (Fig. 3E-G). In FTC-133, dual-targeting led to similar (compared to EGFR-targeting) or decreased (compared to cMET-targeting) MFI levels (Fig. 3H).

Iodide uptake verified the results from the flow cytometry experiments in the three cell lines, with higher uptake in HuH7 (Fig. 3I) and significantly increased uptake in MCF-7 (Fig. 3J) after simultaneously targeting EGFR and cMET. In the low EGFR and cMET-expressing FTC-133 cell line, no advantage of dual- over single-targeting was observed (Fig. 3K). Cell viability was not affected by 45 min incubation with the different polyplexes (Fig. 3L-N).

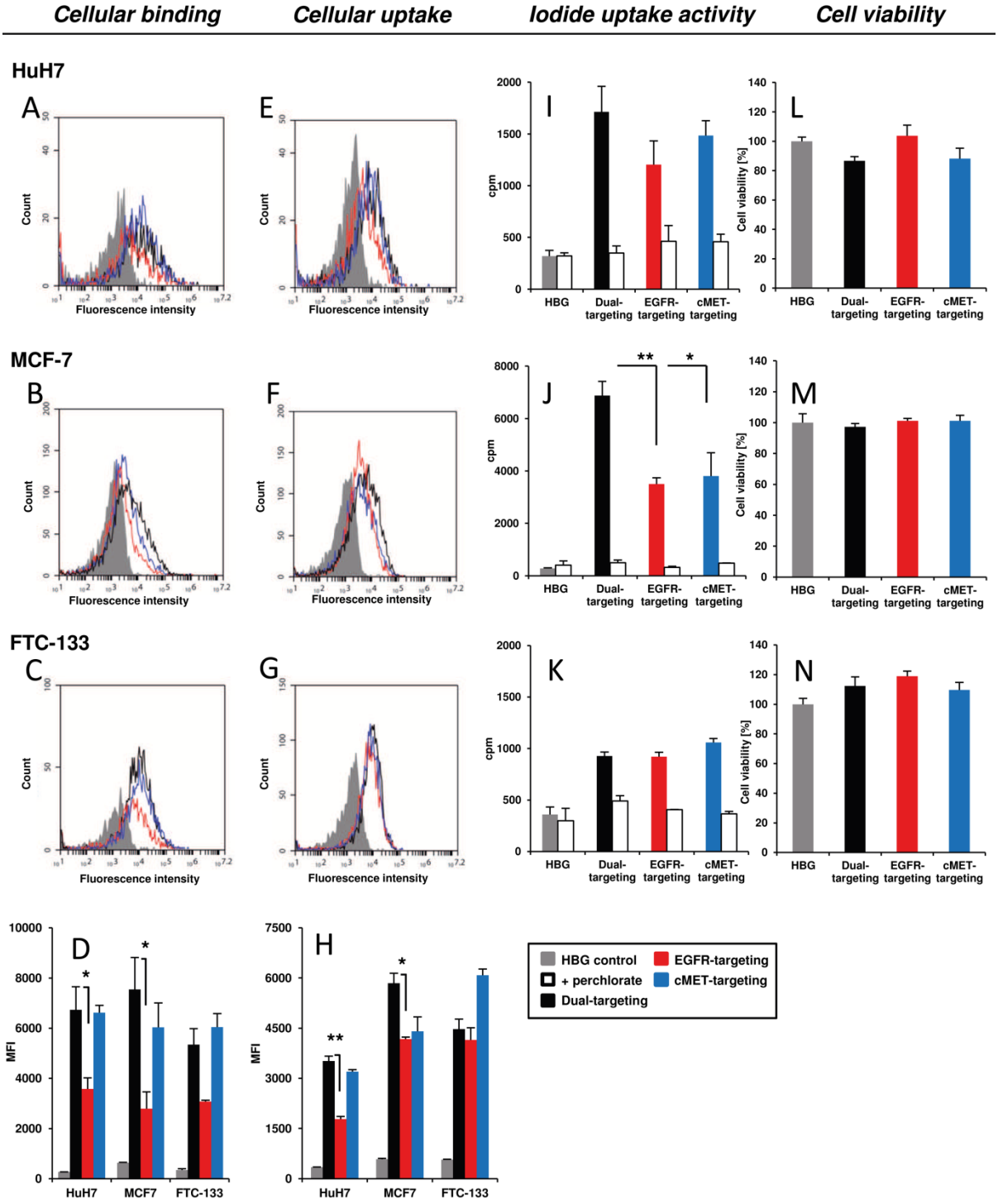

Fig. 3: *Transfection efficiency of polyplexes for single- and dual-targeting was investigated. Cellular binding and cellular uptake were measured by detection of fluorescence intensity of polyplexes containing Cy5-labelled NIS DNA. In high receptor expressing cell lines, binding studies revealed higher MFI values for dual-targeted polyplexes (black bars), whereas MFI values for single-targeted polyplexes were lower (red bars for EGFR-targeting, blue bars for cMET-targeting (A,B). This effect was not obtained with the low EGFR- and cMET-expressing cell line FTC-133 (C,D) (n=3). Uptake levels confirmed binding studies, where a significantly higher MFI after transfection for dual-targeting was detected in HuH7 and MCF-7 cells compared to FTC-133 (E-H) (n=3). NIS mediated 125I uptake verified enhanced NIS expression after simultaneous targeting of EGFR and cMET in HuH7 and MCF-7 cells, while low iodide uptake activity was measured in FTC-133 cells (I-K) (n=4). No toxic effects were measured after incubation with the different polyplex mixtures for 45 min (L-N) (n=3). (*p≤0.05; **p≤0.01). Results are reported as mean ± SEM. Adapted from submitted manuscript.*

Induction of iodide accumulation after systemic tumor-targeted NIS gene transfer in vivo

Based on the promising *in vitro* results, the dual-targeting strategy was further evaluated *in vivo*. An orthotopic HuH7 liver tumor model was established that showed high EGFR (Fig. 4A) and cMET (Fig. 4B) expression. Tumor-bearing mice were systemically injected with either polyplexes for single receptor targeting or dual-targeting. 48 h after NIS gene transfer, mice were injected i.p. with ^{124}I and radioiodide biodistribution was assessed by small-animal PET imaging. Images 1 h after iodide application showed improved distribution and uptake of iodide in tumors of mice that received polyplexes for dual-targeting (Fig. 4C), in comparison to tumors of mice treated with single-targeted polyplexes (Fig. 4D,E). Physiological expression of NIS in thyroid and stomach leads to iodide accumulation in these tissues and renal elimination of radioiodide causes a signal in the bladder. NIS-specificity was verified by i.p. application of the NIS-specific inhibitor sodium perchlorate 30 min prior to radionuclide application in mice treated with dual-targeted polyplexes, which resulted in an almost complete inhibition of iodide uptake in the tumor and organs that physiologically express NIS (Fig. 4F). No additional iodide uptake was recorded in non-target organs such as lung, liver, kidney and spleen (Fig. 4C-F).

Regions of interest (ROI) were quantified and as soon as 1 h after iodide application, a considerably higher tumoral iodide uptake was observed in tumors of mice that received polyplexes for dual-targeting (4.9 ± 0.6% of ID). Lower levels were obtained in tumors of mice treated with polyplexes for single EGFR-targeting (4.7 ± 0.7% of ID) and cMET-targeting (3.2 ± 0.3% of ID). After 3 h, mean iodide uptake after dual-targeting (3.0 ± 0.4% of ID) was 0.8-0.5% higher compared to animals after single-targeting (EGFR-targeting: 2.4 ± 0.5% of ID; cMET-targeting: 2.3 ± 0.3% of ID). ^{124}I scans 5 h after tracer application still showed significantly higher iodide uptake levels demonstrating prolonged tumoral iodide uptake after dual-targeting (2.0 ± 0.4% of ID) compared to EGFR- (1.0 ± 0.1% of ID) and cMET-targeting (1.5 ± 0.3% of ID) (Fig. 4G).

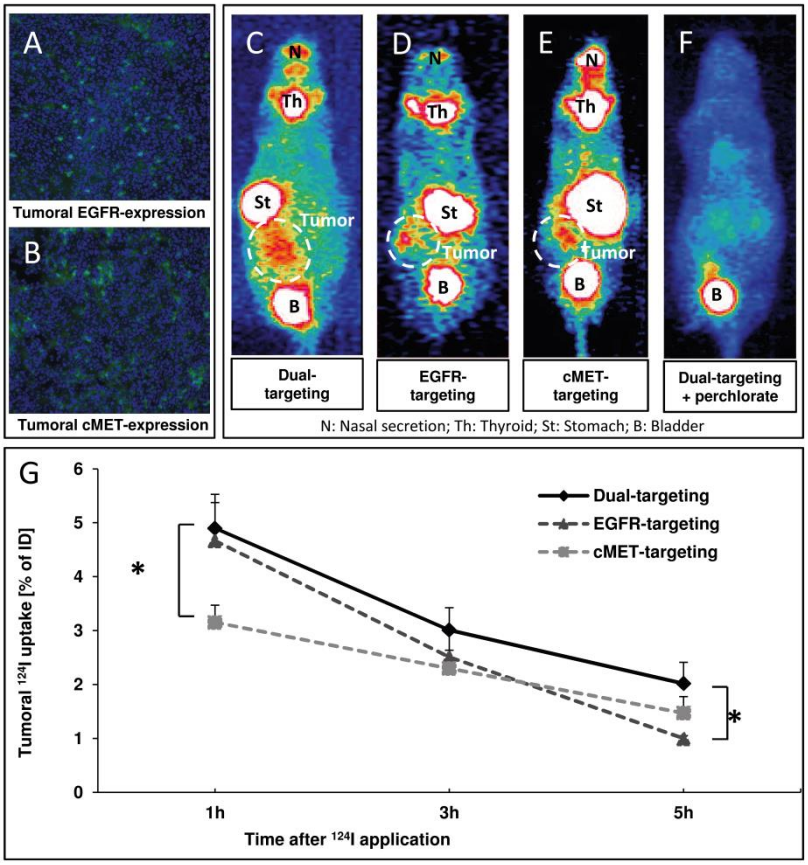

Fig. 4: *Mice bearing orthotopic HuH7 liver tumors that demonstrated high EGFR and cMET expression (A,B) received i.v. polyplexes for single EGFR-targeting (n=6), single cMET-targeting (n=4) or dual-targeting (n=7). At 48 h after NIS gene transfer, mice were injected i.p. with 10 MBq 124I and radioiodide biodistribution was assessed by small-animal PET imaging. PET images 1 h after iodide application showed improved distribution and uptake of iodide in tumors of mice that received polyplexes for dual-targeting in comparison to animals injected with single-targeted polyplexes (C-E). NIS-specificity was verified by pretreatment of mice that received polyplexes for dual-targeting with the NIS-specific inhibitor sodium perchlorate 30 min prior to radionuclide application (n=2). This resulted in an almost complete inhibition of iodide uptake in the tumor and organs that physiologically express NIS (F). ROIs were quantified and higher tumoral iodide uptake over 5 h was observed in tumors of mice that received polyplexes for dual-targeting (*p≤0.05). Results are reported as mean % of ID ± SEM. Adapted from submitted manuscript.*

Tumor-specific NIS protein expression

After the imaging studies, mice from the three different treatment groups were sacrificed and tumors dissected. Immunohistochemical staining of intrahepatic tumor sections revealed NIS-specific staining in all three treatment groups (Fig. 5).

In tumors from mice treated with polyplexes for dual-targeting, a more intense NIS-specific immunostaining and increased amounts of clusters of membrane-associated NIS gene expression in the vicinity of blood vessels was observed (Fig. 5, left panel) compared to tumors from animals that were injected with single EGFR- (Fig. 5, middle panel) and cMET-targeting polyplexes (Fig. 5 right panel).

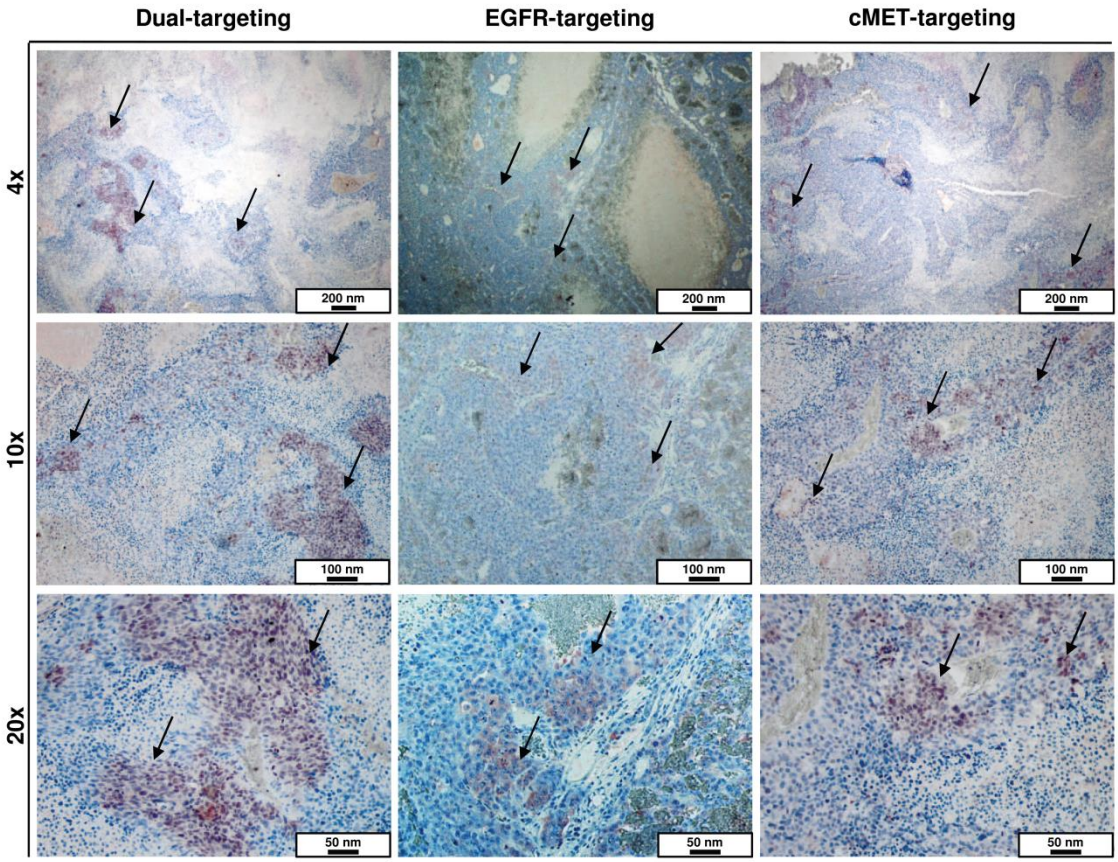

Fig. 5: *Paraffin embedded tumor sections were immunohistochemically stained for NIS expression. Tumors from mice treated with polyplexes for dual-targeting revealed a more intense and increased amount of clusters of membrane-associated NIS gene expression around blood vessels in the tumorous tissue compared to tumors from animals that were injected with polyplexes for single EGFR- and cMET-targeting. Adapted from submitted manuscript.*

Radioiodine therapy studies after in vivo NIS gene transfer

After the proof of concept of effective tumoral NIS transduction using polyplexes for dual-targeting, the therapeutic effect of the dual-targeting NIS gene therapy concept after application of ^{131}I was assessed. Mice developing orthotopic liver carcinomas were treated according to an established treatment protocol [46]. Three weeks after tumor cell inoculation, mice in the therapy group received three cycles of dual-targeted polyplexes i.v. on days 0, 3 and 7, followed by i.p. injections of 55.5 MBq ^{131}I on days 2, 5 and 9 (n=8). Control mice received saline instead of iodide (n=8). Four sonographic measurements were performed on days 2, 9, 15 and 23 after therapy start. Mice in the therapy group exhibited significantly reduced tumor growth (Fig. 6A,B) compared to the control group (Fig. 6A,C), which was associated with significantly prolonged survival up to 45 days after therapy start in comparison to 29 days in the control group (Fig. 6D).

When mice had to be sacrificed due to tumor growth, intrahepatic HCCs were dissected and further processed for immunofluorescence analysis. A Ki67-specific antibody (green) was

used to identify tumor cell proliferation and an antibody against CD31 (red) served for blood vessel labeling (Fig. 6E). The application of dually targeted polyplexes followed by ^{131}I resulted in reduced proliferation and blood vessel density compared to tumors of mice treated with saline instead of iodide (Fig. 6E).

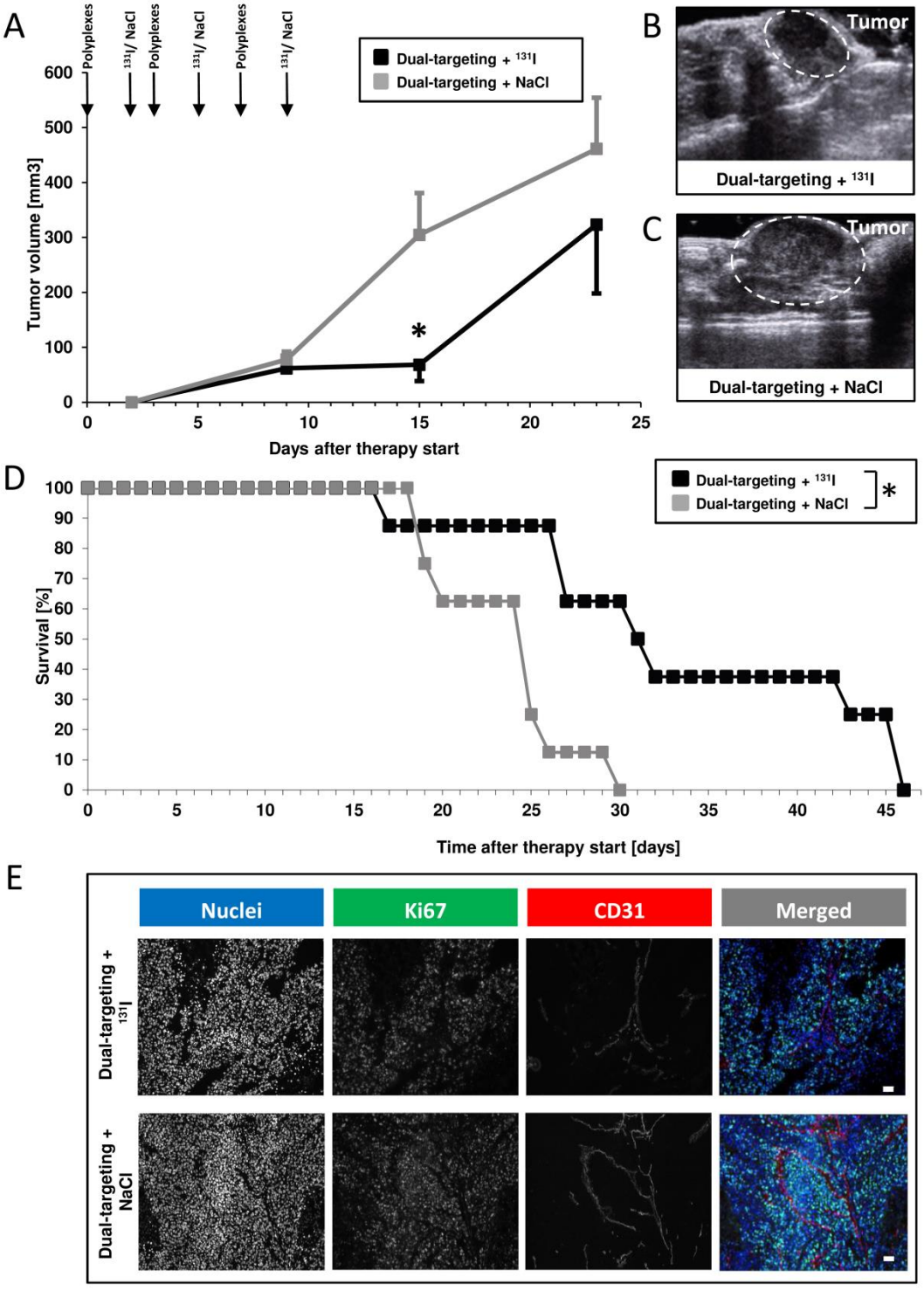

Fig. 6: *The therapeutic effect of the dual-targeting NIS gene therapy approach after application of 131I was assessed. Three weeks after tumor cell inoculation, mice received three cycles of polyplexes for dual-targeting i.v., followed by i.p. injections of 55.5. MBq 131I (n=8). Control mice received saline instead of the therapeutic iodide (n=8). Animals treated with polyplexes for dual-targeting that received radioiodide showed reduced tumor growth during and after therapy (A, B) assessed by conventional sonography in comparison to animals that received saline instead (A, C) (*p≤0.05). This was accompanied by significantly enhanced survival in the therapy group (D) (*p≤0.05). Immunofluorescence analysis of tumors after therapy revealed reduced proliferation (Ki67, green) and blood vessel density (CD31, red) in mice that received the cytoxic iodide compared to tumors of mice treated with saline (E). Results are reported as mean ± SEM or percent for survival blot. Adapted from submitted manuscript.*

Perfusion of intrahepatic tumors determined by CEUS

Two weeks after the last treatment cycle, tumor perfusion was assessed to compare tumors from mice treated with polyplexes for dual-targeting that received ^{131}I with animals that received saline instead. Mice in the therapy group demonstrated an overall reduced contrast agent uptake and a lower maximum signal compared to mice that received saline (Fig. 7A). This was further associated with reduced peak enhancement (PE; 1432.7 ± 534.6) (Fig. 7B), wash-in area under the curve (WiAUC; 7184.2 ± 2197.6) (Fig. 7C) and retention time (RT; 7.98 ± 0.97) (Fig. 7D) of therapy animals in comparison to control animals (PE: 2425.9 ± 260.5; WiAUC: 19633.4 ± 1451.8; RT: 11.39 ± 0.71) (Fig. 7B–D).

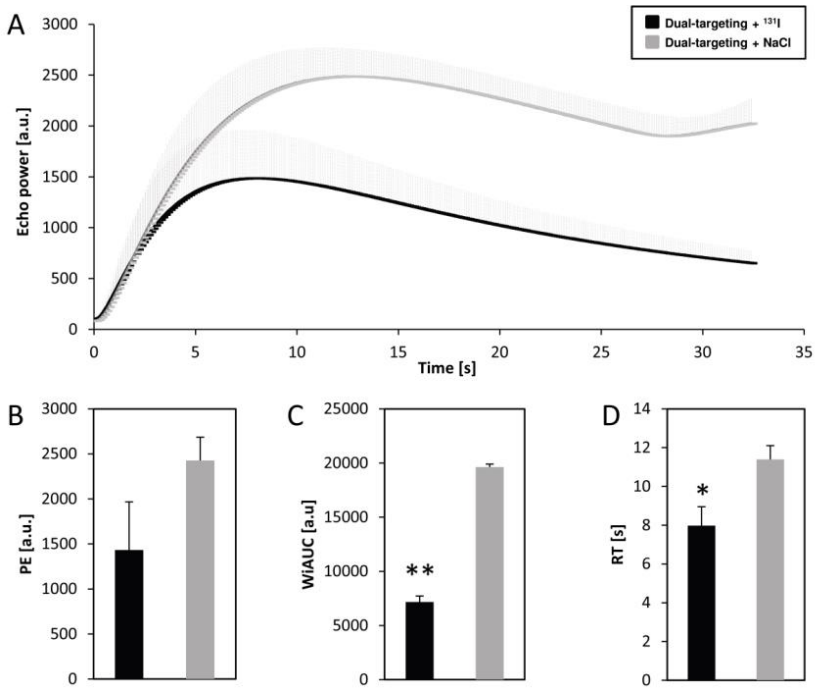

Fig. 7: *Tumors of mice treated with polyplexes for dual-targeting that received 55.5 MBq ^{131}I (n=4) demonstrated an overall reduced contrast agent uptake expressed in arbitrary units (a.u.) compared to mice that received saline instead (A) (n=3). Further, tumors of therapy mice showed reduced PE (1432.66 ± 534.55 (B)), WiAUC (7184.2 ± 2197.6; (C)), RT (7.98 ± 0.97; (D)) after radioiodide therapy as compared to control animals (PE: 2425.9 ± 260.5; WiAUC: 19633.4 ± 1451.8; RT: 11.39 ± 0.71; (B–D)). Results are expressed as mean ± SEM (*p≤0.05; **p≤0.01). Adapted from submitted manuscript.*

5.6 Discussion

In the last decade, intensive research in the field of cancer gene therapy has made big strides towards novel therapeutic options. For clinical application of cancer gene therapy as novel therapeutic alternative, NIS has emerged as an ideal target gene, as it combines the features of a reporter and therapy gene. Due to its endogenous thyroidal expression, NIS has successfully been used over decades for the treatment of thyroid cancer [33]. The high amount of experience gained over the years allows a safe application in humans with a well-known therapeutic-window and minimal side effects. Introducing NIS to non-thyroidal tumor cells offers the possibility to monitor tumor-specific NIS gene expression in a quantitative manner as well as exact localization of tumorous tissue by multimodal imaging techniques with various NIS-specific tracers [49, 173, 176]. At the same time, NIS expression enables application of therapeutic radionuclides (^{131}I, ^{188}Re) for the destruction of cancer cells. The high efficacy of the theranostic function of NIS after gene transfer to non-thyroidal tumors has been demonstrated in several preclinical studies [35-42, 45-47, 92, 93, 126, 151] and showed first promising results in clinical trials after local administration of viral NIS gene delivery vectors [131].

However, in the growing sector of cancer gene therapy, tumor heterogeneity has turned out to be a major bottleneck, resulting in limited and diverging efficacy of therapies. Differences in morphological and phenotypic characteristics that define the behavior of the tumor lesion exist both between different tumors (inter-tumoral heterogeneity) and within tumors (intra-tumoral heterogeneity) [5]. On the molecular level, intra-tumoral heterogeneity is mirrored by diverging cell populations evolved from different subclones [177]. This often lead to great differences in surface receptor expression, release of growth factors and cytokines, cellular metabolism and stromal architecture [178, 179] and hence to a discrepancy in therapy response.

Also in HCC tumor heterogeneity is a well characterized phenomenon that is at least in part responsible for its poor prognosis due to therapy resistance and aggressive tumor progression [180-182]. For advanced HCC the multi-kinase inhibitors sorafenib and regorafenib [166], which only slightly improve progression-free survival and quality of life, and the second-line therapeutics Nivolumab, which is approved for application after therapy failure with sorafenib [183], are the only currently available systemic treatment options.

With the ultimate goal of improved therapeutic efficacy and patient outcomes after tumor-targeted NIS gene delivery even in heterogeneic tumors with variable receptor expression levels, nonviral vectors as potent novel gene delivery vehicles have to be designed and applied in a specialized manner for a future clinical translation. Formulation improvement includes the synthesis of a cationic carrier backbone for DNA binding, incorporation of

hydrophilic domains for polyplex shielding and endosomal buffering and integration of targeting ligands that are indispensable for tumor-specific gene delivery. Variable expression patterns of ligand binding surface receptors are often responsible for heterogenous response rates and expression levels of genetic information after targeted gene transfer. Bispecific targeting as well as combination of different therapy approaches are already well-established strategies in the clinical setting in the form of combination of different antibodies and chemotherapeutics with different modes of action to circumvent resistance and enhance efficacy. Thinking along the same lines, a dual-targeting approach was performed in this study focusing on simultaneously targeting the two receptors EGFR and cMET. EGFR and cMET overexpression in many different cancer types, which is often accompanied with poor prognosis, provide the basis for this approach with the aim of increasing the efficacy of targeting and transduction in heterogeneic tumors. Two underlying mechanisms that enhance binding and uptake of polyplexes for dual-targeting are conceivable: (1) the dual approach may mimic virus-like particles that use more than one receptor for uptake [68, 88] and (2) receptor crosslinking may trigger enhanced endocytosis and particle uptake into the lysosome and trafficking to the cell nucleus [84].

As small peptide ligands exhibit favorable characteristics compared to large proteins and antibodies as targeting ligands due to synthesis procedures, the small peptide ligands GE11 for EGFR-targeting and cMBP for cMET-targeting were coupled to a well-established LPEI-PEG_{2kDa}-backbone in this study. Both ligands demonstrated high tumor specificity with high targeting efficacy in former studies [39, 46, 68, 69, 151]. The polyplexes are formed by mixing NIS DNA with either 100% LPEI-PEG-GE11 or 100% LPEI-PEG-cMBP for single receptor targeting or with a solution of polymers containing 50% LPEI-PEG-GE11 and 50% LPEI-PEG-cMBP at a total N/P ratio of 6 for dual-targeting.

To exclude differences in particle formation and size between polyplexes for single- or dual-targeting that may have an impact on transduction efficiency, polyplex solutions were examined by TEM. All three solutions exhibited comparable sizes of round and linear formed particles ranging from 50-200 nm. For particles with these sizes cellular uptake is described to occur via a clathrin-dependent endocytosis pathway [60].

Detailed analysis of binding and uptake of polyplexes after single-receptor and dual-receptor targeting was performed by flow cytometry with labeled NIS DNA in three different cell lines. The HCC cell line HuH7 as well as the breast cancer cell line MCF-7 showed high EGFR and cMET expression, whereas for the thyroid carcinoma cell line FTC-133 low expression of both surface receptors was detected *in vitro*. HuH7 and MCF-7 exhibited higher cellular binding and uptake capacity after simultaneous dual-targeting, which correlated well with iodide uptake levels, compared to results obtained after targeting only one receptor. The low EGFR and cMET expressing cell line FTC-133, however, did not show any advantage of

dual-targeting over single-targeting, confirming that improved transfection efficiency is ligand-dependent and the effect cannot be reproduced in low receptor expressing cells.

As a next step, the reporter function of NIS was used for detailed investigation of NIS gene expression *in vivo* in orthotopic HuH7 HCC tumors by noninvasive small-animal PET imaging using ^{124}I as tracer. A beneficial effect of the dual-targeting strategy over both single-targeting approaches was detected. Images of mice that received dual-targeted polyplexes showed higher levels of NIS-mediated radioiodine uptake in the tumor lesion. Quantification of iodide uptake revealed higher levels after dual-targeting at all imaging time points. Interestingly, single EGFR-targeting showed higher levels of radioiodide uptake 1 h after tracer application compared to cMET-targeting. After 3 h, tumors of both single-targeting approaches showed nearly the same tumoral iodide uptake levels. With dual-targeting an approximately 1% of ID higher uptake was achieved. After 5 h, EGFR-targeting has dropped down more rapidly showing higher levels of iodide efflux and therefore lower iodide retention as compared to dual and cMET-targeting. This is crucial for more effective therapeutic application of ^{131}I, as iodide retention is an essential factor to reach a sufficiently high tumor absorbed dose, especially in the absence of iodide organification in liver tumors [18].

Immunohistochemical staining showed strong tumorous NIS protein expression in all three treatment groups after application of polyplexes. NIS-specific immunostaining was mainly located in the vicinity of blood vessels and occurred in typical clusters. A trend towards more intensive and expanded areas of NIS-specific immunostaining was seen in sections of animals that received polyplexes for dual-targeting.

After confirming the beneficial effect of dual-targeting *in vivo* by imaging of biodistribution and levels of NIS expression, the therapeutic efficacy of this NIS gene delivery strategy was evaluated. Animals were treated with dual-targeted polyplexes followed by application of ^{131}I 48 h later. As control group, animals received saline instead of the therapeutic radioiodide. The therapy regimen was performed according to an established treatment protocol [46, 126] that allows comparison to earlier studies. Tumor growth was monitored by conventional sonography and perfusion was assessed by CEUS with the contrast agent SonoVue®. Animals in the therapy group showed significantly reduced tumor growth and prolonged survival. The therapeutic effect was further investigated by comparing tumor cell proliferation and blood vessel density of the therapy and control group *ex vivo*. Reduced proliferation and a lower amount of blood vessels in tumor sections of therapy animals that received ^{131}I correlated with the reduced progression of the intrahepatic tumors. CEUS perfusion data, which showed reduced peak enhancement, lower wash-in area under the curve and lower retention times in tumors of therapy animals that show lower blood vessel formation complemented the results and confirm the enormous therapeutic efficacy of dual-targeted NIS gene therapy.

In conclusion, this novel simultaneous targeting approach of EGFR and cMET for NIS gene delivery to HCC tumors combines two crucial bispecific approaches: NIS with its innate dual characteristics to function as reporter gene for diagnostic evaluation and as therapeutic gene in synergy with dual-targeting of two receptors that results in enhanced cellular uptake and increased NIS gene expression in the tumor lesion. Our results highlight the benefits of the bifunctional strategy that represents a promising concept for future clinical translation providing two major advantages for clinical application, enhancing safety by molecular imaging of biodistribution and levels of gene expression as well as overcoming the limitations through tumor heterogeneity by designing polyplexes that home to several targets.

5.7 Acknowledgements

We are grateful to Sissy M. Jhiang (Ohio State University, Columbus, OH, USA) for supplying the full length human NIS cDNA. We thank Barbara Ungern-Sternberg, Rosel Oos, Karin Bormann-Giglmaier (Department of Nuclear Medicine, University Hospital of Munich, LMU Munich, Munich, Germany) for their assistance with animal care and imaging studies. We thank Michael Ingrisch for assistance with CEUS analysis.

This work was supported by grants from the Deutsche Forschungsgemeinschaft within the Collaborative Research Center SFB824 (project C 08) to C Spitzweg as well as within the Priority Programme SPP1629 to C Spitzweg (SP 581/6-1, SP581/6-2), the Cluster of Excellence Nanosystems Initiative Munich (NIM) to E Wagner and by a grant from the Wilhelm-Sander-Stiftung to C Spitzweg (2014.129.1).

6. Sequence-defined cMET/HGFR-targeted polymers as gene delivery vehicles for the theranostic sodium iodide symporter (NIS) gene

This chapter has been adapted from:

Urnauer S[1], Morys S[2], Krhac Levacic A[2], Müller AM[1], Schug C[1], Schmohl KA[1], Schwenk N[1], Zach C[3], Carlsen J[3], Bartenstein P[3], Wagner E[2], Spitzweg C[1]. Sequence-defined cMET/HGFR-targeted Polymers as Gene Delivery Vehicles for the Theranostic Sodium Iodide Symporter (NIS) Gene. Mol Ther. 2016 Aug; 24(8):1395-404.

[1]Department of Internal Medicine II, [2]Department of Pharmacy, Center of Drug Research, Pharmaceutical Biotechnology, [3]Department of Nuclear Medicine, LMU Munich, Germany

6.1 Abstract

The sodium iodide symporter (NIS) as well characterized theranostic gene represents an outstanding tool to target different cancer types allowing non-invasive imaging of functional NIS expression and therapeutic radioiodide application. Based on its overexpression on the surface of most cancer types, the cMET/hepatocyte growth factor receptor serves as ideal target for tumor-selective gene delivery. Sequence-defined polymers as non-viral gene delivery vehicles comprising polyethylene glycol (PEG) and cationic (oligoethanoamino) amide cores coupled with a cMET-binding peptide (cMBP2) were complexed with NIS-DNA and tested for receptor-specificity, transduction efficiency and therapeutic efficacy in hepatocellular cancer cells HuH7. *In vitro* iodide uptake studies demonstrated high transduction efficiency and cMET-specificity of NIS-encoding polyplexes (cMBP2-PEG-Stp/NIS) compared to polyplexes without targeting ligand (Ala-PEG-Stp/NIS) and without coding DNA (cMBP2-PEG-Stp/Antisense-NIS). Tumor recruitment and vector biodistribution were investigated *in vivo* in a subcutaneous xenograft mouse model showing high tumor-selective iodide accumulation in cMBP2-PEG-Stp/NIS-treated mice (6.6±1.6% ID/g ^{123}I, biological half-life 3 h) by ^{123}I-scintigraphy. Therapy studies with 3 cycles of polyplexes and ^{131}I application resulted in significant delay in tumor growth and prolonged survival. These data demonstrate the enormous potential of cMET-targeted sequence-defined polymers combined with the unique theranostic function of NIS allowing for optimized transfection efficiency while eliminating toxicity.

6.2 Introduction

As cancer is one of the leading causes of death both in developed and developing countries [184], new therapy approaches are urgently needed, especially for cancer types with poor prognosis, where surgery, chemo- and radiotherapy often prove ineffective, such as advanced hepatocellular cancer [98]. Gene therapy with its broad potential to interact and interfere with aberrant physiological processes has emerged as a powerful tool in oncology in recent years [185]. However, gene therapy still faces hurdles that strongly limit its application [55]. Low tumor selectivity of gene delivery vehicles, immunoreactions after systemic application and limited effectiveness of therapy genes have driven the search for novel biodegradable vectors with improved safety profile and enhanced transduction efficiency [12, 16, 68, 69, 186].

Based on its theranostic function, the sodium iodide symporter (NIS) represents an ideal therapeutic gene [16, 89, 187, 188]. The unique combination of reporter and therapy gene characteristics allows non-invasive imaging of vector biodistribution and functional NIS expression at tumor sites by ^{123}I-scintigraphy and ^{124}I-/^{18}F-tetrafluoroborate positron emission tomography (PET) as well as exact dosimetric calculations before the assessment of therapeutic efficacy after application of ^{131}I. Several groups including our own have successfully demonstrated the capacity of NIS to induce radioiodide accumulation in different non-thyroidal tumor models mediated by various gene delivery vehicles, including mesenchymal stem cells as well as viral and non-viral vectors [35-44, 47, 90, 92, 95, 176, 189].

Further improvement of the NIS gene therapy concept is focused on generation of new shuttle systems with advanced efficiency, specificity and low cytotoxicity. Cationic polymers as a major sector of non-viral vectors offer the advantages of low immunogenicity, good nucleic acid binding and easy up-scaling [53]. In order to improve performance for systemic application and further enhance transduction efficiency, various design strategies have been developed for the synthesis of novel sequence-defined polymers. In this context, we generated small, well biocompatible polymer backbones with precisely integrated functional groups. These include cationic (oligoethanoamino) amide cores for nucleic acid binding, polyethylene glycol (PEG) linkers for surface shielding, targeting ligands for cell binding and protonatable amino acids with buffer function for a higher rate of endosomal escape, leading to optimized and DNA carrier-improved systems for systemic administration [12, 68, 69].

Selective active ligand-mediated tumor-targeting represents an elegant method to further enhance tumor specificity, making use of aberrant tumor physiology that is often accompanied by up-regulation of various receptors on the surface of tumor cells, such as the epidermal growth factor receptor (EGFR) [3]. We recently reported efficient EGFR-targeting

with viral and non-viral gene delivery vehicles, which resulted in high tumoral iodide uptake after systemic NIS gene transfer that was sufficient for a delay in tumor growth and prolonged survival in a subcutaneous hepatocellular cancer xenograft mouse model [36, 39]. Another attractive and important target in cancer therapy is the receptor tyrosine kinase cMET/hepatocyte growth factor receptor (HGFR). High surface expression levels and activation of cMET/HGFR in a broad range of malignancies are implicated in tumor progression and are often associated with poor prognosis [190]. In order to target non-viral gene delivery vehicles to cMET/HGFR, a cMET-binding peptide (cMBP2) was developed via phage-display screening and further identified as ideal ligand with high receptor affinity that specifically enhances nanoparticle adhesion to the target cell [69, 123, 191, 192].

In the current study, we combined the NIS gene therapy concept with novel sequence-defined polymers as non-viral gene delivery vehicles coupled to cMBP2. Based on the dual function of NIS, the potential of this cMET-targeted gene therapy approach was investigated by non-invasive imaging of vector biodistribution and transduction efficiency in a subcutaneous hepatocellular carcinoma mouse model. Subsequently, therapeutic efficacy was assessed by monitoring tumor growth after application of a therapeutic dose of ^{131}I.

6.3 Materials and methods

Cell culture

The human hepatocellular carcinoma cell line HuH7 (JCRB0403; Japanese Collection of Research Bioresources Cell Bank, Osaka, Japan) was cultured in Dulbecco's modified eagle medium (DMEM; 1 g/l glucose; Sigma-Aldrich, St.Louis, Missouri, USA) and the human hepatocellular carcinoma cell line Hep3B (HB-8064; American Type Culture Collection (ATCC), Manassas, VA) was cultured in Eagle's Minimum Essential Medium (EMEM; Sigma-Aldrich). Both media were supplemented with 10% (v/v) fetal bovine serum (FBS Superior, Biochrom/Merck Milipore, Berlin, Germany) and 1% (v/v) penicillin/streptomycin (Sigma-Aldrich).

Cells were maintained at 37°C and 5% CO_2 in an incubator with a relative humidity of 95%. Cell culture medium was replaced every second day and cells were passaged at 80% confluency.

Plasmid and polymer synthesis

The expression vector pCpG-hCMV-NIS driven by the human elongation factor 1α promotor and human cytomegalovirus enhancer element containing the full-length codon-optimized *NIS* cDNA (Geneart, Regensburg, Germany) was generated as described previously [39]. For all *in vitro* and *in vivo* experiments pNIS-DNA produced and purified by Plasmid Factory GmbH (Bielefeld, Germany) was used. Synthesis of polymers was carried out as described previously [69] and polymers were used as 5 mg/ml stock solutions. Polymer syntheses were performed by Stephan Morys (Department of Pharmacy, Pharmaceutical Biotechnology, LMU).

Polyplex formation

For polyplex formation the sequence-defined histidinylated cMET-targeted polymer (cMBP2-PEG-Stp) or a control polymer with alanine instead of the ligand (Ala-PEG-Stp) and a PEG-free three-armed polymer (3-arm-Stp, #689) in a molar ratio of 70:30 to compact polyplexes were used [69]. The polymer blend and plasmid DNA (pDNA) were diluted in same volumes of HEPES buffered glucose (HBG: 20 mmol/l HEPES, 5% glucose (w/v) at pH 7.4). Polymers were added to the DNA by rapid mixing at a N/P (nitrogen/phosphate) ratio (w/w) of 12 and incubated at room temperature for 30 minutes before use. For calculation, only protonatable nitrogen groups were considered. Final DNA concentration for *in vitro* studies was 2 µg/ml, for *in vivo* studies 200 µg/ml.

Transient transfection and ^{125}I uptake assay

To measure the transduction efficiency, cells were grown to 60-80% confluency ($2x10^5$ HuH7 or Hep3B cells/well in 6-well-plates) and incubated for 4 h with DNA/polymer-solutions in serum- and antibiotic-free medium. Medium was then changed to normal growth medium and, 24 h later, iodide uptake activity was measured. NIS-mediated ^{125}I uptake assays were performed as described previously [47]. Results were normalized to cell survival measured by cell viability assay (see below) and expressed as cpm/A620.

Cell viability assay

Cells were incubated with a commercially available MTT reagent (Sigma-Aldrich) for 2 h at 37°C followed by a washing step with PBS (phosphate-buffered saline). Cell viability was measured after incubation with 10% DMSO (dimethyl sulfoxide) in isopropanol at 620 nm in a Sunrise microplate absorbance reader (Tecan, Männedorf, Switzerland).

Flow cytometry analysis

Cell surface cMET/HGF-receptor expression levels were quantified by flow cytometry analysis. HuH7 and Hep3B cells were detached with trypsin and washed with FACS buffer (PBS with 10% FBS). Cells were incubated with an antibody that detects human cMET/HGFR (1:200; monoclonal mouse IgG1, R&D Systems, Minneapolis, USA) for 1 h on ice. As negative control, an IgG-anti-mouse antibody (BD Bioscience, Franklin Lakes, USA) was used. After incubation, cells were washed with FACS-buffer, stained with an AlexaFluor 488-labeled goat anti-mouse secondary antibody (1:400; Jackson ImmunoResearch, West Grove, Pennsylvania, USA) for 1 h on ice, washed and resuspended in FACS buffer. Analysis was performed on a BD Accuri™ C6 flow cytometer (BD Bioscience, Franklin Lakes, USA). Cells were gated by forward/sideward scatter and pulse width for exclusion of doublets. PI (propidium iodine, Sigma-Aldrich) was used for discrimination between viable and dead cells.

Establishment of subcutaneous HuH7 tumors

HuH7 xenografts were established in 6-week-old female CD-1 nu/nu mice (Charles River, Sulzfeld, Germany) by subcutaneous injection of $5x10^6$ HuH7 cells suspended in 100 µl of PBS into the flank region. Animals were maintained under specific pathogen-free conditions with access to mouse chow and water *ad libitum*. Before radionuclide application, mice were pretreated with L-T4 (L-thyroxine, 5 mg/l; Sigma-Aldrich) in drinking water to reduce iodide uptake in the thyroid gland.

Tumor measurements were performed regularly and tumor volume was estimated using the equation: length x width x height x 0.52. Animals were sacrificed when the tumor volume reached a size of 1500 mm^3 or tumors necrotized. The experimental protocol was approved

by the regional governmental commission for animals (Regierung von Oberbayern) and all animal experiments were carried out according to the guidelines of the German law of protection of animal life.

***In vivo* radioiodide imaging and biodistribution studies after NIS gene transfer**

When subcutaneous HuH7 tumors reached a size of 10-15 mm in diameter, polyplex solutions containing 50 μg of pNIS-DNA were applied via the tail vein. Animals were divided into three groups and treated either with cMBP2-PEG-Stp/NIS (n=15), cMBP2-PEG-Stp/Antisense-NIS (n=5) or Ala-PEG-Stp/NIS (n=5). 48 h after polyplex administration, mice received an intraperitoneal injection of 18.5 MBq ^{123}I. To determine NIS specificity, a subgroup of cMBP2-PEG-Stp/NIS-treated mice received $NaClO_4$ (sodium perchlorate; 2 mg/mouse; Sigma-Aldrich), a NIS-specific inhibitor, 30 min prior to radioiodide application (n=6). Vector biodistribution and tumoral NIS expression were determined by measuring the iodide uptake by serial gamma camera imaging (e.cam, Siemens, Munich, Germany; with a low-energy high resolution collimator). Regions of interest were quantified by using the software HERMES GOLD (Hermes Medical Solutions, Stockholm, Sweden) and are shown as percent of injected iodide dose per gram tumor tissue (% ID/g).

***Ex vivo* biodistribution studies**

For *ex vivo* biodistribution studies, mice of the cMBP2-PEG-Stp/NIS group (n=6), cMBP2-PEG-Stp/NIS+$NaClO_4$ (n=3) group, cMBP2-PEG-Stp/Antisense-NIS group (n=3) or Ala-PEG-Stp/NIS group (n=3) received 18.5 MBq ^{123}I to detect iodide accumulation in the tumor and non-target organs. 3 h after injection of ^{123}I, mice were sacrificed and organs were dissected and measured in a Packard Cobra Quantum Gamma Counter (GMI, Ramsey, Minnesota, USA). Results are presented as percent injected dose per organ (% ID/organ).

Immunohistochemical NIS staining

Immunohistochemical NIS staining was performed on dissected frozen tissues of HuH7 tumors 48 h after systemic administration of polyplexes. A NIS specific mouse monoclonal antibody (Millipore, Darmstadt, Germany; 1:1000) was used for NIS detection and staining was performed as described previously [153]. Sections were imaged on an Olympus BX41 microscope (Olympus, Shimjukum Tokio, Japan) equipped with an Olympus XC30 CCD camera (Olympus).

Radioiodide therapy study *in vivo*

Therapy studies started when subcutaneous HuH7 tumors reached a size of 5-6 mm. Three cycles of polyplex administration were performed on day 0, 3 and 7. Mice received either

cMBP2-PEG-Stp/NIS (n=10), cMBP2-PEG-Stp/Antisense-NIS (n=6) or Ala-PEG-Stp/NIS (n=6) followed by an intraperitoneal application of 55.5 MBq ^{131}I 48 h later. As additional controls mice received cMBP2-PEG-Stp/NIS followed by saline (NaCl; n=9). Mouse survival was defined by a maximum tumor volume of 1500 mm^3 at which animals had to be sacrificed.

Analysis of NIS mRNA expression

For quantification of NIS expression, total RNA was isolated from HuH7 tumors using the RNeasy Mini Kit (Quiagen, Hilden, Germany) according to the manufacturer's recommendations. Reverse transcription was performed using SuperScript III First-Strand Synthesis System (Thermo Fisher Scientific, Waltham, Massachusetts, USA). Quantitative real-time PCR was run with the QuantiTect SYBR Green PCR Kit (Qiagen) in a Mastercycler ep gradient S PCR cycler (Eppendorf, Hamburg, Germany). Relative expression levels were calculated from ΔΔCt values normalised to internal β-actin. The following primers were used:
hNIS: (5'ACACCTTCTGGACCTTCGTG-3') and (5'-GTCGCAGTCGGTGTAGAACA-3'),
β-Actin: (5'AGAAAATCTGGCACCACACC-3') and (5'-TAGCACAGCCTGGATAGCAA-3').

Indirect immunofluorescence assay

After treatment, at the end of the observation period, immunofluorescence staining was performed on dissected frozen tissues, which were fixed in 80% methanol at 4°C for 5 min and acetone at -20°C for 2 min. After rehydration in PBS and blocking with 12% bovine serum albumin/PBS for 30 min at room temperature, incubation with a rabbit polyclonal antibody against human Ki67 (Abcam, Cambridge, UK; dilution 1:1000) and a rat monoclonal antibody against mouse CD31 (BD Pharmingen, Heidelberg, Germany; dilution 1:200) was performed. This was followed by incubation with a secondary anti-rabbit Alexa488-conjugated antibody (Jackson ImmunoResearch, West Grove, Pennsylvania, USA) for Ki67 staining and secondary anti-rat Cy3-conjugated antibody (Jackson ImmunoResearch) for CD31 staining. Nuclei were counterstained with Hoechst bisbenzimide (5 mg/ml) and sections were embedded in Fluorescent Mounting Medium (Dako, Hamburg, Germany). Stained sections were examined using an Axiovert 135 TV fluorescence microscope equipped with an AxioCam MRm CCD camera and AxioVision Re. 4.8. software (Carl Zeiss, Munich, Germany). Quantification of proliferation (Ki67-staining) and blood vessel density (CD31-staining) was performed by evaluation of 6 visual fields per tumor using ImageJ software (NIH).

Statistical methods

All *in vitro* experiments were carried out at least in triplicates. Results are expressed as mean ± SEM, mean fold change ± SEM and, for survival plots, in percent. Statistical significance was calculated by two-tailed Student's t-test for *in vitro* and *ex vivo* experiments or Mann-Whitney U test for *in vivo* experiments. *P* values ≤0.05 were considered significant (**p*≤0.05, ***p*≤0.01, ****p*≤0.001).

6.4 Results

In vitro cMET-targeted NIS-gene transfer in HuH7 and Hep3B cells

cMET/HGFR expression levels on the cell surface of HuH7 and Hep3B cells were detected by flow cytometry (Figs. 1a,b). High cMET/HGFR expression levels on HuH7 cells correlated well with high levels of transduction efficiency after incubation with cMET-targeted PEGylated polyplexes cMBP2-PEG-Stp/NIS (Stp=succinoyl-tetraethylene pentamine), while significantly lower transgene expression levels were obtained after transfection of low cMET/HGFR expressing Hep3B cells (Fig. 1c). This led to the selection of the HuH7 cell line as model system for further *in vitro* and *in vivo* experiments. Transduction conditions were optimized by measurement of perchlorate-sensitive iodide uptake activity 24 h after NIS gene transfer and best conditions with lowest cytotoxicity were used in all subsequent experiments. Incubation of HuH7 cells with cMBP2-PEG-Stp/NIS polyplexes resulted in a 12-fold increase in ^{125}I uptake compared to empty polymers, which was completely blocked upon treatment with the NIS-specific inhibitor sodium perchlorate. In contrast, replacement of the targeting ligand cMBP2 by alanine (Ala-PEG-Stp/NIS) showed a significantly lower iodide uptake activity, demonstrating targeting specificity of the targeting ligand cMBP2. No iodide uptake above background levels was seen in HuH7 cells transfected with empty polymers cMBP2-PEG-Stp and cMBP2-PEG-Stp/Antisense-NIS (Fig. 1d). Results were normalized to cell viability. Cell viability was not affected by polyplex-mediated gene transfer (Fig. 1e).

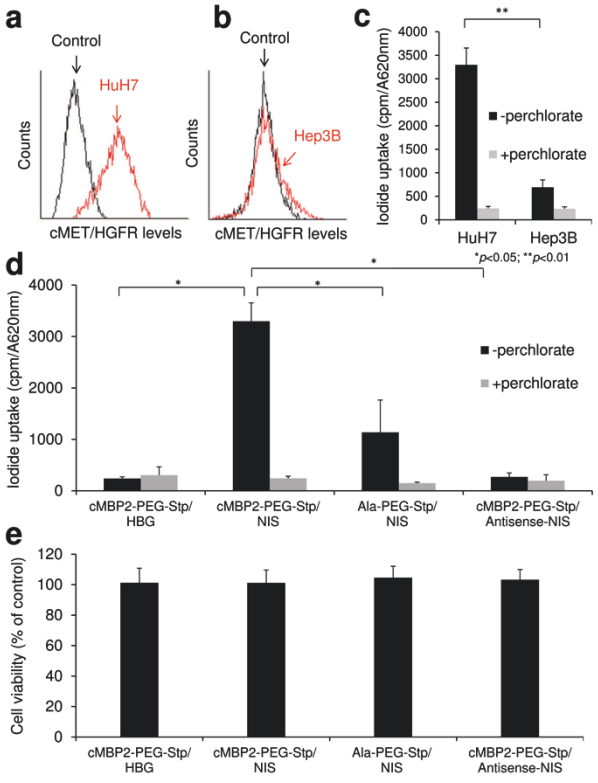

Fig. 1: *Surface expression of cMET/HGFR on HuH7 (**a**) and Hep3B cells (**b**) was analyzed by flow cytometry with an antibody that specifically detects human cMET/HGFR and compared to isotype controls.* ^{125}*I uptake levels were measured in HuH7 and Hep3B cells after in vitro transduction with cMBP2-PEG-Stp/NIS polyplexes (n=3) at an N/P ratio of 12 and results correlated well with cMET/HGFR expression levels (**c**). Further, to identify receptor specificity and NIS-dependency of iodide uptake, HuH7 cells were transfected with untargeted polyplexes Ala-PEG-Stp/NIS (n=3), cMBP2-PEG-Stp/Antisense-NIS (n=3) and polymer without DNA (n=3) (*p<0.05; **p<0.01) (**d**). Cell viability was not affected by polyplex-mediated gene transfer, as determined by MTT assay (n=3) (**f**). Results are reported as mean ± SEM. Polymer syntheses were performed by Stephan Morys (Department of Pharmacy, Pharmaceutical Biotechnology, LMU). Adapted from [46].*

In vivo iodide uptake studies after systemic NIS gene transfer

To evaluate vector biodistribution and functional NIS expression after cMET-targeted gene transfer in HuH7 tumor-bearing mice, animals received an intraperitoneal dose of ^{123}I 24 h or 48 h after intravenous application of polyplexes. Radioiodide biodistribution was assessed by gamma camera imaging and regions of interest were quantified. A considerably higher tumoral iodide uptake was observed in tumors of mice that received ^{123}I 48 h after application of cMBP2-PEG-Stp/NIS polyplexes as compared to 24 h (data not shown). For all subsequent *in vivo* experiments, radionuclide application was conducted 48 h after polyplex administration.

In contrast to high levels of radionuclide accumulation in 80% (7 out of 9) of tumors of mice treated with cMBP2-PEG-Stp/NIS (Fig. 2a), tumors of mice injected with the untargeted control polyplex Ala-PEG-Stp/NIS exhibited only weak tumoral iodide accumulation (Fig. 2b). No tumoral iodide uptake above background levels was measured after treatment with cMBP2-PEG-Stp/Antisense-NIS polyplexes (Fig. 2c). Physiological expression of NIS in thyroid and stomach resulted in iodide accumulation in theses tissues and, due to renal elimination of radioiodide, iodide uptake was also observed in the bladder. No additional iodide uptake was recorded in non-targeted organs such as lung, liver, kidney and spleen. NIS-specificity was confirmed by intraperitoneal application of the NIS-specific inhibitor sodium perchlorate 30 min prior to radionuclide application, which resulted in an almost complete inhibition of iodide uptake in the tumor and organs that physiologically express NIS (Fig. 2d). Serial scanning revealed a maximal ^{123}I accumulation of 6.6±1.6% ID/g (percentage of the injected dose per gram tumor) in NIS-transduced HuH7 xenografts with a biological half-life of 3 h (Fig. 2e). A tumor-absorbed dose of 41 mGy/MBq/g tumor with an effective half-life of 3 h for ^{131}I was calculated.

Ex vivo biodistribution studies after systemic NIS gene transfer

Ex vivo biodistribution was performed to further assess tumor-specific iodide uptake after systemic polyplex administration. 3 h after ^{123}I application, mice were sacrificed, organs dissected and subsequently measured in a gamma counter. *Ex vivo* biodistribution results correlated well with gamma imaging results, showing a perchlorate-sensitive tumoral

radioiodide uptake of 3% of the injected dose per organ in cMBP2-PEG-Stp/NIS-treated mice 3 h after injection of the radionuclide. Moreover, almost no iodide uptake was detected in non-target organs and tumors of control mice that received either Ala-PEG-Stp/NIS, cMBP2-PEG-Stp/Antisense-NIS or cMBP2-PEG-Stp/NIS and sodium perchlorate (Fig. 2f).

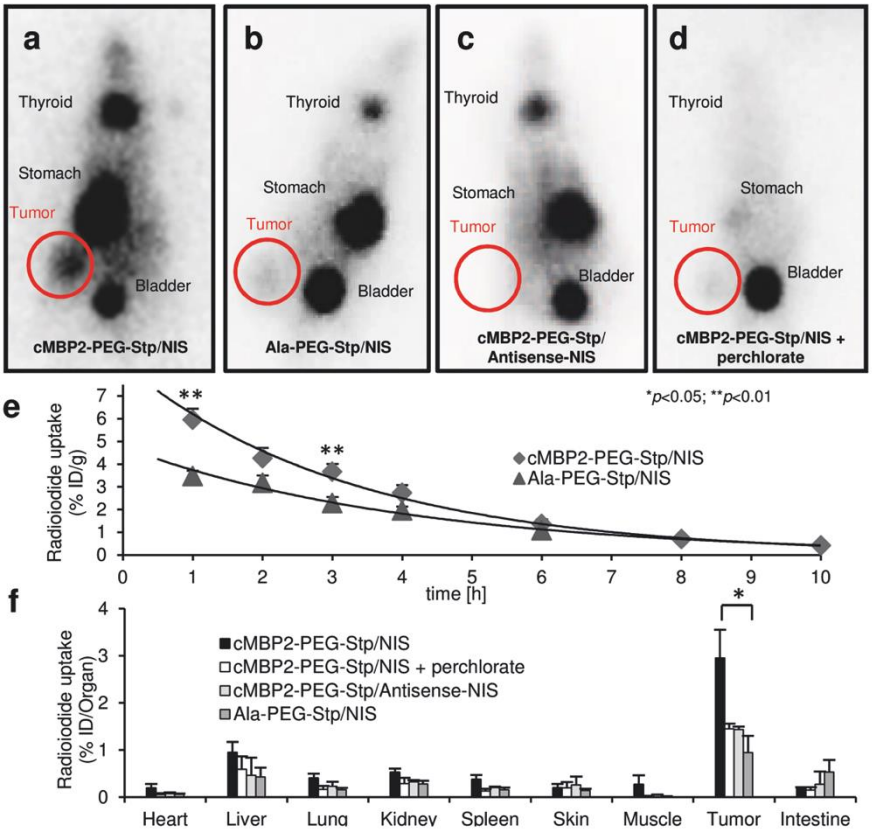

***Fig. 2**: 48 h after polyplex administration, vector biodistribution in mice bearing subcutaneous HuH7 xenografts was analyzed by ^{123}I-scintigraphy. Tumoral iodide uptake of cMBP2-PEG-Stp/NIS-treated mice (n=9) (**a**), Ala-PEG-Stp/NIS-treated mice, where the targeting ligand was replaced by alanine (n=5) (**b**), and cMBP2-PEG-Stp/Antisense-NIS treated mice (n=5) (**c**) was measured 3 h post radioiodide injection. A subset of cMBP2-PEG-Stp/NIS-treated mice was pretreated with the NIS-specific inhibitor perchlorate 30 min before ^{123}I application (n=6) (**d**). Iodide accumulation in tumors over the time and the biological half-life of ^{123}I were monitored by serial scanning (**e**). Ex vivo biodistribution was performed 3 h after injection of the radionuclide. Organs of cMBP2-PEG-Stp/NIS-treated mice without (n=6) and with sodium-perchlorate-pretreatment (n=3), Ala-PEG-Stp/NIS-treated mice (n=3) and cMBP2-PEG-Stp/Antisense-NIS-treated mice (n=3) were dissected and ^{123}I accumulation in single organs was measured by gamma-counting (**f**). Results are reported as mean ± SEM. Adapted from [46].*

Immunohistochemical analysis of NIS protein expression after polyplex-mediated gene transfer

Immunohistochemical analysis of NIS protein expression in HuH7 xenografts 48 h after cMET-targeted polyplex-mediated gene transfer revealed a heterogeneous staining pattern with multiple clusters of NIS-specific immunoreactivity in tumors of mice that received

cMBP2-PEG-Stp/NIS (Figs. 3a,b). In both control groups (Ala-PEG-Stp/NIS, cMBP2-PEG-Stp/Antisense-NIS) no specific NIS expression was detected (Figs. 3c,d), which is comparable to untreated tumor tissue (Fig. 3e).

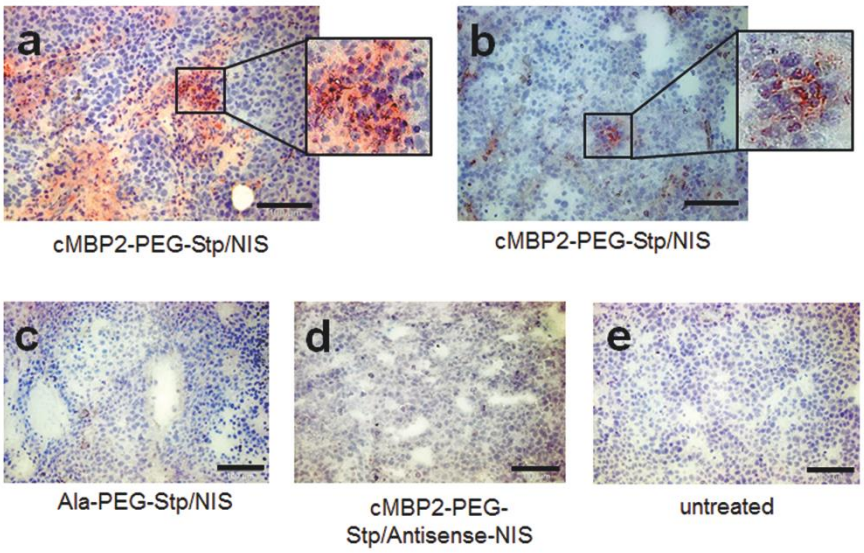

Fig. 3: (a-e) *NIS protein expression in HuH7 xenografts was analyzed by immunohistochemistry 48 h after cMET-targeted polyplex-mediated gene transfer on frozen tumor section from mice that received cMBP2-Stp-PEG/NIS (**a, b**), from mice that received control polyplexes (Ala-PEG-Stp/NIS (**c**), cMBP2-PEG-Stp/Antisense-NIS (**d**)) and from untreated mice (**e**). Scale bar=100 µm. Adapted from [46].*

Quantification of *NIS* mRNA expression by quantitative real-time PCR analysis

To determine *NIS* mRNA levels in HuH7 xenograft, mRNA was analyzed by quantitative real-time PCR (qPCR) 48 h after systemic NIS gene transfer (Fig. 3f). High levels of *NIS* gene expression were measured in tumors of cMBP2-PEG-Stp/NIS-treated mice and tumors of mice that received the NIS-specific inhibitor sodium perchlorate before administration of cMBP2-PEG-Stp/NIS. Lower *NIS* expression levels were observed in tumors of mice treated with Ala-PEG-Stp/NIS. No *NIS* expression above background levels were seen in cMBP2-PEG-Stp/Antisense-NIS-treated mice.

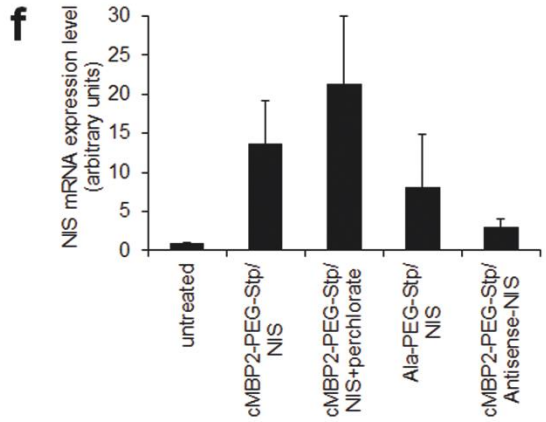

Fig. 3: (F) *Tumoral NIS mRNA expression levels after application of cMBP2-PEG-Stp/NIS with and without sodium-perchlorate pretreatment, Ala-PEG-Stp/NIS and cMBP2-PEG-Stp/Antisense-NIS were examined by qPCR (**f**). Adapted from [46].*

Radioiodide therapy studies after cMET-targeted non-viral NIS gene delivery

Therapeutic efficacy was evaluated after establishment of an optimal time scheme of repetitive polyplex and ^{131}I application. Mice received either cMBP2-PEG-Stp/NIS, Ala-PEG-Stp/NIS or cMBP2-PEG-Stp/Antisense-NIS followed by a therapeutic dose of 55.5 MBq ^{131}I or cMBP2-PEG-Stp/NIS followed by saline 48 h later. The cycle of gene transfer and radioiodine application was conducted three times on days 0/2, 3/5 and 7/9. Mice treated with cMBP2-PEG-Stp/NIS that received radioiodide showed a significant delay in tumor growth as compared to all control groups (Fig. 4a). This was associated with markedly improved survival (Fig. 4b). While mice of control groups had to be sacrificed within 3-4 weeks after onset of the therapy trial due to excessive tumor growth, mice treated with cMBP2-PEG-Stp/NIS and ^{131}I survived up to nearly 7 weeks.

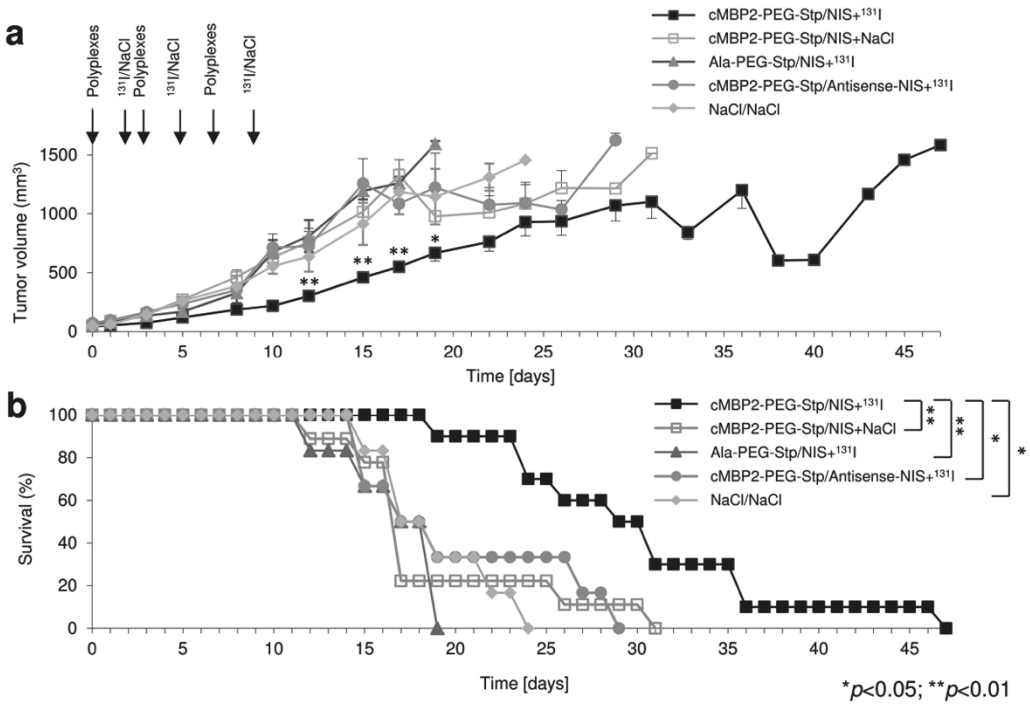

Fig. 4: *The cycle of intravenous gene transfer and radioiodide application was conducted three times on day 0/2, 3/5 and 7/9. Mice were treated either with cMBP2-PEG-Stp/NIS and 55.5 MBq ^{131}I (n=10), cMBP2-PEG-Stp/NIS followed by application of NaCl (n=9), Ala-PEG-Stp/NIS+^{131}I (n=6) or cMBP2-PEG-Stp/Antisense-NIS+^{131}I (n=6). Tumor volumes (**a**) and animal survival (Kaplan-Meier-Plot (**p<0.01)) (**b**) of the different therapy groups were compared. Results are either reported as mean ± SEM for tumor volumes or in percent for survival plots. Adapted from [46].*

Immunofluorescence analysis

After therapy, at the end of the observation period, mice were sacrificed, tumors dissected and tissues further processed for immunofluorescence analysis. A Ki67-specific antibody (green) was used to determine cell proliferation and an antibody against CD31 (red) labeled blood vessels (Figs. 5a-d). Tumors of animals treated with cMBP2-PEG-Stp/NIS that received ^{131}I, exhibited a significantly decreased proliferation and lower blood vessel density as compared to control groups (cMBP2-PEG-Stp/NIS+NaCl; cMBP2-PEG-Stp/Antisense-NIS+^{131}I; Ala-PEG-Stp/NIS+^{131}I) (Fig. 5e,f).

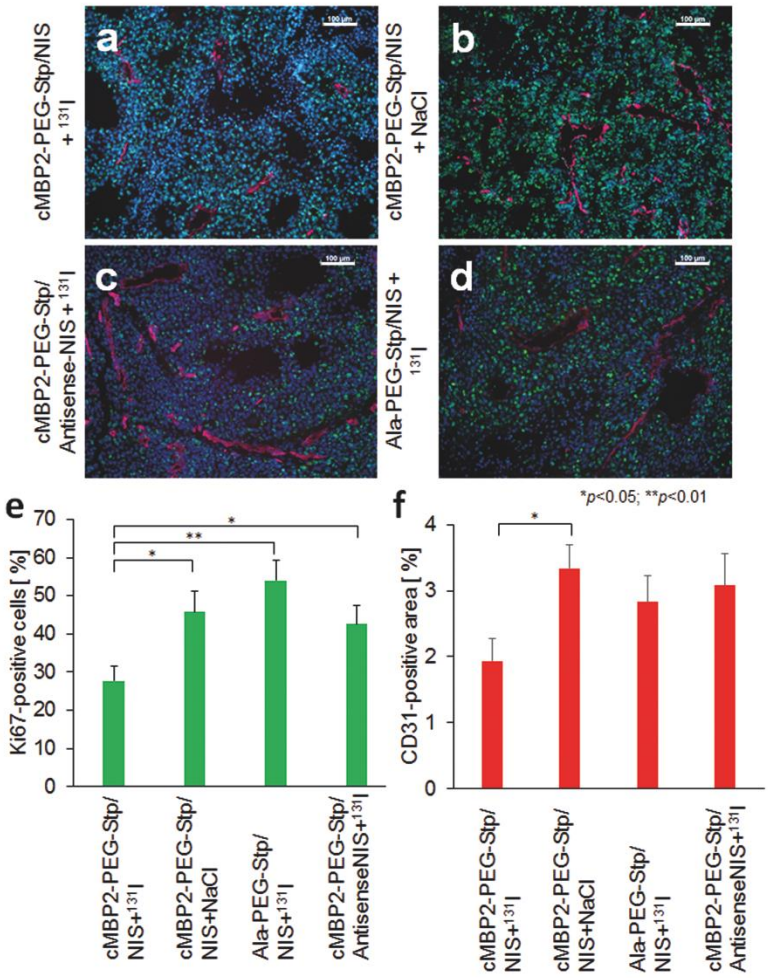

Fig. 5: *After treatment, when tumors reached a size of 1500mm^3, mice were sacrificed and tumors dissected. Frozen sections of tumor tissue were stained with a Ki67-specific antibody (green) to determine cell proliferation and an antibody against CD31 (red) to label blood vessels (**a-d**). Tumor cell proliferation (**e**) and blood vessel density (**f**) in tumors from animals treated with cMBP2-PEG-Stp/NIS that received ^{131}I (n=10) were compared to control groups treated with cMBP2-PEG-Stp/NIS+NaCl (n=8), Ala-PEG-Stp/NIS+^{131}I (n=6) or cMBP2-PEG-Stp/Antisense-NIS+^{131}I (n=6). Nuclei were counterstained with Hoechst. Results are reported as mean ± SEM. Scale bar=100 µm. Adapted from [46].*

6.5 Discussion

Gene therapy is emerging as a highly promising approach to disrupt cancer homeostasis through replacement or silencing of malfunctioning genes and insertion of new genes that directly kill cancer cells [10, 11]. In this context, NIS represents an ideal candidate gene for therapeutic intervention. Its unique capacity to act both as reporter and therapy gene allows us to monitor biodistribution of functional NIS expression by multimodal nuclear medicine imaging modalities and at the same time allows application of a therapeutic dose of ^{131}I [16, 48, 50, 97, 129, 188]. Currently, the NIS gene therapy concept is being evaluated in prostate cancer patients after local adenovirus-mediated NIS gene delivery (NCT00788307) [49, 174]. Moreover, the reporter function of NIS is being tested in various protocols in different cancer types, including head, neck, ovarian and peritoneal cancer to monitor biodistribution of genetically engineered oncolytic measles virus and mesenchymal stem cells that express NIS [51, 94, 130, 173, 193]. However, systemic application with its potential to target metastatic disease requires further improvement of shuttle systems, as the potential of therapeutic genes is highly dependent on efficient and tumor-selective delivery. The delivery pathway from injection site to distant tumor sites poses several major obstacles that need to be overcome [56, 57]. Besides nuclease-dependent stability of nucleic acids in blood circulation, stable complexes of nucleic acid and vector system need to be formed to achieve long-term persistence of systemically applied delivery vehicles. Further requirements include an enhanced safety profile for reduced interactions with blood components and low immunogenicity as well as high targeting specificity to minimize effects on non-target cells and to achieve sufficiently high gene expression levels specifically in tumor tissue. Additionally, after entering the target cell via endocytic cellular uptake, protection from lysosomal degradation along with efficient endosomal escape are crucial steps for intracellular delivery of genetic information [53, 56, 57].

In our previous preclinical studies, we investigated the potential of viral and non-viral vector systems to deliver the NIS gene to non-thyroidal tumor cells after systemic application [35-44, 47, 48, 93, 175, 194]. Viral vectors represent a highly efficient option due to their inherent capacity to insert their genetic material into host cells, as we have shown using different adenoviral vectors [35-37, 41, 93]. However, these vectors bear a series of limitations including high immunogenicity, unspecific cell tropism and uncontrolled insertion of DNA into the host genome [9, 53]. We further demonstrated the feasibility of non-viral delivery vehicles based on biodegradable pseudodendritic oligoamines and EGFR-targeted LPEI-PEG-polymers. Application of pseudodendritic polymers G2-HD-OEI in different tumor models led to high NIS-mediated tumoral iodide accumulation and subsequently high therapeutic efficiency. As there is no specific targeting ligand, tumor selectivity was mostly obtained by

high intrinsic tumor affinity through the so-called “enhanced permeability and retention” effect in these well-vascularized tumors with leaky blood vessel structure [38, 40, 165]. Active EGF-receptor targeting of LPEI-PEG-GE11 polymers via the GE11 ligand resulted in high specific iodide accumulation in tumor tissue. Receptor mediated uptake could be confirmed by pretreatment with the EGFR-specific antibody cetuximab showing significant decrease of polyplex uptake in tumor cells and NIS expression [39]. However, the main drawbacks of these non-viral delivery systems are the variable constitution and polydispersity as well as limited specificity of untargeted pseudodendritic oligoamines and the low biocompatibility and long-term toxicity of LPEI-derivatives. Consequently, for clinical application of synthetic non-viral gene delivery vehicles, it is indispensable to develop highly defined substances with improved efficiency, low immunogenicity and a precise, constant and easily reproducible structure.

These desirable features can be realized through the design of novel sequence-defined polymers with structure-activity relationships by solid-phase synthesis [66], allowing generation of precise backbones and incorporation of multiple functional groups. The optimal balance between the formation of stable polyplexes and efficient release of DNA at the target site is obtained by serial synthesis of artificial amino acid succinoyl-tetraethylenepentamine (Stp) repeats which contain a diaminoethane motif and form the basic polymer structure [68, 69]. This functional site exhibits optimal DNA condensation ability, equips the polymer with buffering amine functions and shows enhanced biodegradability and low toxicity compared to the “gold standard” LPEI. Terminal cysteines further support polyplex stabilization via disulfide bridges. For surface shielding, hydrophilic PEG domains are incorporated that reduce non-specific interactions with serum components, thus leading to a higher safety profile and lower immunogenicity of polyplexes. Additional histidines as protonatable amino acids with high buffering capacity are integrated to improve endosomal escape for adequate release of polymers in target cells [58, 69].

Active ligand-mediated targeting is an elegant method to enhance tumor specificity and thus amplify transgene expression in tumoral tissues while reducing side effects in non-target organs [57]. Active targeting is a prerequisite for clinical application, as polymer accumulation in tumor tissue by passive targeting is highly dependent on retention effects and leaky vascular structure [79, 80]. As growth factor receptors are often overexpressed and play a crucial role in tumor progression, promising candidates that act as ligands have been developed via phage display analysis with a focus on short peptides, as they are easy to synthesize and show high receptor affinity. In previous studies, we have already shown the efficacy of the short peptide GE11 for EGFR targeting [36, 39]. Another attractive target receptor in cancer therapy is cMET/HGFR. High surface expression levels and activation of cMET in a broad range of malignancies are implicated in tumor progression and metastasis

and are often associated with poor prognosis [190]. The cMET-binding peptide cMBP2 was identified as an ideal ligand with high receptor affinity that specifically enhances nanoparticle adhesion to the target cell without activating the receptor [69, 123, 191]. Peptide ligand specificity was confirmed by high cell binding of cMBP2-polyplexes to cMET/HGFR over-expressing prostate cancer cells DU145 [69] and HCC cells HuH7, in contrast to alanine ligand control and four different scrambled sequences of cMBP2 which showed no specific cellular binding [69]. Furthermore, a novel flow method to assess the potential of peptides to specifically bind to their receptors demonstrated sequence-specificity of cMBP2 in binding to the cMET/HGFR expressing HuH7 HCC cell line [123]. Therefore, in this study, we selected cMBP2 as ligand for our innovative sequence-defined cMET-targeted polymers to direct NIS expression to HuH7 HCC xenograft mouse model. The HCC cell line HuH7 represents an attractive platform for cMET-targeted non-viral gene delivery due to its high levels of endogenous surface expression of cMET/HGFR.

High levels of natural cMET expression on HuH7 cells were confirmed via flow cytometry analysis and expression levels were shown to correlate well with *in vitro* transfection efficiency of cMET-targeted polyplexes cMBP2-PEG-Stp/NIS in comparison to the low cMET expressing HCC cell line Hep3B. Further *in vitro* transfection studies using high cMET/HGFR-expressing HuH7 cells revealed an ideal ratio of 12 protonatable nitrogen groups in the polymer backbone per negatively charged phosphate in the nucleic acid (N/P), which resulted in optimal nucleic acid binding, very low toxicity and highest transfection levels. To optimize particle size and DNA compaction for subsequent *in vivo* application, the three-armed non-PEGylated polymer #689 (3-arm-Stp) was added at 30 molar percentage.

As a next step, we took further advantage of the reporter function of NIS to investigate transduction efficiency of cMET-targeted polyplexes *in vivo.* ^{123}I gamma camera imaging of vector biodistribution and functional NIS expression in HuH7 tumor-bearing mice revealed a high tumor-specific iodide uptake of 6.6±1.6% ID/g in cMBP2-Stp-PEG/NIS-treated mice 48 h after intravenous polyplex administration. Significantly lower tumoral iodide accumulation after injection of Ala-PEG-Stp/NIS polyplexes verified improved tumor-selective transduction efficiency of actively targeted polyplexes. The significantly lower, but measureable iodide uptake after transfection with untargeted Ala-PEG-Stp/NIS polyplexes is due to basal transduction efficiency of the untargeted polymer based on passive targeting effects through the so-called “enhanced permeability and retention” effect in well-vascularized tumors [38, 40, 165]. The significant differences in ^{123}I uptake of cMET-targeted polyplexes in comparison to untargeted polyplexes *in vivo* underline the remarkable targeting-effects of the cMBP2 ligand. Pretreatment with the NIS-specific inhibitor sodium perchlorate in a subgroup of cMBP2-PEG-Stp/NIS-treated mice as well as an additional control group treated with cMBP2-PEG-Stp/Antisense-NIS polyplexes led to comparably low iodide uptake

demonstrating NIS-specificity. Data obtained by *ex vivo* biodistribution correlated well with results from gamma camera imaging, showing a tumoral iodide accumulation of 3.0±0.5% ID/organ in cMBP2-PEG-Stp/NIS-treated mice 3 h post ^{123}I application. In addition, no specific iodide accumulation was observed in tumors of control mice and non-target organs, confirming tumor specificity of gene delivery vehicles based on active cMET-targeting. These results clearly demonstrate targeting specificity of cMBP2 as cMET-binding peptide and the efficacy of our novel sequence defined polymers as gene delivery vehicles.

After successfully demonstrating the feasibility of this polyplex-mediated NIS gene therapy approach *in vitro* and *in vivo* taking advantage of NIS in its function as reporter gene, we addressed the question whether tumor-specific transduction is sufficiently high for a therapeutic effect. After three cycles of repetitive polyplex and radioiodide application, a significant reduction in tumor growth was observed in mice treated with cMBP2-PEG-Stp/NIS. This was associated with a prolonged survival of up to nearly 7 weeks, whereas animals of control groups had to be sacrificed within 3-4 weeks. Immunohistochemical staining revealed a heterogenous staining pattern with clusters of membrane associated NIS-specific immunoreactivity. As NIS gene therapy is associated with a high bystander effect based on the crossfire effect of the beta-emitter ^{131}I, the cytotoxic effect is not only limited to transduced cells, but also affects surrounding cells increasing therapeutic effectiveness of the NIS gene therapy concept. These findings were confirmed by immunofluorescence analysis of tumors after treatment: tumors from animals treated with cMBP2-PEG-Stp/NIS exhibited reduced cell proliferation and blood vessel density as compared to all control groups. As the immunofluorescence analysis experiments were performed at the end of the observation period, i.e. at different time points in the control group vs. therapy group, in which mice were sacrificed at a later stage, other factors such as mouse age, might influence the results. However, as mice were sacrificed in the therapy group when significant regrowth of tumors had occurred, our results probably even underestimate the antiproliferative and antiangiogenic effects of ^{131}I therapy following cMBP2-PEG-Stp/NIS-mediated NIS gene transfer.

In our studies, a therapeutic dose of 55.5 MBq ^{131}I (1.5 mCi) was used [35-42, 93] based on initial tests on radiation safety, tolerability and efficacy [35, 93]. The Food and Drug Administration of the United States (FDA) formulated a table of dose conversion factors that allows for allometric adaption from preclinical animal models to humans based on body surface area (BSA) [195]. Using this method, the mouse dose of 55.5 MBq translates to 13.9 GBq (372 mCi) for a 75kg human being, which lies within the dosimetrically determined dose range (300 mCi – 600 mCi) in patients with advanced metastasized differentiated thyroid cancer [91]. In order to keep potential toxicities at a minimum, the calculated dose should not represent a fixed applicable dose, but a dose range that needs to be adjusted in a

personalized manner considering various factors including the radiation sensitivity of the tumor, co-morbidities of the patient and pretreatments. In this context, the concept of the theranostic application of the NIS gene allows optimal adjustment of the ^{131}I dose based on exact dosimetric calculations of doses to the tumor and other organs from radioiodine imaging studies to limit side effects to non-target organs including bone marrow, spinal cord, salivary glands, upper gastrointestinal tract, kidneys and bladder.

Based on these promising preclinical results, the next crucial step towards clinical application will be a toxicity study, specifically designed to assess potential toxicities arising from cMBP2-PEG-Stp/NIS application followed by saline or ^{131}I application. For this purpose, naive mice without tumor will be used, cMBP2-PEG-Stp/NIS will be injected i.v. as well as directly into critical organs such as the liver and lungs, followed by assessment of toxicity by physical examination, blood and tissue sampling at early, intermediate and late time points (such as 1 week up to 3 months).

Our data clearly demonstrate the therapeutic efficacy of cMET-targeted NIS gene therapy. Combined with our previous results targeting NIS to EGFR on tumor cells using the peptide GE11, this opens the exciting prospect of a possible future combination of these two targeting agents. The concept of dual targeting mimicks the natural process of viral cellular uptake, as several viruses, including adenoviruses, target two receptor types for so-called biphasic cell entry. The synergistic effects of targeting the receptors for EGF and transferrin using synthetic polymers have already been explored *in vitro* [68]. Studies postulating crosstalk between EGFR and cMET on cancer cells further substantiate the potential of dual targeting of these two receptors, especially as cMET amplification has been implicated in resistance mechanisms to escape EGFR-targeted therapy [85, 86, 196, 197].

In conclusion, our data demonstrate the enormous potential of sequence-defined polymers for cMET-targeted NIS gene delivery. The precise synthesis of these novel polymers allows for optimized transfection efficiency while eliminating adverse effects such as toxicity or high immunogenicity. High cMET expression levels on many cancer cells make this receptor an ideal target in cancer therapy. Combined with the unique theranostic function of NIS, our targeting strategy led to significant tumoral iodide uptake that was sufficient for potent therapeutic effects after ^{131}I application. This innovative concept of active receptor-targeted non-viral gene delivery is of high clinical relevance as it optimizes efficacy and safety of systemic NIS gene delivery and opens the exciting prospect of application in metastatic disease.

6.6 Acknowledgments

We are grateful to Sissy M Jhiang (Ohio State University, Columbus, OH, USA) for supplying the full length human NIS cDNA. We thank Roswitha Beck, Rosel Oos, Franz-Josef Gildehaus and Andreas Delker (Department of Nuclear Medicine, Ludwig-Maximilians-University, Munich, Germany), as well as Eva Kessel and Markus Kovac (Department of Pharmacy, Center of Drug Research, Pharmaceutical Biotechnology, Ludwig-Maximilians-University, Munich, Germany) for their assistance with animal care and imaging studies. This work was supported by grants from the Deutsche Forschungsgemeinschaft within the Collaborative Research Center SFB824 (project C 08) to C Spitzweg as well as within the Priority Programme SPP1629 to C Spitzweg and PJ Nelson (SP 581/6-1, SP581/6-2, NE 648/5-2), the Cluster of Excellence Nanosystems Initiative Munich (NIM) to E Wagner and by a grant from the Wilhelm-Sander-Stiftung to C Spitzweg (2014.129.1).

7. EGFR targeting and shielding of pDNA lipopolyplexes via bivalent attachment of a sequence-defined PEG agent

This chapter has been adapted from:

Morys S[1+], **Urnauer S**[2+], Spitzweg C[2], Wagner E[1]. EGFR targeting and shielding of pDNA lipopolyplexes via bivalent attachment of a sequence-defined PEG agent. Macromol Biosci. 2017. [in press]

[1]Pharmaceutical Biotechnology, Center for System-Based Drug Research and Center for Nanoscience (CeNS), LMU Munich, 81377 Munich, Germany, [2]Department of Internal Medicine IV, University Hospital of Munich, LMU Munich, 81377 Munich, Germany

[+] *Authors contributed equally*

Stephan Morys performed syntheses of polymers as well as analytical and chemical experiments. Sarah Urnauer performed all cell association and uptake studies as well as transfection experiments. Contributions of authors to the experiments are listed in the respective passage.

7.1 Abstract

For successful nonviral gene delivery, cationic polymers are promising DNA carrier which need to comprise several functionalities. The current work focuses on the post-incorporation of epidermal growth factor receptor (EGFR) targeted PEGylation agents onto lipopolyplexes for pDNA delivery. T-shaped lipo-oligomers were previously found to be effective sequence-defined carriers for pDNA and siRNA. Here, the bis-oleoyl-oligoaminoethanamide ***454*** containing tyrosine trimer-cysteine ends was applied for complex formation with pDNA coding for luciferase or sodium iodide symporter (NIS). In a second step, the lipopolyplexes were modified via disulfide formation with sequence-defined monovalent or bivalent PEGylation agents containing one or two 3-nitro-2-pyridinesulfenyl (NPys)-activated cysteines, respectively. For targeting, the PEG agents comprise the EGFR targeting peptide GE11. In comparison of all transfection complexes, ***454*** lipopolyplexes modified with the bidentate PEG-GE11 agent showed the best, EGFR-dependent uptake as well as luciferase or NIS gene expression into receptor-positive tumor cells.

7.2 Introduction

The growing global incidence of cancer entailed intense research for novel alternative treatment strategies [146]. One promising direction is cancer gene therapy, which offers the possibility to interfere in the complex process of tumorigenesis, invasion and metastasis formation [10, 198]. However, the capability to change, add, modulate and knock-out tumor specific gene information is highly dependent on the efficacy of nucleic acid delivery systems. These carriers should ensure high tumor specific transfection efficiency along with sustained stability and biocompatibility. As viral vector particles face disadvantages concerning immunobiocompatibility, safety and toxicity, nonviral vectors might present an alternative nanoscale delivery platform with flexible design strategies [9, 53, 56, 65, 105, 199].

First-generation cationic polymers, like polyethylenimine (PEI) and polyamidoamine (PAMAM) dendrimer, demonstrated high efficiency but at the same time exhibited drawbacks regarding polydispersity, low degradability and toxicity. Within the last two decades these drawbacks have been dealt with by introducing biodegradable polymers and functional modifications including shielding and targeting domains [56]. Precision polymers can be generated with improved polymer chemistry; alternatively, sequence-defined peptide-like polymers can be generated by solid-phase assisted synthesis (SPS) [56]. Our work initiated from the chemical repeat unit of PEI, which is thought to be responsible for favorable nucleic acid binding as well as endosomal buffering [63], and resulted in the development of artificial amino acids containing the aminoethylene motif [66, 200, 201]. These artificial building blocks were assembled by SPS together with other artificial or natural units into sequence-defined oligomers for use in intracellular nucleic acid or protein delivery [58, 83, 139, 202-209]. Colloidal and biological characteristics of nucleic acid nanoparticles can be improved by incorporation of hydrophilic polymers such as polyethylene glycol (PEG) or *N*-(2-hydroxypropyl)methacrylamide (HPMA). These and related agents [71-73, 210-215] were found to shield against aggregation or undesired biological interactions. However, covalent modification of cationic carriers with hydrophilic chains may also diminish nanoparticle compaction and other favorable properties [76, 77, 215]. Post-integration of shielding agents into preformed nanoparticles emerged as encouraging alternative to avoid such unfavorable effects [75, 133, 216-222]. Use of shielding agents with multivalent attachment sites proved to be especially effective, as improved shielding synergizes with lateral stabilization of the nanoparticle by crosslinking the carrier molecules [216, 217, 219, 222].

In the present study, our aim was to generate novel shielded pDNA lipopolyplexes by either monovalent or bivalent attachment of targeted PEG agents. For the assembly of pDNA core nanoparticles, we selected a T-shaped, cysteine-containing bis-oleoyl-oligoethanaminoamide

(compound ***454***). This lipo-oligomer was originally developed for siRNA delivery and contains nanoparticle-stabilizing tyrosine trimers and cysteines [204]. After polyplex with internal disulfide formation, the remaining cysteine thiols on the polyplex surface are supposed to be available for reacting with 3-nitro-2-pyridinesulfenyl (Npys) activated Cys-PEG reagents. For tumor-targeting, shielding should go hand in hand with active targeting [223, 224]. For this purpose, specific attachment to the epidermal growth factor receptor (EGFR) by the phage library-derived peptide GE11 was considered. EGFR is overexpressed in most cancer types [151, 225] and has already been shown as an effective target for nucleic acid delivery by using various receptor-binding ligands [39, 68, 119, 138, 151, 218, 226-232]. Thus, as described in the following, four different PEGylation agents, without or with GE11 targeting peptide, with monovalent or bivalent attachment linkers, were synthesized by sequence-controlled SPS. A clear effect of the ligand and the linker bivalency was demonstrated in cellular uptake and gene transfer studies into receptor-positive Huh7 and MCF-7 tumor cells. The transfection efficacy of the most effective bidentate PEG-GE11 pDNA nanoparticle was further demonstrated and confirmed on a functional level by using the theranostic sodium iodide symporter (NIS) gene [29, 30, 33, 38, 42, 46, 47, 151].

7.3 Materials and methods

Materials

2-Chlorotrityl chloride resin was obtained from Iris Biotech (Marktredwitz, Germany), Fmoc-Ala-Wang resin was obtained from Novabiochem (Darmstadt, Germany), 2-(1*H*-benzotriazol-1-yl)-1,1,3,3-tetramethyluronium-hexafluorophosphate (HBTU), benzotriazole-1-yl-oxy-tris-pyrrolidino-phosphonium hexafluorophosphate (PyBOP) and syringe reactors (PP reactor with PE frit) from Multisyntech GmbH (Witten, Germany). The synthesis of the cationic building block Fmoc-Stp(Boc)3-OH was prepared as described by Schaffert et al [66]. All amino acids, dimethylformamide (DMF) as well as *N*-methylpyrrolidon (NMP) both peptide grade, *N*,*N*-diisopropylethylamine (DIPEA) and trifluoroacetic acid (TFA) were used from Iris Biotech (Marktredwitz, Germany). Dithiothreitol (DTT), 5,5'-dithiobis-(2-nitrobenzoic acid (DTNB), 1-hydroxy-benzotriazole (HOBt), triisopropylsilane (TIS), dimethylsulfoxide (DMSO), 3-(4,5-dimethylthiazol-2-yl)-2,5-diphenyltetrazolium bromide (MTT), *N*-Fmoc-*N´*-succinyl-4,7,10-trioxa-1,13-tridecanediamine (STOTDA), oleic acid and Triton X-100 as well as 1,2-ethanedithiol (EDT) were purchased from Sigma-Aldrich (Munich, Germany). *N*-hexane and *tert*-butyl methyl ether (MTBE) were obtained from Brenntag (Mühlheim an der Ruhr, Germany). Dichloromethane (DCM) was obtained from Bernd Kraft (Duisburg, Germany). Fmoc-*N*-amido-dPEG24-acid® was purchased from Quanta Biodesign (Powell, OH, USA). All solvents and other reagents were acquired from Sigma-Aldrich (Munich, Germany), Iris Biotech (Marktredwitz, Germany), Merck (Darmstadt, Germany) or AppliChem (Darmstadt, Germany). All cell culture consumables were obtained from Sarstedt (Nümbrecht, Germany). DMEM and DMEM/F12 were purchased from Sigma Aldrich (Munich, Germany). Fetal bovine serum (FBS), cell culture media, and antibiotics were purchased from Invitrogen (Karlsruhe, Germany), glucose from Merck (Darmstadt, Germany), HEPES from Biomol GmbH (Hamburg, Germany), and sodium chloride from Prolabo (Haasrode, Belgium). Agarose NEEO Ultra-Qualität was obtained from Carl Roth GmbH (Karlsruhe, Germany) and GelRed™ from VWR (Darmstadt, Germany). Heparin sulfate was purchased from Ratiopharm (Ulm, Germany) with 5000 IU/mL. Luciferase cell culture 5× lysis buffer and D-luciferin sodium were obtained from Promega (Mannheim, Germany). DNA plasmids (pCMVLuc [233]; CMV: cytomegalovirus promotor and enhancer*;* Luc: firefly luciferase gene and pCpG-hCMV-NIS [39]; human NIS plasmid DNA driven by the human elongation factor 1α promotor and human cytomegalovirus enhancer element) were prepared by Plasmid Factory GmbH (Bielefeld, Germany).

Peptide synthesis

All syntheses were performed by Stephan Morys (Department of Pharmacy, Pharmaceutical Biotechnology, LMU). Peptide synthesis was carried out using Fmoc-chemistry and L-amino acids. Prior to synthesis, 2-chlorotrityl chloride resins were loaded with the appropriate C-terminal amino acids. For synthesis of GE11 targeting peptide (YHWYGYTPQNVI), a resin preloaded with Fmoc-L-Ile-OH was used. The peptide sequence was assembled with an automated Syro Wave (Biotage, Uppsala, Sweden) peptide synthesizer equipped with a microwave cavity. Double couplings were performed at 50 °C for 12 min prior to 5 repetitive washing steps. Per coupling and free amine 4 equivalent (eq) of HBTU, 8 eq of DIPEA, 4 eq of HOBt, and 4 eq of Fmoc-protected amino acid were added on the solid support; the solution was supplemented with 1% Triton X-100 (*v*/*v*). Amino acids and HOBt were dissolved in NMP, supplemented with Triton-X. HBTU was dissolved in DMF and DIPEA diluted with NMP. Fmoc removal was conducted by standard deprotection methods with 40% piperidine in DMF (*v*/*v*) supplemented with 1% Triton-X for 5 × 10 min. The peptide sequence was built by sequentially coupling Fmoc-L-Val-OH, Fmoc-L-Asn(Trt)-OH, Fmoc-L-Gln(Trt)-OH, Fmoc-L-Pro-OH, Fmoc-L-Thr(tBu)-OH, Fmoc-L-Tyr(tBu)-OH, Fmoc-L-Gly-OH, Fmoc-L-Tyr(tBu)-OH, Fmoc-L-Trp(Boc)-OH, Fmoc-L-His(Trt)-OH and Fmoc-L-Tyr(tBu)-OH. After the last coupling an analytical cleavage of a small fraction for MALDI-MS and HPLC was done. Data can be found in Figure S14 and S15.

In case of pre-PEGylated oligomer ***440*** a commercially available Wang resin, preloaded with Fmoc-L-Ala-OH low-loaded (LL) was deprotected as described in SI, in case of ***835***, the GE11 peptide loaded resin (prepared as described above) was used. As coupling of $dPEG_{24}$ represents a crucial step in synthesis, this step was conducted manually, and successful coupling and deprotection was monitored by Kaiser test [234]. Coupling was performed for 1 h under steady shaking with 4 eq of PyBOP, 8 eq of DIPEA, 4 eq of HOBt and 4 eq of Fmoc-*N*-amido-$dPEG_{24}$-acid dissolved in 50:50 (v/v) of DCM/DMF. Deprotection was performed as described before by addition of 40% piperidine in DMF (v/v) for 5 × 10 min. Then both reactors were placed in the automated Syro Wave (Biotage, Uppsala, Sweden) peptide synthesizer and cationic backbones were synthesized in parallel. Reagents were prepared as for synthesis of GE11 and double couplings were performed at RT for 1 h each. First Fmoc-L-His(Trt)-OH, followed by Fmoc-L-Lys(Fmoc)-OH for symmetrical branching, was attached. Fmoc-L-His(Trt) and our novel building block Fmoc-Stp$(boc)_3$-OH (Stp: succinyl-tetraethylene pentamine; Boc: *tert*-butyloxycarbonyl) were attached alternately four times, leading to five histidines and four Stp units. Synthesis was terminated by coupling of Boc-L-Cys(Trt)-OH.

Oligomer ***454*** was synthesized on a 2-chlorotrityl chloride resin preloaded with Fmoc-L-Cys(Trt)-OH. The resin was placed in the microwave cavity of the Syro Wave peptide synthesizer (Biotage, Uppsala, Sweden). The cationic backbone, was attached using the

protocol described above. First Fmoc-L-Tyr(tBu)-OH was coupled three times, then the artificial amino acid Fmoc-Stp(boc)$_3$-OH was coupled twice. Fmoc-L-Lys(Dde)-OH served as a mirror axis so again two Fmoc-Stp(boc)3-OH and three times Fmoc-L-Tyr(tBu)-OH were coupled. Coupling of Boc-L-Cys(Trt)-OH at room temperature for 2 x 1 h terminated the cationic backbone. To introduce the hydrophobic domains, Dde removal was conducted with 4% hydrazine in DMF (v/v) for 15 cycles lasting 3 min each. Then Fmoc-L-Lys(Fmoc)-OH was coupled for symmetrical branching prior to attaching oleic acid on both arms.

PEGylation agents were either synthesized on a preloaded Ala-Wang resin (for the Ala control reagent) or were attached to GE11 previously assembled on the solid support as described above (for the targeting reagent). First Fmoc-*N*-amido-dPEG$_{24}$-acid was coupled manually. Then each resin was split in two parts, and either Boc-L-Cys(Npys) in case of monovalent reagent, or Fmoc-L-Lys(Fmoc)-OH in case of the bivalent reagent, was coupled. In case of the bivalent PEG agents, STOTDA was introduced as a short spacer before terminating the sequence by coupling of Boc-L-Cys(NPys)-OH. The resins were dried under high vacuum and then cleavage was conducted. In case of oligomers ***440***, ***835*** and ***454*** a cleavage cocktail TFA/EDT/H_2O/TIS 94:2.5:2.5:1 (v/v) at a ratio of 10 mL/g resin and in case of post-PEGylation agents TFA/H_2O/TIS 95:2.5:2.5 was chosen. Cleavage was conducted for 90 min with the exception of ***454***, here the cleavage solution was precooled to 4°C and cleavage was only performed for 30 min to prevent side reaction at the double bond of the oleic acid (S. Reinhard, W. Zhang, E. Wagner, accepted manuscript). The cleaved oligomers were precipitated in a 50:50 (v/v) mixture of n-hexane/MTBE and purified by size exclusion chromatography (SEC) performed with 10 mM hydrochloric acid/acetonitrile 7:3 as solvent. An ÄKTA purifier system (GE Healthcare Biosciences, Uppsala, Sweden) equipped with a Sephadex G-10 column and a P-900 solvent pump module, a UV-900 spectrophotometrical detector, a pH/C-900 conductivity module and a Frac-950 automated fractionator were used. The product fractions were collected and combined prior to lyophilization. Analytical data (MS data (Maldi or ESI respectively) and RP-HPLC) of all structures can be found in Figures S14-S28. LPEI-PEG$_{2k}$-GE11 was synthesized and analyzed as described before [139].

Polyplex formation

Indicated amounts of pDNA and oligomer at a nitrogen/phosphate (N/P) ratio of 12 were diluted in separate tubes. If not mentioned otherwise, suspension media was 20 mM HEPES buffered 5% glucose at pH 7.4 (HBG 7.4). Diluted oligomer and diluted pDNA were mixed at similar volume. For N/P ratio calculation, only the protonatable amino groups of the Stp units and N-terminal amines of cysteine residues were considered (N number) and related to the anionic phosphate groups (P number) in pDNA. The nucleic acid was added to the oligomer, mixed vigorously, and incubated for 30 min at room temperature under air exposure to

enhance disulfide formation. In case of ***454***, if indicated, PEGylation agents calculated as molar eq per –SH in ***454*** were added, carefully mixed and incubated for further 15 min.

Particle size and zeta potential

Particle size and zeta potential of polyplexes were measured by Stephan Morys (Department of Pharmacy, Pharmaceutical Biotechnology, LMU) by dynamic laser-light scattering (DLS) using a Zetasizer Nano ZS (Malvern Instruments, Worcestershire, UK) and transmission electron microscopy (TEM) with a JEM 1011 (Jeol, Freising, Germany).

For DLS measurements, 2 µg pDNA was dissolved in 30 µL HBG and was added to an amount of oligomers corresponding to N/P 12 in 30 µL HBG. After 30 min of incubation at room temperature, 0.5 or 1.0 eq of PEGylation agents were added, if indicated and after incubation at RT for further 15 min, 740 µL of 10 mM sodium chloride solution (pH 7.4) was added and the samples were measured. Results were plotted as Z-Average and SD out of three runs with 12 sub-runs each. Zeta potential (ZP) is displayed as average (mV) of three runs with up to 15 sub-runs each.

For TEM, samples were prepared as follows. The formvar/carbon-coated 300 mesh copper grids (Ted Pella Inc., Redding, CA, USA) were activated by mild plasma cleaning. Afterwards, the grids were incubated with 20 µL of the polyplex solution at N/P 12 for 2.5 min. Polyplexes were previously prepared in water with 1 µg pDNA / 0.1 ml. Excess liquid was blotted off using filter paper until the grid was almost dry. Prior to staining, the grids were washed with 5 µL of staining solution for 5 s. Then, the copper grids were incubated with 5 µL of a 2% aqueous uranylformate solution for 5 s, excess liquid was blotted off using filter paper, followed by air-drying for 30 min. Samples were then analyzed at 80 kV.

Ethidium bromide compaction assay and polyanionic stress test

Experiments were performed by Stephan Morys (Department of Pharmacy, Pharmaceutical Biotechnology, LMU). Polyplexes containing 2 µg pDNA were formed at N/P ratio of 12 in a total volume of 200 µL HBG. LPEI polyplexes formed at N/P 12 served as positive control. If indicated, PEG agents were added at indicated ratios. HBG buffer (200 µL) served as blank and 2 µg pDNA in 200 µL HBG buffer was considered as maximum ethidium bromide (EtBr) fluorescence intensity (100% value). These samples were prepared in parallel to the polyplexes. After incubation at room temperature, 700 µL of EtBr solution (c = 0.5 µg/mL) was added. The fluorescence intensity of EtBr was measured after an additional 3 min incubation using a Cary Eclipse spectrophotometer (Varian, Germany) at the excitation wavelength λex = 510 nm and emission wavelength λem = 590 nm. The fluorescence intensity of EtBr was determined in relation to free pDNA. As a further experiment, 250 IU of

heparin (Ratiopharm, Ulm, Germany) was added to the samples after EtBr addition to investigate polyplex stability against polyanionic stress.

Cell culture

The human hepatocellular carcinoma cell line Huh7 was cultured in Dulbecco's Modified Eagle's Medium (DMEM) (1 g/L glucose), the human breast cancer cell line MCF-7 was cultured in DMEM high glucose (4.5 g/L glucose) and the human follicular thyroid carcinoma cell line FTC-133 was cultured in DMEM/F12. All media were supplemented with 10% fetal bovine serum (FBS), 100 U/mL penicillin and 100 µg/mL streptomycin. Cell lines were cultured at 37 °C and 5% CO2 in an incubator with a relative humidity of 95%.

In vitro gene transfer and metabolic activity of transfected cells (MTT assay)

Cells were seeded 24 h prior to pDNA delivery. For determining luciferase activity, 10,000 cells/well were seeded in 96-well plates. Transfection efficiency of oligomers at N/P 12 was evaluated using 200 ng pCMVLuc per well. Where indicated, PEGylated complexes were used. Before treatment, cells received 80 µL of fresh medium containing 10% FBS. Polyplex solution (20 µL) was added to each well and incubated on cells at 37 °C for either 45 min or 24 h. In the first case, medium was replaced 45 min after transfection by fresh medium. In the second case, cells were incubated with polyplex solution for 24 h after initial transfection. All experiments were performed in quintuplicate. LPEI or LPEI-PEG_{2k}-GE11 (N/P 6) was used as a positive control and HBG buffer served as negative control. Luciferase activity of cells was determined after lysis with 100 µL lysis buffer using a Centro LB 960 plate reader luminometer (Berthold Technologies, Bad Wildbad, Germany) and LAR buffer supplemented with 1 mM luciferin. Transfection efficiency was evaluated as relative light units (RLU) per well.

For determining iodide uptake activity after NIS gene delivery, 200,000 cells/well were plated in 6-well plates. Transfection efficiency of oligomers at N/P 12 was evaluated using 2 µg hNIS pDNA. After 24 h incubation with polyplexes, cells were washed with HBSS (Hank's Balanced Salt Solution; Thermo Fisher Scientific, Waltham, USA) and then incubated with HBSS supplemented with 10 µm NaI, 0.1 µCi of $Na^{125}I$ / ml and 10 mm HEPES at pH 7.3 for 45 min at 37°C. Sodium perchlorate (NaClO4; 100 µM) as NIS-specific inhibitor was added to control wells. After incubation with iodide, cells were washed with HBSS and trapped iodide was removed from cells by a 20 min incubation in 1 M NaOH and measured by γ-counting and expressed as counts per minute (cpm).

Metabolic activity of transfected cells was determined 24 h after initial transfection. 10 µL of MTT (5 mg/mL) was added to each well in 96-well plates and 200 µL was added to each well

in 6-well plates. Medium with unreacted dye was removed after incubation for 2 h at 37 °C and washed with PBS (phosphate-buffered saline).
Absorbance was determined after incubation with 10% DMSO (dimethyl sulfoxide) in isopropanol by using a Sunrise microplate absorbance reader (Tecan, Männedorf, Switzerland) at 620 nm. The relative cell viability (%) related to the buffer-treated control cells was calculated as ([A] test/[A] control) × 100%.

Cellular association and internalization

Huh7 and MCF-7 cells were seeded 24 h prior to transfection into 24-well plates at a density of 50,000 cells/well. Culture medium was replaced with 400 µL fresh growth medium 24 h after seeding the cells. pDNA polyplexes were formed with oligomers (N/P 12) and 1 µg pCMVLuc (20% of Cy5-labeled pCMVLuc) and incubated for 30 min in 100 µL HBG. PP-agents were, if indicated, co-incubated for further 15 min prior to addition to cells. In case of cellular association, polyplexes were added to cells and incubated for 30 min on ice. Subsequently, cells were washed twice with 500 µL PBS, detached with trypsin/EDTA and resuspended in PBS with 10% FBS.
Cellular internalization was determined after polyplex addition and incubation at 37 °C for 45 min. Subsequently, cells were incubated with 500 µL PBS containing 1000 IU heparin for 15 min on ice to remove any polyplexes sticking to the cell surface and afterwards washed once with 500 µL PBS. Cells were detached with trypsin/EDTA and resuspended in PBS with 10% FBS.
Cellular association and internalization of polyplexes was measured by excitation of Cy5 at 635 nm and detection of emission at 665 nm. PI was used to discriminate between viable and dead cells. Cells were properly gated by forward/sideward scatter and pulse width for exclusion of doublets.

Statistical analysis

Statistical analysis of the results (mean ± SD) was evaluated by unpaired t test: *$p < 0.05$; **$p<0.01$; ***$p < 0.001$; ****$p < 0.0001$.

7.4 Results and discussion

pDNA nanoparticle design, peptide and oligomer syntheses

As published in 2001 by Blessing et al [218], EGF-PEG-PEI pDNA polyplexes were successfully generated by two different methods; either via pre-conjugation of PEI (25 kDa) with EGF before pDNA complex formation, or by post-modification of previously formed PEI/pDNA polyplexes. Also in the current study, the pre- and post-modification strategy was compared for generation of EGFR-targeted polyplexes. Instead of PEI 25kDa, in the novel investigation shorter sequence-defined oligomers were applied as pDNA carriers, with far higher biocompatibility and chemical precision (Table 1). Instead of EGF as targeting ligand, the phage-display derived EGFR targeting peptide GE11 (YHWYGYTPQNVI) [235] was applied; and instead of polydisperse PEG linkers, a precise monodisperse PEG of exactly 24 ethylenoxide repeats ($dPEG_{24}$) was used. Like all other components, also the PEG agents required for the post-modification strategy (Table 2) were synthesized in precise fashion by solid-phase synthesis, with the majority of steps performed in an automated form using a peptide synthesizer. Analytical data can be found in Figures S14-S28 [performed by Stephan Morys (Department of Pharmacy, Pharmaceutical Biotechnology, LMU].

ID	Abbreviation	Sequence
440	2-arm-PEG_{24}-His-Ala	$(C\text{-}(H\text{-}Stp)_4\text{-}H)_{\alpha,\varepsilon}$-K-$dPEG_{24}$-A
835	2-arm-PEG_{24}-His-GE11	$(C\text{-}(H\text{-}Stp)_4\text{-}H)_{\alpha,\varepsilon}$-K-$dPEG_{24}$-YHWYGYTPQNVI
454	T-shape	$C\text{-}Y_3\text{-}Stp_2\text{-}K\text{-}(K(OleA)_{\alpha,\varepsilon})\text{-}Stp_2\text{-}Y_3\text{-}C$

Table 1. *List of oligomers as pDNA carriers used in this study. An internal ID, an abbreviation as well as its sequence (N to C terminus) are displayed. Detailed chemical structures can be found in Figure S1. Synthesis of polymers was performed by Stephan Morys (Department of Pharmacy, Pharmaceutical Biotechnology, LMU).Table adapted from [67].*

Abbreviation	Sequence
Cys-PEG_{24}-Ala	Cys(NPys)-$dPEG_{24}$-A
Cys-PEG_{24}-GE11	Cys(NPys)-$dPEG_{24}$-YHWYGYTPQNVI
$(Cys)_2$-PEG_{24}-Ala	$(Cys(NPys)\text{-}STOTDA)_{\alpha,\varepsilon}$-K-$dPEG_{24}$-A
$(Cys)_2$-PEG_{24}-GE11	$(Cys(NPys)\text{-}STOTDA)_{\alpha,\varepsilon}$-K-$dPEG_{24}$-YHWYGYTPQNVI

Table 2. *Sequences of PEGylation agents (N to C terminus) as well as used abbreviation are displayed. Detailed chemical structures can be found in Figure S2. Synthesis of polymers was performed by Stephan Morys (Department of Pharmacy, Pharmaceutical Biotechnology, LMU). Table adapted from [67].*

The pre-conjugation strategy is based on a 2-arm oligomer topology of ligand-PEG-STP/His, which had already proven as effective for receptor targeted gene transfer *in vitro* as well as *in vivo* for several receptor/ligand combinations [46, 58, 69, 139]. Two cationizable alternating Stp/histidine repeats provide effective nucleic acid binding and endosomal buffering [58, 236], a lysine as symmetrical branching point links the $dPEG_{24}$ molecule, which is end-modified with the targeting ligand. In the current case, the EGFR targeted oligomer ***835*** contains GE11, whereas the analogous control structure ***440*** contains alanine instead (Table 1). These oligomers also contain terminal cysteines for polyplex-stabilizing disulfide cross-link formation.

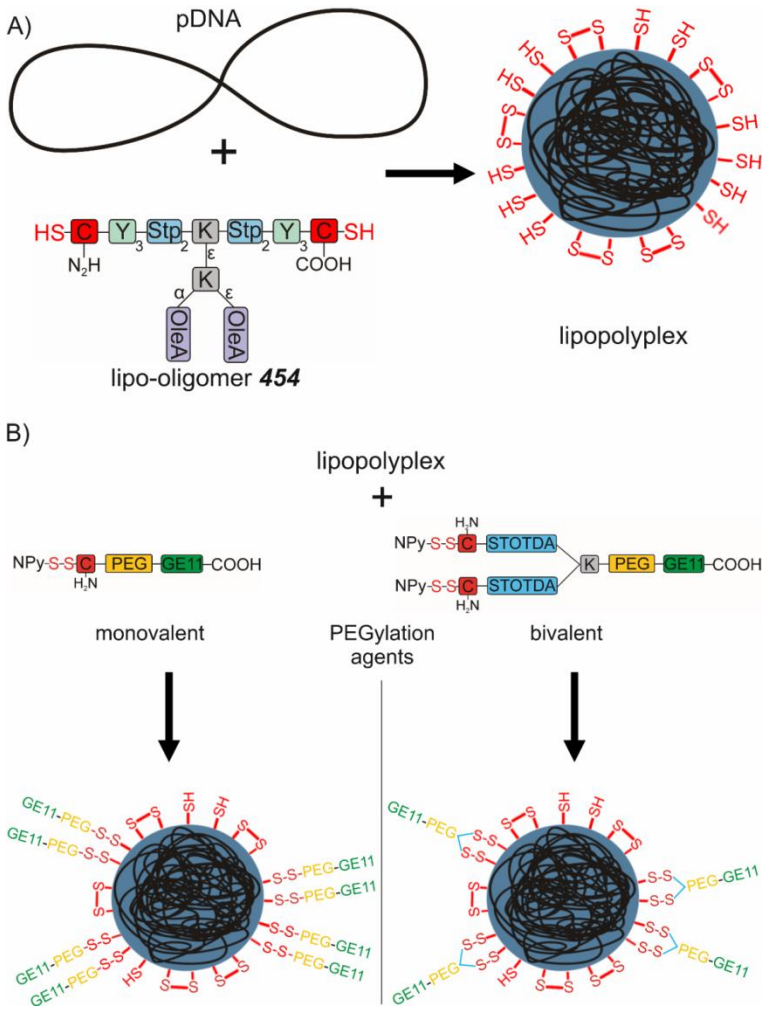

Scheme 1. *EGFR-targeted pDNA lipopolyplexes designed by post-modification of* ***454*** *(Table 1) core complexes with mono- or bi-valent PEG agents (Table 2). (A) Lipopolyplex formation. (B) Post-PEGylation via disulfide exchange. Scheme adapted from [67].*

In the novel post-modification strategy (Scheme 1), activated disulfide exchange chemistry was used for introduction of the targeted PEG reagents. Core pDNA lipopolyplexes were formed using the T-shaped lipo-oligomer ***454*****,** which had been designed to mediate efficient siRNA knockdown due to its optimized structure [58]. Four units of the cationizable artificial amino acid Stp (12 protonatable nitrogens in total) provide nucleic acid binding and endosomal buffering [58, 66, 237], two centrally placed oleic acids contribute to hydrophobic polyplex stability and have lytic potential upon acidification within the endosome [202, 204, 238]. Peripheral tyrosine trimers (Y3) increase polyplex stability via inter-oligomeral π-π stacking of aromatic rings [239]; C-terminal as well as N-terminal cysteine residues provide additional, disulfide triggered polyplex stabilization [237] as well as anchors for the subsequent post-PEGylation. This oligomer has been extensively investigated as core oligomer for receptor dependent siRNA delivery *in vitro* as well as *in vivo*, e.g. via folate receptor [75], transferrin receptor [207] as well as EGFR [232], but has been never used as

core carrier for receptor targeted pDNA delivery. Pre-PEGylation of ***454*** before polyplex formation was unsuccessful, resulting in polyplex aggregation (SM, unpublished results).
For modification of ***454***/pDNA polyplexes via activated disulfide exchange, monovalent or bivalent PEGylation agents, comprising precise $dPEG_{24}$ with GE11 or alanine as control, were synthesized by SPS with introduction of Boc-L-Cys(NPys)-OH as terminal coupling. In case of the bivalent agent, the diamino acid Fmoc-L-lysine(Fmoc)-OH was inserted for symmetrical branching following the PEG domain, and a short PEG spacer (STOTDA) was introduced for increasing flexibility of the reagent. The sequence was terminated by introduction of Boc-L-Cys(NPys)-OH on both branches.

Physicochemical polyplex characterization

Oligomer/pDNA interaction was examined in different assays, focusing on pDNA binding ability, stability and compaction. Polyplexes with and without post-PEGylation were evaluated. First, complete binding of 200 ng of pDNA by oligomers at N/P 12 was verified by agarose gel electrophoresis shift assays (Figure S3A). N/P 12 was previously determined as the required ratio for complete pDNA binding of ***454*** and therefore was chosen for all further experiments [204]. Most important, it is to note that post-modification of ***454*** polyplexes did not influence pDNA binding, independent of the amounts attached to the core particle (Figure S3B).
Also pre-PEGylated polyplexes, consisting of targeted or untargeted 2-arm-His-PEG_{24} and 200 ng of pDNA, showed complete pDNA retention (Figure S3A) at N/P 12. It was reported that lower N/P ratios for these kinds of carriers were sufficient to completely bind pDNA [69, 215]. For reasons of comparability between post-PEGylated lipopolyplexes and pre-PEGylated 2-arm polyplexes, all further experiments were conducted with N/P 12. After pDNA binding was confirmed, particle sizes and zeta potential were determined by dynamic light scattering. Results with ***454*** (post-PEGylated) polyplexes revealed very homogenous particles with a polydispersity index (PDI) between 0.11 and 0.20, where 1.0 represents the highest polydispersity (Table 3 as well as Table S1).
At the same time polyplexes formed with 2-arm PEG-oligomers ***440*** and ***835*** showed very inhomogeneous particle populations with a PDI between 0.4 and 0.5. This non-homogeneity resulted in DH values (displayed as Z-Average in nm) of more than 1000 nm (Table 3) for pre-PEGylated polyplexes. This could be explained by the high degree of PEGylation in comparison with a rather small cationizable pDNA compacting domain and the associated large amount of hydrophobic GE11 peptide; it is known that hydrophobic peptides tend to cause aggregation [240, 241].

.

Polymer	Size (nm)	PDI	ZP (mV)
440	1367 ± 134.0	0.39 ± 0.11	1.2 ± 0.2
835	1947 ± 211.7	0.51 ± 0.04	4.5 ± 0.1
454	81.4 ± 5.2	0.18 ± 0.02	29.9 ± 1.3
454 - 1.0 eq Cys-PEG_{24}-Ala	82.4 ± 0.4	0.15 ± 0.01	14.7 ± 0.9
454 - 1.0 eq Cys-PEG_{24}-GE11	121.1 ± 0.8	0.12 ± 0.01	16.9 ± 1.3
454 - 1.0 eq $(Cys)_2$-PEG_{24}-Ala	83.8 ± 0.8	0.12 ± 0.02	15.6 ± 0.9
454 - 1.0 eq $(Cys)_2$-PEG_{24}-GE11	283.8 ± 0.4	0.17 ± 0.01	17.7 ± 2.0

Table 3*. Particle size (Z-average), PDI and zeta potential of pDNA polyplexes formed in HBG buffer determined with DLS. Mean of three measurements of the same sample is indicated. Polymer at N/P 12 and 2 µg pDNA were separately diluted with HBG pH 7.4 to 30 µL each. Then solutions were mixed and incubated for 30 min. If indicated, post-PEGylation was carried out with 1.0 eq for further 15 min. Polyplexes then were diluted to 800 µl with 10 mM NaCl pH 7.4 prior to measurement. Polyplexes post-PEGylated with 0.5 eq can be found in Table S1. Measurements were performed by Stephan Morys (Department of Pharmacy, Pharmaceutical Biotechnology, LMU).Table adapted from [67].*

Unmodified ***454*** polyplexes exhibited a size of approximately 80 nm. It is to note that the polyplex size increased after post-modification with the monovalent GE11 reagent up to 121 nm and with the bidentate reagent up to 284 nm (1.0 eq each). In contrast, post-PEGylation with alanine containing reagents (independent of its topology or amount up to 1.0 eq) did not influence polyplex size. Similar findings of increasing polyplex size after post-PEGylation were observed for ***454/***siRNA polyplexes post-modified with GE11-PEG_{28}-maleimide [232]. In sum, these data indicate a special property of the hydrophobic GE11 ligand which can be better handled by the post-modification strategy. At the same time the zeta potential of post-shielded polyplexes was reduced from 30 mV (unmodified ***454***) as far as 15 mV, thereby indicating the successful post-modification. To validate post-PEGylation, UV spectra of a ***454*** polyplex before and after addition of 1.0 eq of $(Cys)_2$-PEG_{24}-Ala was recorded and compared to the reagents solely. A change in absorbance around 350-400 nm compared to the unconjugated PEGylation agent demonstrates the successful release of NPys. Data can be found in Figure S4.

Further on, quantitative evidence of successful PEGylation of the ***454***/pDNA lipoplexes is provided by determination of free lipooligomer thiols (Figure S5A) as well as release of 3-nitro-2-thiopyridone from PEGylation reagent (Figure S5B). Significant reduction of free thiols

(100% in free oligomers) to approximately 80% after polyplex formation and to 15% after PEGylation was observed.

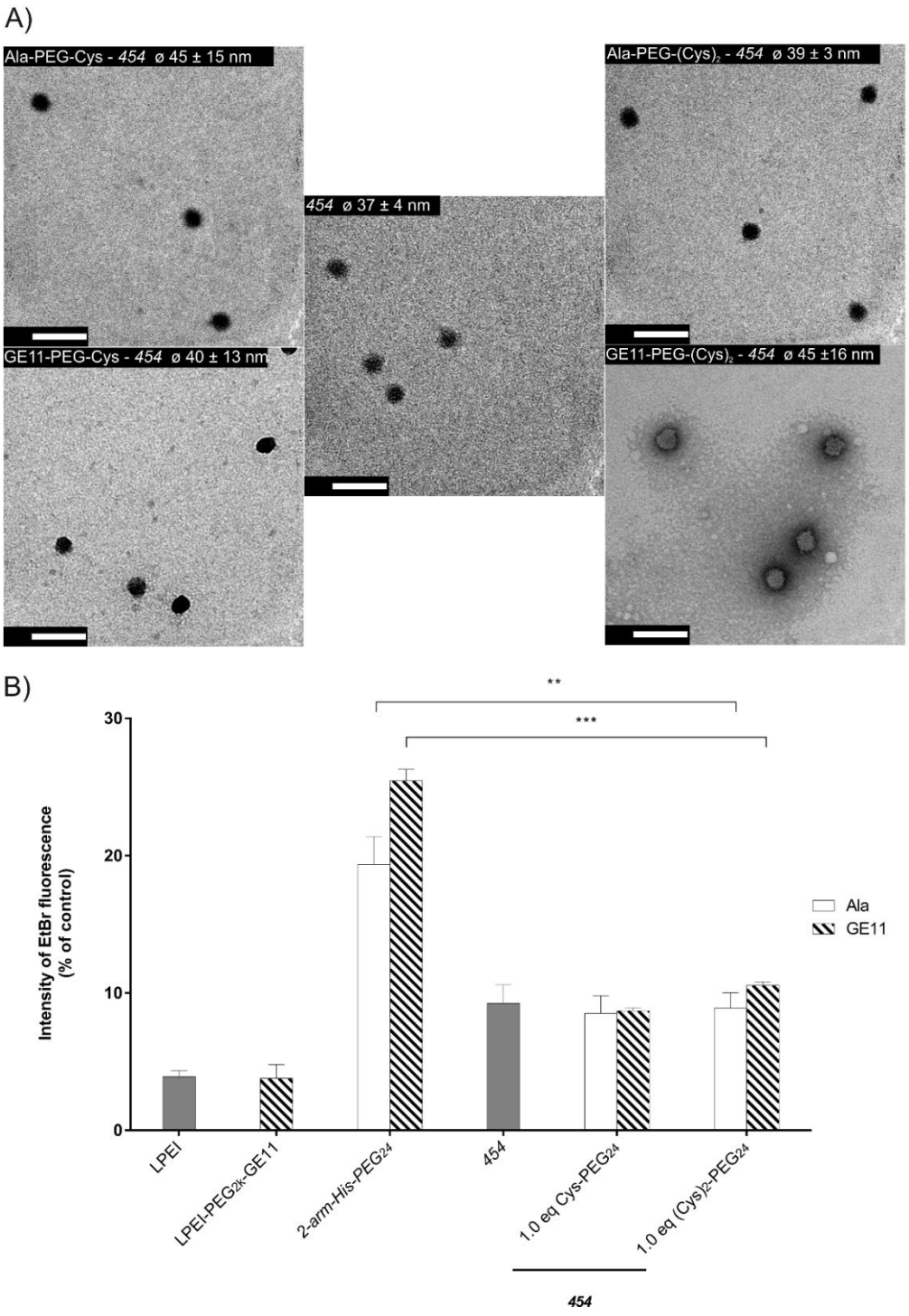

Fig. 1. (***A***) *Transmission electron microscopy images (TEM) of polyplexes formed with 1 µg of pDNA at N/P 12. Average diameters (nm) of polyplexes (n=5) ± SD are displayed. Scale bar represents 100 nm. (**B**) pDNA compaction of polyplexes determined with an EtBr assay. Untargeted controls are displayed in white, while polyplexes targeted with GE11 peptide are marked with pattern. For post-PEGylation 1.0 eq was used, additional EtBr data can be found in Figure S6. Measurements were performed by Stephan Morys (Department of Pharmacy, Pharmaceutical Biotechnology, LMU). Figure adapted from [67].*

Next, transmission electron microscopy was performed to investigate polyplex size and shape. In Figure 1A and Figure S6A TEM images of pre- as well as post-PEGylated polyplexes are shown. Polyplexes of ***835*** and ***440*** exhibited a homogeneous size of around 50 nm, appearing in short rods, while aggregation as determined by DLS, could not be seen. These findings indicate that bigger particles can either not be detected by TEM, or that they only occurred in minor extend, influencing size distribution by intensity in a severe manner.

At the same time, non-PEGylated ***454*** polyplexes form globules of around 40 nm, not undergoing significant changes due to post-modification, regardless of the topology of applied reagents (monovalent or bivalent). These findings suggest that the mean particle size could be much smaller as determined by dynamic light scattering, facilitating cellular uptake by standard pathways [62].

Next, the ability of the oligomers to compact pDNA was investigated by an ethidium bromide (EtBr) compaction assay. Interestingly, a significant difference between 2-arm-PEG_{24}-His and post-PEGylated ***454*** polyplexes was found (Figure 1B). While in the first group the remaining EtBr fluorescence was determined as more than 20% (compared to untreated pDNA). In comparison to polyplexes formed with ***440*** and ***835***, EtBr compaction of polyplexes formed with ***454*** was decreased by 50% to approximately 10% in total, even in case of post-functionalization with 1.0 eq.

No difference between modified (data for 0.5 eq can be found in Figure S6B) and unmodified ***454*** polyplex was observed, indicating that post-PEGylation does not have an influence on pDNA compaction of the core particle. Also no difference between C-terminal alanine or the GE11 peptide was found. The highest pDNA compaction nevertheless can be achieved by LPEI, a far larger polycation, with a remaining EtBr fluorescence of less than 5%. To the same samples 250 IU of heparine sulfate was added to determine anionic stress tolerance (Figure S6C). Here we found, as reported previously [215], that LPEI polyplexes are very sensitive, leading to 100% EtBr fluorescence corresponding to full pDNA release. These effects were minor pronounced for LPEI-PEG_{2k}-GE11, retaining approximately 13% pDNA, nevertheless they were notably increased in comparison to ***454*** based polyplexes, where only 70% could be released. By increasing the cationic charge, even better pDNA retention could be achieved. While no difference between unmodified ***454***/pDNA polyplexes and post-PEGylated could be observed, pre-PEGylated polyplexes were also very prone to heparine stress and fully released pDNA. This could be explained by the increased size, also leading to looser polyplexes.

Stability of polyplexes in the protein environment presents a most critical issue. Therefore, polyplexes have been investigated by DLS after incubation with 10% FBS supplemented cell culture media or full serum (FBS). Pre-PEGylated polyplexes formed with ***440*** and ***835*** underwent immediate aggregation under both conditions (Figure S7C-F). Non-modified ***454***

polyplexes increased from 80 nm to 250 nm with no further changes over time. ***454*** polyplexes post-modified with the monovalent structures showed immediate size increase from 100 nm in 10 mM NaCl to approximately 200 nm in both conditions. Between 4 h and 24 h these polyplexes aggregated to particles >800 nm (Figure S7I-L). For ***454*** post-modified with 1.0 eq $(Cys)_2$-PEG_{24}-GE11 a size of 280 nm in 10 mM NaCl was determined that changed to approximately 300 nm after addition of full serum or cell culture media. Between 4 h and 24 h these polyplexes underwent no changes in full serum (Figure S7O). As in ***454*** polyplexes post-modified with the bivalent structures $(Cys)_2$-PEG_{24}-Ala/GE11 the aggregation was less profound, higher stability is suggested.

Luciferase gene transfections

For evaluation of pDNA transfection efficiency, the hepatocellular cell line Huh7 (Figure 2A) and the breast cancer cell line MCF-7 (Figure 2B), both showing high EGFR cell surface expression (Figure S8), as well as the low EGFR expressing cell line FTC-133 (Figure S11) were used. Cells were either incubated for 45 min or 24 h with pDNA complexes and luciferase intensity was determined after 24 h. Polyplexes post-PEGylated (with monovalent or bivalent polymers) were compared to PEG-free core particle complexes (***454***) and 2-arm histidine-containing pre-PEGylated polymers. LPEI-PEG_{2k}-GE11, which already has shown high transduction efficacy and EGFR specificity *in vitro* and *in vivo*, was used as positive control [39, 68, 151].

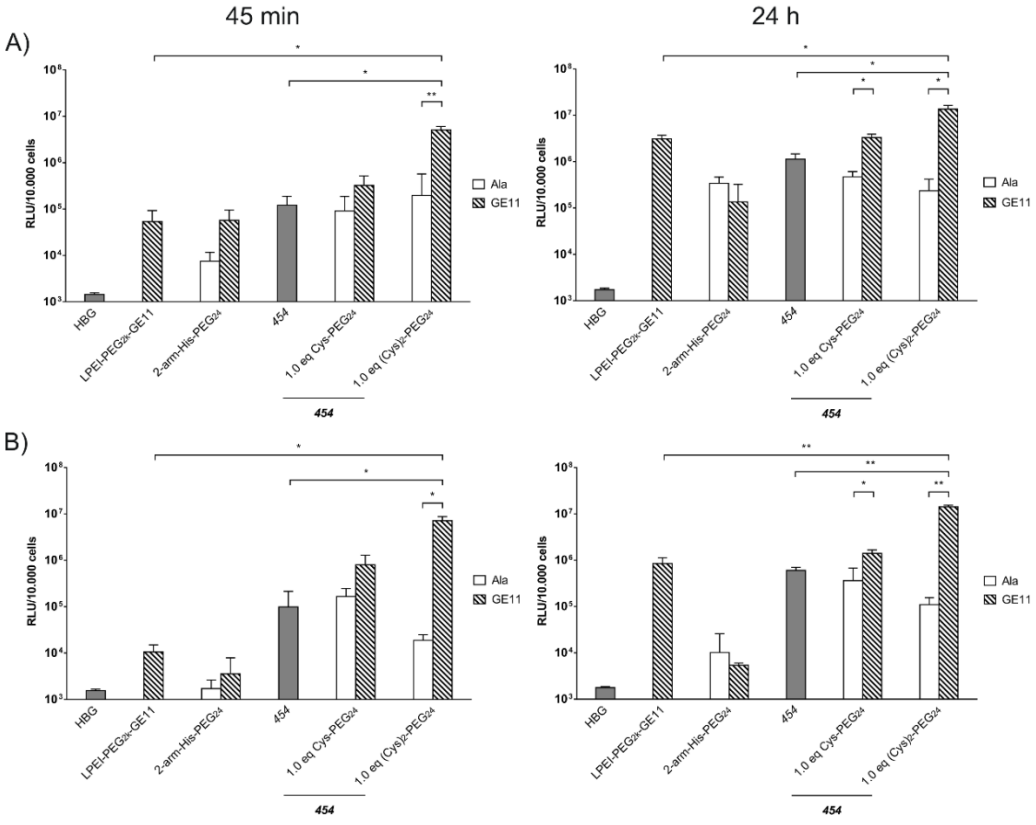

Fig. 2: *Luciferase reporter gene expression in two EGFR positive human cancer cell lines. (**A**) Human hepatocellular cancer cells Huh7 and (**B**) human breast cancer cell line MCF-7. pCMVLuc polyplexes were incubated on cells for 45 min (left) or 24 h (right). Untargeted controls are displayed in white, while polyplexes targeted with GE11 peptide are marked with pattern. Figure adapted from [67].*

The EGFR-targeted bivalent structure $(Cys)_2$-PEG_{24}-GE11 coupled to ***454*** core polyplexes at a molar ratio of 1.0 eq demonstrated a strong EGFR-targeting effect in both cell lines, in contrast to the alanine containing structure. Moreover, significantly higher expression levels compared to all other polymers were detected. The pre-PEGylated polyplexes (***835*** and ***440*** *control*) revealed similar transfection level as LPEI-PEG_{2k}-GE11 in Huh7 cells and even lower results in MCF-7 cells. Based on sizes measured by DLS, which showed sizes over 1 µm for both pre-PEGylated polymers, transfection efficacy might be attributed to high aggregation and not due to specific uptake. Transfection of non-PEGylated ***454*** demonstrated equal (in Huh7) or slightly higher (MCF-7) expression level compared to LPEI-PEG-GE11. None of the polyplexes mediated cytotoxicity after 45 min and 24 h of incubation (Figure S9) For post-integration of PEG onto core polyplexes, monovalent and bivalent structures were compared at two different molar ratios. One eq proved to be more efficient than 0.5 eq. Results for 0.5 eq are displayed in Figure S10A-B, with no occurring cytotoxicity (Figure S10C-D). Interestingly, transduction efficacy was not influenced by post-modification of ***454*** polyplexes with up to 1.0 eq of $(Cys)_2$-PEG_{24}-Ala in comparison to the unshielded core polyplexes, thereby highlighting this approach as possibility to circumvent the so called "PEG-dilemma" of pre-PEGylated structures [103]. It is widely accepted that PEI-like polyplexes require a combined effect of osmotic endosomal eruption and direct phospholipid destabilization by the cationized vehicle for endosomal escape [56, 65, 105]. PEG obviously can interfere with this direct cationic membrane destabilization. Consistently, bioreversible PEGylation was introduced to resolve this dilemma [69, 230, 231] and also the disulfide conjugation of oligomer and PEG used in the present work could possibly be cleaved off by intracellular glutathion (GSH) as demonstrated in other work [61, 208, 242].

In comparison to Huh7 and MCF-7 cells that demonstrated strong EGFR dependency of transfection rates, this was not detected in low EGFR expressing FTC-133 cells. FTC-133 cells demonstrated no differences in transfection rates of post-PEGylated monovalent and bivalent structures coupled to either GE11 or Ala after 45 min incubation time. This further indicates the beneficial EGFR targeting strategy of polyplexes post-modified with GE11 targeted PEGylation reagents (Figure S11A). At the same time, no polyplex mediated cytotoxicity was observed after 45 min of incubation (Figure S11B).

After 24 h of polyplex incubation, an overall increased transduction efficacy was measurable due to unspecific uptake mechanisms that occur after long-time incubation. Due to residual positive charge polyplexes tend to adhere unspecifically to the negatively charged cell membrane and particles get taken up unspecifically over time, leading to a diminished

targeting effect. Nevertheless, the advantageous bivalent conjugation of EGFR-targeted PEG to ***454*** is still evident after 24 h of incubation.

Cellular binding and internalization of bivalent post-PEGylated polyplexes

For a more detailed investigation, cellular association and uptake of Cy5 labeled pDNA complexes were determined by flow cytometry. Best-performing condition (1 eq) was used. Binding efficiency of bivalent post-PEGylated (EGFR-targeted and untargeted) lipopolyplexes in comparison to unshielded lipopolyplexes (***454***) was examined (Figure 3). All three lipoplexes showed efficient binding after 30 min incubation on ice. Far higher Cy5 fluorescence intensity was measured in cells transfected with the post-PEGylated EGFR-targeted bidentate structure. This emphasizes the suitability of GE11 as EGFR specific ligand and at the same time demonstrates that the bidentate structure represents the most promising post-PEGylation reagent. Shielding with PEG did not result in diminished interaction with cell surface, as can be seen by comparing fluorescence activity between non-shielded ***454*** and bivalent post-PEGylated alanine control. No difference in fluorescence activity was detected. Experiments were also performed with monovalent PEGylation reagents, which did not result in any enhancement of binding in comparison to ***454*** and the alanine control in Huh7 and MCF-7 (Figure S12A,C). Complementary uptake and binding results of LPEI-PEG_{2k}-GE11 and 2-arm pre-PEGylated structures are shown in Figure S13A,C.

Results of uptake studies were consistent with binding studies, showing highest intracellular uptake after transfection with the bivalent post-PEGylated structure in comparison to unshielded ***454*** and alanine control (Figure 3) and lower uptake was obtained after transfection with LPEI-PEG_{2k}-GE11, pre-PEGylated structures and monovalent post-PEGylation complexes (Figure S12B,D and S13B,D).

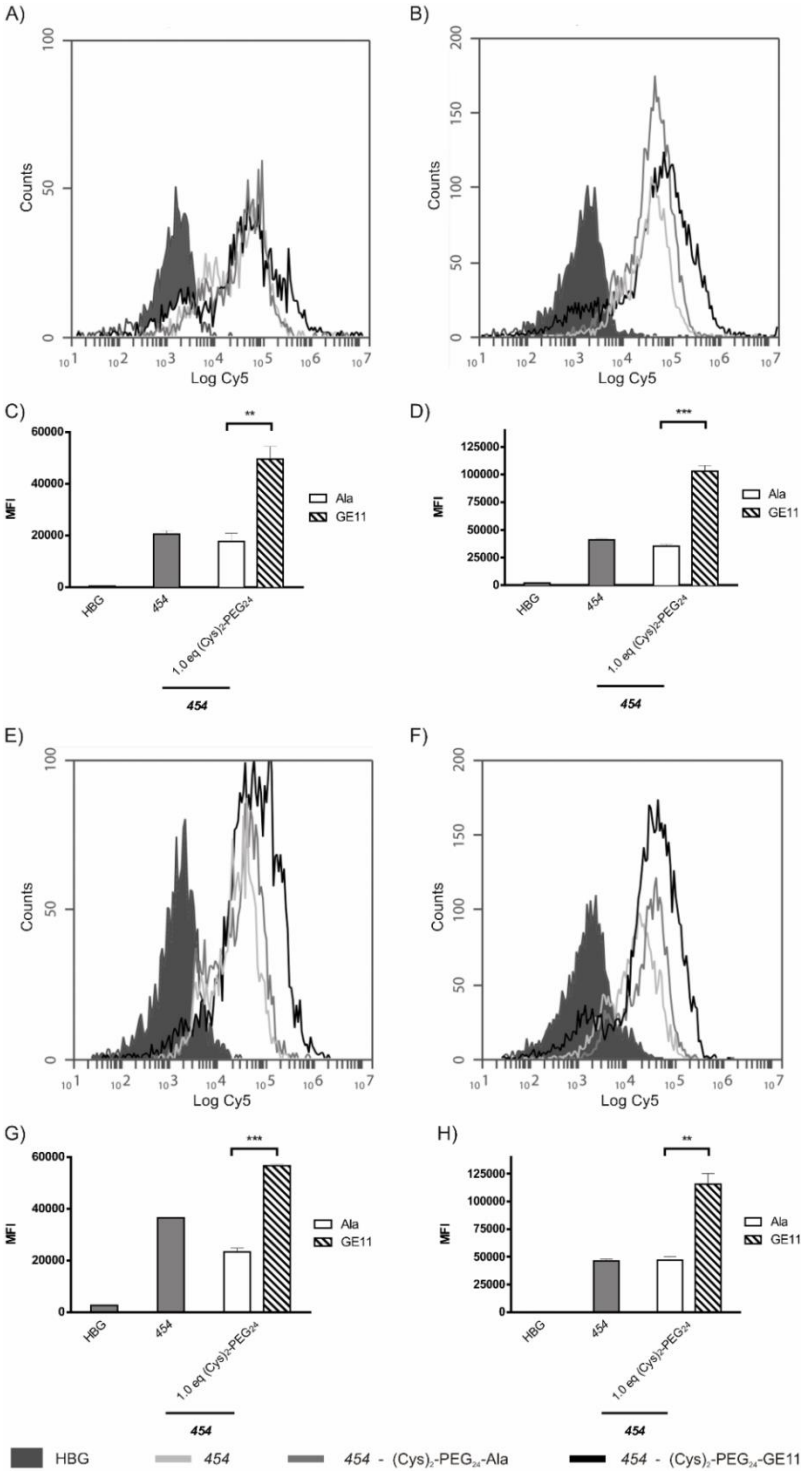

Fig. 3: *Cellular association of **454** polyplexes post-PEGylated with 1.0 eq of bidentate reagents on Huh7 (**A**) and MCF-7 (**B**) after 30 min incubation at 4 °C was determined by flow cytometry. In (**C**) and (**D**) corresponding mean fluorescence intensity (MFI) values are displayed. Cellular internalization of polyplexes after 45 min of incubation at 37 °C followed by removal of extracellularly bound polyplexes is displayed in (**E**) and (**F**). Corresponding MFI values can be found in (**G**) and (**H**). Logarithmic X-scale in (**A**) and (**B**) as well as (**E**) and (**F**) represents Cy5 fluorescence of polyplexes. Figure adapted from [67].*

For nanoparticles different uptake pathways are described depending on cell type, nanoparticle formulation, nanoparticle size and incorporation of ligands for active targeting. Various studies have been performed to rule out the exact mechanisms.

Size-dependent uptake studies determined that particles up to 500 nm were internalized into cells by energy based processes [60, 62]. A clathrin-dependent uptake mechanism, as well as caveolae assistant uptake, was detected for particles up to 200 nm. For lipoplexes, the clathrin dependent way is the major mechanism, whereas for polyplexes, both ways are possible [60].

The lipoplexes used in this study lay around 200 nm or smaller, which suggests a clathrin dependend uptake. However, uptake is not only size dependent, but also ligand dependent. Referring to this point, a study comparing the ligand GE11 and EGF for receptor mediated uptake revealed following that GE11 targeted polyplexes were taken up into the cell via clathrin-mediated endocytosis. This GE11-mediated uptake showed no activation of EGFR with constant EGFR levels after transfection and demonstrated an alternative actin-dependent pathway [243].

In conclusion, EGFR-targeted lipoplexes in this study are designed to achieve characteristics for an active targeted, clathrin-dependent uptake mechanism, which was proved to be the process of lipoplexes and polyplexes with the GE11 ligand [243].

After the successful uptake into endosomes, the endosomal buffer capacity of the Stp units in the oligomer backbone of the lipoplexes leads to protonation. The cationic function as well as the hydrophobic domains lead to enhanced interaction with the lysosomal membrane followed by destabilization of the membrane and degradation of the lipoplex and hence release of the pDNA in the cytosol.

Iodide uptake activity after hNIS gene delivery

After the proof of concept using the sensitive luciferase reporter capability for quantifying transduction efficacy, the sodium iodide symporter (NIS) was used as a clinically more relevant target gene. NIS features the beneficial dual characteristic as diagnostic and therapeutic gene [60, 62]. This theranostic function gives the possibility of exact determination of tumoral NIS gene expression *in vivo* by non-invasive imaging modalities as well as therapeutic investigation by application of cytotoxic radionuclides [35-39, 41, 42, 45-47, 126, 151].

In cell culture studies, NIS gene expression after lipopolyplex mediated delivery can be detected by measuring iodide (^{125}I) uptake activity of transfected cells by gamma-counter analysis. To verify NIS-dependent ^{125}I cell uptake, cells were pretreated with the NIS-specific inhibitor perchlorate ($NaClO_4$) that results in a blockade of NIS mediated iodide uptake.

As already observed in transfection, binding and uptake studies with the luciferase reporter gene, superiority of the post-integration approach of EGFR-targeted bidentate structures over non- and pre-PEGylated structures as well as untargeted complexes were confirmed (Figure 4A). Measured iodide uptake was perchlorate-sensitive verifying NIS mediated

uptake. No effects on cell viability were observed after transfection (Figure 4B). The advantageous new EGFR specific delivery vehicles combine high transduction efficacy, high biocompatibility, ideal size along with optimal shielding that was introduced by post-integration of the bivalent (Cys(NPys)-STOTDA)$_{\alpha,\varepsilon}$-K-dPEG$_{24}$ via disulfide exchange reaction.

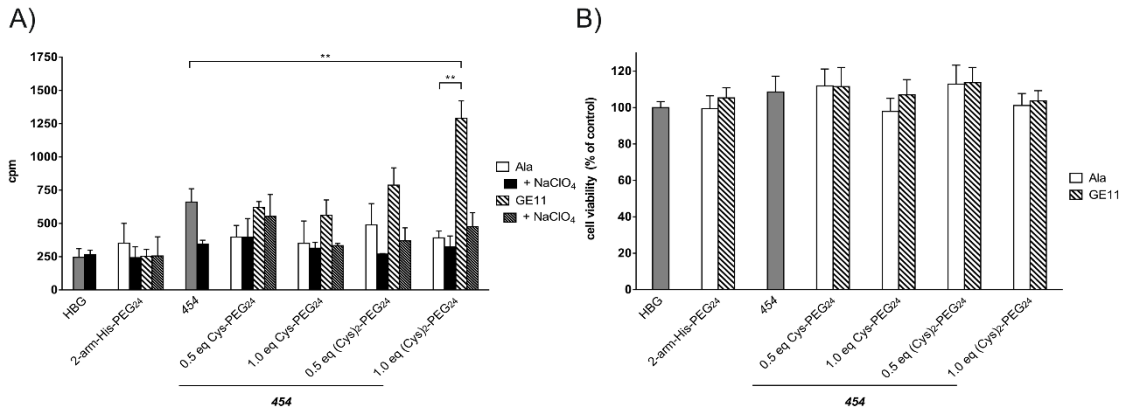

Fig. 4: *(**A**) Transfection of polyplexes on Huh7 cells. A sodium iodide symporter (NIS) coding pDNA was used. After ^{125}I application, iodide uptake was determined as counts per minute (cpm). Results are displayed with (black) and without (white) blockade of NIS by application of $NaClO_4$ prior to measurement. (**B**) MTT performed in parallel to transfections. Untargeted controls are displayed in white, while polyplexes targeted with GE11 peptide are marked with pattern. Figure adapted from [67].*

7.5 Conclusions

pDNA polyplexes can be functionalized with shielding and targeting domains either by pre-conjugation or by post-modification strategies. The current study aimed at the design of EGFR-targeted pDNA polyplexes, based on precise sequence-defined oligomers available by SPS. A side-by-side comparison was made for polyplexes which were obtained from a pre-conjugation strategy using GE11-PEG-STP/His 2-arm oligomers, with lipopolyplexes that were post-modified with mono- or bivalent PEG-GE11 reagents. These studies identified peculiarities of the alternative approaches and the best-performing carrier for EGFR specific pDNA gene delivery. Pre-conjugation was previously found as effective for the targeting ligands folate or a c-met binding peptide, however was hampered by the hydrophobicity of GE11 and resulting in significant polyplex aggregation. For post-integration into core lipopolyplexes, the bivalent structure Cys(Npys)$_2$-PEG$_{24}$-GE11 was found to be the best agent, yielding highly specific, EGFR dependent gene transfer, demonstrated with luciferase marker gene and sodium iodide symporter (NIS) gene expression studies. Previous work already pointed out that post-modification represents a promising tool for shielding and targeting pDNA [36-43] as well as siRNA polyplexes [75, 207, 232]. The superior effect of the bivalent over monovalent linkage is well consistent with similar findings using multivalent coatings of nucleic acid nanoparticles [216, 217, 219].

7.6 Supporting information

7.6.1 Supporting methods

Oligomer syntheses and analytical experiments were performed by Stephan Morys (Department of Pharmacy, Pharmaceutical Biotechnology, LMU).

Resin loading

Loading of a chlorotrityl chloride resin with Fmoc-L-Ile-OH

Experiments were performed by Stephan Morys (Department of Pharmacy, Pharmaceutical Biotechnology, LMU). Chlorotrityl chloride resin (1.2 mmol chloride, 750 mg) was swollen in 7 mL dry DCM for 10 min, a solution of 0.3 eq Fmoc-L-Ile-OH (119.3 mg) in 5 mL dry DCM and 173.3 µL DIPEA (0.9 eq) were added and the resin was shaken for 1 h in an overhead shaker. The reaction solvent was drained and 5 mL of a mixture of dry DCM/MeOH/DIPEA (80/15/5) was added for 30 min. After the removal of the reaction mixture, the resin was washed 5 times with DCM.

Forty mg of the wet resin were separated and dried to determine the loading of the resin. Therefore, an exactly weighted amount of the dry resin was treated with 1 mL deprotection solution (20% piperidine in DMF) for 1 h. Afterwards, the solution was diluted and absorption was measured at 301 nm. The loading was then calculated according to the equation: resin load [mmol/g] = (A × 1000)/(m [mg] × 7800 × df) with df as dilution factor.

The resin was treated five times with 20% piperidine in DMF to remove the fmoc protection group. Successful deprotection was evaluated by Kaiser test [234]. Afterwards, the resin was washed with DMF, DCM and n-hexane and dried in vacuum.

Loading of a chlorotrityl chloride resin with Fmoc-Cys(Trt)-OH

Experiments were performed by Stephan Morys (Department of Pharmacy, Pharmaceutical Biotechnology, LMU). Chlorotrityl chloride resin (1.2 mmol chloride, 750 mg) was swollen in 7 mL dry DCM for 10 min, a solution of 197.7 mg Fmoc-Cys(Trt)-OH (0.3 eq) in 5 mL DCM and 173.3 µL DIPEA (0.9 eq) were added and the resin was shaken for 1 h in an overhead shaker. From now on the same protocol was applied as mentioned above.

pDNA binding assay by electrophoresis

Experiments were performed by Stephan Morys (Department of Pharmacy, Pharmaceutical Biotechnology, LMU). For investigation of the pDNA binding ability of the oligomers, a 1% agarose gel was prepared. Therefore, agarose was suspended in TBE buffer (trizma base 10.8 g, boric acid 5.5 g, EDTA 0.75 g per 1 L of water) and the mixture was heated until boiling and total dissolution. After cooling down to approximately 60 °C, GelRed (Biotium

Inc., Hayward, CA, USA) for detection of the nucleic acid was added and the agarose solution was casted into an electrophoresis unit and left to form a solid gel. Then polyplexes consisting of oligomers at N/P 12 were prepared with 200 ng pDNA in a total volume of 20 µL. After 30 min (and if indicated, further 15 min of post-modification), 4 µL of 6x loading buffer (6 mL of glycerol, 1.2 mL of 0.5 M EDTA, 2.8 mL of H_2O, 0.02 g of bromophenol blue) was added to each sample and applied to the gel. Electrophoresis was performed for 80 min at 120 V.

UV spectrometrical investigation of polyplex modification

Experiments were performed by Stephan Morys (Department of Pharmacy, Pharmaceutical Biotechnology, LMU). Polyplexes consisting of 8 µg pDNA and 454 at N/P 12 in 50 µL HBG were prepared. After 30 min samples were either diluted to 100 µL HBG or post-modified with 1.0 eq of Ala-PEG_{24}-$Cys(NPys)_2$ for 15 min prior to dilution. HBG served as blank; 8µg pDNA in HBG, its correlating amount of 454 at N/P 12 and 1.0 eq of Ala-PEG_{24}-K-(STOTDA-$(Cys(NPys))_2$ were treated as controls. For all samples UV/Vis spectra from 200-700 nm were recorded with a Genesys 10S UV-VIS spectrophotometer (Thermo Scientific, Schwerte, Germany).

Ellman's assay

Experiments were performed by Stephan Morys (Department of Pharmacy, Pharmaceutical Biotechnology, LMU). Polyplexes were formed in 50 µL HBG (containing 8µg pDNA and 454 at N/P 12). Solutions containing unmodified 454/pDNA polyplexes as well as post-modified polyplexes (15 min with 1.0 eq $(Cys)_2$-PEG_{24}-Ala), were diluted with 275 µL Ellman's Buffer (0,2M Na_2HPO_4, 1mM EDTA, pH 8,0) and eight µL of a DTNB solution (4mg/ml dissolved in MeOH). After addition of DTNB, both solutions were incubated for 15 min at 37 °C and A_{412} was measured. Post-modified polyplex absorption was measured at 412 nm prior and after DTNB addition in order to exclude distortion mediated by 3-nitro-2-thiopyridone, which is released during post-modification. A Genesys 10S UV-VIS spectrophotometer (Thermo Scientific, Schwerte, Germany) was used for measurement. A_{412} of PEGylated polyplexes then was calculated according to the following formula: A_{412} (Sample) = A_{412} (+DTNB) – A_{412} (-DTNB). The percentage of free mercapto groups is based on the theoretical amount (100%) of thiols.

Release of 3-Nitro-2-Thiopyridone

Experiments were performed by Stephan Morys (Department of Pharmacy, Pharmaceutical Biotechnology, LMU). The amount of $(Cys)_2$-PEG_{24}-Ala corresponding to 1.0 molar eq of 454 was diluted with HBG (pH 7.4) to 300 µL and 33 µL of a 1M DTT (dithiothreitol) solution was

added to the solution. As determined in previous experiments (see Figure S4), the maximum absorbance of 3-nitro-2-thiopyridone was detected at 324 nm. Absorbance at A_{324} was measured and compared to the amount released from the PEGylated polyplex. Therefore 50 µL of polyplex solution (containing 8 µg of pDNA, and 454 at N/P 12) was post-modified with 1.0 eq $(Cys)_2$-PEG_{24}-Ala for 15 min and the polyplex solution was diluted with 275 µL of Ellman's Buffer prior to measurement. Absorbance of $(Cys)_2$-PEG_{24}-Ala reduced with 1M DTT was considered as 100% and was correlated to 3-nitro-2-thiopyridone release after PEGylation.

Stability of polyplexes in serum and media

Experiments were performed by Stephan Morys (Department of Pharmacy, Pharmaceutical Biotechnology, LMU). Determination of polyplex stability in full serum (FBS) as well as in DMEM supplemented with 10% serum was determined by DLS. Polyplexes were prepared as described previously with 8 µg pDNA and oligomers at N/P 12 in a total volume of 50 µL HBG. After incubation for 30 min, if indicated, polyplexes were PEGylated for 15 min, then HBG and FBS or DMEM were added. 60 µL were placed in a DTS1070 cuvette and t=0 min was determined. Polyplexes in serum or media were incubated under steady shaking at 37 °C and aliquots were taken for further measurements after 4 and 24 h. Each time point represents one measurement averaged from 6 sub runs.

EGF receptor measurement

1×10^6 Huh7, MCF-7 or FTC-133 cells were detached with trypsin, washed with PBS supplemented with 10% FBS and incubated with an EGFR-specific antibody (1:100; monoclonal mouse IgG1 - Dako, Glostrup, Denmark) or with an IgG-anti-mouse antibody (BD Bioscience, Franklin Lakes, USA) as negative control for 1 h on ice. Afterwards cells were washed with PBS supplemented with 10% FBS and incubated with an AlexaFluor 488 labeled goat anti-mouse secondary antibody (1:400 - Invitrogen, Langenselbold, Germany) for 1 h on ice. After a final washing step, cells were resuspended in PBS supplemented with 10% FBS and flow cytometry analysis was performed on a BD Accuri C6 flow cytometer (BD Bioscience, Franklin Lakes, USA). Cells were gated by forward/sideward scatter and pulse width for exclusion of doublets. PI (propidium iodide, Sigma-Aldrich) was used for discrimination between viable and dead cells.

7.6.2 Analytical methods

Analytical experiments were performed by Stephan Morys (Department of Pharmacy, Pharmaceutical Biotechnology, LMU).

ESI mass spectrometry

Experiments were performed by Stephan Morys (Department of Pharmacy, Pharmaceutical Biotechnology, LMU). Electrospray ionization (ESI) mass spectrometry was carried out using a Thermoscientific LTQ FT Ultra Fourier transform ion cyclotron and an IonMax source. Samples were dissolved in water containing 1% formic acid to a concentration of 1 mg/ml. Data is shown after positive ionization (M+H).

MALDI mass spectrometry

Experiments were performed by Stephan Morys (Department of Pharmacy, Pharmaceutical Biotechnology, LMU). One µL matrix consisting of a saturated solution of Super-DHB (mixture of 2,5-dihydroxybenzoic acid and 2-hydroxy-5-methoxybenzoic acid) in acetonitrile / water (1:1) containing 0.1% (v/v) trifluoroacetic acid was applied on a MTP AnchorChip (Bruker Daltonics, Bremen, Germany). After the Super-DHB matrix dried and crystalized, one µL of the sample solution (10 mg/mL in water) was added to the matrix spot. Samples were analyzed using an Autoflex II mass spectrometer (Bruker Daltonics, Bremen, Germany).

Analytical RP-HPLC

Experiments were performed by Stephan Morys (Department of Pharmacy, Pharmaceutical Biotechnology, LMU). Reversed-phase HPLC (RP-HPLC) was carried out with a VWR-Hitachi Chromaster 5160 Pump System (VWR, Darmstadt, Germany), VWR-Hitachi Chromaster 5260 Autosampler (VWR, Darmstadt, Germany) and a Diode Array Detector (VWR-Hitachi Chromaster 5430; VWR, Darmstadt, Germany) at 214 nm detection wavelength. As a column either a YMC Hydrosphere 302 C^{18} (YMC Europe, Dinslaken, Germany) or a Waters Sunfire C^{18} (Waters, Saint-Quentin en Yvelines Cedex, France) was used. A gradient starting at 95:5 (water / acetonitrile) to 0:100 within 20 min was applied. All solvents were supplemented with 0.1% trifluoroacetic acid.

Proton NMR spectroscopy

Experiments were performed by Stephan Morys (Department of Pharmacy, Pharmaceutical Biotechnology, LMU). ^{1}H-NMR spectra were recorded using an AVANCE III HD500 (500 MHz) by Bruker with a 5 mm CPPBBO probe. Spectra were recorded without TMS as internal standard and therefore all signals were calibrated to the residual proton signal of the deuterium oxide (D_2O) solvent. Chemical shifts are reported in ppm and refer to the solvent

as internal standard (D_2O at 4.79). Integration was performed manually. The spectra were analyzed using MestreNova (Ver.9.0 by MestReLab Research). Integrals were normalized to the succinic acid peaks.

7.6.3 Supplemental figures and tables

Polymer	Size (nm)	PDI	ZP (mV)
454 - 0.5 eq Cys-PEG_{24}-Ala	85.1 ± 1.3	0.13 ± 0.01	17.8 ± 0.3
454 - 0.5 eq Cys-PEG_{24}-GE11	95.2 ± 0.3	0.11 ± 0.01	20.8 ± 1.4
454 - 0.5 eq $(Cys)_2$-PEG_{24}-Ala	79.3 ± 0.5	0.18 ± 0.01	14.7 ± 0.8
454 - 0.5 eq $(Cys)_2$-PEG_{24}-GE11	189.0 ± 1.4	0.20 ± 0.02	22.0 ± 1.5

Table S1. *Particle size (Z-average), PDI and zeta potential of pDNA polyplexes formed in HBG buffer determined with DLS. Mean of three measurements of the same sample is indicated. Polymer at N/P 12 and 2 µg pDNA were separately diluted with HBG pH 7.4 to 30 µL each. Then solutions were mixed and incubated for 30 min. If indicated, PEGylation was carried out with 0.5 eq for further 15 min. Polyplexes then were diluted to 800 µl with 10 mM NaCl pH 7.4 prior to measurement. Measurements were performed by Stephan Morys (Department of Pharmacy, Pharmaceutical Biotechnology, LMU). Table adapted from [67] supplemental information.*

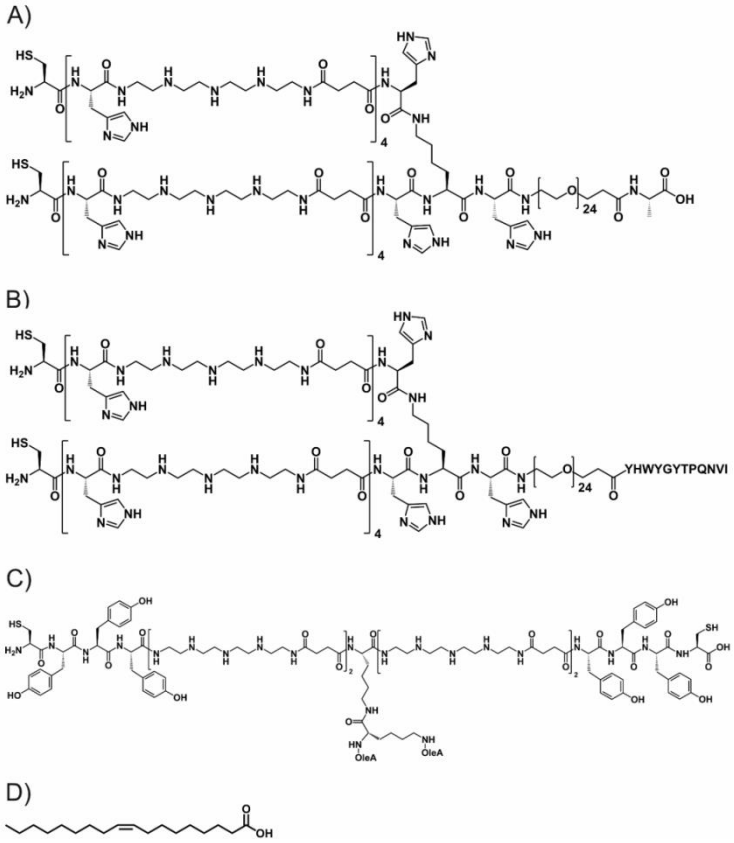

Figure S1*. Chemical structures from N to C terminus of oligomers* ***440*** *(**A**),* ***835*** *(**B**) and* ***454*** *(**C**). Oleic acid (OleA) is shown in (**D**). Figure adapted from [67] supplemental information.*

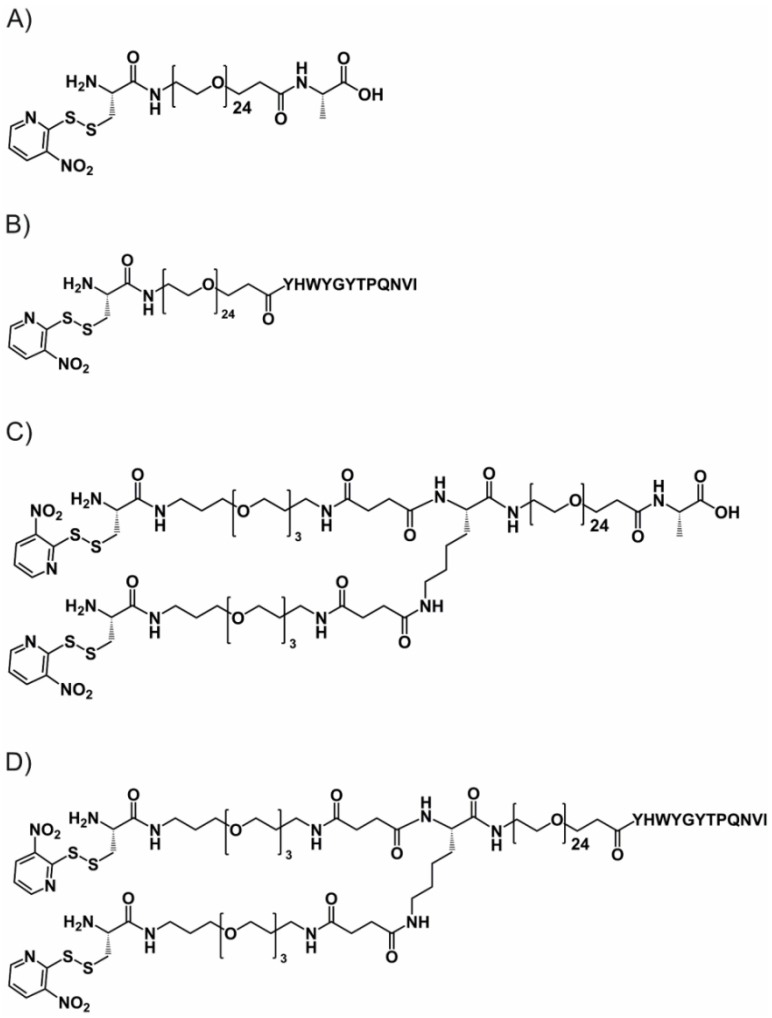

***Figure S2**. Chemical structures from N- to C- terminus of Cys(NPys)-dPEG$_{24}$-Ala (**A**), Cys(NPys)-dPEG$_{24}$-GE11 (**B**), (Cys(NPys)-STOTDA)α,ε-K-dPEG$_{24}$-Ala (**C**) and (Cys(NPys)-STOTDA)α,ε-K-dPEG$_{24}$-GE11 (**D**). Figure adapted from [67] supplemental information.*

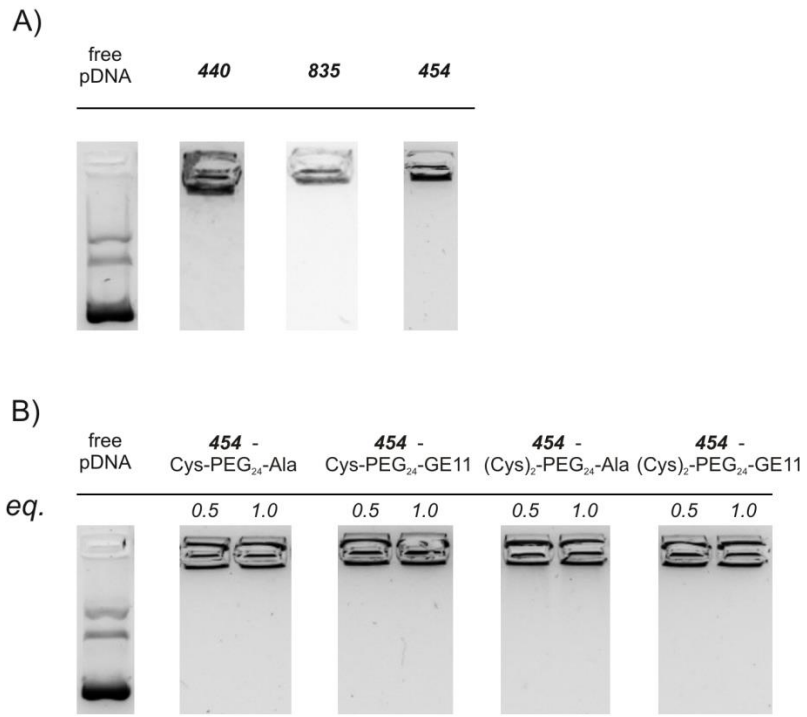

***Figure S3**. Retardation of formed pDNA complexes in agarose gel at N/P 12. (**A**) Pre-conjugated 2-arm-His-PEG$_{24}$ (**440** and **835**) as well as unmodified **454**. (**B**) Post-PEGylated **454** polyplexes with indicated PEGylation agents. Measurements were performed by Stephan Morys (Department of Pharmacy, Pharmaceutical Biotechnology, LMU). Figure adapted from [67] supplemental information.*

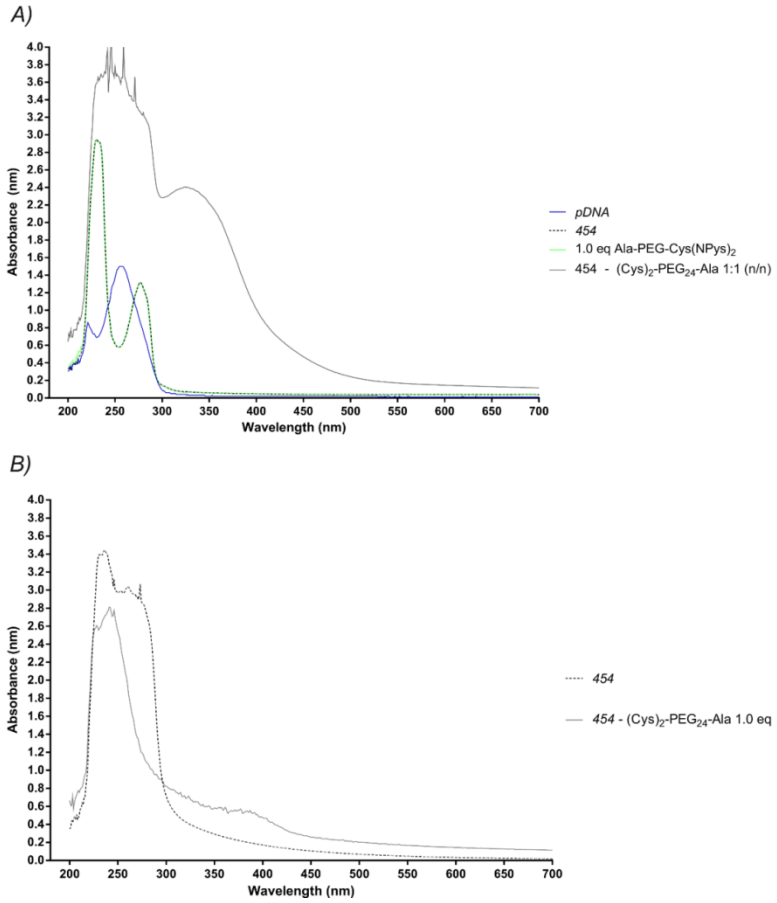

***Figure S4**. UV/Vis detection of PEGylation reaction. (**A**) 8 µg of pDNA, corresponding amount of **454** at N/P 12 and 1.0 eq of Ala-PEG$_{24}$-K-(STOTDA-Cys(NPys))$_2$ were used. **454** - (Cys(NPys)-STOTDA)$_2$-K-PEG$_{24}$-Ala mixed without pDNA served as positive control (mol Cys **454** / mol Cys(Npys)). (**B**) The same reagents were used to form polyplexes. **454**/pDNA, as well as **454**/pDNA PEGylated with 1.0 eq of (Cys)$_2$-PEG$_{24}$-Ala indicated successful reaction. Measurements were performed by Stephan Morys (Department of Pharmacy, Pharmaceutical Biotechnology, LMU). Figure adapted from [67] supplemental information.*

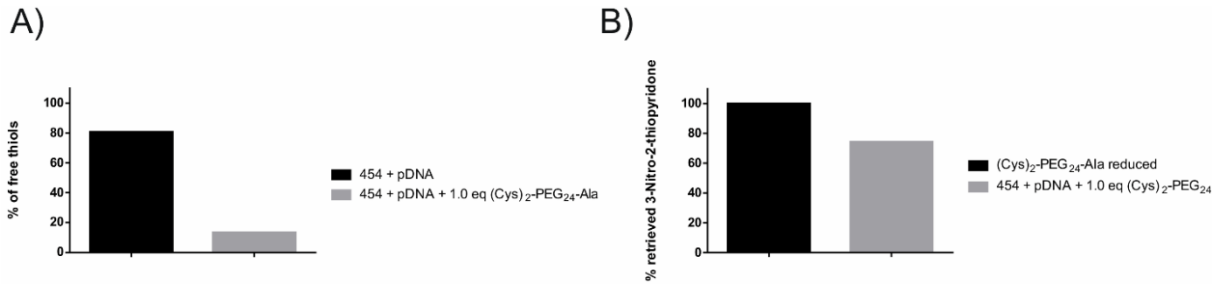

***Figure S5.** (A) Percentage of residual cysteine mercapto (SH) groups as determined with Ellman's assay for **454** polyplexes before (black) and after (grey) modification with 1.0 molar eq of (Cys)$_2$-PEG$_{24}$-Ala. The percentage of free mercapto groups is based on the theoretical amount (100%) of cysteines (two molar eq in Oligomer **454**) applied in the polyplex formation. (B) Release of 3-nitro-2-thiopyridone (detected at 324 nm) from 1.0 molar eq (Cys)$_2$-PEG$_{24}$-Ala after reduction. Complete 3-nitro-2-thiopyridone release after addition of 1M DTT solution (black bar) and after addition to a **454**/pDNA polyplex for further 15 min (grey bar) is displayed. Measurements were performed by Stephan Morys (Department of Pharmacy, Pharmaceutical Biotechnology, LMU). Figure adapted from [67] supplemental information.*

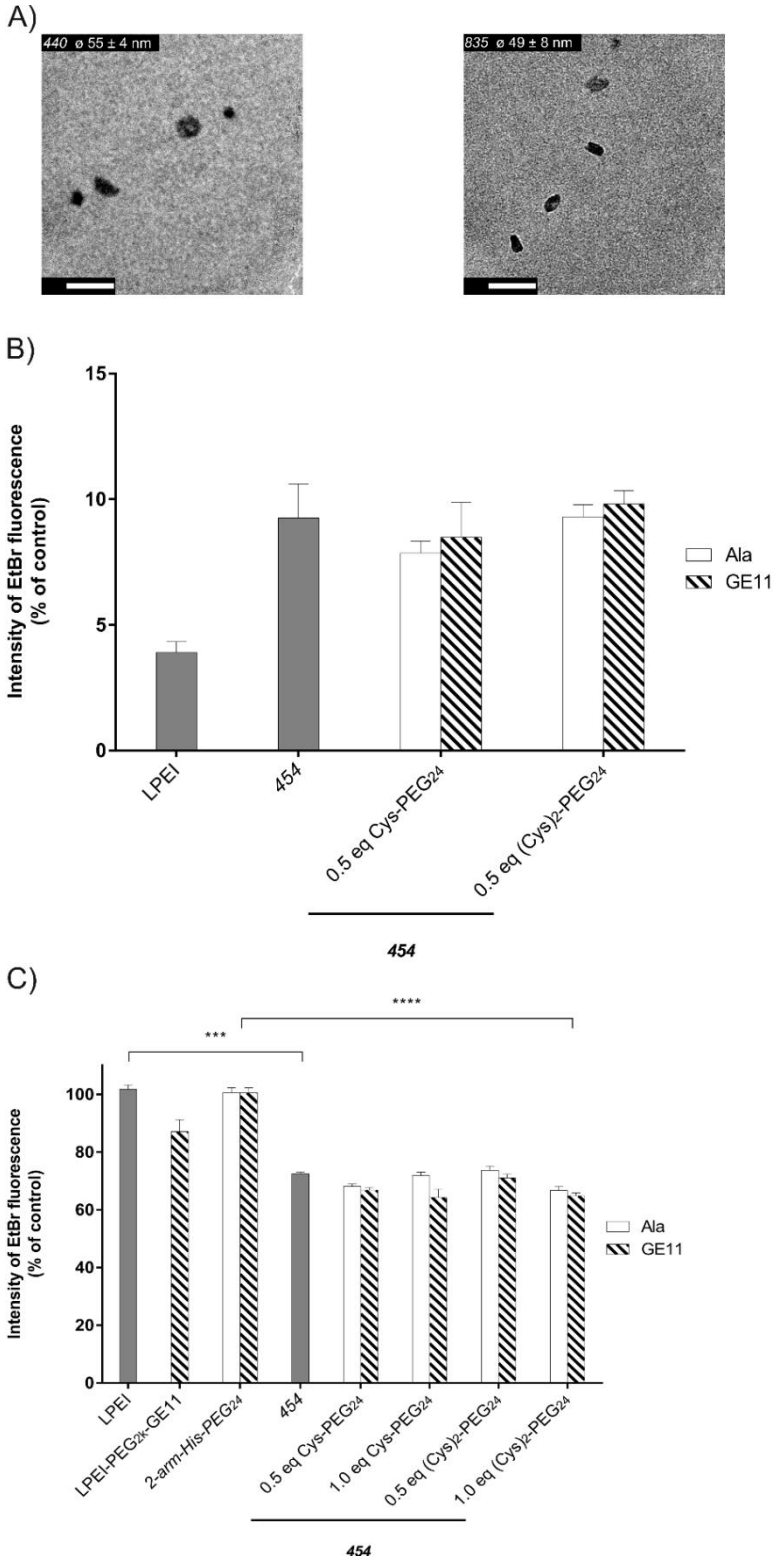

Figure S6. *(A) Transmission electron microscopy images (TEM) of pre-conjugated polyplexes **440** and **835** formed with 1 µg of pDNA at N/P 12. Average diameters (nm) of polyplexes (n=5) ± SD are displayed. Scale bar represents 100 nm. (B) displays pDNA compaction of polyplexes post-PEGylated with 0.5 eq of reagents determined with EtBr assay. (C) shows polyplex stability in presence of 250 IU heparine determined with EtBr assay. Untargeted controls are displayed in white, while polyplexes targeted with GE11 peptide are marked with pattern. Measurements were performed by Stephan Morys (Department of Pharmacy, Pharmaceutical Biotechnology, LMU). Figure adapted from [67] supplemental information.*

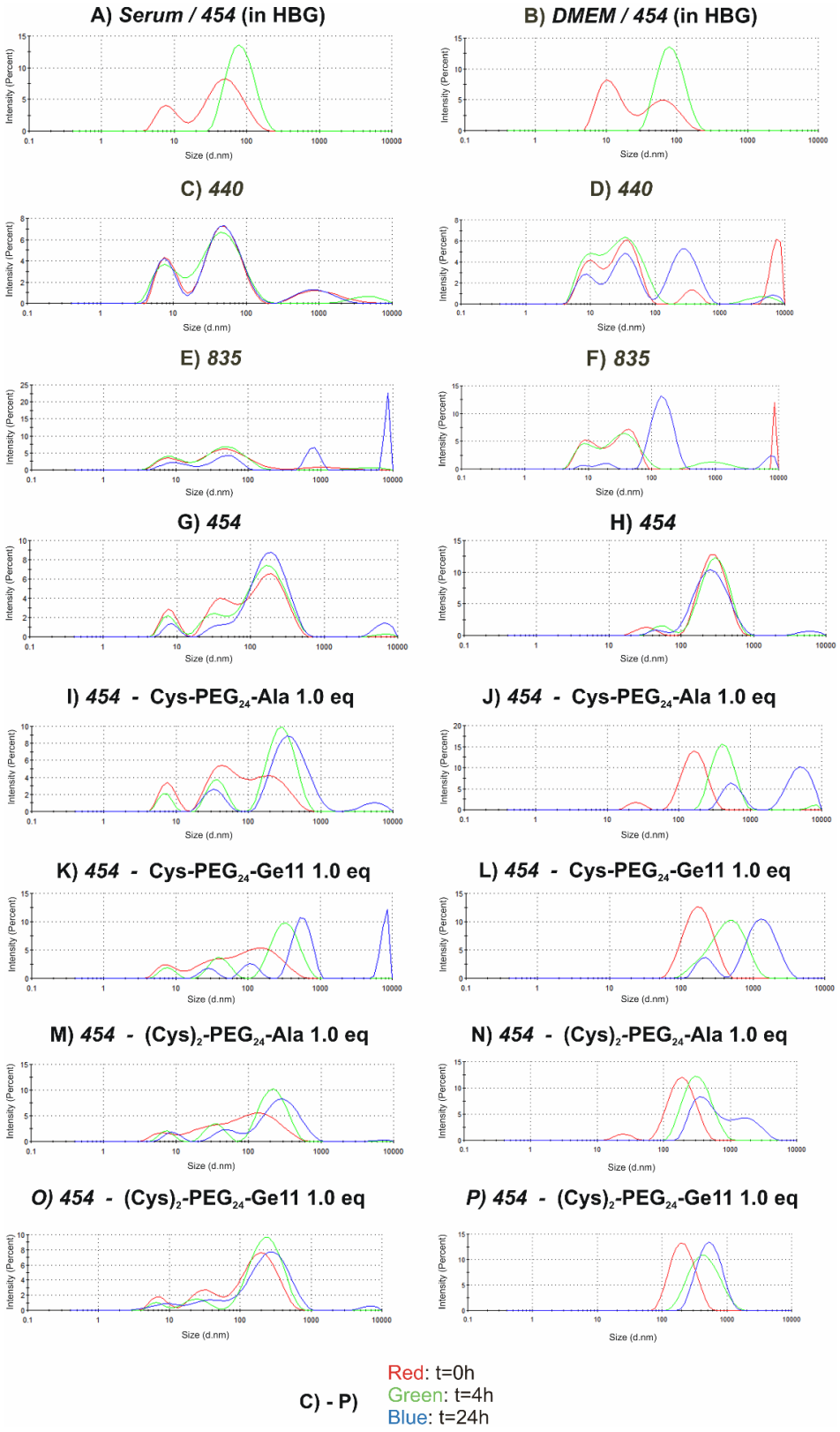

Figure S7. *Intensity mean curves maintained by DLS. Full serum (A) or DMEM (supplemented with 10% FBS) (B) is displayed in green and polyplexes of the **454**/pDNA in 10 mM NaCl in red. These references should help to discriminate between polyplex and serum (left column) /media (right column) peaks. (C) – (P) Display behavior of polyplexes with indicated oligomers in FBS (left) / DMEM (right) over time. Measurements were performed by Stephan Morys (Department of Pharmacy, Pharmaceutical Biotechnology, LMU). Figure adapted from [67] supplemental information.*

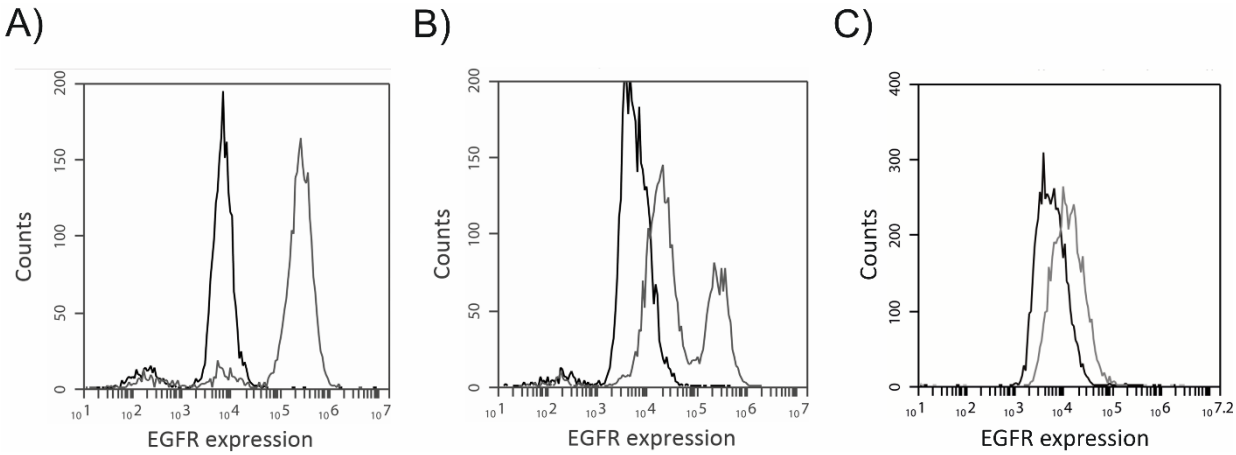

Figure S8. *EGFR expression of EGFR positive cell lines Huh7 (A), MCF-7 (B) as well as low EGFR expressing cell line FTC-133 (C) are displayed, obtained with a monoclonal mouse anti-human EGFR antibody and IgG control. Alexa 488-labeled goat anti-mouse secondary antibody was used for the detection of receptor expression by flow cytometry. Control cells are presented in black, EGFR positive cells are presented in grey. Figure adapted from [67] supplemental information.*

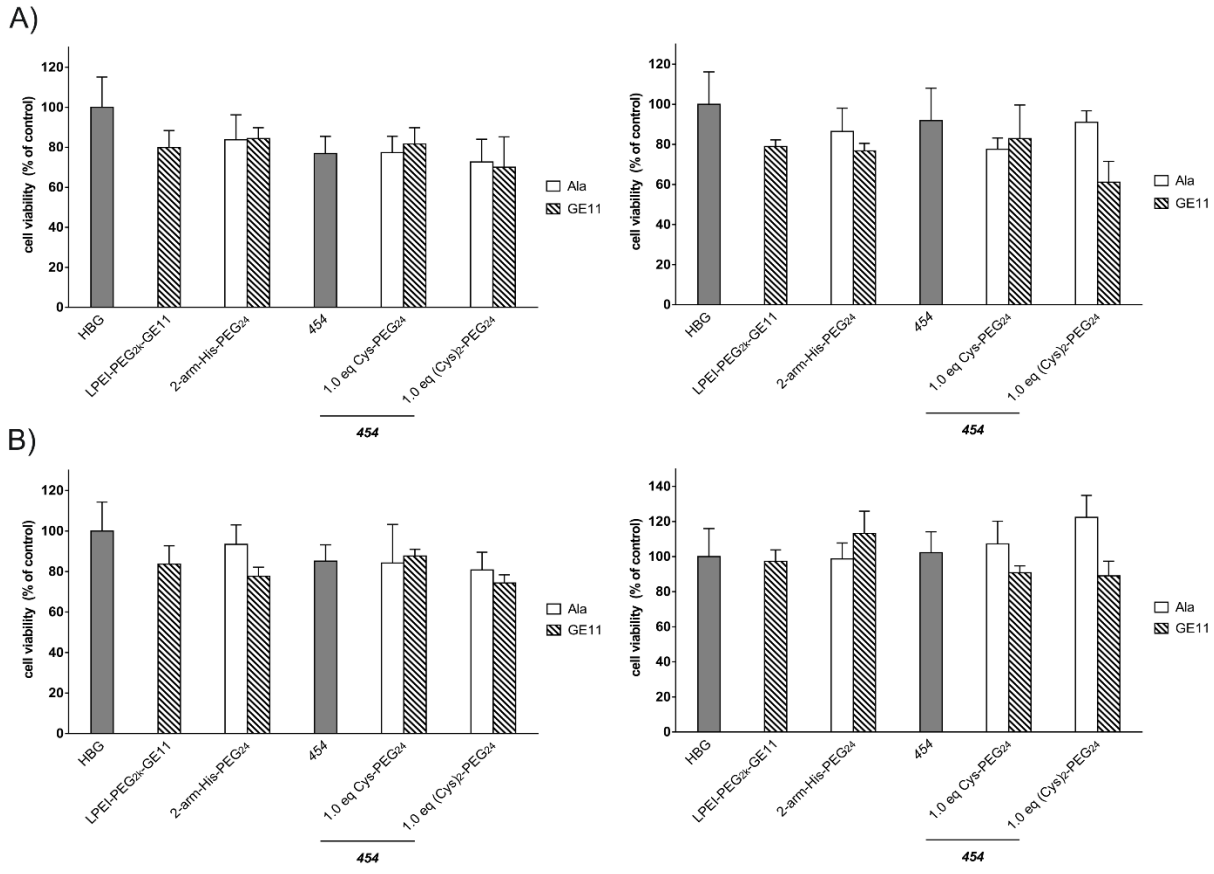

Figure S9. *Cell viability assay of (A) Huh7 and (B) MCF-7 was performed in parallel to luciferase transfection. MTT was performed after 45 min (left), and after 24 h (right). Figure adapted from [67] supplemental information.*

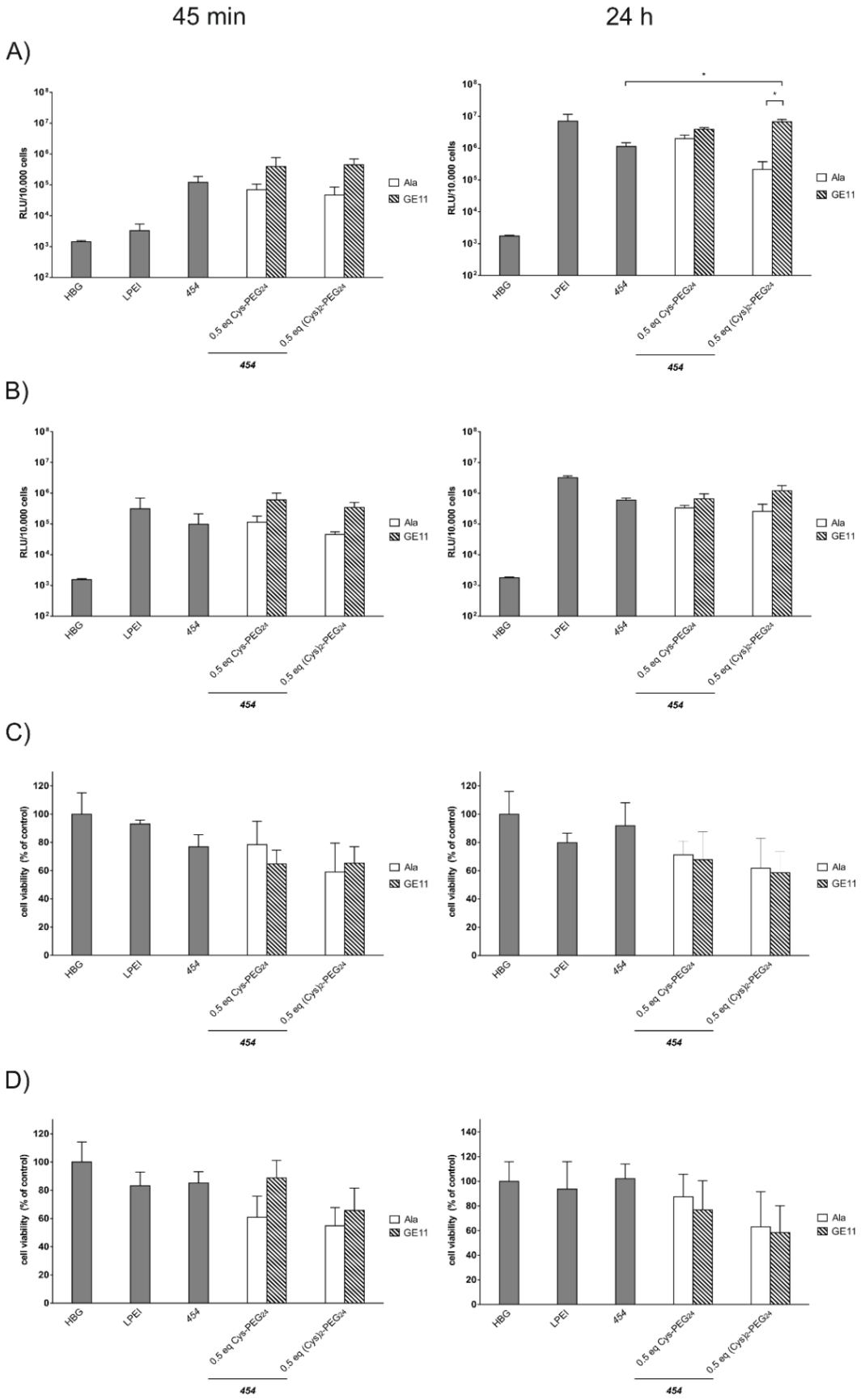

Figure S10. *Transfection of **454** polyplexes PEGylated with 0.5 eq after 45 min (left) and 24 h (right) are shown. Luciferase gene expression was determined on Huh7 (A) and MCF-7 (B), corresponding MTT assays were performed in parallel and are displayed in (C) and (D) respectively. Figure adapted from [67] supplemental information.*

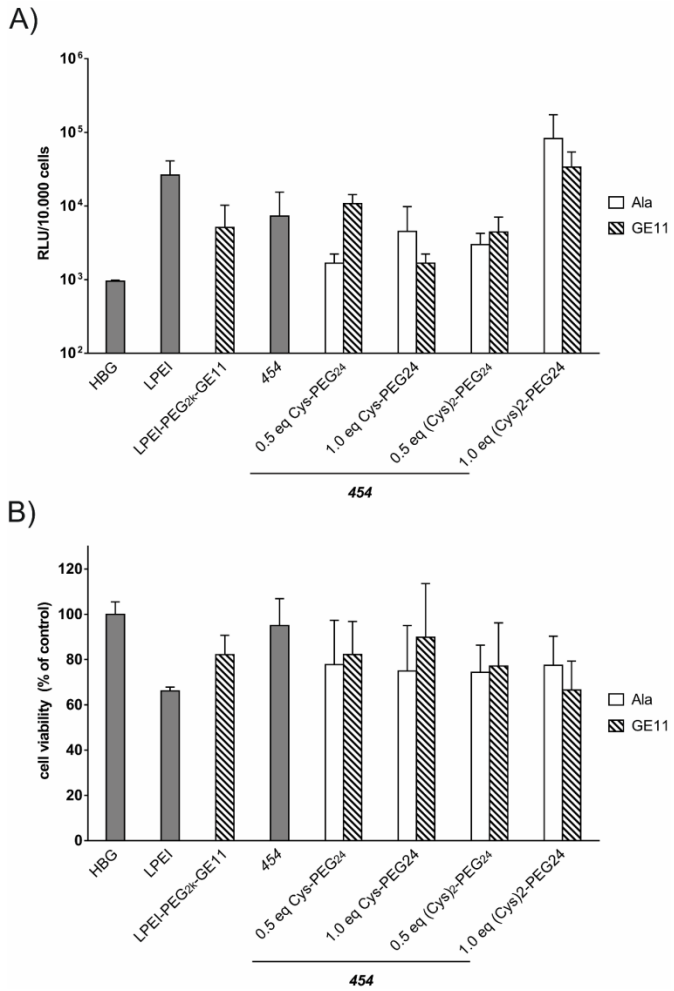

Figure S11. *Luciferase gene expression was determined on the low EGFR expressing cell line FTC-133 (A). Transfection results after 45 min of polyplex incubation are shown. The corresponding MTT assay was performed in parallel is displayed in (B). Figure adapted from [67] supplemental information.*

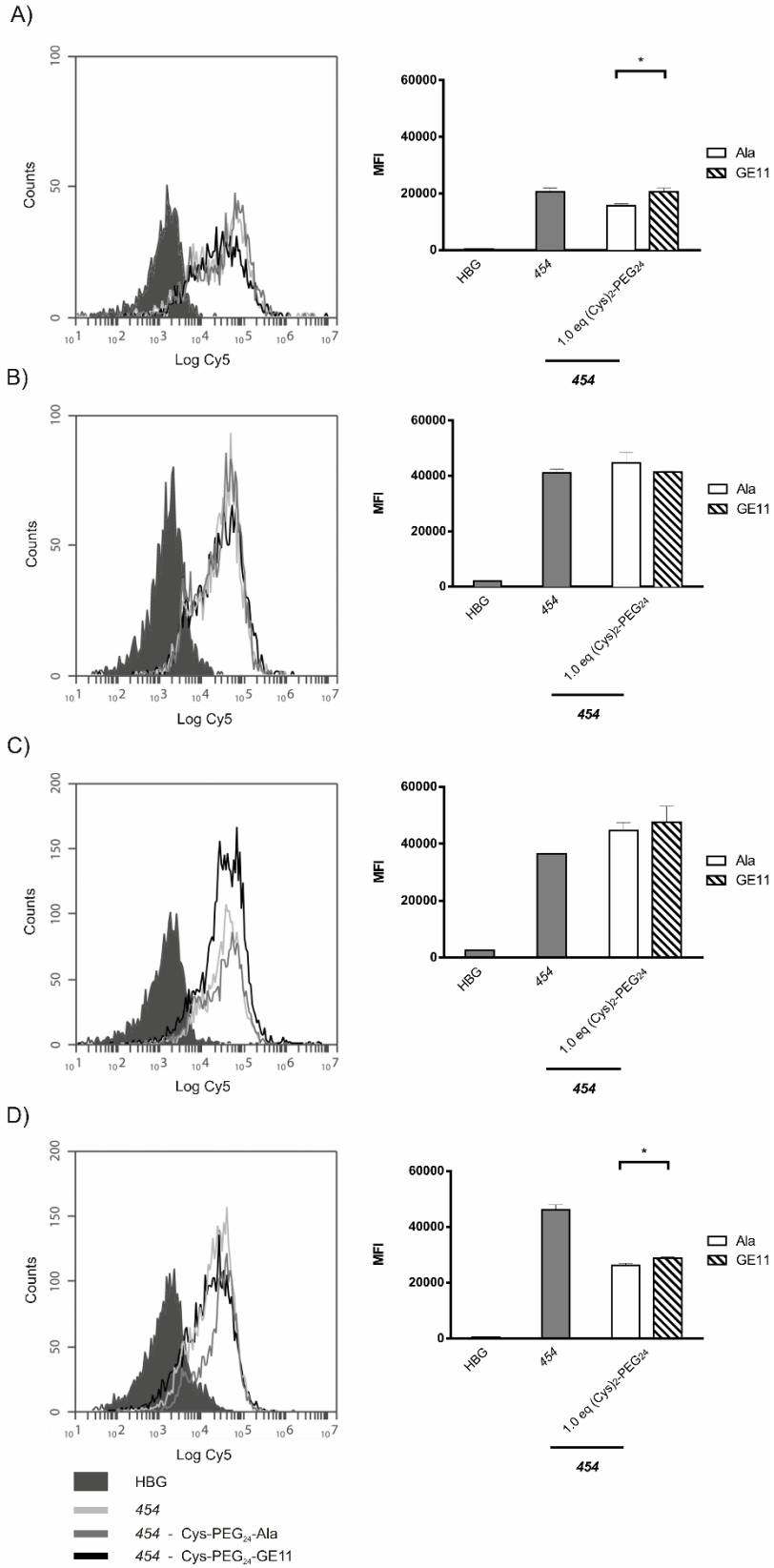

Figure S12. *Flow cytometry results of **454** polyplexes PEGylated with 1.0 eq of monovalent reagents as well as corresponding mean fluorescence intensity are displayed. Cellular association of polyplexes on Huh7 (A) and MCF-7 (C) after 30 min incubation at 4 °C was determined by flow cytometry. In (B) and (D) cellular internalization of polyplexes after 45 min of incubation at 37 °C followed by removal of extracellularly bound polyplexes is displayed. Logarithmic X-scale in (A) - (D) represents Cy5 fluorescence of polyplexes. Figure adapted from [67] supplemental information.*

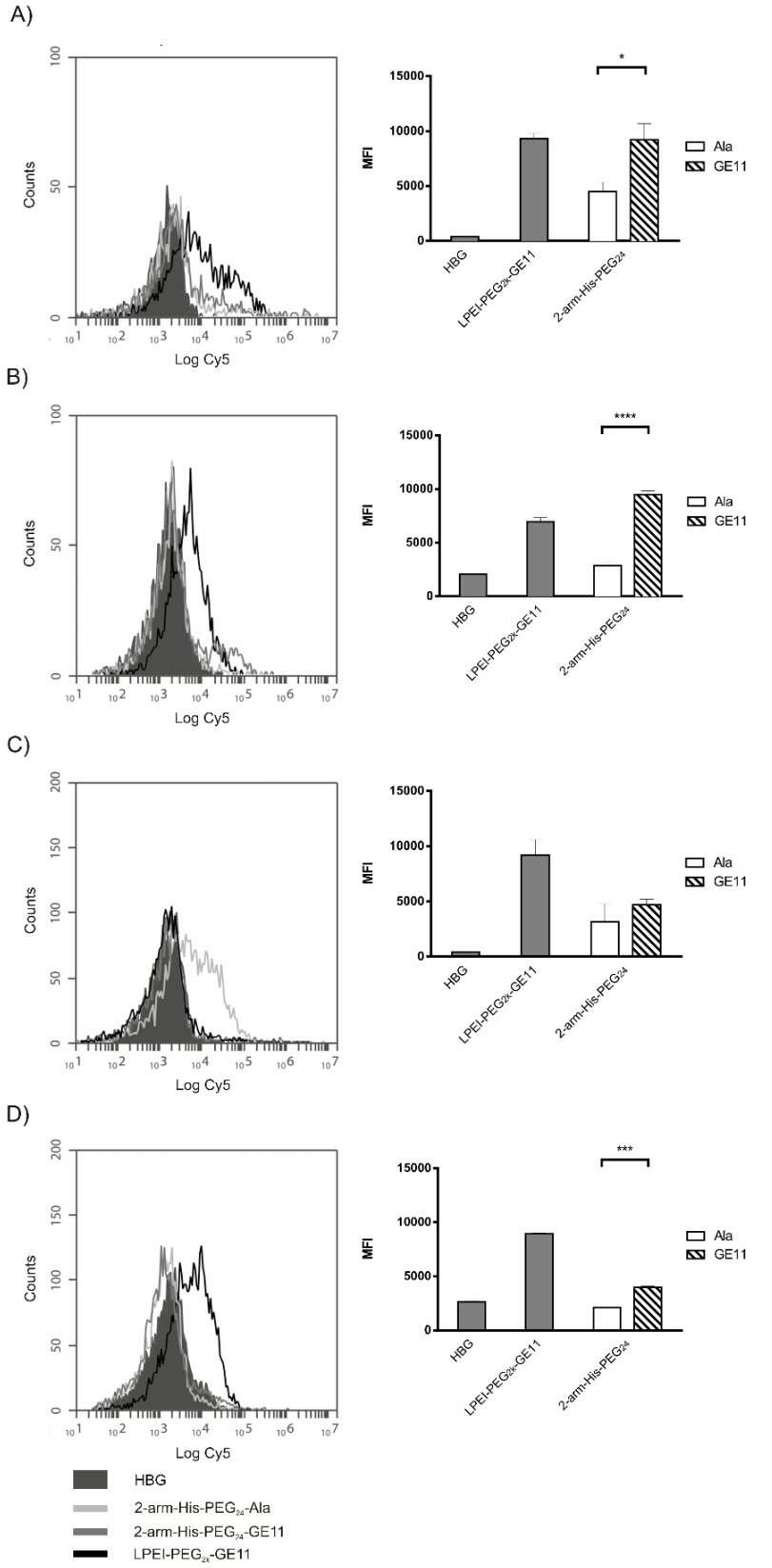

***Figure S13**. Flow cytometry results of pre-conjugated polyplexes as well as corresponding mean fluorescence intensity. Cellular association of polyplexes on Huh7 (A) and MCF-7 (C) after 30 min incubation at 4 °C was determined by flow cytometry. In (B) and (D) cellular internalization of polyplexes after 45 min of incubation at 37 °C followed by removal of extracellularly bound polyplexes is displayed. Logarithmic X-scale in (A) - (D) represents Cy5 fluorescence of polyplexes. Figure adapted from [67] supplemental information.*

Analytical data

Analytical experiments were performed by Stephan Morys (Department of Pharmacy, Pharmaceutical Biotechnology, LMU). Figures adapted from [67] supplemental information.

Maldi-MS and RP-HPLC of GE11 peptide

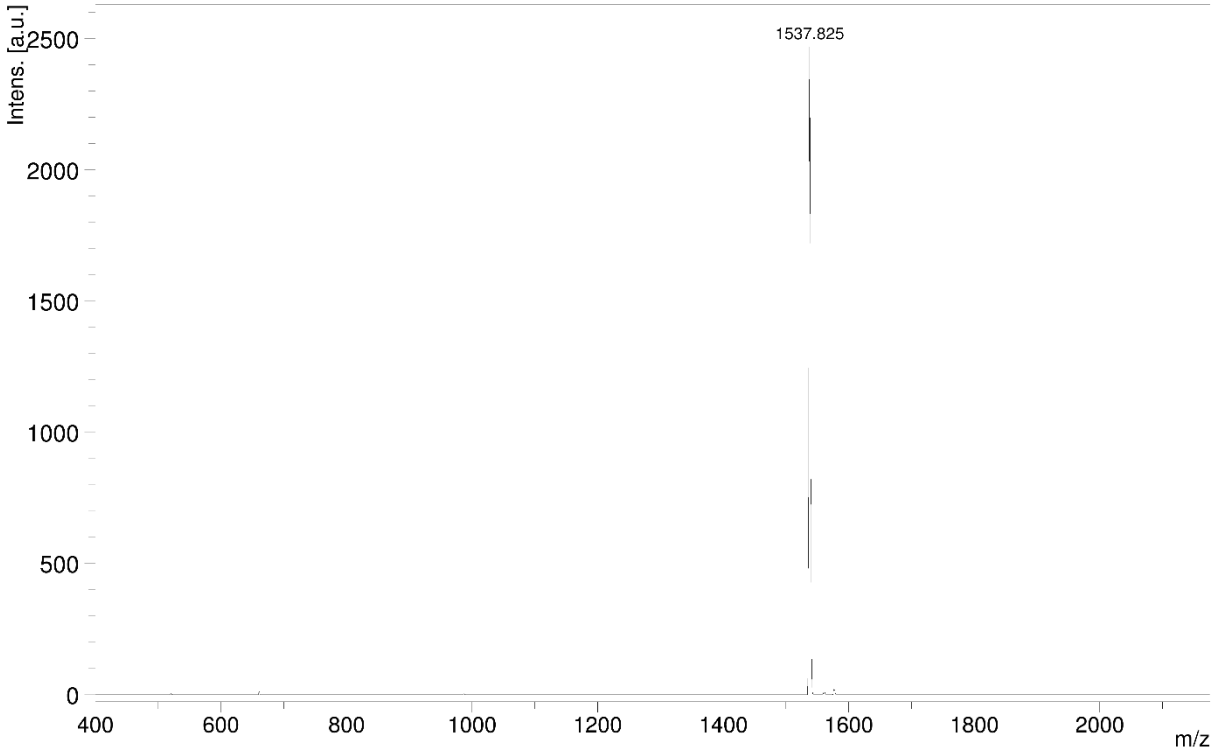

***Figure S14**. MALDI-MS of GE11 peptide: Calculated mass [M+H] of $C_{75}H_{97}N_{17}O_{19}$: 1541.70 g/mol. Adapted from [67] supplemental information.*

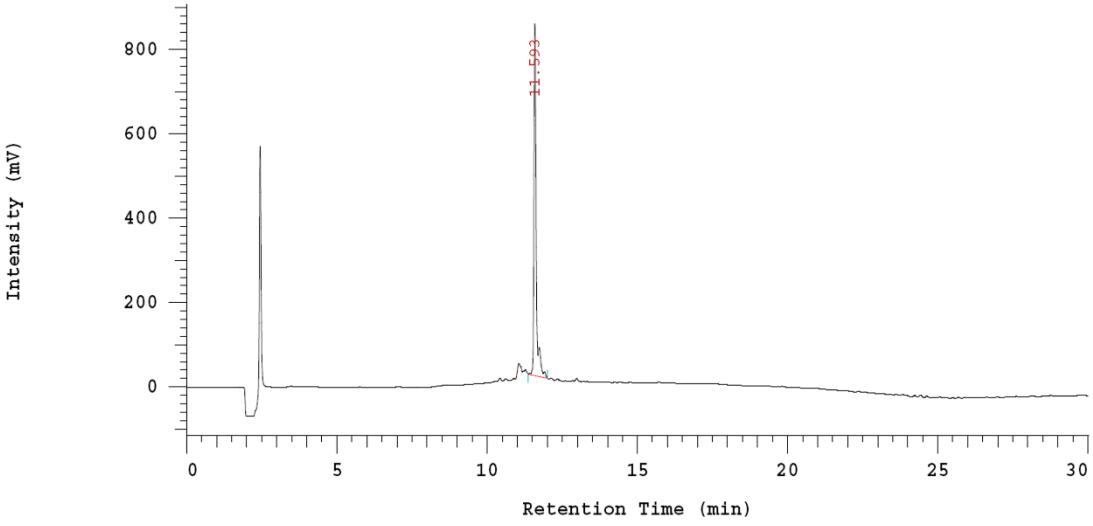

Figure S15. *RP-HPLC of GE11 peptide. Adapted from [67] supplemental information.*

^{1}H-NMR and RP-HPLC of oligomer *440*

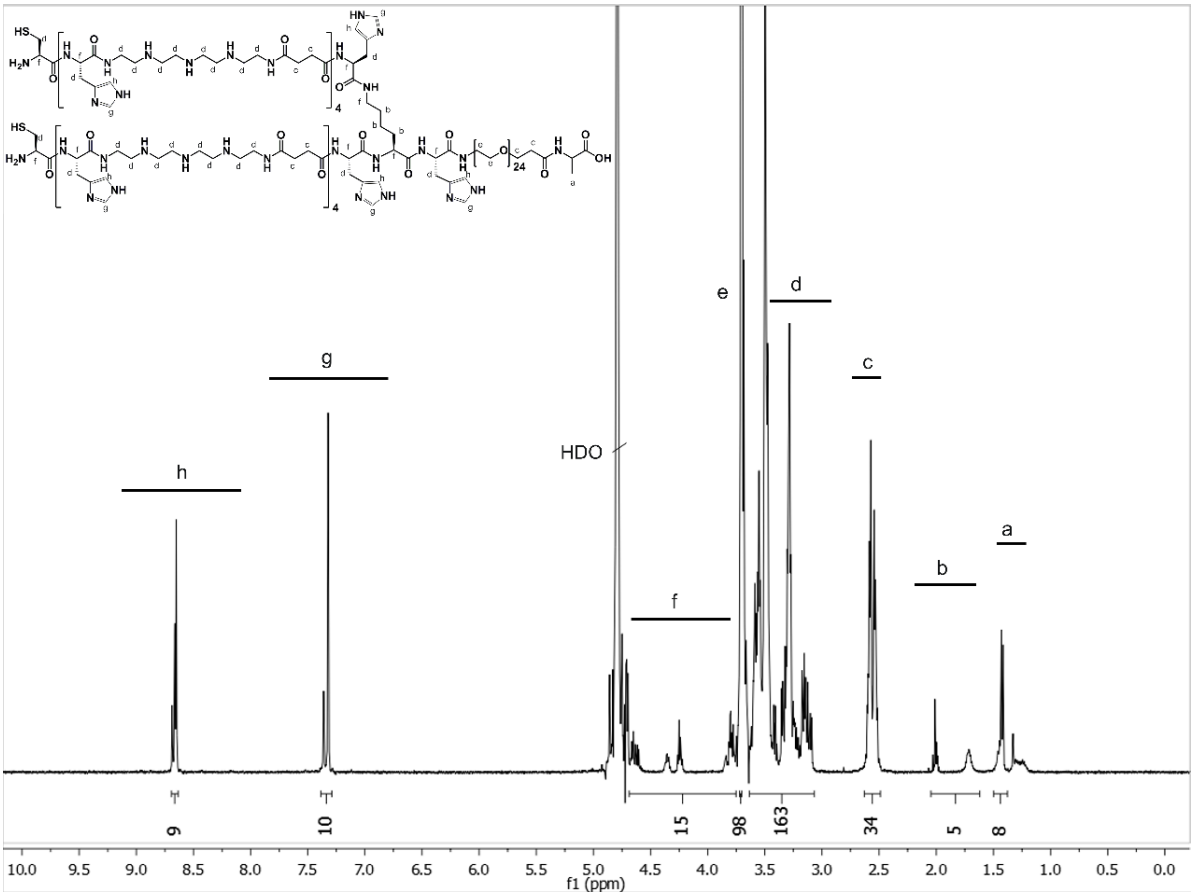

Figure S16. *^{1}H-NMR spectrum of **440** in D_2O. δ (ppm) = 1.3-1.45 (comp, 3H, βH alanine), 1.6-2.0 (comp, 6H, βγδH lysine), 2.4-2.6 (comp, 34 H, -CO-CH_2-CH_2-CO- succinic acid -CO-CH2-dPEG$_{24}$), 3.0 -3.65 (comp, 156 H, -CH_2- tepa, H lysine, βH cysteine, βH histidine), 3.70 (s, 98H, -CH2-O-dPEG$_{24}$, -CH2-N-dPEG$_{24}$), 3.75-4.75 (comp, 15 H, αH cysteine, lysine, histidine), 4.79 (s, HDO), 7.2-7.4 (m, 11 H, aromatic H histidine), 8.5-8.7 (m, 11 H, aromatic H histidine). comp indicates a group of overlaid protons. Adapted from [67] supplemental information.*

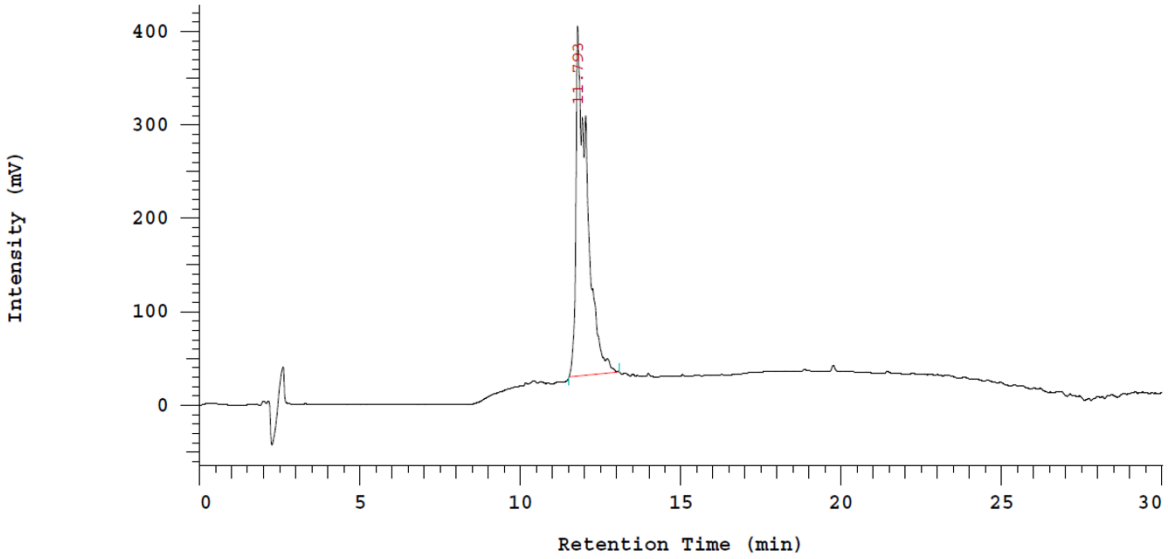

Figure S17. RP-HPLC of ***440.*** *Adapted from [67] supplemental information.*

^{1}H-NMR and RP-HPLC of oligomer *835*

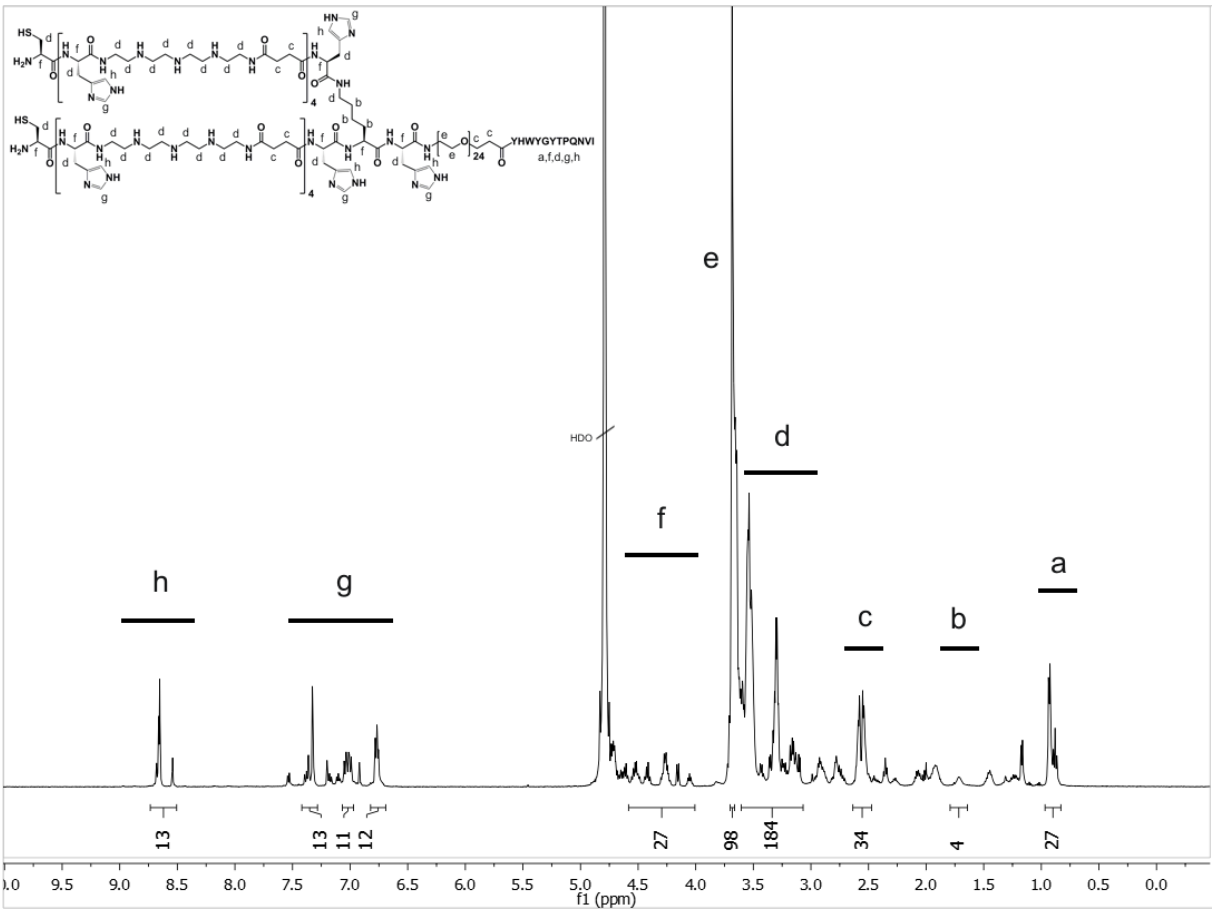

Figure S18. *^{1}H-NMR spectrum of **835** in D_2O δ (ppm) = 0.75-1.0 (m, 19H, γH threonine β-CH_3 γδH isoleucine, β-CH_3 valine), 1.60-1.80 (m, 6H, βγδH lysine), 2.35-2.54 (m, 34 H, -CO-CH_2-CH_2-CO- succinic acid, -CO-CH_2-dPEG24), 3.1-3.65 (m, 174 H, -CH_2- tepa, H asparagine, βH cysteine, βH histidine, βH tryptophan, βH tyrosine, δH proline, βH asparagine, βH valine, εH lysine), 3.74-3.8 (m, 98 H, -CH_2-O- dPEG24, -CH_2-N- dPEG24), 4.1-4.65 (m, 26 H, αH amino acids), 4.75 (s, HDO), 6.7-7.42 (m, 29 H, aromatic ring H tyrosine, tryptophan, imidazole), 8.52-8.70 (m, 11 H, imidazole). Adapted from [67] supplemental information.*

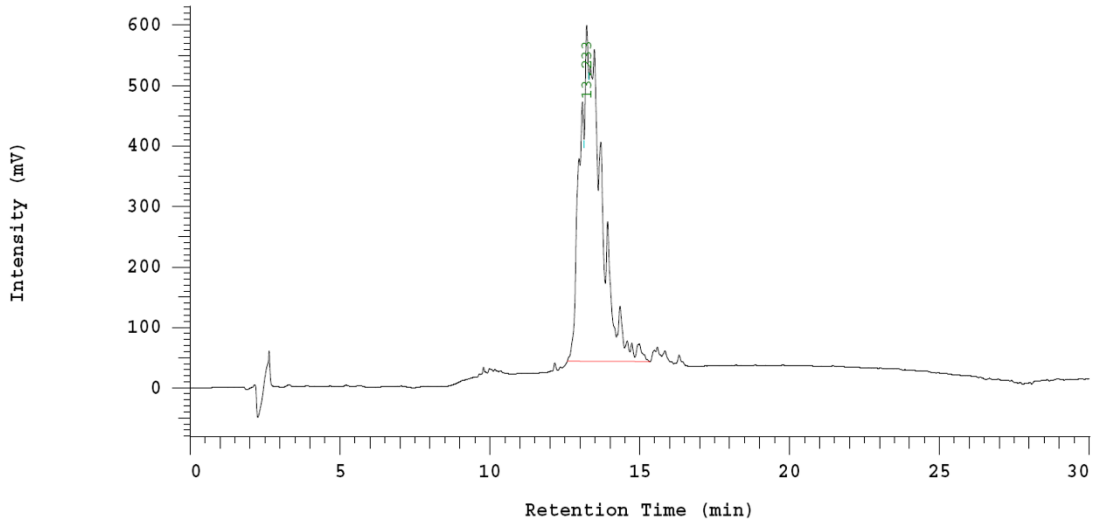

Figure S19. *RP-HPLC of* ***835.*** *Adapted from [67] supplemental information.*

Maldi-MS of oligomer *454*

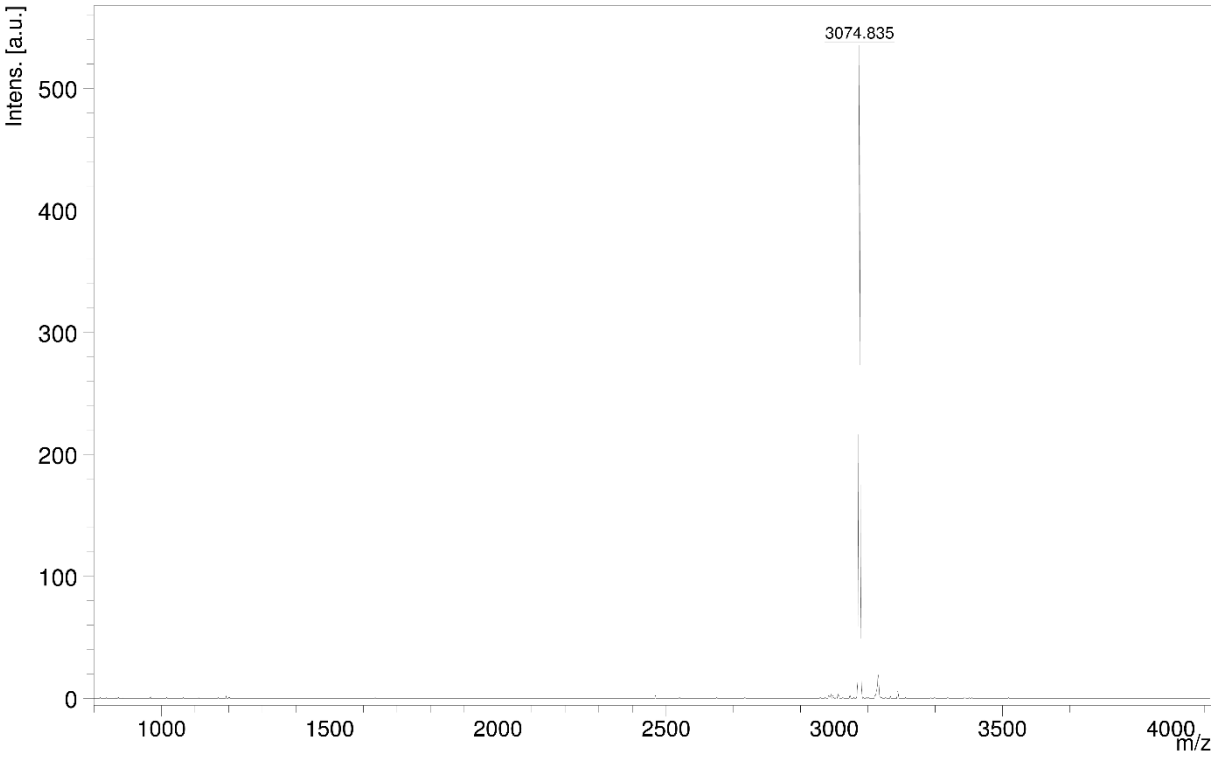

Figure S20. *MALDI MS of* ***454****: Calculated mass [M-H] of* $C_{234}H_{421}N_{62}O_{63}S_2$*: 3074.07 g/mol. Adapted from [67] supplemental information.*

ESI MS and RP-HPLC of Ala-PEG$_{24}$-Cys(NPys)

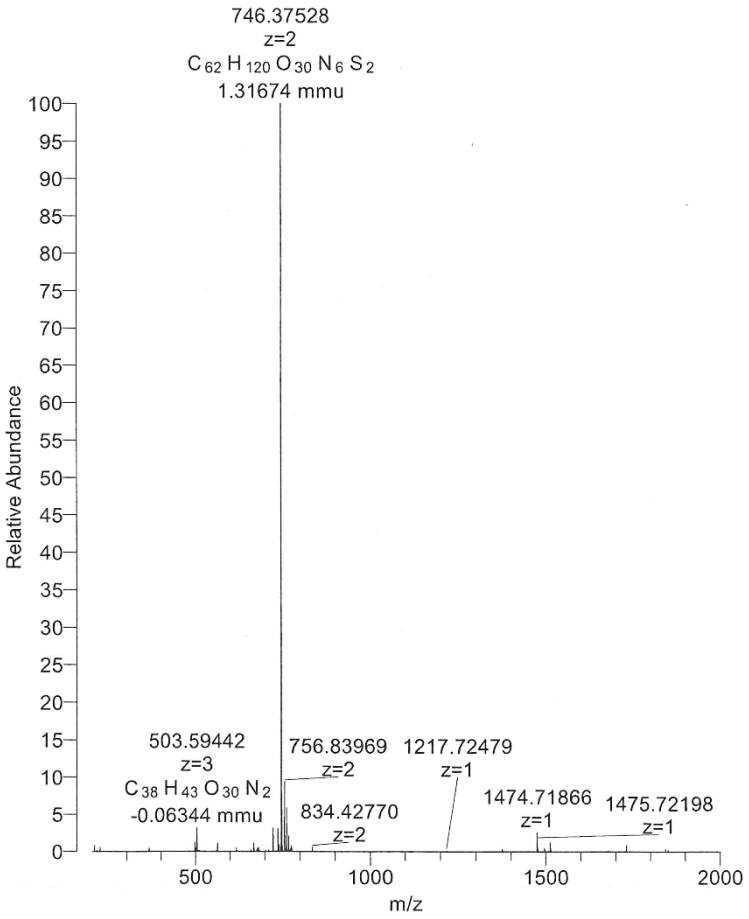

Figure S21. *ESI MS of Ala-PEG$_{24}$-Cys(NPys): Calculated Mass [M+Na] of $C_{62}H_{114}N_5O_{30}S_2Na$: 1495.71 g/mol. Adapted from [67] supplemental information.*

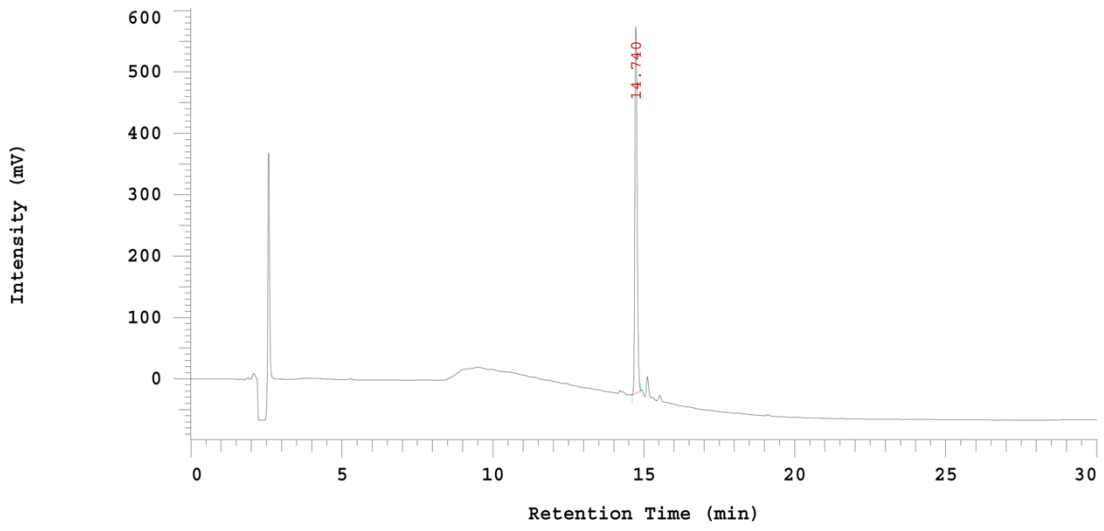

Figure S22. *RP-HPLC of Ala-PEG$_{24}$-Cys(NPys). Adapted from [67] supplemental information.*

ESI MS and RP-HPLC of GE11-PEG$_{24}$-Cys(NPys)

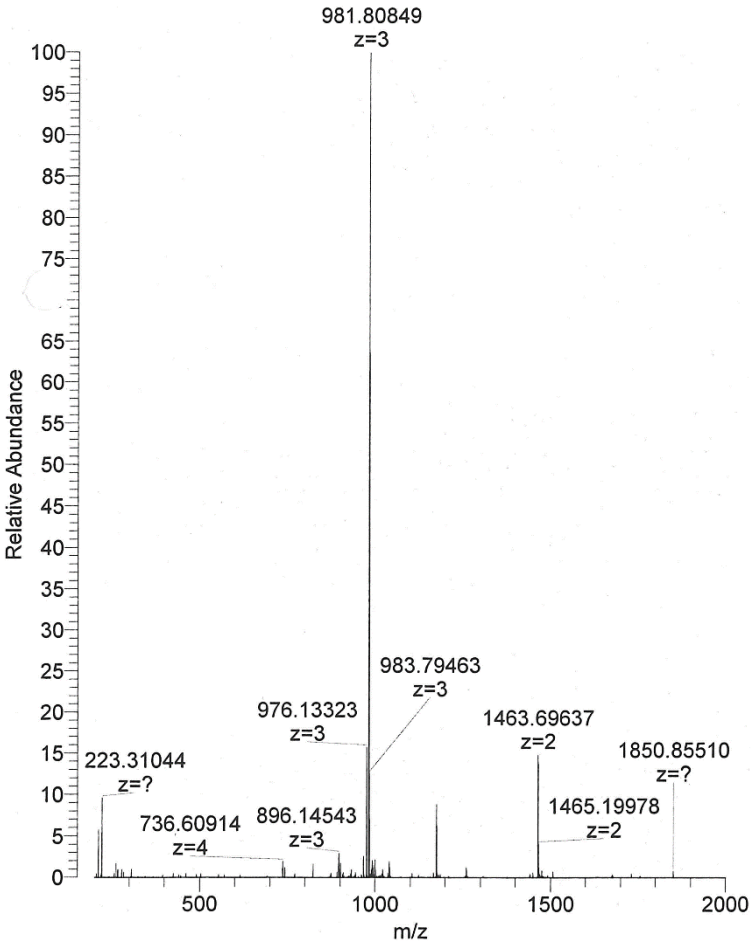

Figure S23. *ESI MS of GE11-PEG$_{24}$-Cys(NPys): Calculated Mass [M+Na] of $C_{134}H_{204}N_{21}O_{47}S_2Na$: 2948.33 g/mol. Adapted from [67] supplemental information.*

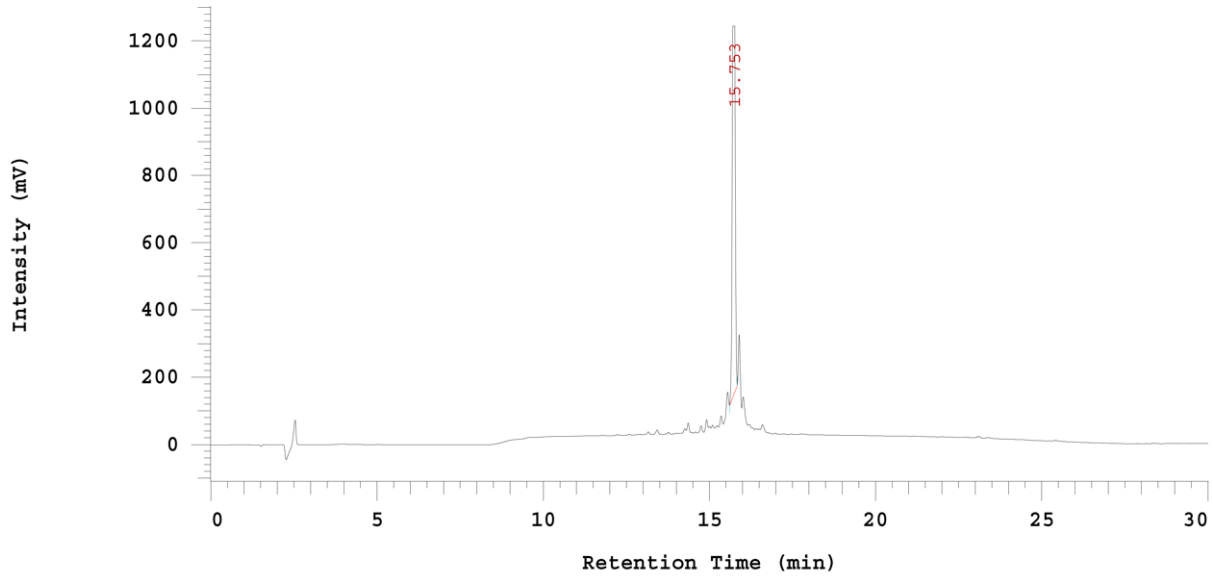

Figure S24. *RP-HPLC of GE11-PEG$_{24}$-Cys(NPys). Adapted from [67] supplemental information.*

ESI MS and RP-HPLC pf Ala-PEG$_{24}$-Cys(NPys)$_2$

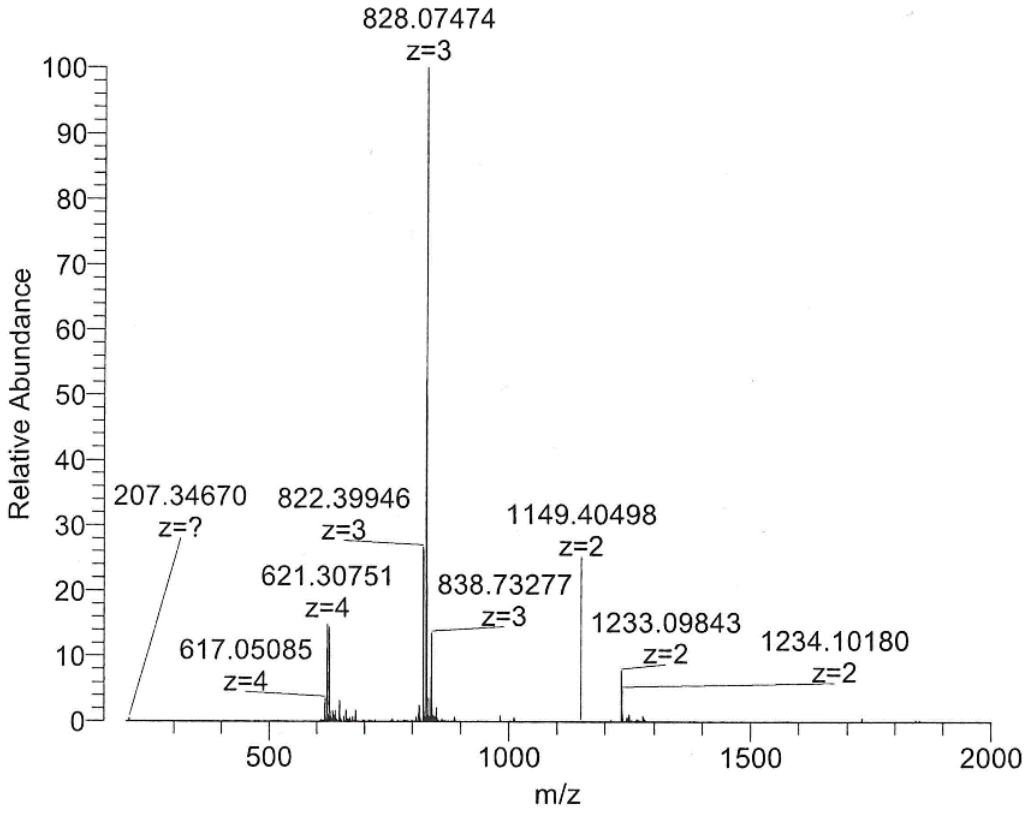

Figure S25. *ESI MS of Ala-PEG$_{24}$-Cys(NPys)$_2$: Calculated Mass [M+Na] of $C_{104}H_{185}N_{14}O_{44}S_4Na$: 2486.93 g/mol. Adapted from [67] supplemental information.*

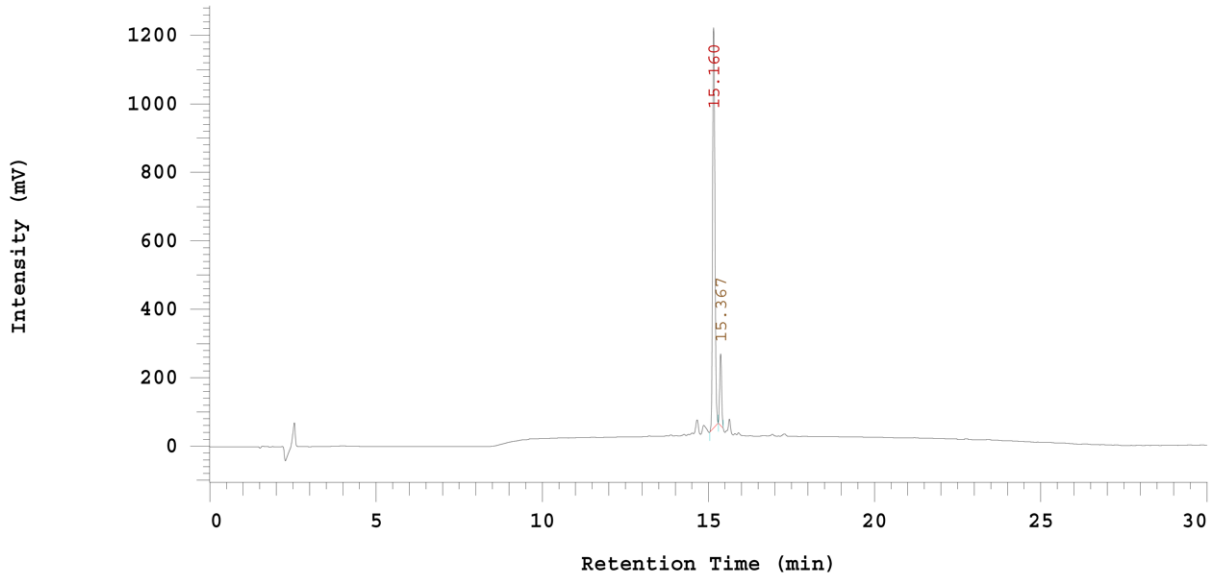

Figure S26. *RP-HPLC of Ala-PEG$_{24}$-Cys(NPys)$_2$. Adapted from [67] supplemental information.*

ESI MS and RP-HPLC pf GE11-PEG$_{24}$-Cys(NPYS)$_2$

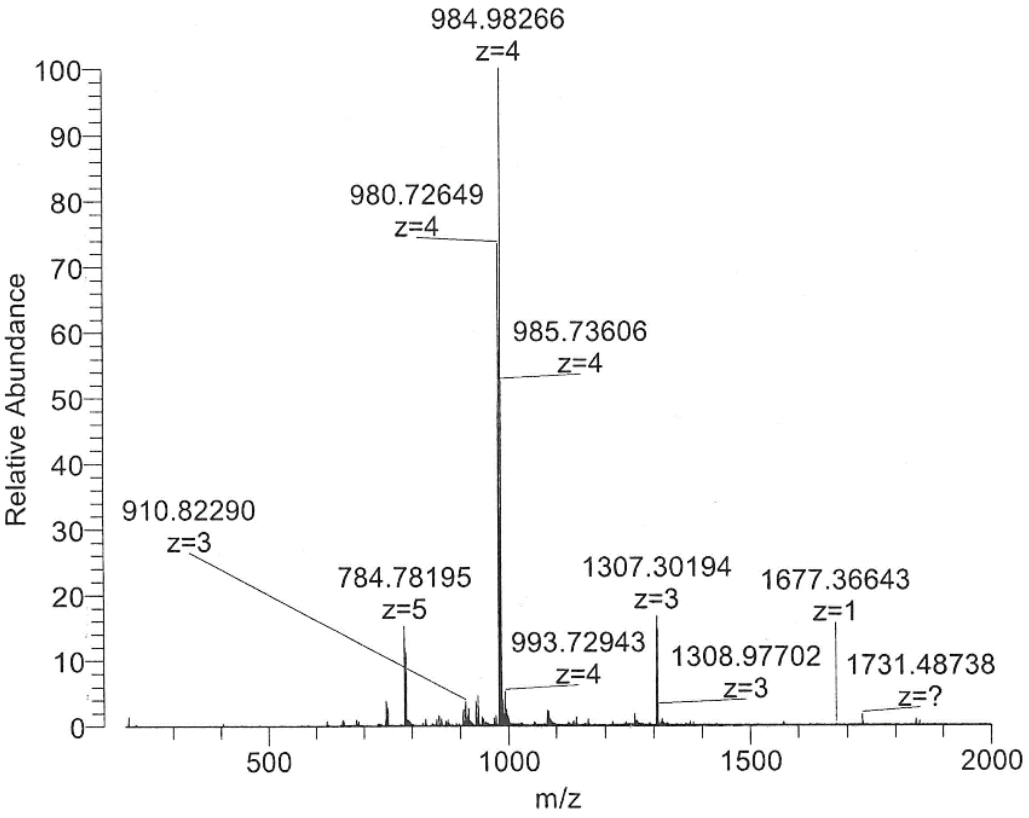

Figure S27. *ESI MS of GE11-PEG$_{24}$-Cys(NPys)$_2$: Calculated Mass [M+Na] of $C_{176}H_{275}N_{30}O_{61}S_4Na$: 3938,53 g/mol. Adapted from [67] supplemental information.*

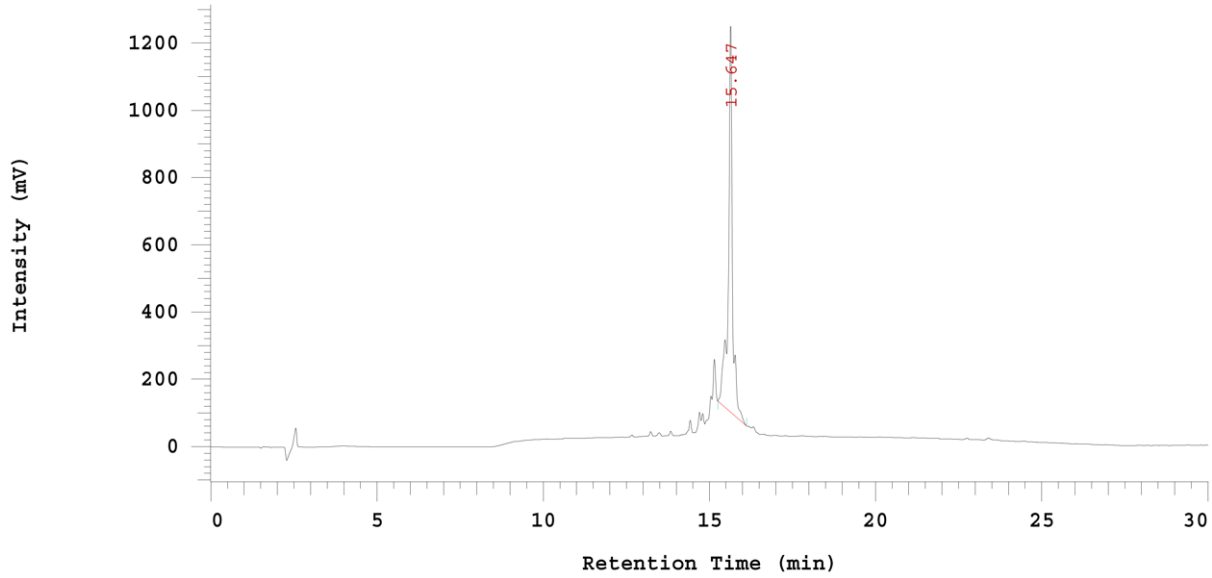

Figure S28. *RP-HPLC of GE11-PEG$_{24}$-Cys(NPys)$_2$. Adapted from [67] supplemental information.*

Conjugate	Calculated Mass (g/mol)	Detected Mass (g/mol)
GE11 Peptide	1541.70 [M+H]	1537.83
454	3074.07 [M-H]	3074.84
Ala-PEG_{24}-Cys(NPys)	1495.71 [M+Na]	1492.76
GE11-PEG_{24}-Cys(NPys)	2948.33 [M+Na]	2945.43
Ala-PEG_{24}-$Cys(NPys)_2$	2486.93 [M+Na]	2484.3
GE11-PEG_{24}-$Cys(NPys)_2$	3939.53 [M+Na]	3939.96

Table S2. *Calculated and detected mass of conjugates. Adapted from [67] supplemental information.*

7.7 Acknowledgements

We want to thank Susanne Kempter and Caroline Hartl (Department of Physics, LMU Munich) for providing TEM images of polyplexes, Dr. Werner Spahl (Department of Chemistry, LMU Munich) for ESI mass spectroscopy and Dr. Ulrich Lächelt for scientific discussion. We also want to thank Olga Brück for secretarial assistance and Wolfgang Rödl for technical support.

This work was supported by grants from the Deutsche Forschungsgemeinschaft within the Collaborative Research Center SFB824 (project C 08) to C. Spitzweg and E. Wagner, SFB1032 (project B 04 to E. Wagner), SFB1066 (project B5 to E. Wagner), as well as within the Priority Program SPP1629 to C. Spitzweg (SP 581/6-1, SP581/6-2), the Cluster of Excellence Nanosystems Initiative Munich (NIM) to E. Wagner, a grant from the Wilhelm-Sander-Stiftung to C. Spitzweg (2014.129.1) and the Sino-German Center research grant GZ995 to E Wagner.

8. Summary

Polymers as gene delivery vehicles gained great success for cancer gene therapy over the last years. At the same time, the sodium iodide symporter (NIS) emerged as outstanding therapy gene. The combinatorial “theranostic” function as a reporter and therapy gene, based on the capacity to transport various radionuclides into the cell, allows for exact quantification of NIS gene expression in the tumor lesion by multimodal imaging of radionuclide uptake as well as therapeutic intervention by application of cytotoxic radionuclides. However, one of the biggest obstacles for nonviral polymer-mediated NIS gene therapy is the design of safe, specific and efficient carriers.

The innovative concept of active receptor-targeted nonviral NIS gene delivery owns enormous potential with high clinical relevance for systemic treatment of solid tumors as well as metastases. But despite the current standard, major progress must be made in the further development of the polymeric delivery systems to improve efficacy, in particular in heterogeneic tumors, biocompatibility, safety, selectivity, uptake and endosomal escape. In the course of this thesis, novel tumor-targeted systems were established and applied for image-guided NIS gene therapy.

The first step was, to set up a broad repertoire of highly efficient and tumor specific ligands. This enables application of the ligand-mediated NIS gene delivery in a broad range of malignancies that exhibit different receptor expression profiles. The peptide ligands B6 (high tumor-cell binding affinity), GE11 (targeting EGFR) and cMBP (targeting cMET) were coupled to the well-established LPEI-PEG_{2kDa} backbone, which had already been verified as advantageous system with improved performance *in vivo*. B6-conjugated nonviral delivery vehicles specifically introduce NIS to cancer tissue with high efficacy after systemic application, which was assessed by ^{123}I gamma-camera imaging. In a therapy trial, significant NIS-mediated ^{131}I accumulation induced decelerated tumor growth with prolonged animal survival.

As a next step, EGFR-targeted LPEI-PEG_{2kDa} polyplexes were applied in a colon cancer metastases model. This valuable tool was selected to reflect the clinical situation on a morphological and molecular level including the natural tumor microenvironment and tumor stroma to allow a better prediction of therapy outcome. Using the novel NIS PET-tracer ^{18}F-TFB, specific imaging of NIS gene expression in single metastases was obtained. Images demonstrated high resolution with exact mapping of metastases that showed significantly increased tracer uptake after EGFR-targeting compared to animals treated with untargeted control polyplexes. Subsequent evaluation of the therapeutic efficacy of the EGFR-targeted

NIS gene delivery approach resulted in reduced hepatic metastases load of animals treated with ^{131}I, monitored by contrast-enhanced ultrasound, and prolonged animal survival.

With respect to a future translation to humans, where tumor heterogeneity displays a major hurdle causing therapy resistance and limited efficacy, a combinatorial ligand set-up was applied to cope with variable receptor expression levels. Simultaneous targeting of EGFR and cMET for NIS gene therapy combined two outstanding bispecific approaches: (1) application of NIS with its innate dual characteristics to function as reporter and therapy gene and (2) using the synergy of dual-targeting of two receptors. Enhanced uptake and increased NIS gene expression *in vitro* and *in vivo* highlighted the benefits of the bifunctional strategy. Therapeutic intervention by application of cytotoxic ^{131}I resulted in efficient cancer treatment mirrored by reduced tumor growth and improved animal survival and allows successful application even in heterogeneic tumors.

To further improve applicability of delivery vectors, solid-phase methodology was applied for synthesis and design of novel functionalized nanosystems that contain precise numbers of molecules with structure-activity relationship. The precise synthesis allowed for integration of DNA binding sites, shielding domains, amino acids with high buffering capacity and specific ligands that resulted in optimized transfection efficiency, while adverse effects such as toxicity or high immunogenicity were reduced. Based on high cMET expression level on many cancer cells, this receptor serves as an ideal target for cancer therapy. Coupling novel sequence defined polymers to a cMET-binding peptide ligand, systemic NIS gene delivery led to significant tumoral NIS mediated iodide uptake that was sufficiently high for a potent therapeutic effect after ^{131}I application.

To optimize particle structure and performance of shielded PEGylated vectors, a postintegration strategy was conducted. Preformed oleic acid containing sequence defined oligomers were complexed with luciferase or NIS pDNA. As a second step, 1-arm and 2-arm structures composed of PEG coupled to the EGFR-specific peptide ligand GE11 were added to the preformed lipopolyplexes. Chemical characteristics and transfection efficiency were determined *in vitro* and superiority of 2-arm structures was detected. This strategy forms the basis for a future application *in vivo* with the advantage of exact formed lipopolyplexes were the effect on size and looser compaction of the shielding domain can be reduced and hydrophobic ligands can be introduced.

In conclusion, in the course of this thesis, the concept of active receptor targeted nonviral NIS gene therapy has been refined. High efficacy and tumor specificity in advanced tumor models was obtained and together with further development of LPEI-based delivery vectors to defined systems, a more efficient and safe application of the image-guided NIS gene therapy was performed. This highlights the enormous potential of nonviral polymeric systems

as gene transfer systems as well as the outstanding property of NIS in cancer therapy and forms the basis for successful future clinical translation of the NIS gene therapy concept.

9. Publications

9.1 Original papers

Urnauer S, Schmohl KA, Tutter M, Schug C, Schwenk N, Morys S, Ziegler S, Bartenstein P, Clevert DA, Wagner E, Spitzweg C. Dual-targeting strategy for improved nonviral gene transfer of the theranostic sodium iodide symporter. [Submitted manuscript]

Urnauer S, Müller AM, Schug C, Schmohl KA, Tutter M, Schwenk N, Rödl W, Morys S, Ingrisch M, Bertram J, Bartenstein P, Clevert DA, Wagner E, Spitzweg C. EGFR-targeted nonviral NIS gene transfer for bioimaging and therapy of disseminated colon cancer metastases. Oncotarget. 2017 Sep 16;8(54):92195-92208

Morys S, **Urnauer S**, Spitzweg C, Wagner E. EGFR targeting and shielding of pDNA lipopolyplexes via bivalent attachment of a sequence-defined PEG agent. Macromol Biosci. 2017. [in press]; SM and SU contributed equally to this work

Morys S, Levacic AK, **Urnauer S**, Kempter S, Kern S, Rädler JO, Spitzweg C, Wagner E. Influence of defined hydrophilic blocks within oligoaminoamide copolymers: compaction versus shielding of pDNA nanoparticles. Polymers. 2017. [in press]

Urnauer S, Klutz K, Grünwald GK, Morys S, Schwenk N, Zach C, Gildehaus FJ, Rödl W, Ogris M, Wagner E, Spitzweg C. Systemic tumor-targeted sodium iodide symporter (NIS) gene therapy of hepatocellular carcinoma mediated by B6 peptide polyplexes. J Gene Med. 2017 May;19(5). SU and KK contributed equally to this work

Müller AM, Schmohl KA, Knoop K, Schug C, **Urnauer S**, Hagenhoff A, Clevert DA, Ingrisch M, Niess H, Carlsen J, Zach C, Wagner E, Bartenstein P, Nelson PJ, Spitzweg C. Hypoxia-targeted 131I therapy of hepatocellular cancer after systemic mesenchymal stem cell-mediated sodium iodide symporter gene delivery. Oncotarget. 2016 Aug 23;7(34):54795-54810.

Urnauer S, Morys S, Krhac Levacic A, Müller AM, Schug C, Schmohl KA, Schwenk N, Zach C, Carlsen J, Bartenstein P, Wagner E, Spitzweg C. Sequence-defined cMET/HGFR-targeted polymers as gene delivery vehicles for the theranostic sodium iodide symporter (NIS) gene. Mol Ther. 2016 Aug;24(8):1395-404.

9.2 Manuscripts in preparation

Schug C, Sievert W, **Urnauer S**, Müller AM, Schmohl KA, Wechselberger A, Schwenk N, Lauber K, Schwaiger M, Multhoff G, Nelson PJ, Spitzweg C. External beam radiation therapy enhances mesenchymal stem cell-mediated sodium iodide symporter gene delivery.

Schug C, Gupta A, **Urnauer S**, Schmohl KA, Steiger K, Trajkovic-Arsic M, Schwenk N, Schwaiger M, Nelson PJ, Siveke JT, Spitzweg C. Mesenchymal stem cell-mediated NIS gene delivery – a novel approach for imaging-guided 131I therapy of pancreatic ductal adenocarcinoma

9.3 Oral presentations

40th Annual Meeting of the European Thyroid Association, Belgrade, Serbia, September 2017. **Urnauer S**, Müller AM, Schug C, Schmohl KA, Tutter M, Schwenk N, Rödl W, Morys S, Ingrisch M, Bertram J, Bartenstein P, Clevert DA, Wagner E, Spitzweg C. EGFR-targeted nonviral NIS gene transfer for bioimaging and therapy of disseminated colon cancer metastases.

60th Annual Meeting of the German Society of Endocrinology, Würzburg, Germany, April 2017. **Urnauer S**, Müller AM, Schug C, Schmohl KA, Tutter M, Schwenk N, Rödl W, Morys S, Ingrisch M, Bertram J, Bartenstein P, Clevert DA, Wagner E, Spitzweg C. EGFR-targeted polyplex-mediated NIS gene therapy of metastatic colorectal cancer.

15th International Thyroid Congress, Orlando, Florida, USA, October 2015. **Urnauer S**, Morys S, Levacic AK, Schug C, Schwenk N, Carlsen J, Zach C, Wagner E, Spitzweg C. Systemic non-viral cMET/HGFR-targeted gene delivery using the theranostic function of the sodium iodide symporter (NIS)

9.4 Poster presentations

87th Annual Meeting of the American Thyroid Association, Victoria, Canada, October 2017. **Urnauer S**, Schmohl KA, Morys S, Tutter M, Schwenk N, Schug C, Oos R, Bartenstein P, Clevert DA, Wagner E, Spitzweg C. Dual receptor targeting for improved systemic tumor-specific delivery of the sodium iodide symporter (NIS) gene.

60th Annual Meeting of the German Society of Endocrinology, Würzburg, Germany, April 2017. **Urnauer S**, Müller AM, Schug C, Schmohl KA, Tutter M, Schwenk N, Rödl W, Morys S, Ingrisch M, Bertram J, Bartenstein P, Clevert DA, Wagner E, Spitzweg C. EGFR-targeted polyplex-mediated NIS gene therapy of metastatic colorectal cancer.

86th Annual Meeting of the American Thyroid Association, Denver, USA, October 2016. **Urnauer S**, Müller AM, Morys S, Oos R, Bartenstein P, Clevert DA, Wagner E, Spitzweg C. Systemic epidermal growth factor receptor-targeted sodium iodide symporter (NIS) gene therapy in an advanced tumor model of hepatic colon cancer metastasis

59th Annual Meeting of the German Society of Endocrinology, Munich, Germany, May 2016. **Urnauer S**, Morys S, Levacic AK, Müller AM, Schug C, Schmohl KA, Schwenk N, Zach C, Carlsen J, Bartenstein P, Wagner E, Spitzweg C. Sequence defined cMET/HGFR-targeted polymers as gene delivery vehicles for the theranostic sodium iodide symporter (NIS) gene.

59th Annual Meeting of the German Society of Endocrinology, Munich, Germany, May 2016. **Urnauer S**, Morys S, Müller AM, Oos R, Carlsen J, Bartenstein P, Wagner E, Spitzweg C. Systemic epidermal growth factor receptor-targeted gene delivery using the theranostic sodium iodide symporter (NIS) gene in an advanced orthotopic tumor model.

18th Congress of European Endocrinology, Munich, Germany, May 2016. **Urnauer S**, Morys S, Müller AM, Oos R, Carlsen J, Bartenstein P, Wagner E, Spitzweg C. Systemic epidermal growth factor receptor-targeted gene delivery using the theranostic sodium iodide symporter (NIS) gene in an advanced orthotopic tumor model.

18th Congress of European Endocrinology, Munich, Germany, May 2016. **Urnauer S**, Morys S, Levacic AK, Müller AM, Schug C, Schmohl KA, Schwenk N, Zach C, Carlsen J, Bartenstein P, Wagner E, Spitzweg C. Sequence defined cMET/HGFR-targeted polymers as gene delivery vehicles for the theranostic sodium iodide symporter (NIS) gene.

9.5 Awards

Participation at the 87th Annual Meeting of the American Thyroid Association Trainee Grant Program, Victoria, Canada, October 2017

Travel grant, European Thyroid Association
40th Annual Meeting of the European Thyroid Association, Belgrade, Serbia, September 2017. Urnauer S, Müller AM, Schug C, Schmohl KA, Tutter M, Schwenk N, Rödl W, Morys S, Ingrisch M, Bertram J, Bartenstein P, Clevert DA, Wagner E, Spitzweg C. EGFR-targeted nonviral NIS gene transfer for bioimaging and therapy of disseminated colon cancer metastases.

Travel grant, German Society of Endocrinology
60th Annual Meeting of the German Society of Endocrinology, Würzburg, Germany, April 2017. Urnauer S, Müller AM, Schug C, Schmohl KA, Tutter M, Schwenk N, Rödl W, Morys S, Ingrisch M, Bertram J, Bartenstein P, Clevert DA, Wagner E, Spitzweg C. EGFR-targeted polyplex-mediated NIS gene therapy of metastatic colorectal cancer.

Travel grant, German Society of Endocrinology
86th Annual Meeting of the American Thyroid Association, Denver, USA, October 2016. Urnauer S, Müller AM, Morys S, Oos R, Bartenstein P, Clevert DA, Wagner E, Spitzweg C. Systemic epidermal growth factor receptor-targeted sodium iodide symporter (NIS) gene therapy in an advanced tumor model of hepatic colon cancer metastasis

Participation at the 86th Annual Meeting of the American Thyroid Association Trainee Grant Program, Denver, USA, October 2016

Travel grant, German Society of Endocrinology
15th International Thyroid Congress, Orlando, Florida, USA, October 2015. Urnauer S, Morys S, Levacic AK, Schug C, Schwenk N, Carlsen J, Zach C, Wagner E, Spitzweg C. Systemic non-viral cMET/HGFR-targeted gene delivery using the theranostic function of the sodium iodide symporter (NIS)

Travel grant, European Society of Endocrinology
15th International Thyroid Congress, Orlando, Florida, USA, October 2015. Urnauer S, Morys S, Levacic AK, Schug C, Schwenk N, Carlsen J, Zach C, Wagner E, Spitzweg C. Systemic non-viral cMET/HGFR-targeted gene delivery using the theranostic function of the sodium iodide symporter (NIS)

10. References

1. Sharma S, Kelly TK and Jones PA. Epigenetics in cancer. Carcinogenesis. 2010; 31(1):27-36.

2. You JS and Jones PA. Cancer genetics and epigenetics: two sides of the same coin? Cancer Cell. 2012; 22(1):9-20.

3. Hanahan D and Weinberg RA. Hallmarks of cancer: the next generation. Cell. 2011; 144(5):646-674.

4. Torre LA, Siegel RL, Ward EM and Jemal A. Global Cancer Incidence and Mortality Rates and Trends--An Update. Cancer Epidemiol Biomarkers Prev. 2016; 25(1):16-27.

5. Jamal-Hanjani M, Quezada SA, Larkin J and Swanton C. Translational implications of tumor heterogeneity. Clin Cancer Res. 2015; 21(6):1258-1266.

6. Urruticoechea A, Alemany R, Balart J, Villanueva A, Vinals F and Capella G. Recent advances in cancer therapy: an overview. Curr Pharm Des. 2010; 16(1):3-10.

7. Seidlin SM, Marinelli LD and Oshry E. Radioactive iodine therapy; effect on functioning metastases of adenocarcinoma of the thyroid. J Am Med Assoc. 1946; 132(14):838-847.

8. Touchefeu Y, Harrington KJ, Galmiche JP and Vassaux G. Review article: gene therapy, recent developments and future prospects in gastrointestinal oncology. Aliment Pharmacol Ther. 2010; 32(8):953-968.

9. Ediriwickrema A and Saltzman WM. Nanotherapy for Cancer: Targeting and Multifunctionality in the Future of Cancer Therapies. ACS Biomater Sci Eng. 2015; 1(2):64-78.

10. Rosland GV and Engelsen AS. Novel points of attack for targeted cancer therapy. Basic Clin Pharmacol Toxicol. 2015; 116(1):9-18.

11. Ortiz R, Melguizo C, Prados J, Alvarez PJ, Caba O, Rodriguez-Serrano F, Hita F and Aranega A. New gene therapy strategies for cancer treatment: a review of recent patents. Recent Pat Anticancer Drug Discov. 2012; 7(3):297-312.

12. He D and Wagner E. Defined polymeric materials for gene delivery. Macromol Biosci. 2015; 15(5):600-612.

13. Ledford H. Engineered cell therapy for cancer gets thumbs up from FDA advisers. Nature. 2017; 547(7663):270.

14. Maude SL, Frey N, Shaw PA, Aplenc R, Barrett DM, Bunin NJ, Chew A, Gonzalez VE, Zheng Z, Lacey SF, Mahnke YD, Melenhorst JJ, Rheingold SR, Shen A, Teachey DT, Levine BL, et al. Chimeric antigen receptor T cells for sustained remissions in leukemia. N Engl J Med. 2014; 371(16):1507-1517.

15. Zhang C, Liu J, Zhong JF and Zhang X. Engineering CAR-T cells. Biomark Res. 2017; 5:22.

16. Hingorani M, Spitzweg C, Vassaux G, Newbold K, Melcher A, Pandha H, Vile R and Harrington K. The biology of the sodium iodide symporter and its potential for targeted gene delivery. Curr Cancer Drug Targets. 2010; 10(2):242-267.

17. Spitzweg C and Morris JC. Sodium iodide symporter (NIS) and thyroid. Hormones (Athens). 2002; 1(1):22-34.

18. Portulano C, Paroder-Belenitsky M and Carrasco N. The Na+/I- symporter (NIS): mechanism and medical impact. Endocr Rev. 2014; 35(1):106-149.

19. Carrasco N. Iodide transport in the thyroid gland. Biochim Biophys Acta. 1993; 1154(1):65-82.

20. Eskandari S, Loo DD, Dai G, Levy O, Wright EM and Carrasco N. Thyroid Na+/I- symporter. Mechanism, stoichiometry, and specificity. J Biol Chem. 1997; 272(43):27230-27238.

21. Dadachova E and Carrasco N. The Na+/I- symporter (NIS): imaging and therapeutic applications. Semin Nucl Med. 2004; 34(1):23-31.

22. Spitzweg C, Joba W, Eisenmenger W and Heufelder AE. Analysis of human sodium iodide symporter gene expression in extrathyroidal tissues and cloning of its complementary deoxyribonucleic acids from salivary gland, mammary gland, and gastric mucosa. J Clin Endocrinol Metab. 1998; 83(5):1746-1751.

23. Perron B, Rodriguez AM, Leblanc G and Pourcher T. Cloning of the mouse sodium iodide symporter and its expression in the mammary gland and other tissues. J Endocrinol. 2001; 170(1):185-196.

24. Vayre L, Sabourin JC, Caillou B, Ducreux M, Schlumberger M and Bidart JM. Immunohistochemical analysis of Na+/I- symporter distribution in human extra-thyroidal tissues. Eur J Endocrinol. 1999; 141(4):382-386.

25. Cheng L, Liu M, Ruan M and Chen L. Challenges and strategies on radioiodine treatment for differentiated thyroid carcinoma. Hell J Nucl Med. 2016; 19(1):23-32.

26. Magnander K and Elmroth K. Biological consequences of formation and repair of complex DNA damage. Cancer Lett. 2012; 327(1-2):90-96.

27. Dingli D, Russell SJ and Morris JC, III. In vivo imaging and tumor therapy with the sodium iodide symporter. J Cell Biochem. 2003; 90(6):1079-1086.

28. Kelkar SS and Reineke TM. Theranostics: combining imaging and therapy. Bioconjug Chem. 2011; 22(10):1879-1903.

29. Smanik PA, Liu Q, Furminger TL, Ryu K, Xing S, Mazzaferri EL and Jhiang SM. Cloning of the Human Sodium Iodide Symporter. Biochem Biophys Res Commun. 1996; 226(2):339-345.

30. Dai G, Levy O and Carrasco N. Cloning and characterization of the thyroid iodide transporter. Nature. 1996; 379(6564):458-460.

31. Spitzweg C and Heufelder AE. The sodium iodide symporter: its emerging relevance to clinical thyroidology. Eur J Endocrinol. 1998; 138(4):374-375.

32. Spitzweg C, Bible KC, Hofbauer LC and Morris JC. Advanced radioiodine-refractory differentiated thyroid cancer: the sodium iodide symporter and other emerging therapeutic targets. Lancet Diabetes Endocrinol. 2014; 2(10):830-842.

33. Ravera S, Reyna-Neyra A, Ferrandino G, Amzel LM and Carrasco N. The Sodium/Iodide Symporter (NIS): Molecular Physiology and Preclinical and Clinical Applications. Annu Rev Physiol. 2017; 79:261-289.

34. Wapnir IL, Goris M, Yudd A, Dohan O, Adelman D, Nowels K and Carrasco N. (2004). The Na+/I- Symporter Mediates Iodide Uptake in Breast Cancer Metastases and Can Be Selectively Down-Regulated in the Thyroid. Clin Cancer Res. 2004; 10(13):4294-4302.

35. Grünwald GK, Klutz K, Willhauck MJ, Schwenk N, Senekowitsch-Schmidtke R, Schwaiger M, Zach C, Goke B, Holm PS and Spitzweg C. Sodium iodide symporter (NIS)-mediated radiovirotherapy of hepatocellular cancer using a conditionally replicating adenovirus. Gene Ther. 2013; 20(6):625-633.

36. Grünwald GK, Vetter A, Klutz K, Willhauck MJ, Schwenk N, Senekowitsch-Schmidtke R, Schwaiger M, Zach C, Wagner E, Goke B, Holm PS, Ogris M and Spitzweg C. EGFR-Targeted Adenovirus Dendrimer Coating for Improved Systemic Delivery of the Theranostic NIS Gene. Mol Ther Nucleic Acids. 2013; 2:e131.

37. Grünwald GK, Vetter A, Klutz K, Willhauck MJ, Schwenk N, Senekowitsch-Schmidtke R, Schwaiger M, Zach C, Wagner E, Goke B, Holm PS, Ogris M and Spitzweg C. Systemic image-guided liver cancer radiovirotherapy using dendrimer-coated adenovirus encoding the sodium iodide symporter as theranostic gene. J Nucl Med. 2013; 54(8):1450-1457.

38. Klutz K, Russ V, Willhauck MJ, Wunderlich N, Zach C, Gildehaus FJ, Goke B, Wagner E, Ogris M and Spitzweg C. Targeted radioiodine therapy of neuroblastoma tumors following systemic nonviral delivery of the sodium iodide symporter gene. Clin Cancer Res. 2009; 15(19):6079-6086.

39. Klutz K, Schaffert D, Willhauck MJ, Grunwald GK, Haase R, Wunderlich N, Zach C, Gildehaus FJ, Senekowitsch-Schmidtke R, Goke B, Wagner E, Ogris M and Spitzweg C. Epidermal growth factor receptor-targeted (131)I-therapy of liver cancer following systemic delivery of the sodium iodide symporter gene. Mol Ther. 2011; 19(4):676-685.

40. Klutz K, Willhauck MJ, Dohmen C, Wunderlich N, Knoop K, Zach C, Senekowitsch-Schmidtke R, Gildehaus FJ, Ziegler S, Furst S, Goke B, Wagner E, Ogris M and Spitzweg C. Image-guided tumor-selective radioiodine therapy of liver cancer after systemic nonviral delivery of the sodium iodide symporter gene. Hum Gene Ther. 2011; 22(12):1563-1574.

41. Klutz K, Willhauck MJ, Wunderlich N, Zach C, Anton M, Senekowitsch-Schmidtke R, Goke B and Spitzweg C. Sodium iodide symporter (NIS)-mediated radionuclide ((131)I, (188)Re) therapy of liver cancer after transcriptionally targeted intratumoral in vivo NIS gene delivery. Hum Gene Ther. 2011; 22(11):1403-1412.

42. Knoop K, Kolokythas M, Klutz K, Willhauck MJ, Wunderlich N, Draganovici D, Zach C, Gildehaus FJ, Boning G, Goke B, Wagner E, Nelson PJ and Spitzweg C. Image-guided, tumor stroma-targeted 131I therapy of hepatocellular cancer after systemic mesenchymal stem cell-mediated NIS gene delivery. Mol Ther. 2011; 19(9):1704-1713.

43. Knoop K, Schwenk N, Dolp P, Willhauck MJ, Zischek C, Zach C, Hacker M, Goke B, Wagner E, Nelson PJ and Spitzweg C. Stromal targeting of sodium iodide symporter using mesenchymal stem cells allows enhanced imaging and therapy of hepatocellular carcinoma. Hum Gene Ther. 2013; 24(3):306-316.

44. Knoop K, Schwenk N, Schmohl K, Muller A, Zach C, Cyran C, Carlsen J, Boning G, Bartenstein P, Goke B, Wagner E, Nelson PJ and Spitzweg C. Mesenchymal stem cell-mediated, tumor stroma-targeted radioiodine therapy of metastatic colon cancer using the sodium iodide symporter as theranostic gene. J Nucl Med. 2015; 56(4):600-606.

45. Müller AM, Schmohl KA, Knoop K, Schug C, Urnauer S, Hagenhoff A, Clevert DA, Ingrisch M, Niess H, Carlsen J, Zach C, Wagner E, Bartenstein P, Nelson PJ and Spitzweg C. Hypoxia-targeted 131I therapy of hepatocellular cancer after systemic mesenchymal stem cell-mediated sodium iodide symporter gene delivery. Oncotarget. 2016; 7(34):54795-54810.

46. Urnauer S, Morys S, Krhac Levacic A, Muller AM, Schug C, Schmohl KA, Schwenk N, Zach C, Carlsen J, Bartenstein P, Wagner E and Spitzweg C. Sequence-defined cMET/HGFR-targeted Polymers as Gene Delivery Vehicles for the Theranostic Sodium Iodide Symporter (NIS) Gene. Mol Ther. 2016; 24(8):1395-1404.

47. Spitzweg C, Zhang S, Bergert ER, Castro MR, McIver B, Heufelder AE, Tindall DJ, Young CY and Morris JC. Prostate-specific antigen (PSA) promoter-driven androgen-inducible expression of sodium iodide symporter in prostate cancer cell lines. Cancer Res. 1999; 59(9):2136-2141.

48. Spitzweg C, Dietz AB, O'Connor MK, Bergert ER, Tindall DJ, Young CY and Morris JC. In vivo sodium iodide symporter gene therapy of prostate cancer. Gene Ther. 2001; 8(20):1524-1531.

49. Dwyer RM, Schatz SM, Bergert ER, Myers RM, Harvey ME, Classic KL, Blanco MC, Frisk CS, Marler RJ, Davis BJ, O'Connor MK, Russell SJ and Morris JC. A preclinical large animal model of adenovirus-mediated expression of the sodium-iodide symporter for radioiodide imaging and therapy of locally recurrent prostate cancer. Mol Ther. 2005; 12(5):835-841.

50. Merron A, Peerlinck I, Martin-Duque P, Burnet J, Quintanilla M, Mather S, Hingorani M, Harrington K, Iggo R and Vassaux G. SPECT/CT imaging of oncolytic adenovirus propagation in tumours in vivo using the Na/I symporter as a reporter gene. Gene Ther. 2007; 14(24):1731-1738.

51. Peerlinck I, Merron A, Baril P, Conchon S, Martin-Duque P, Hindorf C, Burnet J, Quintanilla M, Hingorani M, Iggo R, Lemoine NR, Harrington K and Vassaux G. Targeted radionuclide therapy using a Wnt-targeted replicating adenovirus encoding the Na/I symporter. Clin Cancer Res. 2009; 15(21):6595-6601.

52. Faivre J, Clerc J, Gerolami R, Herve J, Longuet M, Liu B, Roux J, Moal F, Perricaudet M and Brechot C. Long-term radioiodine retention and regression of liver cancer after sodium iodide symporter gene transfer in wistar rats. Cancer Res. 2004; 64(21):8045-8051.

53. Pack DW, Hoffman AS, Pun S and Stayton PS. Design and development of polymers for gene delivery. Nat Rev Drug Discov. 2005; 4(7):581-593.

54. Nayerossadat N, Maedeh T and Ali PA. Viral and nonviral delivery systems for gene delivery. Adv Biomed Res. 2012; 1:27.

55. Akinc A, Thomas M, Klibanov AM and Langer R. Exploring polyethylenimine-mediated DNA transfection and the proton sponge hypothesis. J Gene Med. 2005; 7(5):657-663.

56. Lächelt U and Wagner E. Nucleic Acid Therapeutics Using Polyplexes: A Journey of 50 Years (and Beyond). Chem Rev. 2015; 115(19):11043-11078.

57. Wang T, Upponi JR and Torchilin VP. Design of multifunctional non-viral gene vectors to overcome physiological barriers: dilemmas and strategies. Int J Pharm. 2012; 427(1):3-20.

58. Lächelt U, Kos P, Mickler FM, Herrmann A, Salcher EE, Rodl W, Badgujar N, Brauchle C and Wagner E. Fine-tuning of proton sponges by precise diaminoethanes and histidines in pDNA polyplexes. Nanomedicine. 2014; 10(1):35-44.

59. Choi HS, Liu W, Liu F, Nasr K, Misra P, Bawendi MG and Frangioni JV. Design considerations for tumour-targeted nanoparticles. Nat Nanotechnol. 2010; 5(1):42-47.

60. Rejman J, Bragonzi A and Conese M. Role of clathrin- and caveolae-mediated endocytosis in gene transfer mediated by lipo- and polyplexes. Mol Ther. 2005; 12(3):468-474.

61. Truebenbach I, Gorges J, Kuhn J, Kern S, Baratti E, Kazmaier U, Wagner E and Lächelt U. Sequence-Defined Oligoamide Drug Conjugates of Pretubulysin and Methotrexate for Folate Receptor Targeted Cancer Therapy. Macromol Biosci. 2017; 17(10)

62. Rejman J, Oberle V, Zuhorn IS and Hoekstra D. Size-dependent internalization of particles via the pathways of clathrin- and caveolae-mediated endocytosis. Biochem J. 2004; 377(Pt 1):159-169.

63. Boussif O, Lezoualc'h F, Zanta MA, Mergny MD, Scherman D, Demeneix B and Behr JP. A versatile vector for gene and oligonucleotide transfer into cells in culture and in vivo: polyethylenimine. Proc Natl Acod Sci USA.1995; 92(16):7297-7301.

64. Neu M, Fischer D and Kissel T. Recent advances in rational gene transfer vector design based on poly(ethylene imine) and its derivatives. J Gene Med. 2005; 7(8):992-1009.

65. Hall A, Lachelt U, Bartek J, Wagner E and Moghimi SM. Polyplex Evolution: Understanding Biology, Optimizing Performance. Mol Ther. 2017; 25(7):1476-1490.

66. Schaffert D, Badgujar N and Wagner E. Novel Fmoc-polyamino acids for solid-phase synthesis of defined polyamidoamines. Org Lett. 2011; 13(7):1586-1589.

67. Morys S, Urnauer S, Spitzweg C and Wagner E. EGFR Targeting and Shielding of pDNA Lipopolyplexes via Bivalent Attachment of a Sequence-Defined PEG Agent. Macromol Biosci. 2017.

68. Kos P, Lachelt U, He D, Nie Y, Gu Z and Wagner E. Dual-targeted polyplexes based on sequence-defined peptide-PEG-oligoamino amides. J Pharm Sci. 2015; 104(2):464-475.

69. Kos P, Lachelt U, Herrmann A, Mickler FM, Doblinger M, He D, Krhac Levacic A, Morys S, Brauchle C and Wagner E. Histidine-rich stabilized polyplexes for cMet-directed tumor-targeted gene transfer. Nanoscale. 2015; 7(12):5350-5362.

70. Burke RS and Pun SH. Extracellular Barriers to in Vivo PEI and PEGylated PEI Polyplex-Mediated Gene Delivery to the Liver. Bioconjug Chem. 2008; 19(3):693-704.

71. Wolfert MA, Schacht EH, Toncheva V, Ulbrich K, Nazarova O, Seymour LW, Dash PR and Oupicky D. Characterization of vectors for gene therapy formed by self-assembly of DNA with synthetic block co-polymers 724. Hum Gene Ther. 1996; 7:2123-2133.

72. Toncheva V, Wolfert MA, Dash PR, Oupicky D, Ulbrich K, Seymour LW and Schacht EH. Novel vectors for gene delivery formed by self-assembly of DNA with poly(L-lysine) grafted with hydrophilic polymers. Biochim Biophys Acta. 1998; 1380:354-368.

73. Petersen H, Fechner PM, Martin AL, Kunath K, Stolnik S, Roberts CJ, Fischer D, Davies MC and Kissel T. Polyethylenimine-graft-Poly(ethylene glycol) Copolymers: Influence of Copolymer Block Structure on DNA Complexation and Biological Activities as Gene Delivery System. Bioconjug Chem. 2002; 13(4):845-854.

74. Petersen H, Merdan T, Kunath K, Fischer D and Kissel T. Poly(ethylenimine-co-L-lactamide-co-succinamide): a biodegradable polyethylenimine derivative with an advantageous pH-dependent hydrolytic degradation for gene delivery. Bioconjug Chem. 2002; 13(4):812-821.

75. Müller K, Kessel E, Klein PM, Hohn M and Wagner E. Post-PEGylation of siRNA Lipo-oligoamino Amide Polyplexes Using Tetra-glutamylated Folic Acid as Ligand for Receptor-Targeted Delivery. Mol Pharm. 2016; 13(7):2332-2345.

76. Williford JM, Archang MM, Minn I, Ren Y, Wo M, Vandermark J, Fisher PB, Pomper MG and Mao HQ. Critical Length of PEG Grafts on lPEI/DNA Nanoparticles for Efficient in Vivo Delivery. ACS Biomater Sci Eng. 2016; 2(4):567-578.

77. Roberts MJ, Bentley MD and Harris JM. Chemistry for peptide and protein PEGylation. Adv Drug Deliv Rev. 2002; 54(4):459-476.

78. Hatakeyama H, Akita H, Kogure K, Oishi M, Nagasaki Y, KIHIRA Y, Ueno M, Kobayashi H, Kikuchi H and Harashima H. Development of a novel systemic gene delivery system for cancer therapy with a tumor-specific cleavable PEG-lipid. Gene Ther. 2007; 14(1):68-77.

79. Smrekar B, Wightman L, Wolschek MF, Lichtenberger C, Ruzicka R, Ogris M, Rodl W, Kursa M, Wagner E and Kircheis R. Tissue-dependent factors affect gene delivery to tumors in vivo. Gene Ther. 2003; 10(13):1079-1088.

80. Zhou Y and Kopecek J. Biological rationale for the design of polymeric anti-cancer nanomedicines. J Drug Target. 2013; 21(1):1-26.

81. Maeda H. The enhanced permeability and retention (EPR) effect in tumor vasculature: the key role of tumor-selective macromolecular drug targeting. Adv Enzyme Regul. 2001; 41:189-207.

82. Bertrand N, Wu J, Xu X, Kamaly N and Farokhzad OC. Cancer nanotechnology: the impact of passive and active targeting in the era of modern cancer biology. Adv Drug Deliv Rev. 2014; 66:2-25.

83. Zhang W, Rodl W, He D, Doblinger M, Lachelt U and Wagner E. Combination of sequence-defined oligoaminoamides with transferrin-polycation conjugates for receptor-targeted gene delivery. J Gene Med. 2015; 17(8-9):161-172.

84. Moody PR, Sayers EJ, Magnusson JP, Alexander C, Borri P, Watson P and Jones AT. Receptor Crosslinking: A General Method to Trigger Internalization and Lysosomal Targeting of Therapeutic Receptor:Ligand Complexes. Mol Ther. 2015; 23(12):1888-1898.

85. Jo M, Stolz DB, Esplen JE, Dorko K, Michalopoulos GK and Strom SC. Cross-talk between epidermal growth factor receptor and c-Met signal pathways in transformed cells. J Biol Chem. 2000; 275(12):8806-8811.

86. Puri N and Salgia R. Synergism of EGFR and c-Met pathways, cross-talk and inhibition, in non-small cell lung cancer. J Carcinog. 2008; 7:9.

87. Meng S, Su B, Li W, Ding Y, Tang L, Zhou W, Song Y, Li H and Zhou C. Enhanced antitumor effect of novel dual-targeted paclitaxel liposomes. Nanotechnology. 2010; 21(41):415103.

88. Nie Y, Schaffert D, Rodl W, Ogris M, Wagner E and Gunther M. Dual-targeted polyplexes: one step towards a synthetic virus for cancer gene therapy. J Control Release. 2011; 152(1):127-134.

89. Spitzweg C and Morris JC. The sodium iodide symporter: its pathophysiological and therapeutic implications. Clin Endocrinol. 2002; 57(5):559.

90. Miller A and Russell SJ. The use of the NIS reporter gene for optimizing oncolytic virotherapy. Expert Opin Biol Ther. 2016; 16(1):15-32.

91. Van Nostrand D, Atkins F, Yeganeh F, Acio E, Bursaw R and Wartofsky L. Dosimetrically determined doses of radioiodine for the treatment of metastatic thyroid carcinoma. Thyroid. 2002; 12(2):121-134.

92. Spitzweg C, O'Connor MK, Bergert ER, Tindall DJ, Young CY and Morris JC. Treatment of prostate cancer by radioiodine therapy after tissue-specific expression of the sodium iodide symporter. Cancer Res. 2000; 60(22):6526-6530.

93. Willhauck MJ, Sharif Samani BR, Klutz K, Cengic N, Wolf I, Mohr L, Geissler M, Senekowitsch-Schmidtke R, Goke B, Morris JC and Spitzweg C. Alpha-fetoprotein promoter-targeted sodium iodide symporter gene therapy of hepatocellular carcinoma. Gene Ther. 2008; 15(3):214-223.

94. Russell SJ, Federspiel MJ, Peng KW, Tong C, Dingli D, Morice WG, Lowe V, O'Connor MK, Kyle RA, Leung N, Buadi FK, Rajkumar SV, Gertz MA, Lacy MQ and Dispenzieri A. Remission of disseminated cancer after systemic oncolytic virotherapy. Mayo Clin Proc. 2014; 89(7):926-933.

95. Trujillo MA, Oneal MJ, McDonough SJ and Morris JC. Viral dose, radioiodide uptake, and delayed efflux in adenovirus-mediated NIS radiovirotherapy correlates with treatment efficacy. Gene Ther. 2013; 20(5):567-574.

96. Jauregui-Osoro M, Sunassee K, Weeks AJ, Berry DJ, Paul RL, Cleij M, Banga JP, O'Doherty MJ, Marsden PK, Clarke SE, Ballinger JR, Szanda I, Cheng SY and Blower PJ. Synthesis and biological evaluation of [(18)F]tetrafluoroborate: a PET imaging agent for thyroid disease and reporter gene imaging of the sodium/iodide symporter. Eur J Nucl Med Mol Imaging. 2010; 37(11):2108-2116.

97. Groot-Wassink T, Aboagye EO, Glaser M, Lemoine NR and Vassaux G. Adenovirus biodistribution and noninvasive imaging of gene expression in vivo by positron emission tomography using human sodium/iodide symporter as reporter gene. Hum Gene Ther. 2002; 13(14):1723-1735.

98. Davis GL, Dempster J, Meler JD, Orr DW, Walberg MW, Brown B, Berger BD, O'Connor JK and Goldstein RM. Hepatocellular carcinoma: management of an increasingly common problem. Proc (Bayl Univ Med Cent). 2008; 21(3):266-280.

99. Felgner PL, Barenholz Y, Behr JP, Cheng SH, Cullis P, Huang L, Jessee JA, Seymour L, Szoka F, Thierry AR, Wagner E and Wu G. Nomenclature for synthetic gene delivery systems. Hum Gene Ther. 1997; 8(5):511-512.

100. Ambegia E, Ansell S, Cullis P, Heyes J, Palmer L and MacLachlan I. Stabilized plasmid-lipid particles containing PEG-diacylglycerols exhibit extended circulation lifetimes and tumor selective gene expression. Biochim Biophys Acta. 2005; 1669(2):155-163.

101. Li SD and Huang L. Gene therapy progress and prospects: non-viral gene therapy by systemic delivery. Gene Ther. 2006; 13(18):1313-1319.

102. Schäfer J, Hobel S, Bakowsky U and Aigner A. Liposome-polyethylenimine complexes for enhanced DNA and siRNA delivery. Biomaterials. 2010; 31(26):6892-6900.

103. Hatakeyama H, Akita H and Harashima H. A multifunctional envelope type nano device (MEND) for gene delivery to tumours based on the EPR effect: a strategy for overcoming the PEG dilemma. Adv Drug Deliv Rev. 2011; 63(3):152-160.

104. Mevel M, Haudebourg T, Colombani T, Peuziat P, Dallet L, Chatin B, Lambert O, Berchel M, Montier T, Jaffres PA, Lehn P and Pitard B. Important role of phosphoramido linkage in imidazole-based dioleyl helper lipids for liposome stability and primary cell transfection. J Gene Med. 2016; 18(1-3):3-15.

105. Miyata K, Nishiyama N and Kataoka K. Rational design of smart supramolecular assemblies for gene delivery: chemical challenges in the creation of artificial viruses. Chem Soc Rev. 2012; 41(7):2562-2574.

106. Wei H, Volpatti LR, Sellers DL, Maris DO, Andrews IW, Hemphill AS, Chan LW, Chu DS, Horner PJ and Pun SH. Dual responsive, stabilized nanoparticles for efficient in vivo plasmid delivery. Angew Chem Int Ed Engl. 2013; 52(20):5377-5381.

107. Leng Q and Mixson AJ. The neuropilin-1 receptor mediates enhanced tumor delivery of H2K polyplexes. J Gene Med. 2016; 18(7):134-144.

108. Coll JL, Chollet P, Brambilla E, Desplanques D, Behr JP and Favrot M. In vivo delivery to tumors of DNA complexed with linear polyethylenimine. Hum Gene Ther. 1999; 10(10):1659-1666.

109. Poulain L, Ziller C, Muller CD, Erbacher P, Bettinger T, Rodier JF and Behr JP. Ovarian carcinoma cells are effectively transfected by polyethylenimine (PEI) derivatives. Cancer Gene Ther. 2000; 7(4):644-652.

110. Aoki K, Furuhata S, Hatanaka K, Maeda M, Remy JS, Behr JP, Terada M and Yoshida T. Polyethylenimine-mediated gene transfer into pancreatic tumor dissemination in the murine peritoneal cavity. Gene Ther. 2001; 8(7):508-514.

111. Sidi AA, Ohana P, Benjamin S, Shalev M, Ransom JH, Lamm D, Hochberg A and Leibovitch I. Phase I/II marker lesion study of intravesical BC-819 DNA plasmid in H19 over expressing superficial bladder cancer refractory to bacillus Calmette-Guerin. J Urol. 2008; 180(6):2379-2383.

112. Anwer K, Barnes MN, Fewell J, Lewis DH and Alvarez RD. Phase-I clinical trial of IL-12 plasmid/lipopolymer complexes for the treatment of recurrent ovarian cancer. Gene Ther. 2010; 17(3):360-369.

113. Neuberg P and Kichler A. Recent developments in nucleic acid delivery with polyethylenimines. Adv Genet. 2014; 88:263-288.

114. Bonnet ME, Erbacher P and Bolcato-Bellemin AL. Systemic delivery of DNA or siRNA mediated by linear polyethylenimine (L-PEI) does not induce an inflammatory response. Pharm Res. 2008; 25(12):2972-2982.

115. Gofrit ON, Benjamin S, Halachmi S, Leibovitch I, Dotan Z, Lamm DL, Ehrlich N, Yutkin V, Ben-Am M and Hochberg A. DNA based therapy with diphtheria toxin-A BC-819: a phase 2b marker lesion trial in patients with intermediate risk nonmuscle invasive bladder cancer. J Urol. 2014; 191(6):1697-1702.

116. Plank C, Mechtler K, Szoka FC, Jr. and Wagner E. Activation of the complement system by synthetic DNA complexes: a potential barrier for intravenous gene delivery. Hum Gene Ther. 1996; 7(12):1437-1446.

117. Hall A, Larsen AK, Parhamifar L, Meyle KD, Wu LP and Moghimi SM. High resolution respirometry analysis of polyethylenimine-mediated mitochondrial energy crisis and cellular stress: Mitochondrial proton leak and inhibition of the electron transport system. Biochim Biophys Acta. 2013; 1827(10):1213-1225.

118. Merkel OM, Urbanics R, Bedocs P, Rozsnyay Z, Rosivall L, Toth M, Kissel T and Szebeni J. In vitro and in vivo complement activation and related anaphylactic effects associated with polyethylenimine and polyethylenimine-graft-poly(ethylene glycol) block copolymers. Biomaterials. 2011; 32(21):4936-4942.

119. Schaffert D, Kiss M, Rodl W, Shir A, Levitzki A, Ogris M and Wagner E. Poly(I:C)-mediated tumor growth suppression in EGF-receptor overexpressing tumors using EGF-polyethylene glycol-linear polyethylenimine as carrier. Pharm Res. 2011; 28(4):731-741.

120. Kichler A, Chillon M, Leborgne C, Danos O and Frisch B. Intranasal gene delivery with a polyethylenimine-PEG conjugate. J Control Release. 2002; 81(3):379-388.

121. Kursa M, Walker GF, Roessler V, Ogris M, Roedl W, Kircheis R and Wagner E. Novel Shielded Transferrin-Polyethylene Glycol-Polyethylenimine/DNA Complexes for Systemic Tumor-Targeted Gene Transfer. Bioconjug Chem. 2003; 14(1):222-231.

122. Xia H, Anderson B, Mao Q and Davidson BL. Recombinant human adenovirus: targeting to the human transferrin receptor improves gene transfer to brain microcapillary endothelium. J Virol. 2000; 74(23):11359-11366.

123. Broda E, Mickler FM, Lachelt U, Morys S, Wagner E and Brauchle C. Assessing potential peptide targeting ligands by quantification of cellular adhesion of model nanoparticles under flow conditions. J Control Release. 2015; 213:79-85.

124. Russ V, Elfberg H, Thoma C, Kloeckner J, Ogris M and Wagner E. Novel degradable oligoethylenimine acrylate ester-based pseudodendrimers for in vitro and in vivo gene transfer. Gene Ther. 2008; 15(1):18-29.

125. Willhauck MJ, Sharif Samani BR, Gildehaus FJ, Wolf I, Senekowitsch-Schmidtke R, Stark HJ, Goke B, Morris JC and Spitzweg C. Application of 188rhenium as an alternative radionuclide for treatment of prostate cancer after tumor-specific sodium iodide symporter gene expression. J Clin Endocrinol Metab. 2007; 92(11):4451-4458.

126. Urnauer S, Klutz K, Grunwald GK, Morys S, Schwenk N, Zach C, Gildehaus FJ, Roedl W, Ogris M, Wagner E and Spitzweg C. Systemic tumor-targeted sodium iodide symporter (NIS) gene therapy of hepatocellular carcinoma mediated by B6 peptide polyplexes. J Gene Med. 2017; 19(5)

127. Torre LA, Bray F, Siegel RL, Ferlay J, Lortet-Tieulent J and Jemal A. Global cancer statistics, 2012. CA Cancer J Clin. 2015; 65(2):87-108.

128. Kuczynski EA, Sargent DJ, Grothey A and Kerbel RS. Drug rechallenge and treatment beyond progression-implications for drug resistance. Nat Rev Clin Oncol. 2013; 10(10):571-587.

129. Penheiter AR, Wegman TR, Classic KL, Dingli D, Bender CE, Russell SJ and Carlson SK. Sodium iodide symporter (NIS)-mediated radiovirotherapy for pancreatic cancer. AJR Am J Roentgenol. 2010; 195(2):341-349.

130. Merron A, Baril P, Martin-Duque P, de la Vieja A, Tran L, Briat A, Harrington KJ, McNeish IA and Vassaux G. Assessment of the Na/I symporter as a reporter gene to visualize oncolytic adenovirus propagation in peritoneal tumours. Eur J Nucl Med Mol Imaging. 2010; 37(7):1377-1385.

131. Barton KN, Stricker H, Brown SL, Elshaikh M, Aref I, Lu M, Pegg J, Zhang Y, Karvelis KC, Siddiqui F, Kim JH, Freytag SO and Movsas B. Phase I study of noninvasive imaging of adenovirus-mediated gene expression in the human prostate. Mol Ther. 2008; 16(10):1761-1769.

132. McErlean EM, McCrudden CM and McCarthy HO. Delivery of nucleic acids for cancer gene therapy: overcoming extra- and intra-cellular barriers. Ther Deliv. 2016; 7(9):619-637.

133. Ogris M, Brunner S, Schuller S, Kircheis R and Wagner E. PEGylated DNA/transferrin-PEI complexes: reduced interaction with blood components, extended circulation in blood and potential for systemic gene delivery. Gene Ther. 1999; 6(4):595-605.

134. Smith RJ, Beck RW and Prevette LE. Impact of molecular weight and degree of conjugation on the thermodynamics of DNA complexation and stability of polyethylenimine-graft-poly(ethylene glycol) copolymers. Biophys Chem. 2015; 203-204:12-21.

135. Erbacher P, Bettinger T, Belguise-Valladier P, Zou S, Coll JL, Behr JP and Remy JS. Transfection and physical properties of various saccharide, poly(ethylene glycol), and antibody-derivatized polyethylenimines (PEI). J Gene Med. 1999; 1(3):210-222.

136. Wagner E, Zenke M, Cotten M, Beug H and Birnstiel ML. Transferrin-polycation conjugates as carriers for DNA uptake into cells. Proc Natl Acad Sci USA. 1990; 87(9):3410-3414.

137. Harbottle RP, Cooper RG, Hart SL, Ladhoff A, McKay T, Knight AM, Wagner E, Miller AD and Coutelle C. An RGD-oligolysine peptide: a prototype construct for integrin-mediated gene delivery. Hum Gene Ther. 1998; 9(7):1037-1047.

138. Wolschek MF, Thallinger C, Kursa M, Rossler V, Allen M, Lichtenberger C, Kircheis R, Lucas T, Willheim M, Reinisch W, Gangl A, Wagner E and Jansen B. Specific systemic nonviral gene delivery to human hepatocellular carcinoma xenografts in SCID mice. Hepatology. 2002; 36(5):1106-1114.

139. He D, Muller K, Krhac Levacic A, Kos P, Lachelt U and Wagner E. Combinatorial Optimization of Sequence-Defined Oligo(ethanamino)amides for Folate Receptor-Targeted pDNA and siRNA Delivery. Bioconjug Chem. 2016; 27(3):647-659.

140. Liu Z, Gao X, Kang T, Jiang M, Miao D, Gu G, Hu Q, Song Q, Yao L, Tu Y, Chen H, Jiang X and Chen J. B6 peptide-modified PEG-PLA nanoparticles for enhanced brain delivery of neuroprotective peptide. Bioconjug Chem. 2013; 24(6):997-1007.

141. Meng T, Liu J, Wen L, Yuan M, Cheng B, Hu Y, Zhu Y, Liu X, Yuan H and Hu F. Multi-cycle chemotherapy with the glycolipid-like polymeric micelles evade cancer stem cell enrichment in breast cancer therapy. Oncotarget. 2016; 7(45):72978-72989.

142. Dingli D, Peng K-W, Harvey ME, Greipp PR, O'Connor MK, Cattaneo R, Morris JC and Russell SJ. Image-guided radiovirotherapy for multiple myeloma using a recombinant measles virus expressing the thyroidal sodium iodide symporter. Blood. 2004; 103(5):1641-1646.

143. Stanta G, Jahn SW, Bonin S and Hoefler G. Tumour heterogeneity: principles and practical consequences. Virchows Arch. 2016; 469(4):371-384.

144. Crystal AS, Shaw AT, Sequist LV, Friboulet L, Niederst MJ, Lockerman EL, Frias RL, Gainor JF, Amzallag A, Greninger P, Lee D, Kalsy A, Gomez-Caraballo M, Elamine L, Howe E, Hur W, et al. Patient-derived models of acquired resistance can identify effective drug combinations for cancer. Science. 2014; 346(6216):1480-1486.

145. Luqmani YA. Mechanisms of drug resistance in cancer chemotherapy. Med Princ Pract. 2005; 14 Suppl 1:35-48.

146. Siegel RL, Miller KD and Jemal A. Cancer statistics, 2016. CA Cancer J Clin. 2016; 66(1):7-30.

147. Cisterna BA, Kamaly N, Choi WI, Tavakkoli A, Farokhzad OC and Vilos C. Targeted nanoparticles for colorectal cancer. Nanomedicine (Lond). 2016; 11(18):2443-2456.

148. Mittal VK, Bhullar JS and Jayant K. Animal models of human colorectal cancer: Current status, uses and limitations. World J Gastroenterol. 2015; 21(41):11854-11861.

149. Karim BO and Huso DL. Mouse models for colorectal cancer. Am J Cancer Res. 2013; 3(3):240-250.

150. Vatandoust S, Price TJ and Karapetis CS. Colorectal cancer: Metastases to a single organ. World J Gastroenterol. 2015; 21(41):11767-11776.

151. Schmohl KA, Gupta A, Grunwald GK, Trajkovic-Arsic M, Klutz K, Braren R, Schwaiger M, Nelson PJ, Ogris M, Wagner E, Siveke JT and Spitzweg C. Imaging and targeted therapy of pancreatic ductal adenocarcinoma using the theranostic sodium iodide symporter (NIS) gene. Oncotarget. 2017; 8(20):33393-33404.

152. Engelstaedter V, Boda J, Volklein C, Engel J, Jeschke U, Kirchner T and Mayr D. Lack of prognostic relevance of Her-2/neu, topoisomerase IIalpha and EGFR in advanced ovarian carcinoma. Exp Ther Med. 2012; 3(5):828-834.

153. Spitzweg C, Baker CH, Bergert ER, O'Connor MK and Morris JC. Image-guided radioiodide therapy of medullary thyroid cancer after carcinoembryonic antigen promoter-targeted sodium iodide symporter gene expression. Hum Gene Ther. 2007; 18(10):916-924.

154. Eichhorn ME, Klotz LV, Luedemann S, Strieth S, Kleespies A, Preissler G, Lindner M, Jauch KW, Reiser MF and Clevert DA. Vascular targeting tumor therapy: non-invasive contrast enhanced ultrasound for quantitative assessment of tumor microcirculation. Cancer Biol Ther. 2010; 9(10):794-802.

155. Urnauer S, Müller A, Schug C, Schmohl K, Tutter M, Schwenk N, Rödl W, Morys S, Ingrisch M, Bertram J, Bartenstein P, Clevert DA, Wagner E and Spitzweg C. EGFR-targeted nonviral NIS gene transfer for bioimaging and therapy of disseminated colon cancer metastases. Oncotarget. 2017; 8(54):92195-92208

156. Italiano A, Saint-Paul MC, Caroli-Bosc FX, Francois E, Bourgeon A, Benchimol D, Gugenheim J and Michiels JF. Epidermal growth factor receptor (EGFR) status in primary colorectal tumors correlates with EGFR expression in related metastatic sites: biological and clinical implications. Ann Oncol. 2005; 16(9):1503-1507.

157. Alliot C. Relevance of EGFR expression in colorectal cancer. Ann Oncol. 2005; 16(9):1557-1558; author reply 1558-1559.

158. Lisziewicz J, Bakare N, Calarota SA, Banhegyi D, Szlavik J, Ujhelyi E, Toke ER, Molnar L, Lisziewicz Z, Autran B and Lori F. Single DermaVir immunization: dose-dependent expansion of precursor/memory T cells against all HIV antigens in HIV-1 infected individuals. PLoS One. 2012; 7(5):e35416.

159. D'Onofrio M, Crosara S, De Robertis R, Canestrini S and Mucelli RP. Contrast-Enhanced Ultrasound of Focal Liver Lesions. AJR Am J Roentgenol. 2015; 205(1):W56-66.
160. Rubenthaler J, Reiser M and Clevert DA. Diagnostic vascular ultrasonography with the help of color Doppler and contrast-enhanced ultrasonography. Ultrasonography. 2016; 35(4):289-301.
161. Danila M, Popescu A, Sirli R, Sporea I, Martie A and Sendroiu M. Contrast enhanced ultrasound (CEUS) in the evaluation of liver metastases. Med Ultrason. 2010; 12(3):233-237.
162. Eschbach RS, Clevert DA, Hirner-Eppeneder H, Ingrisch M, Moser M, Schuster J, Tadros D, Schneider M, Kazmierczak PM, Reiser M and Cyran CC. Contrast-Enhanced Ultrasound with VEGFR2-Targeted Microbubbles for Monitoring Regorafenib Therapy Effects in Experimental Colorectal Adenocarcinomas in Rats with DCE-MRI and Immunohistochemical Validation. PLoS One. 2017; 12(1):e0169323.
163. Baron Toaldo M, Salvatore V, Marinelli S, Palama C, Milazzo M, Croci L, Venerandi L, Cipone M, Bolondi L and Piscaglia F. Use of VEGFR-2 targeted ultrasound contrast agent for the early evaluation of response to sorafenib in a mouse model of hepatocellular carcinoma. Mol Imaging Biol. 2015; 17(1):29-37.
164. Cosgrove D and Blomley M. Liver tumors: evaluation with contrast-enhanced ultrasound. Abdom Imaging. 2004; 29(4):446-454.
165. Iyer AK, Khaled G, Fang J and Maeda H. Exploiting the enhanced permeability and retention effect for tumor targeting. Drug Discov Today. 2006; 11(17-18):812-818.
166. Lu LC, Hsu CH, Hsu C and Cheng AL. Tumor Heterogeneity in Hepatocellular Carcinoma: Facing the Challenges. Liver Cancer. 2016; 5(2):128-138.
167. Hammoud GM and Ibdah JA. Are we getting closer to understanding intratumor heterogeneity in hepatocellular carcinoma? Hepatobiliary Surg Nutr. 2016; 5(2):188-190.
168. Quader S and Kataoka K. Nanomaterial-Enabled Cancer Therapy. Mol Ther. 2017; 25(7):1501-1513.
169. Schaffert D and Ogris M. Nucleic acid carrier systems based on polyethylenimine conjugates for the treatment of metastatic tumors. Curr Med Chem. 2013; 20(28):3456-3470.
170. Saeidnia S, Manayi A and Abdollahi M. From in vitro Experiments to in vivo and Clinical Studies; Pros and Cons. Curr Drug Discov Technol. 2015; 12(4):218-224.
171. Al-Lazikani B, Banerji U and Workman P. Combinatorial drug therapy for cancer in the post-genomic era. Nat Biotechnol. 2012; 30(7):679-692.
172. Stabile LP, Rothstein ME, Keohavong P, Lenzner D, Land SR, Gaither-Davis AL, Kim KJ, Kaminski N and Siegfried JM. Targeting of Both the c-Met and EGFR Pathways Results in Additive Inhibition of Lung Tumorigenesis in Transgenic Mice. Cancers (Basel). 2010; 2(4):2153-2170.

173. Penheiter AR, Dingli D, Bender CE, Russell SJ and Carlson SK. Monitoring the initial delivery of an oncolytic measles virus encoding the human sodium iodide symporter to solid tumors using contrast-enhanced computed tomography. J Gene Med. 2012; 14(9-10):590-597.

174. Barton KN, Stricker H, Elshaikh MA, Pegg J, Cheng J, Zhang Y, Karvelis KC, Lu M, Movsas B and Freytag SO. Feasibility of adenovirus-mediated hNIS gene transfer and 131I radioiodine therapy as a definitive treatment for localized prostate cancer. Mol Ther. 2011; 19(7):1353-1359.

175. Willhauck M, Samani B-R, Wolf I, Senekowitsch-Schmidtke R, Stark H-J, Meyer G, Knapp W, Göke B, Morris J and Spitzweg C. The potential of 211Astatine for NIS-mediated radionuclide therapy in prostate cancer. Eur J Nucl Med Mol Imaging. 2008; 35(7):1272-1281.

176. Trujillo MA, Oneal MJ, McDonough S, Qin R and Morris JC. A steep radioiodine dose response scalable to humans in sodium-iodide symporter (NIS)-mediated radiovirotherapy for prostate cancer. Cancer Gene Ther. 2012; 19(12):839-844.

177. Swanton C. Intratumor heterogeneity: evolution through space and time. Cancer Res. 2012; 72(19):4875-4882.

178. O'Connor JP, Rose CJ, Waterton JC, Carano RA, Parker GJ and Jackson A. Imaging intratumor heterogeneity: role in therapy response, resistance, and clinical outcome. Clin Cancer Res. 2015; 21(2):249-257.

179. Junttila MR and de Sauvage FJ. Influence of tumour micro-environment heterogeneity on therapeutic response. Nature. 2013; 501(7467):346-354.

180. Huang A, Zhao X, Yang XR, Li FQ, Zhou XL, Wu K, Zhang X, Sun QM, Cao Y, Zhu HM, Wang XD, Yang HM, Wang J, Tang ZY, Hou Y, Fan J, et al. Circumventing intratumoral heterogeneity to identify potential therapeutic targets in hepatocellular carcinoma. J Hepatol. 2017; 67(2):293-301.

181. Siddique O, Yoo ER, Perumpail RB, Perumpail BJ, Liu A, Cholankeril G and Ahmed A. The importance of a multidisciplinary approach to hepatocellular carcinoma. J Multidiscip Healthc. 2017; 10:95-100.

182. Hectors SJ, Wagner M, Bane O, Besa C, Lewis S, Remark R, Chen N, Fiel MI, Zhu H, Gnjatic S, Merad M, Hoshida Y and Taouli B. Quantification of hepatocellular carcinoma heterogeneity with multiparametric magnetic resonance imaging. Sci Rep. 2017; 7(1):2452.

183. El-Khoueiry AB, Sangro B, Yau T, Crocenzi TS, Kudo M, Hsu C, Kim TY, Choo SP, Trojan J, Welling THR, Meyer T, Kang YK, Yeo W, Chopra A, Anderson J, Dela Cruz C, et al. Nivolumab in patients with advanced hepatocellular carcinoma (CheckMate 040): an open-label, non-comparative, phase 1/2 dose escalation and expansion trial. Lancet. 2017; 389(10088):2492-2502.

184. Fitzmaurice C, Dicker D, Pain A, Hamavid H, Moradi-Lakeh M, MacIntyre MF, Allen C, Hansen G, Woodbrook R, Wolfe C, Hamadeh RR, Moore A, Werdecker A, Gessner BD, Te Ao B, McMahon B, et al. The Global Burden of Cancer 2013. JAMA Oncol. 2015; 1(4):505-527.

185. Amer MH. Gene therapy for cancer: present status and future perspective. Mol Cell Ther. 2014; 2:27.

186. Roder R and Wagner E. Sequence-defined shuttles for targeted nucleic acid and protein delivery. Ther Deliv. 2014; 5(9):1025-1045.

187. Harrington KJ, Spitzweg C, Bateman AR, Morris JC and Vile RG. Gene therapy for prostate cancer: current status and future prospects. J Urol. 2001; 166(4):1220-1233.

188. Spitzweg C, Harrington KJ, Pinke LA, Vile RG and Morris JC. The Sodium Iodide Symporter and Its Potential Role in Cancer Therapy. J Clin Endocrinol Metab. 2001; 86(7): 3327-3335.

189. Oneal MJ, Trujillo MA, Davydova J, McDonough S, Yamamoto M and Morris JC, 3rd. Effect of increased viral replication and infectivity enhancement on radioiodide uptake and oncolytic activity of adenovirus vectors expressing the sodium iodide symporter. Cancer Gene Ther. 2013; 20(3):195-200.

190. Blumenschein GR, Jr., Mills GB and Gonzalez-Angulo AM. Targeting the hepatocyte growth factor-cMET axis in cancer therapy. J Clin Oncol. 2012; 30(26):3287-3296.

191. Kim EM, Park EH, Cheong SJ, Lee CM, Jeong HJ, Kim DW, Lim ST and Sohn MH. In vivo imaging of mesenchymal-epithelial transition factor (c-Met) expression using an optical imaging system. Bioconjug Chem. 2009; 20(7):1299-1306.

192. Kim EM, Park EH, Cheong SJ, Lee CM, Kim DW, Jeong HJ, Lim ST, Sohn MH, Kim K and Chung J. Characterization, biodistribution and small-animal SPECT of I-125-labeled c-Met binding peptide in mice bearing c-Met receptor tyrosine kinase-positive tumor xenografts. Nucl Med Biol. 2009; 36(4):371-378.

193. Galanis E, Atherton PJ, Maurer MJ, Knutson KL, Dowdy SC, Cliby WA, Haluska P, Jr., Long HJ, Oberg A, Aderca I, Block MS, Bakkum-Gamez J, Federspiel MJ, Russell SJ, Kalli KR, Keeney G, et al. Oncolytic measles virus expressing the sodium iodide symporter to treat drug-resistant ovarian cancer. Cancer Res. 2015; 75(1):22-30.

194. Willhauck M, Sharif-Samani B, Senekowitsch-Schmidtke R, Wunderlich N, Göke B, Morris J and Spitzweg C. Functional sodium iodide symporter expression in breast cancer xenografts in vivo after systemic treatment with retinoic acid and dexamethasone. Breast Cancer Res Treat. 2008; 109(2):263-272.

195. USFDA. Guidance for Industry: Estimating the Maximum Safe Starting Dose in Adult Healthy Volunteer. US Food and Drug Administration. 2005:Rockville.

196. Zhang YW, Staal B, Essenburg C, Lewis S, Kaufman D and Vande Woude GF. Strengthening context-dependent anticancer effects on non-small cell lung carcinoma by inhibition of both MET and EGFR. Mol Cancer Ther. 2013; 12(8):1429-1441.

197. Van Der Steen N, Pauwels P, Gil-Bazo I, Castanon E, Raez L, Cappuzzo F and Rolfo C. cMET in NSCLC: Can We Cut off the Head of the Hydra? From the Pathway to the Resistance. Cancers (Basel). 2015; 7(2):556-573.

198. Merdan T, Kopecek J and Kissel T. Prospects for cationic polymers in gene and oligonucleotide therapy against cancer. Adv Drug Deliv Rev. 2002; 54(5):715-758.

199. Whitehead KA, Dorkin JR, Vegas AJ, Chang PH, Veiseh O, Matthews J, Fenton OS, Zhang Y, Olejnik KT, Yesilyurt V, Chen D, Barros S, Klebanov B, Novobrantseva T, Langer R and Anderson DG. Degradable lipid nanoparticles with predictable in vivo siRNA delivery activity. Nat Commun. 2014; 5:4277.

200. Salcher EE, Kos P, Fröhlich T, Badgujar N, Scheible M and Wagner E. Sequence-defined four-arm oligo(ethanamino)amides for pDNA and siRNA delivery: Impact of building blocks on efficacy. J Control Release. 2012; 164(3):380-386.

201. Morys S, Wagner E and Lächelt U. From Artificial Amino Acids to Sequence-Defined Targeted Oligoaminoamides. Methods Mol Biol. 2016; 1445:235-258.

202. Schaffert D, Troiber C, Salcher EE, Fröhlich T, Martin I, Badgujar N, Dohmen C, Edinger D, Kläger R, Maiwald G, Farkasova K, Seeber S, Jahn-Hofmann K, Hadwiger P and Wagner E. Solid-phase synthesis of sequence-defined T-, i-, and U-shape polymers for pDNA and siRNA delivery. Angew Chem Int Ed Engl. 2011; 50(38):8986-8989.

203. Fröhlich T, Edinger D, Russ V and Wagner E. Stabilization of polyplexes via polymer crosslinking for efficient siRNA delivery. Eur J Pharm Sci. 2012; 47(5):914-920.

204. Troiber C, Edinger D, Kos P, Schreiner L, Kläger R, Herrmann A and Wagner E. Stabilizing effect of tyrosine trimers on pDNA and siRNA polyplexes. Biomaterials. 2013; 34(5):1624-1633.

205. Klein PM, Müller K, Gutmann C, Kos P, Krhac Levacic A, Edinger D, Hohn M, Leroux JC, Gauthier MA and Wagner E. Twin disulfides as opportunity for improving stability and transfection efficiency of oligoaminoethane polyplexes. J. Control. Release. 2015; 205:109-119.

206. Lee DJ, Kessel E, Edinger D, He D, Klein PM, Voith von Voithenberg L, Lamb DC, Lächelt U, Lehto T and Wagner E. Dual antitumoral potency of EG5 siRNA nanoplexes armed with cytotoxic bifunctional glutamyl-methotrexate targeting ligand. Biomaterials. 2016; 77:98-110.

207. Zhang W, Müller K, Kessel E, Reinhard S, He D, Klein PM, Höhn M, Rödl W, Kempter S and Wagner E. Targeted siRNA Delivery Using a Lipo-Oligoaminoamide Nanocore with an Influenza Peptide and Transferrin Shell. Adv Healthc Mater. 2016; 5(12):1493-1504.

208. Klein PM, Reinhard S, Lee DJ, Muller K, Ponader D, Hartmann L and Wagner E. Precise redox-sensitive cleavage sites for improved bioactivity of siRNA lipopolyplexes. Nanoscale. 2016; 8(42):18098-18104.

209. Zhang P, He D, Klein PM, Liu X, Röder R, Döblinger M and Wagner E. Enhanced Intracellular Protein Transduction by Sequence Defined Tetra-Oleoyl Oligoaminoamides Targeted for Cancer Therapy. Adv Funct Mater. 2015; 25(42):6627-6636.

210. Walker GF, Fella C, Pelisek J, Fahrmeir J, Boeckle S, Ogris M and Wagner E. Toward synthetic viruses: endosomal pH-triggered deshielding of targeted polyplexes greatly enhances gene transfer in vitro and in vivo. Mol Ther. 2005; 11(3):418-425.

211. Neu M, Germershaus O, Behe M and Kissel T. Bioreversibly crosslinked polyplexes of PEI and high molecular weight PEG show extended circulation times in vivo. J control Release. 2007; 124(1-2):69-80.

212. Noga M, Edinger D, Rödl W, Wagner E, Winter G and Besheer A. Controlled shielding and deshielding of gene delivery polyplexes using hydroxyethyl starch (HES) and alpha-amylase. J Control Release. 2012; 159(1):92-103.

213. Heller P, Birke A, Huesmann D, Weber B, Fischer K, Reske-Kunz A, Bros M and Barz M. Introducing PeptoPlexes: polylysine-block-polysarcosine based polyplexes for transfection of HEK 293T cells. Macromol Biosci. 2014; 14(10):1380-1395.

214. Du J, Tian C, Ling J and Wang Y. R8-modified polysarcosine-b-polylysine polypeptide to enhance circulation stability and gene delivery efficiency. J Control Release. 2015; 213:e50-51.

215. Morys S, Krhac Levacic A, Urnauer S, Kempter S, Kern S, Rädler JO, Spitzweg C, Lächelt U and Wagner E. Influence of Defined Hydrophilic Blocks within Oligoaminoamide Copolymers: Compaction versus Shielding of pDNA Nanoparticles. Polymers. 2017; 9(142).

216. Fisher KD, Ulbrich K, Subr V, Ward CM, Mautner V, Blakey D and Seymour LW. A versatile system for receptor-mediated gene delivery permits increased entry of DNA into target cells, enhanced delivery to the nucleus and elevated rates of transgene expression. Gene Ther. 2000; 7(15):1337-1343.

217. Oupicky D, Howard KA, Konak C, Dash PR, Ulbrich K and Seymour LW. Steric stabilization of poly-L-Lysine/DNA complexes by the covalent attachment of semitelechelic poly[N-(2-hydroxypropyl)methacrylamide]. Bioconjugate Chem. 2000; 11(4):492-501.

218. Blessing T, Kursa M, Holzhauser R, Kircheis R and Wagner E. Different strategies for formation of pegylated EGF-conjugated PEI/DNA complexes for targeted gene delivery. Bioconjug Chem. 2001; 12(4):529-537.

219. Oupicky D, Ogris M, Howard KA, Dash PR, Ulbrich K and Seymour LW. Importance of lateral and steric stabilization of polyelectrolyte gene delivery vectors for extended systemic circulation. Mol Ther. 2002; 5(4):463-472.

220. Peeters L, Sanders NN, Jones A, Demeester J and De Smedt SC. Post-pegylated lipoplexes are promising vehicles for gene delivery in RPE cells. J Control Release. 2007; 121(3):208-217.

221. Fella C, Walker GF, Ogris M and Wagner E. Amine-reactive pyridylhydrazone-based PEG reagents for pH-reversible PEI polyplex shielding. Eur J Pharm Sci. 2008; 34(4-5): 309-320.

222. Beckert L, Kostka L, Kessel E, Krhac Levacic A, Kostkova H, Etrych T, Lächelt U and Wagner E. Acid-labile pHPMA modification of four-arm oligoaminoamide pDNA polyplexes balances shielding and gene transfer activity in vitro and in vivo. Eur J Pharm Biopharm. 2016; 105:85-96.

223. Wagner E. Programmed drug delivery: nanosystems for tumor targeting. Expert Opin Biol Ther. 2007; 7(5):587-593.

224. Wagner E. Advances in cancer gene therapy: tumor-targeted delivery of therapeutic pDNA, siRNA, and dsRNA nucleic acids. J BUON. 2007; 12 Suppl 1:S77-82.

225. Mendelsohn J and Baselga J. Epidermal growth factor receptor targeting in cancer. Semin Oncol. 2006; 33(4):369-385.

226. Chen J, Gamou S, Takayanagi A and Shimizu N. A novel gene delivery system using EGF receptor-mediated endocytosis 97. FEBS Lett. 1994; 338:167-169.

227. Cristiano RJ and Roth JA. Epidermal growth factor mediated DNA delivery into lung cancer cells via the epidermal growth factor receptor. Cancer Gene Ther. 1996; 3(1):4-10.

228. Fominaya J, Uherek C and Wels W. A chimeric fusion protein containing transforming growth factor-alpha mediates gene transfer via binding to the EGF receptor. Gene Ther. 1998; 5(4):521-530.

229. Liu X, Tian P, Yu Y, Yao M, Cao X and Gu J. Enhanced antitumor effect of EGF R-targeted p21WAF-1 and GM-CSF gene transfer in the established murine hepatoma by peritumoral injection. Cancer Gene Ther. 2002; 9(1):100-108.

230. Schäfer A, Pahnke A, Schaffert D, van Weerden WM, de Ridder CM, Rödl W, Vetter A, Spitzweg C, Kraaij R, Wagner E and Ogris M. Disconnecting the yin and yang relation of epidermal growth factor receptor (EGFR)-mediated delivery: a fully synthetic, EGFR-targeted gene transfer system avoiding receptor activation. Hum Gene Ther. 2011; 22(12):1463-1473.

231. Abourbeh G, Shir A, Mishani E, Ogris M, Rödl W, Wagner E and Levitzki A. PolyIC GE11 polyplex inhibits EGFR-overexpressing tumors. IUBMB Life. 2012; 64(4):324-330.

232. Müller K, Klein PM, Heissig P, Roidl A and Wagner E. EGF receptor targeted lipo-oligocation polyplexes for antitumoral siRNA and miRNA delivery. Nanotechnology. 2016; 27(46):464001.

233. Plank C, Zatloukal K, Cotten M, Mechtler K and Wagner E. Gene transfer into hepatocytes using asialoglycoprotein receptor mediated endocytosis of DNA complexed with an artificial tetra-antennary galactose ligand. Bioconjug Chem. 1992; 3(6):533-539.

234. Kaiser E, Colescott RL, Bossinger CD and Cook PI. Color test for detection of free terminal amino groups in the solid-phase synthesis of peptides. Anal Biochem. 1970; 34(2):595-598.

235. Li Z, Zhao R, Wu X, Sun Y, Yao M, Li J, Xu Y and Gu J. Identification and characterization of a novel peptide ligand of epidermal growth factor receptor for targeted delivery of therapeutics. Faseb J. 2005; 19(14):1978-1985.

236. Leng Q, Goldgeier L, Zhu J, Cambell P, Ambulos N and Mixson AJ. Histidine-lysine peptides as carriers of nucleic acids. Drug News Perspect. 2007; 20(2):77-86.

237. Schaffert D, Troiber C and Wagner E. New sequence-defined polyaminoamides with tailored endosomolytic properties for plasmid DNA delivery. Bioconjugate Chem. 2012; 23(6):1157-1165.

238. Fröhlich T, Edinger D, Klager R, Troiber C, Salcher E, Badgujar N, Martin I, Schaffert D, Cengizeroglu A, Hadwiger P, Vornlocher HP and Wagner E. Structure-activity relationships of siRNA carriers based on sequence-defined oligo (ethane amino) amides. J Control Release. 2012; 160(3):532-541.

239. Hunter CA and Sanders JKM. The nature of .pi.-.pi. interactions. J Am Chem Soc. 1990; 112(14):5525–5534.

240. Fink AL. Protein aggregation: folding aggregates, inclusion bodies and amyloid. Fold Des. 1998; 3(1):R9-23.

241. Veronese FM, Mero A, Caboi F, Sergi M, Marongiu C and Pasut G. Site-specific pegylation of G-CSF by reversible denaturation. Bioconjugate Chem. 2007; 18(6):1824-1830.

242. Saito G, Swanson JA and Lee KD. Drug delivery strategy utilizing conjugation via reversible disulfide linkages: role and site of cellular reducing activities. Adv Drug Deliv Rev. 2003; 55(2):199-215.

243. Mickler FM, Mockl L, Ruthardt N, Ogris M, Wagner E and Brauchle C. Tuning nanoparticle uptake: live-cell imaging reveals two distinct endocytosis mechanisms mediated by natural and artificial EGFR targeting ligand. Nano Lett. 2012; 12(7):3417-3423.

11. Acknowledgements

Over the last years, so many people contributed to this thesis and I would like to thank them for their great help and support.

First and foremost, I would like to thank Prof. Dr. Christine Spitzweg for giving me the possibility to work on this exciting project and to perform my thesis in her group. I very much appreciate her professional guidance, scientific support, trust, beneficial advice and encouragement to develop own ideas and to grow with the demands.

Furthermore, I would like to thank Prof. Dr. Ernst Wagner for accepting me as an external PhD student, for his scientific support, always helpful advice, many fruitful discussions and for a great collaboration. Thanks to all of his lab members for including me as an external in the lab and for all their help. Many thanks especially to Stephan for the good collaboration and the continuous supply of oligomers.

I am very grateful to all my group members for the best working atmosphere ever, for always having something to laugh about, spending so much time (day and night) together and our crazy travels. My deepest gratitude goes to Christina my seat-neighbor, for her support in all these years. Additionally, I would like to express my deepest thankfulness to Katy for introducing me to scientific writing and being the best reviewer I can imagine. Furthermore, I would like to thank Nathalie for constant support and help and for keeping the lab running. Many thanks to my like-minded pharma girl Mariella, for being my flight partner and Andrea for so many experiments we did together and reminding me not to wear my pyjamas in the lab.

I would further like to thank the members of the Department of Nuclear Medicine at the Klinikum Großhadern (director: Prof. Dr. P. Bartenstein), especially Rosel, Karin and Barbara for the great support as well as personal and technical assistance during the imaging and therapy studies.

Special thanks to Prof. Dr. Dirk-Andre Clevert and Dr. Michael Ingrisch for an excellent collaboration and for helping me with CEUS imaging studies, which represent a highly significant part of my work.

I am also grateful to all members of the SFB 824 for their collaboration, for providing the professional infrastructure and many helpful discussions.

Finally, I owe my deepest gratitude to my family and family-in-law, who have always been there for me, supported me and gave me the best advice for any problem and in any difficult situation. Thank you, Jürgen, for being at my side for many years, for supporting me and for always believing in me.